# COMPARATIVE STUDY OF CHARACTERISTICS OF SOLVENT FREE ORGANIC COATING WITH CONVENTIONAL AND NANO FILLER

**The Thesis Submitted to the Faculty Council of Interdisciplinary studies, Law & Management (ISLM), Jadavpur University, Kolkata**

**For the Award the Degree of Doctor of Philosophy in Engineering**

**Submitted by**

**UJJWAL GHOSH**

**Registration No. – D-7/ISLM/54/16**

**Supervised by**

**Under Guidance of**

**DR. AKSHAY KR. PRAMANICK**
**PROFESSOR**
**MET AND MAT ENGG DEPTT.**
**JADAVPUR UNIVERSITY**
**KOLKATA-700032, INDIA**

**DR. BUDDHADEB DUARI**
**NACE CORROSION & COATING SPECIALIST AND SSPC PROTECTIVE COATING SPECIALIST**

**Faculty Council of Interdisciplinary Studies, Law & Management (ISLM)**

**JADAVPUR UNIVERSITY**

**KOLKATA-700032, INDIA**

**2023**

II

INDEX No. D-7/ISLM/54/16

## 1. Title of the thesis:

**COMPARATIVE STUDY OF CHARACTERISTICS OF SOLVENT FREE ORGANIC COATING WITH CONVENTIONAL AND NANO FILLER**

## 2. Name Designation & Institution of the Supervisors:

I.

**DR. AKSHAY KR. PRAMANICK**

PROFESSOR

MET AND MAT ENGG DEPTT

JADAVPUR UNIVERSITY

KOLKATA- 700032, INDIA

e-mail: akshay99.ju@gmail.com

II.

**DR. BUDDHADEB DUARI**

NACE CORROSION & COATING

SPECIALIST AND SSPC PROTECTIVE

COATING SPECIALIST

e-mail: bduari@yahoo.co.in

# CERTIFICATE FROM SUPERVISORS

This is to certify that the thesis entitled "**COMPARATIVE STUDY OF CHARACTERISTICS OF SOLVENT FREE ORGANIC COATING WITH CONVENTIONAL AND NANO FILLER**" submitted by **SHRI. UJJWAL GHOSH (Reg. No. D-7/ISLM/54/16)**, who got his name registered on **14.07.2016** for the award of **Ph.D. (Engg)** degree of **Jadavpur University** is absolutely based upon his own work under the supervision of **Prof.(Dr.)Akshay Kr. Praminck** and **Dr. Buddhadeb Duari** and that neither his thesis nor any part of the thesis has been submitted for any degree or any other academic award anywhere before.

I. Signature of supervisor

12/07/2023

**DR. AKSHAY KR. PRAMANICK**

**PROFESSOR**
**MET AND MAT ENGG DEPTT.**
**JADAVPUR UNIVERSITY**
**KOLKATA-700032, INDIA**

(Signature of the supervisor and date with official seal)

Dr. Akshay Kr. Pramanick
Professor
Department of Metallurgical & Material Engineering
Jadavpur University, Kolkata-700 032

II. Signature of supervisor

12/7/2023

**DR. BUDDHADEB DUARI**

**NACE CORROSION & COATING SPECIALIST AND SSPC PROTECTIVE COATING SPECIALIST**

(Signature of the supervisor and date with official seal)

NACE CORROSION SPECIALIST CERT NO. 14687

NACE COATING SPECIALIST CERT NO. 14687

SSPC COATING SPECIALIST

# Statement of Originality

I, **Ujjwal Ghosh** registered on **14.07.2016** do hereby declare that this thesis entitled "**COMPARATIVE STUDY OF CHARACTERISTICS OF SOLVENT FREE ORGANIC COATING WITH CONVENTIONAL AND NANO FILLER**" contains literature survey and original research work done by the undersigned candidate as part of Doctoral studies.

All information in this thesis have been obtained and presented in accordance with existing academic rules and ethical conduct. I declare that, as required by these rules and conduct, I have fully cited and referred all materials and results that are not original to this work.

I also declare that I have checked this thesis as per the "Policy on Anti Plagiarism, Jadavpur University, 2019", and the level of similarity as checked by iThenticate software is **1%**.

Ujjwal Ghosh

Signature of Candidate:

Date: 12/07/2023

Certified by Supervisor(s):

(Signature with date, seal)

I. 12/07/2023

Dr. Akshay K. Pramanick
Professor
Department of Metallurgical & Material Engineering
Jadavpur University, Kolkata-700 032

II. 12/7/2023

CORROSION SPECIALIST CERT NO. 14687

CERT. NO. 14687

CERT NO. 2010-625-153

# *Dedicated to*

*My Parents*

*Sri. Ashesh Ghosh, Smt. Padma Ghosh*

*&*

*Elder Brother*

*Sri. Shyamal Ghosh*

*"I haven't failed.*

*I've just found*

*10,000 ways*

*that won't work "*

*Thomas Alva Edison*

# ACKNOWLEDGEMENT

I convey most sincere regards, respect and deepest gratitude to **Prof. Akshay Kumar Pramanick** (Department of Metallurgical and Material Engineering, Jadavpur University) and **Dr. Buddhadeb Duari** (NACE Corrosion, Coating Specialist and SSPC Protective coating Specialist) for their inspiration, encouragement and valuable guidance throughout the work.

I thank Prof. P.C.Chakrabaty, HOD, Met & Mat Engg Deptt, Jadavpur University. I am deeply indebted to all the faculty members of Department and technical staff, senior scholars and also the junior scholars for their help and support.

I take this opportunity to express gratitude to **Mr. Sunil Ghosh**, retired technologist of protective coating of Shalimar Paint Limited, Kolkata. I would like to express my deepest appreciation to Sudhir Ghosh, Pankaj Bhadra, Shimadri Majumdar, Jayanta Bhattcharjee, Anik Chowdhuri, Amithabh Das, Bighneswar Besera, Sujit Kumar Guchhait, Subrata Kundu, Pangita Deka, Sourav Debnath, Soumojit Roy and Tanmoy Mondal. I am extremely grateful to Surya Kanta Ghosh, Krishna Kumar Sarkar, Bubai Bag, Arnab Adhikary, Sumon Biswas, Mithun Biswas, Mithun Majumdar and special thanks to Koushik Duari. I would like to express my deepest gratitude to Late Manik Mondal, Debjit Karmarkar, Arghadeep Banerjee, Ayan Chaterjee, Avijit Halder, Mrinmoy Pal, Asit Banerjee, Soumendra Nath Das, Tarasankar Sarkar, Dipayan Chatterjee, Toton Ghosh, Santanu Mukherjee and Sadai Bauri. I also thankful to my childhood friends Totan Roy and Utpal Ghosh. I would like to thank all the members of “Aalo”, a NGO group. I am extremely grateful to Vijoy Solvent and Thinner. Kolkata, Mr. Paras Kr Shah, Lalita Infra Project Ltd. Kolkata and Aglow lab, Kolkata.

I also thank my parents Ashesh Ghosh, Padma Ghosh, elder brother Shyamal Ghosh and also Nabanita Das for the unceasing encouragement, support and attention. I could not have undertaken this journey without my friends, and all the well wishers.

I would also like to express my thanks to all my respected teachers for their help and support.

Sincere words of gratitude to the office of the Principal Secretary and Dean, Faculty of ISLM, for allowing me to formally proceed with my work all these year.

It would be unfair if I don't mention the financial support of **"UGC BSR-2014-15"** fellowship scheme for this research work.

**Department of** **Ujjwal Ghosh**

**Metallurgical and Material Engineering,**

**Jadavpur University**

**Kolkata**

**Dated:**

# Abstract

In this recent research come in contact nano coating as nano structured material which will give a lot of efforts and improve coating technologies mostly like corrosion resistant because of greater surface activity with well dispersion of nanoparticales, in the resin through containing cross linking agent with lot of linkage group and gives three dimensional network rigid structures with desirable properties. These molecular networks form a very high crosslink density coating with remarkable physical properties including extreme scratch resistance, ultra high gloss, very high water and chemical resistance, extreme UV resistance, remarkable flexibility and cleaning properties. Such nanoparticles when incorporated in coating, physical properties of the system get altered without affecting the clarity. Tiny size of nanoparticles produces extra ordinary high surface energy. From the last decade convectional and nano filler like ZnO, $ZrO_2$, clay, $SiO_2$, $Fe_2O_3$, $MoS_2$, Zeolite, halloysite, $TiO_2$, $Al_2O_3$, $SiO_2$ and $CaCO_3$ are mostly studied in the paints industry. But our focus should be out of these, fumed silica is is selected for nano filler which finely dispersed, amorphous form of silica. It is produced through high-temperature hydrolysis of silicon tetrachloride in an oxyhydrogen gas flame, give highly pure product. In the Aerosil (R972) manufacturing process, the primary particles that are created are nearly spherical and devoid of pores. This product exhibits a specific surface area (measured using the BET method) of 110 ± 20 $m^2g^{-1}$, with a primary particle size (PPS) of 12 nm and achieved by treating $SiO_2$ with dimethyl dichloro silane (DDS). Hydrophobic fumed silica is employed to enhance and sustain the flow characteristics of

powders, thicken water-resistant systems, and develop anticorrosive coatings. It offers rheology control for intricate liquid systems and displays water resistance, facilitating hydrophobization of liquid systems. In coatings, it serves as an anti-settling agent, aids in pigment stabilization. Different formed of silica is also economically and environmentally eco friend which is easily available and industrial affordable. Quartz silica used as conventional filler which is used for comparative study of both composite coatings. The used of silica particles in different polymers such as Epoxy, Polyurethane, Coal Tar Epoxy and Vinyl Ester matrix, which leads to significant improvements in the Physico-Mechanical, thermal properties and also corrosion behaviors of the developed nanocomposite coatings. Conventional and nano filler based composite coating were developed through solution blending route and cured by hardener and characterized by FTIR, XRD, SEM and TGA-DTA analysis. The size of the nano particles was confirmed by transmission electron microscopy (TEM). Physico-Mechanical and corrosion studies of silica (micro and nano) based composites coatings were determined by ASTM method. Extreme improvement of wear index data observed in every nano composite coatings. Corrosion behaviors of the coated mild steel specimens were evaluated by salt spray chamber (SSC) test, cathodic disbondment (CD) test, $E_{corr}$ & $I_{corr}$ i.e. (PD) and electro-chemical impedance spectroscopy (EIS) measurements immersion in 3.5% NaCl solution. Optical images are taken both types of coatings before and after corrosion test. SSC test was performed by 2200 hours of both types of MS coated samples and cured film in 5% NaCl solution. Water absorption and chemical resistance also studied of composite coatings for 65 days. Moreover, all nanocomposite based coatings have showed excellent results all over experiment than conventional based composite coating.

# List of Publications

## ➢ Journal Publications:

- **(Scopus index)**

1. **Ujjwal Ghosh**, Akshay Kumar Pramanick, Buddhadeb Duari, Koushik Duari, Sourav Debnath, Comparative Studies of Wear and Corrosion Behaviors of Conventional and Nano Filler Based Solvent Free Tar-free epoxy-amine Coatings, Journal of Mines metals & fuels, Vol.71, 2023. (Accepted)

- **(SCI index)**

2. **Ujjwal Ghosh**, Buddhadeb Duari, Kaushik Duari, Sujit Kumar Guchhait , Akshay Kr Pramanick, Study of Corrosion Behaviors of Conventional and Nano Filler Based Solvent Free Organic Coatings, (Communicated)

3. **Ujjwal Ghosh,** Akshay Kr Pramanick, Buddhadeb Duari, Koushik Duari Tanmoy Mondal, Sujit Kumar Guchhait, Wear Resistance and Anticorrosion Properties of Conventional and Nano Filler Based Solvent Free PU Composite Coatings, (Communicated)

## ➢ Book Chapter:

1. **Ujjwal Ghosh**, Sourav Debnath, Buddhadeb Duari, Kaushik Duari, Totan Roy, Akshay Kumar Pramanick, "Wear and Thermal Behaviours of micro and nano Filler Based Solvent Free Epoxy-phenalkamine Composite Coatings," (Accepted for publication in Taylor & Francis, CRC Press).

## ➢ Patent/ Copyright:

1. **Ujjwal Ghosh**, Sourav Debnath, Samrat Paul, Akshay Kumar Pramanick, Buddhadeb Duari, Kaushik Duari, Anindya Sundar Das, "Comparative Studies of

Wear resistance and Anti corrosion Behaviors of Conventional and Nano filler Based Solvent free 160N Glass flake-epoxy Composite Coating." (Intellectual Property Rights Application ID: 105/IPR/OTH/May 2023/2/2)

- **Paper Presented in International Conferences :**

1. **Ujjwal Ghosh**, Akshay Kumar Pramanick, Buddhadeb Duari, Koushik Duari, Sourav Debnath "Comparative Studies of Wear and Corrosion Behaviors of Conventional and Nano Filler Based Solvent Free Tar-free epoxy-amine Coatings." International Conference on Engineering Design and Computing (ICEDC)-2023 held from 28th – 29th January 2023 at Swami Vivekananda University, Kolkata.

2. **Ujjwal Ghosh**, Sourav Debnath, Buddhadeb Duari, Kaushik Duari, Totan Roy, Akshay Kumar Pramanick, "Wear and Thermal Behaviours of micro and nano Filler Based Solvent Free Epoxy-phenalkamine Composite Coatings," Industry 5.0: Revolution, Innovation and Efficiency (ICIRIE-2023) held on 4th—5th March, 2023 at Swami Vivekananda Institute of Science & Technology, Kolkata 700145.

# CONTENTS

CHAPTER PAGE NO

CHAPTER PAGE NO

CHAPTER PAGE NO

CHAPTER PAGE NO

CHAPTER PAGE NO

# LIST OF SYMBOLS AND ABBREVIATIONS

| | | |
|---|---|---|
| ASTM | - | American Society for Testing and Materials |
| Å | - | Angstrom |
| $\Delta E/\Delta I$ | - | Applied Potential and Response Current |
| CC | - | Chromium-containing compounds |
| $I_{corr}$ | - | Corrosion Current |
| $E_{corr}$ | - | Corrosion Potential |
| CE | - | Counter Electrode |
| °C | - | Degree Celsius |
| °F | - | Degree Fahrenheit |
| DETA | - | Diethylenetriamine |
| EIS | - | Electrochemical Impedance Spectroscopy |
| $e^-$ | - | Electron |
| eV | - | Electron Volts |
| $Fe^{2+}$ | - | Ferrous |
| FTIR | - | Fourier Transform -Infrared spectroscopy |
| FRA | - | Frequency Response Analyzer |
| Hz | - | Hertz |
| HCl | - | Hydrochloric acid |
| $H_2$ | - | Hydrogen |

| | | |
|---|---|---|
| $H^+$ | - | Hydrogen ion |
| OH | - | Hydroxyl |
| Fe | - | Iron |
| $Fe(OH)_2$ | - | Iron (II) hydroxide |
| $Fe_2O_3$ | - | Iron (III) oxide |
| µm | - | Micrometer |
| MS | - | Mild Steel |
| $SiO_2$ | - | Silicon Dioxide |
| $TiO_2$ | - | Titanium Dioxide |
| ZnO | - | Zinc oxide |
| HCl | - | Hydrochloric acid |
| NaCl | - | Sodium chloride |
| Rct | - | Charge Transfer Resistance |
| $R_{PO}$ | - | Double Layer Capacitance |
| $R_p$ | - | Pore Resistance |
| XRD | - | X-ray Diffraction studies |
| CD | - | Cathodic Disbondment |
| PD | - | Potentiodynamic Polarization |
| DFT | - | Dry Film Thickness |

| | | |
|---|---|---|
| SSC | - | Salt Spray Chamber studies |
| $H_2SO_4$ | - | Sulphuric acid |
| TGA-DTA | - | Thermo Gravimetric Analysis-Differential Thermal Analysis |
| CPE | - | Constant Phase Element |
| PU | - | Polyurethane |
| EP | - | Epoxy |
| VE | - | Vinyl Ester |
| CTEP | - | Coal Tar Epoxy |
| MIBK | - | Methyl Isobutyl Ketone |
| MDI | - | Methylene Diphenyl Diisocyanate |
| DGEBA | - | Diglycidyl Ether of Bisphenol-A |
| AC | - | Alternating Current |
| DC | - | Direct Current |
| $\beta a$ | - | Anodic Slope |
| $\beta c$ | - | Cathodic Slope |
| $J_{corr}$ | - | Corrosin Current Density |
| $R_S$ | - | Solution Resistance |
| NaOH | - | Sodium Hydroxide |
| WE | - | Working Electrode |

# List of Figures

**Figure No & Title** **Page No**

# LIST OF TABLES

**Table No & Title** **Page No**

# CHAPTER-1

# Introduction

# 1. Introduction

This chapter focuses on the progress of corrosion research across various industries and applications. It discusses not only traditional corrosion studies but also explores coating methods for polymer nanocomposites.

Metals and alloys are considered to be the most important materials in engineering and thus can say that corrosion of metals is one of the most crucial problems faced by different scientist and engineers over a long period of time. Over the past century and a half, the field of corrosion control has developed into a significant area of research. In addition to this, the prevention of metal corrosion through the application of protective surface coatings has become an expansive subject. The visual allure of these coatings further augments their appearance in various applications, including structures, vehicles, aircraft, maritime vessels, household and commercial devices.

The matter encompasses concerns related to public safety, substantial economic repercussions, environmental consequences, and the preservation of materials. Corrosion is frequently likened to rusting and pertains to the deterioration of a metal due to exposure and interaction with its surroundings. The process of "corrosion" which is the interaction between a metal and its surrounding environment that leads to alterations in the metal's characteristics. This interaction can potentially harm the metal itself, the surrounding environment, or the larger technical system of which the metal is a component [1, 2]. Corrosion is not limited to just metals, it can indeed affect a wide range of materials, including nonmetallic materials like polymers, ceramics, semiconductors, and more. This broader definition of corrosion encompasses the degradation of various types of natural and synthetic materials, including biomaterials etc. Corrosion is as an irreversible

interfacial process involving a substance such as metal, ceramic or polymer and its surroundings. This interaction leads to either the material being consumed or a constituent from the surroundings dissolving into the material [3]. NACE defined corrosion as the weakening or degradation of a metal/material, caused by its interaction with the surrounding environment [4].

Corrosion has far-reaching consequences across economic, health, safety, technological, and cultural domains in society. The economic aspect is particularly pivotal, driving a significant amount of research in the field. Its impact on a nation's economy is substantial, with industries annually incurring substantial expenses due to corrosion, a figure that continues to rise. Numerous publications have addressed the financial toll of corrosion, with the initial notable report by Uhlig in 1949 estimating the United States' yearly corrosion cost at 5.5 billion dollars, equivalent to 2.1% of the total Gross National Product (GNP) for that year [5]. In the sixties, the significance of corrosion became more apparent as it became clear that it was inflicting economic harm on industrialized nations. This was evident through the wastage of resources due to anti-metallurgical processes and the reduction in the lifespan of manufactured goods [6]. Subsequently, in the late seventies, a significant and all-encompassing study regarding the economic impacts of corrosion was revealed in the USA [7]. The study's findings revealed that in 1975, the collective financial impact of corrosion amounted to $70 billion, equivalent to around 5% of the Gross National Product (GNP) for that year. The study categorized corrosion costs into two groups: avoidable costs and unavoidable costs. The avoidable costs, which could have been minimized by employing existing corrosion control methods, were notably high at $10 billion, constituting approximately 15% of the overall corrosion expenses. Subsequently, in 2002, the U.S. Federal Highway Administration (FHWA) published a groundbreaking study

that calculated the direct expenses linked to metallic corrosion within the U.S. industrial sector. This study, initiated by NACE International and mandated by the U.S. Congress as part of the Transportation Equity Act for the 21st century (TEA-21), not only offered contemporary cost assessments but also outlined strategies on a national scale to mitigate the repercussions of corrosion [8]. The study published an annual direct corrosion cost of $276 billion, roughly 3.1% of the US GDP. This prompted other countries like the UK, Japan, Australia, Kuwait, Germany, Finland, Sweden, India, and China to study corrosion costs. They found that corrosion expenses range from about 1% to 5% of each nation's GNP. A recent publication by NACE International in 2016 estimated global corrosion-related economic losses at an astonishing $2.5 trillion [9]. While the precise numerical values might be subject to debate, the significance of corrosion-related challenges is undeniable in contemporary societies. In India, for instance, a direct corrosion cost assessment conducted for the year 1984-85 amounted to Rs. 4076 Crores, with Rs. 1804 Crores of this cost being deemed avoidable [10]. Another study focusing on India's corrosion expenses indicated yearly losses of Rs. 25,000 crores, equivalent to 4% of the Gross National Product (GNP) [11]. According to NACE International's recent global study, the corrosion-related impact on India's economy is currently estimated at 4.2% of the Gross Domestic Product (GDP).

The surface coatings are used to protect iron and steel and the main areas on behind this is its huge volume of production. Majority of the steel products are varnished with polymeric coatings. Polymer coating are basically filled polymer system which are based on three principal components. The basic components are as follows:-

1) Polymeric binder which monitors in the drying characteristics physical and chemical properties of the coatings.

2) Pigments are basically insoluble fillers mixed with binding media.
3) Solvents which provide the desirable properties for applying the coating on metal as well as control the viscosity.

Nowadays, nanoparticles play a significant role in polymeric systems as a promising filler. The reason is that nanoparticles can impart very low concentrations of physical, chemical, and biological properties. When polymers are modified with nano fillers it becomes polymer nanocomposites. The two most active areas of research in corrosion-resistant coating technology are as follows: (i) Conductive polymeric coatings (ii) Polymeric nanocomposite coatings. However, conductive polymeric coatings alone may not be an effective barrier due to their potentially brittle nature [12,13].

The surface modification of metallic substrates through the application of polymer nanocomposite coatings is a crucial method aimed at improving various surface properties, including wear resistance, oxidation resistance, and corrosion resistance. A range of traditional techniques are employed to deposit the desired materials onto the metallic substrate. These techniques are used to achieve surface modifications that provide enhanced protection for the substrate. Polymer nanocomposite coatings applied to metallic substrates serve as efficient barriers between the metal and oxidative environments. As a result, they effectively hinder the occurrence of corrosion. As a result, current research efforts have been directed towards the creation of innovative polymer nanocomposite materials that incorporate potent anticorrosive agents. This focus aims to address the need for effective corrosion protection.

Polymer nanocomposites offer a novel alternative to traditionally filled polymers. By integrating nanoparticles at the nanometer scale and ensuring proper filler

dispersion, polymer nanocomposites demonstrate significantly enhanced properties compared to pure polymers or conventional composites.

Although these protection systems are effective and in current use, a significant challenge is their susceptibility to being compromised due to easy application. If the protective shield becomes dislodged or the coating gets damaged, the underlying substrate becomes vulnerable to harm. Thus, integrating a protective coating into the polymer nanocomposite could present a more advantageous approach.

# CHAPTER-2

# Literature Survey

# &

# Scope of the Investigation

## 2.1. Literature Survey

Corrosion and physico-mechanical properties of mild steel protection by organic coating has been widely studied. The corrosion inhibition efficiency of organic compounds is related to their extender properties of coating. Studies reported that the organic coating mainly depends on some physicochemical properties of the molecule such as functional groups of main extender that is filler. Show high surface area can absorb more resin, hydrophobic in nature, anti-settling agent, pigment stabilization, leading to the formation of a corrosion protecting film.

The effectiveness of nanocomposite coatings in protecting mild steel substrates was attributed to their superior barrier properties when compared to pure epoxy coatings. The key factor influencing these barrier properties and corrosion protection in nanocomposite coatings is the quality of graphene oxide (GO) dispersion within the polymer coating investigated by Pourhashem et al [1]. Frigione et all showed organic-inorganic hybrid nanostructured epoxies have been introduced, and their significant potential in various applications has been emphasized. [2]. A solvent-free method creates functionalized graphene platelets and epoxy nanocomposites without the requirement for graphene surface modification. This is achieved by transforming a graphene precursor into functionalized graphene platelets within the epoxy at around 200°C studied by Losic et al [3]. Zeng et al investigated that gelatin, an economical protein, serves as an effective and environmentally friendly bio-surfactant for functionalizing carbon nanomaterials. This enables the development of advanced multifunctional polymeric nanocomposites [4]. The composite coatings exhibited exceptional barrier properties against water molecules when compared to the pure epoxy coating. By corrosion studies confirmed that the corrosion rate in the composite coatings containing 0.5 wt% graphene was significantly lower, by an order of

magnitude, than that observed in the pure epoxy coating studied by Shaun et al [5]. Xiong et al studied The corrosion resistance of the epoxy (EP) coating can be greatly enhanced by incorporating a novel inorganic nanofiller called OMSEP. The EP coating exhibits the highest level of corrosion resistance when it contains 3 wt% OMSEP [6]. Tomic et al studied at a volume fraction of 4.1%, the rheological properties exhibited a notable improvement of epoxy/clay nanocomposite. This enhancement was attributed to the formation of a continuous network comprising tactoids, each consisting of 45-layer-thick tactoids [7]. The enhanced abrasion-resistant coating, achieved by adding bentonite clay nanoparticles, is versatile and can be used to protect various surfaces such as floors, pipes, automotive components and more investigated by Madhup et al [8]. Milena et al studied the release of DOC from the TNTs is sensitive to both time and pH conditions. Furthermore, the nanocomposite coatings exhibited better anticorrosion properties at pH 2 compared to pH 5 [9]. The mechanical properties of the composite are significantly affected by the particular interface conditions between silica nanoparticles and polyimide, especially when dealing with nanoparticle radii less than 1,000 Å reported by Odegard et al [10]. The incorporating of PANI/OMMT nanocomposite into epoxy paint leads to enhanced anticorrosion properties, surpassing those of PANI/MMT and pure PANI coatings demonstrated by Navarchian et al [11]. The inclusion of the PAni.DBSA/$SiO_2$ hybrid in the epoxy system especially when prepared with CTAB leads to a substantial one-order increase in coating resistance, validating its strong anticorrosion performance studied by Caldas et al [12]. Abd El-Fattah et al reported the DMA analysis in this study reveals that chitosan can enhance the viscoelastic properties of epoxy coatings. Additionally, both mechanical and chemical resistance are improved, and this improvement becomes more pronounced as the chitosan loading increases, up to and including 15% chitosan [13]. The coating's thermal and abrasion resistances

improved with increasing SNPs content. The coatings with 5% SNP content exhibited the highest mechanical, thermal, and abrasion properties studied by Alam et al [14]. Alam et al investigated the coatings displayed the highest corrosion resistance when they contained 5% $SiO_2$ nanoparticles, especially when the immersion time was extended to 30 days [15]. Ray et al investigated the preparation of nanocomposites using layered silicates has been extensively explored in various polymers, with a specific focus on biodegradable polymers. These resulting PLS nanocomposites offer several advantages [16]. Tsaneva et al investigated the nano-hybrid coatings exhibited strong mechanical properties and effective corrosion protection, both with and without the use of an industrial topcoat system [17]. Li et al investigated based on the analysis of non-volatile matter and the impact strength of the coating film, it was determined that 12% of 3601 serves as the most suitable amount of reactive diluents [18]. The 430SS coated with intermetallic compound coating exhibits superior corrosion resistance compared to that coated with base coat studied by Hong Bin et al [19]. Dhoke et al investigated at a lower concentration by 0.1% weight, the addition of nano-ZnO particles to the coatings improved corrosion resistance, UV resistance and mechanical properties without affecting the optical transparency of the coating. [20]. Shen et al studied nanosilica was effectively dispersed in both polyester and polyurethane materials at the nanoscale, resulting in enhanced hardness, abrasion resistance and tensile properties when a small amount of nanosilica was added to the polymer films [21]. The uniform dispersion of modified ZnO nanoparticles within the WPU coating prevents the movement of corrosive substances to the substrate, thus effectively averting corrosion reported by Christopher et al [22]. Tamboura et al suggested that silicone-PU based paint systems have low water absorption and the newly developed multilayer silicone-urethane-based paint systems are suitable as anticorrosion primers [23]. Immersion tests showed that the

fouling behavior of the PTU/t-ZnO composite with 1 wt% t-ZnO filler decreased compared to pure PTU. Moreover, the composite with 5 wt% t-ZnO filler exhibited nearly no biofouling studied by Holken et al [24]. Jia-Hu et al investigated the adhesive's performance reached its optimum when the concentration of nano-$SiO_2$ was within the range of 2.0% to 2.5%. [25]. Explored the properties of polyurethane/clay composites specifically focusing on strength, swelling behavior and morphology reported by Arifin et al [26]. Adapala et al investigated to polyurethane anti-graffiti coatings were created by adding different quantities of OH-functional Silicone modified polyacrylate [27]. Garcıa et al suggested that when applied to carbon steel, polyurethane coatings exhibit superior adhesion and improved anticorrosion protection compared to when applied to galvanized steel. [28]. Thomas et al reported the studies of the electrochemical performance of anti corrosion behaviors of polyaniline-polyurethane (PANi-PU) antifouling coating when exposed to a 3.5 wt% Nacl solution using electrochemical impedance spectroscopy (EIS). [29].

Valentini et al investigated the study assessed the effectiveness of epoxy coatings in protecting mild steel when exposed to a 3.5% Nacl solution. This evaluation was conducted using electrochemical noise analysis and EIS [30]. How erosion affects the corrosion behavior of coal tar epoxy coatings. It utilizes EIS measurements to evaluate this impact studied by Atapour et al [31]. Diogenes et al suggested using Kraft lignin, a bio-polyphenol that is both safe and sourced as waste from the pulp and paper industry, as an alternative to create an epoxy coating without coal tar [32]. To replace coal tar, various alternative approaches have been suggested, including bitumen (BIT), hydrocarbon resin (HR), flexibilizer (FL), and curing agents like polyamide (PAD) or polyamine (PAM). The study formulated four distinct coal tar-free coatings using these different approaches investigated by Jagtap et al [33]. Zhang et al reported the study analyzed and discussed the

electrochemical impedance spectra, breakpoint frequency (fb) and electrical resistance of the coating in relation to both titanium content and immersion time. This analysis also involved calculating the permittivity of the coating [34]. The study focused on developing a light-colored epoxy coating system that uses modified amine curing. This system provides excellent long-term protection without the use of coal tar making it a safer and more environmentally friendly option studied by Bum Sung et al [35]. Babic et al reported the steel panels coated with a coal tar epoxy composition. It examined their impedance spectroscopy characteristics both in a dry condition and while exposed to synthetic seawater and a 10% NaOH solution [36]. The enamel coating exhibited the lowest corrosion resistance because of its interconnected pore structure. Additionally prior damage significantly reduced the corrosion resistance of both pure and double enamel-coated rebar.studied by Tang et al [37]. Tang et al investigated that pure and double enamel coatings offer superior protection to steel rebar compared to mixed enamel coatings. This enhanced protection is attributed to their denser microstructures with isolated pores [38]. Chaudhary reported a diglycidyl aniline epoxy resin (DGA) was modified by treating it with crotonic acid to create a vinyl ester resin (VER) [39]. The study explored how nano $TiO_2$ and nano $SiO_2$ impact the bonding performance and structural characteristics of PVAc investigated by Bardak et al [40]. Ghadami et al evaluated the comparative study between the effect of micro and nano glass flake on anticorrosion performance of epoxy vinyl ester coatings [41]. Nanoscale analysis of vinyl ester anti-corrosion coatings containing glass flakes on mild steel studied by Barbhuiya et al [42]. Various concentrations of prepared nanocomposites were mixed with poly(vinyl acetate) as the primary matrix and then applied as a coating on carbon steel investigated by Khademian et al [43]. This study centered on the synthesis of vinyl ester resins by reacting epoxy resin, specifically 2,6-dimethylol-4-bromonaphthol with methyl

acrylate and ethyl acrylate in the presence of triethylamine and hydroquinone reported by Chaudhary et al [44]. Kang et al demonstrated how well polymer coatings dissolved or mixed with vinyl ester resin indicating that better solubility and miscibility resulted in a higher Interfacial Shear Strength (IFSS). [45]. This study presented both near-infrared (NIR) and rheological analyses of interpenetrating polymer networks composed of epoxy and vinyl ester.reported by Dean et al [46]. Epoxy resin of the diglycidyl ether of bisphenol-A type, when cured with diamino diphenyl sulfone was employed as a matrix in the production of fiber-reinforced composites to enhance their mechanical and thermal properties studied by Hameed et al [47]. Ray et al investigated in the composites, both flexural strength and breaking energy decreased compared to the unfilled resin. However, the flexural modulus value increased by 13%. [48]. The study systematically investigated how different isothermal temperatures affect the curing extent, gel time, dynamic rheological properties, and mechanical characteristics of vinyl ester resins (VERs)reported by Zhang et al [49].

## 2.2. Scope of the Investigation

Now a day, nanoparticle plays a very important role in polymeric systems as a promising filler. The reason behind it is they can provide very low concentration of physical, chemical and biological properties when polymers are modified with nano fillers then it becomes polymer nanocomposites. The two most active areas of rearch in corrosion resistant coating technology as follows

(a) Conductive polymeric coating

(b) Polymeric nano composite coating

But conductive polymeric coating alone is not an effective barrier due to perhaps brittle in nature. After investigation, of this study is to concentrate on the incorporation of nano filler into polymers to create nano filler based polymer nanocomposites. These enhance the corrosion resistance of the polymers and are regarded as one of the most effective materials for polymeric coatings. In many cases, the addition of pigments is unnecessary [50,51].

### 2.2.1. Chemistry of Corrosion and Its Mechanism

Generally shaped metals possessed from their ores which are naturally occurring compounds by the consumption of large amounts of energy. Hence, these structural metals can considered as being in a metastable from. And it will attend to loss their energy by regress to compounds more or less similar to their initial state. Whereas most of the metallic compounds particularly corrosion product have low wear as well as mechanical strength and severely corroded portion of metal substrate is entirely useless for its actual purpose.

Actually, all type of corrosion reactions are consider electrochemical in nature. In anodic reaction on the surface of iron undertake in solution formed as ferrous ions at anodic site. By oxidation iron atoms under go to ions releases electrons and metal build up charged negatively quickly and get into prevention of further anodic reaction or “corrosion”.

Involvements of dissolution of iron as corresponding iron ions with the salvation of free electrons and the cathodic reaction eat up these electrons with either progression of hydrogen and absorbed oxygen, it also depend upon essence of corrosive environment of electrolyte. According to Fraday’s Law, the rates of anodic and cathodic reaction must be equivalent resolved by the total flow of electrons from anode to cathode which is named by “corrosion current” ($I_{corr}$). By

ionic conduction the corrosion current pass through the electrolyte and its conductivity affected by course of action in which corrosion cell operate. The corroding iron piece is expressed as a “mixed electrode” hence anodic and cathodic reactions are proceeding on metal surface. Simultaneously mixed electrode system goes a complete electrochemical cell reaction on one surface of metal.

At anodic reaction (Corrosion)

$$Fe \rightarrow Fe^{2+} + 2e^{-} \qquad \text{(i)}$$

At cathodic reaction (Simplified)

$$2H^{+} + 2e^{-} \rightarrow H_2 \qquad \text{(ii)}$$

$$H_2O + ½\ O_2 + 2e^{-} \rightarrow 2OH^{-} \qquad \text{(iii)}$$

Reaction of (ii) is generally in acidic the range of PH is (6.5 to 8.5) and reaction (iii) represents oxygen reduction. Commonly corrosion is associated by the composition of solid corrosion scrap from the between anodic and cathodic reaction products.

$$Fe^{2+} + 2OH^{-} \rightarrow Fe(OH)_2, \text{ Iron (II) hydroxide} \qquad \text{(iv)}$$

Pure iron (II) hydroxide shows white but the material initially formed by corrosion is generally in air partial oxidation greenish colour formed.

$$2Fe(OH)_2 + H_2O + ½\ O_2 \rightarrow 2Fe(OH)_3, \text{ Iron (III) hydroxide} \qquad \text{(v)}$$

Moreover by hydration and oxidation reactions take place and the redish rust forms lastly which is mixture of complex formation will depend on other trace elements which are existent. As a result of secondary reaction the rust is precipitated and attends to act as a sort of harmful layer which promotes further corrosion. At first, during anodic oxidation solid corrosion product is formed which is act as a highly

protective film and retards further corrosion, then the surface of metal said to be "passive".

$$2Fe + 3H_2O \rightarrow Fe_2O_3 + 6H^+ + 6e^-$$

At elevated temperature and oxidizing conditions, the production of an oxide film formed on iron in water.

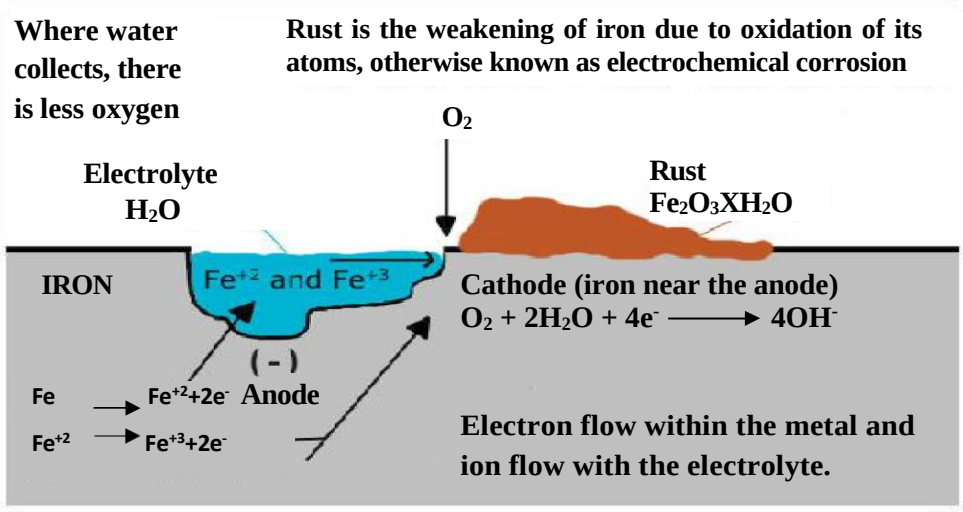


**Fig.2.1:** Rust formation

**Fig.2.2:** Water pipeline Corrosion


**Fig.2.3:** (A) Gas pipeline corrosion (B) Inner view of corroded pipeline (C) Microbial corrosion in pipeline (D) Corrosion in boilers

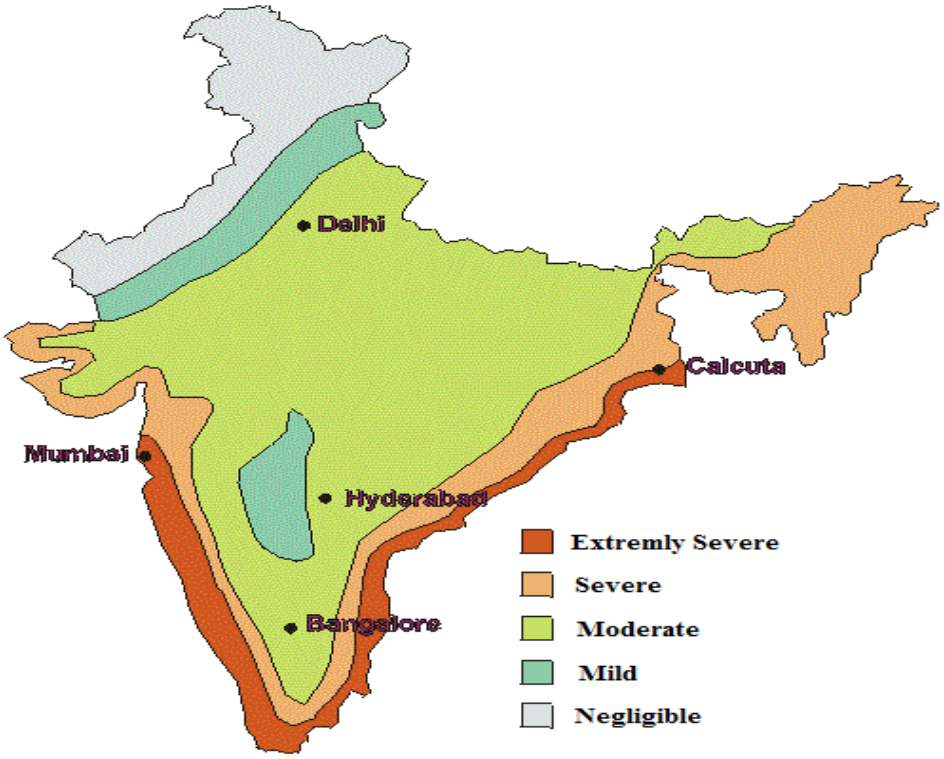


**Fig.2.4**: Map describing corrosion patterns in India

## 2.2.2. Consequences of Corrosion

The consequences of corrosion are diverse and wide-ranging, and their impact on the secure, dependable, and effective functioning of equipment or structures is frequently more significant than mere metal loss. Different types of failures and the requirement for costly substitutions can arise, even when the quantity of corroded metal is relatively minor. A few of the key adverse consequences of corrosion can be succinctly stated as follows:

- Decreased metal thickness can result in the deterioration of mechanical strength, leading to structural failure or breakdown. When metal loss occurs in specific localized regions, creating a structure resembling cracks, even a small amount of metal erosion can cause substantial weakening.
- Dangers or physical harm to individuals resulting from structural failures or collapses, for instance in cases involving bridges, automobiles, and aircraft.
- Downtime due to the unavailability of industrial equipment used for profile manufacturing.
- Diminished value of products resulting from the deterioration of their appearance.
- Contamination of fluids within containers and pipelines (for example, beer becoming cloudy due to the release of small amounts of heavy metals caused by corrosion).
- Penetration of vessels and pipes leading to the leakage of their contents and potential harm to the environment. For instance, a leaking household radiator can result in costly damage to carpets and decorations, and corrosive seawater might enter power station boilers if the condenser tubes become perforated.

- Depletion of crucial surface characteristics of a metal component. These attributes might encompass properties like friction and bearing capabilities, the smoothness of fluid flow across pipe surfaces, electrical conductivity in contacts, surface reflectivity, or the ability to conduct heat across a surface.
- Mechanical damage to valves, pumps, and similar equipment, or the obstruction of pipelines due to the presence of solid corrosion byproducts.
- Increased intricacy and costs associated with designing equipment that must withstand a certain level of corrosion and facilitate the convenient replacement of corroded components.

### 2.2.3. Corrosion and its Control

The control of corrosion can be dependent on economics, well being assertion and a number of technical remuneration. The experimental methods available for the conservation of metal against corrosion are assorted. These are commonly based on

- Protective/ Organic/ Polymeric coating
- Metallic coating
- Electrochemical Control
    - Cathodic protection
    - Anodic protection
- Use of inhibitors

These are procedures can be used discretely or in meld to control the corrosion. Among the various techniques available for controlling corrosion, protective coatings are considered the optimal choice in terms of both efficiency and cost-effectiveness in the industrial scale.

## 2.2.4. Corrosion Monitoring Technique

The area of corrosion measurement, control, and prevention encompasses a wide range of technical tasks. In the domain of preventing and controlling corrosion, there exist technical choices like cathodic and anodic protection, selecting materials, using chemicals, and applying coatings. Corrosion measurement employs diverse methods to gauge environmental corrosiveness and the speed of metal loss. It's the quantitative way to assess the efficiency of corrosion control and prevention techniques, offering feedback to optimize these methods.

- **Physico-Chemical method**
  - Weight loss method
  - Gasometric method
- **Electrochemical method**
- **AC Method:**
  - Tafel extrapolation method
  - Linear polarization method
- **DC Method:**
  - EIS (Electro Impedance Spectroscopy)
  - Faradic Rectification method

## 2.2.5. Mild Steel/Carbon Steel

Carbon steel stands out as the most extensively utilized form of steel. Its attributes are chiefly influenced by the quantity of carbon it holds. Generally, carbon steel contains less than 1% carbon. This type of steel finds application across a diverse array of products, spanning from structural beams and car bodies to kitchen appliances and containers. Essentially, three categories of plain carbon steel exist: low carbon steel, medium carbon steel, and high carbon steel. As implied by their

names, these variants differ in their carbon content. To be precise, high plain carbon steel contains a maximum carbon content of 1.5%, in addition to minor proportions of silica, sulphur, phosphorus, and manganese.

## 2.2.6. Chemistry of Organic Coating

Polymeric coatings play a vital role in corrosion prevention by using pigmented solutions bound by polymers. The coating's physical and chemical traits are determined by the polymer, which is influenced by pigment type and proportion. The volatile component regulates paint viscosity for manufacturing and application. Formulating coatings for specific purposes remains a technological art, as predicting their combined properties is challenging. Common polymers like alkyds, epoxies, and polyurethanes are favored for their corrosion resistance, adhesion, and low shrinkage, making them prominent in coating applications.

### ❖ Constitution of paint

Paint is a liquid substance that, when applied thinly onto a surface, transforms into a strong, clinging, and unified layer. This fluid paint consists of three key elements: a binder or film-forming agent, pigment, and solvent. The ratios of these components can be adjusted to create films with specific physical and application properties according to need.

### ➢ Binders

The binder needs to transform into a compact, solid film that adheres well to all surfaces. It imparts consistency and unity to any coating structure. The capacity of the binder to create a dense, closely packed film is directly linked to its molecular dimensions and intricacy [52].

## ❖ Epoxy resin

Epoxy resin falls within the category of thermosetting polymers and is distinguished by several exceptional attributes. These encompass impressive mechanical robustness and rigidity, resistance to chemicals and corrosion, long-lasting nature, resilience when facing diverse environmental situations, minimal contraction upon solidification, and superb bonding to various substances [53]. Glycidyl ether epoxy resin is the most commonly employed variant, produced through the condensation reaction involving two molecules of epichlorohydrin and one molecule of either bisphenol-A or diglycidyl ether of bisphenol-A (DGEBA). These resins are transparent and devoid of color, and easily common in various grades with varying viscosities. The properties of the resin are contingent on the degree of the reaction. Typically, these resins are employed in solution format for coating purposes. The epoxy functionality increases the cross-linking density also increases, resulting in the creation of a more rigid polymer [54].

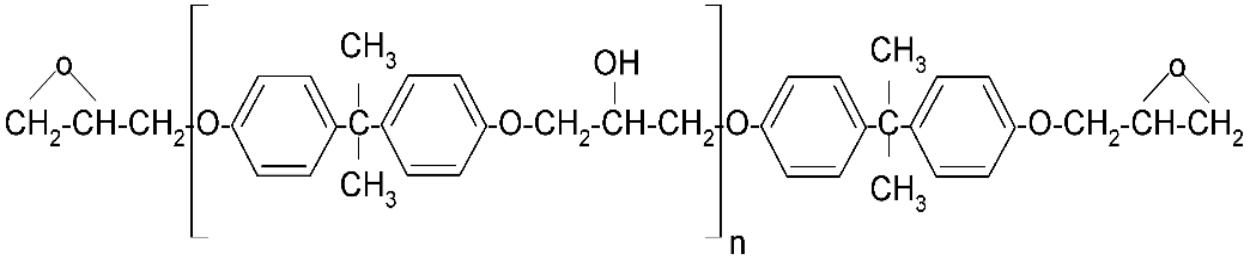

**Fig.2.5:** Structures of DGEBA (YD128)

## ▪ Curing agents/crosslinkers for epoxy resin

Aliphatic amines act as curing agents that can solidify epoxy resin at room temperature. The active hydrogen within primary amines reacts with an epoxy group to produce a secondary amine. This secondary amine then engages with another epoxy group, resulting in a tertiary amine. This tertiary amine is effective in initiating the polymerization of epoxy groups. The nature of the amine cured

epoxy be based on the curing speed, amount of hardener added and the grade of epoxy resin Aromatic amines, owing to the hinderance posed by their aromatic rings, cure slowly at room temperature. Epoxy cured with aliphatic amines exhibits strong adhesive characteristics and exceptional resilience against water and solvents. Anhydrides, known for their extended pot life, are commonly used as curing agents.

Phenalkamine is derived from the reaction of cardanol with formaldehyde and alkylamines through the Mannich reaction. The aromatic structure of phenalkamine imparts stiffness to the epoxy resin network, while the aliphatic side chain provides flexibility when employed as a curing agent for epoxy resin. The phenolic hydroxyl group renders it highly reactive even at low temperatures, while the alkylamine side chain contributes to the high up cross-linked density [56].

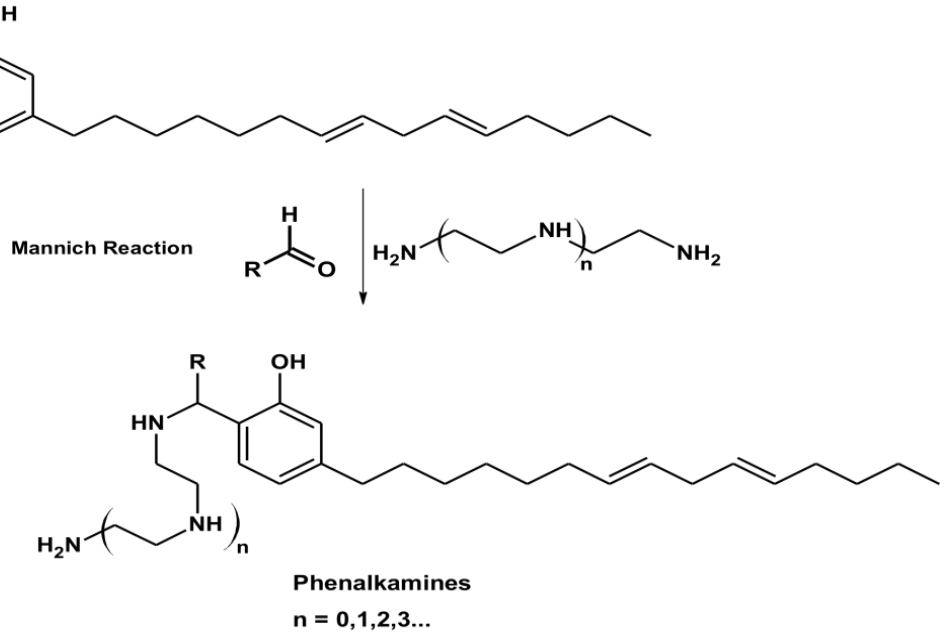


**Fig.2.6:** Structures of phenalkamine

## ❖ Polyol Resin (Polyurethane)

Polyurethanes (PUs) are polymers with a urethane linkage [NH–C(O)–O], formed by reacting components with hydroxyl (–OH) groups, like polyols and isocyanates (–N=C=O). For the PU polymerization process, the isocyanate component must possess a minimum of two isocyanate groups [57]. The typical representation of castor oil's structure is triricinolein shown in Fig.7. However, it primarily consists of about 90% ricinoleic acid and the remaining portion comprises majorly oleic and linoleic acids. Ricinoleic acid has a hydroxyl group on the 12th carbon and a double bond between the 9th and 10th carbons. Castor oil is liquid at room temperature due to its double bonds, with a viscosity of approximately 700 mPa.s at 25°C and around 1000-1500 mPa.s at 20°C. Hydrogenated castor oil is solid and has a melting point of 86°C. Castor oil is a mixture of triols (approximately 70%), diols (around 21%), and monols (about 7%). When castor oil polyol crosslinked with methylene diphenyl diisocyanate (MDI), it forms a hard elastomeric polymer [58-60].

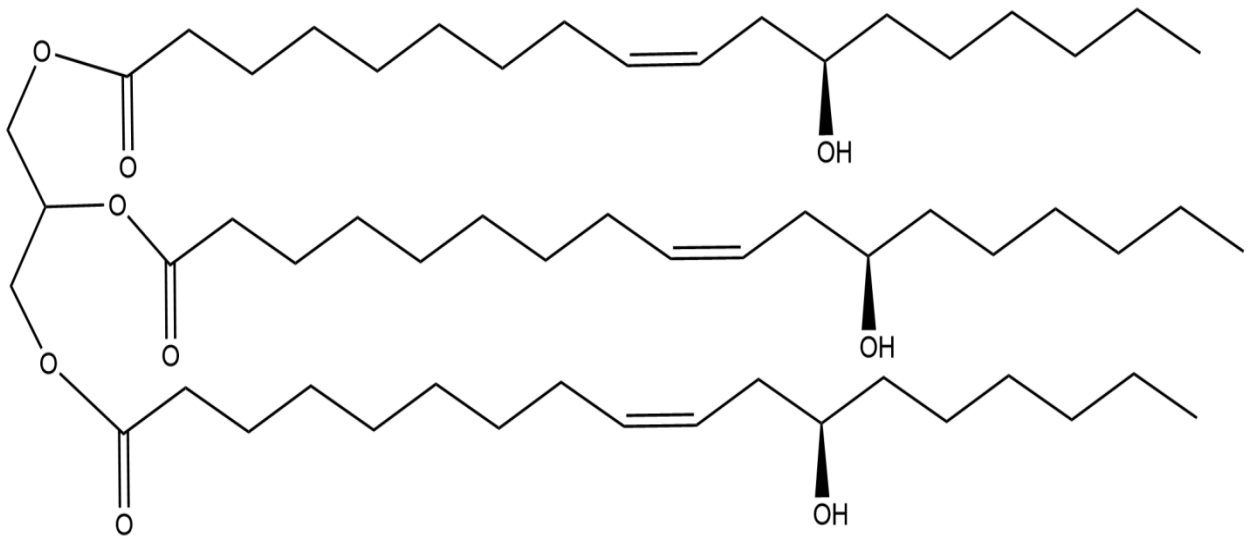


**Fig.2.7:** Structures of castor oil ricinoleic based polyol

- **Curing agents/crosslinkers for polyol resin**

Isocyanates play a crucial role in producing polyurethane (PU). They consist of the chemical group R–N=C=O. The positions of the isocyanate groups determine their reactivity. In 4,4'-MDI, the two isocyanate groups are equivalent. However, in 2,4'-MDI, the two groups exhibit significantly different reactivities. The isocyanate group at the 4-position is approximately four times more reactive than the one at the 2-position due to steric hindrance [61].

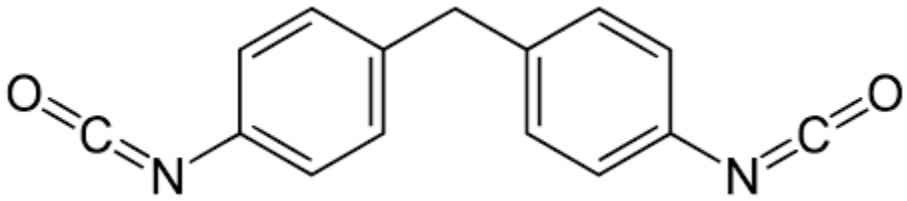


**Fig.2.8:** Structures of 4,4´- Methyl Diphenyl Diisocyanate (MDI)

- **Coal Tar Epoxy Resin**

Coal tar-based coatings have been widely employed for over a century to safeguard steel structures and underground pipes. Coal tar has been utilized to enhance the anticorrosive properties of various polymeric resin binders, including epoxy, chlorinated rubber, vinyl, and polyurethane. Coaltar epoxy paint coating has found extensive application in marine environments, particularly in underwater areas, due to its exceptional qualities such as extremely low permeability, high electrolytic resistance, and strong adhesion even on surfaces with limited preparation [62]. Fractional distillation is used for the distillation of coal tar. It involves separating components in a chemical mixture based on their differing boiling points. In the context of tar, fractional distillation is used to separate its components by utilizing their varying boiling points. The residual substance after distillation is known as coal tar pitch. This material undergoes additional processing to achieve the desired

chemical and physical characteristics of coal tar pitch. The primary goal of the coal tar distillation process is to generate various tar acid products from the crude tar. Coal tar epoxy coatings play a crucial role in providing effective protection for steel structures, even when exposed to challenging atmospheric conditions and submerged environments. Our research involved developing a light-colored epoxy coating system cured with revised amines. This system demonstrates excellent protective performance over an extended service period, without the need for tar [63].

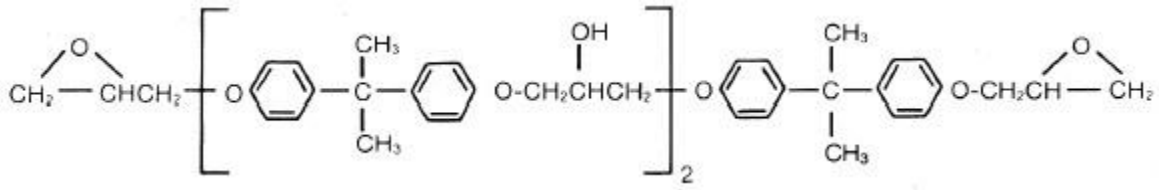

**Fig.2.9:** Structures of high build epoxy of DGEBA (Epotech, 1000F)

- **Curing agents/crosslinkers for coal tar epoxy resin**

Diethylene Triamine (DETA) is a linear ethylene amine compound that contains two primary and one secondary nitrogen atom. It is clear and colorless appearance, along with an odor reminiscent of ammonia. DETA exhibits high solubility in both water and organic solvents. Its aqueous solution possesses alkaline properties due to its nature as a weak base. Notably, DETA is produced as a byproduct during the manufacturing process of ethylene diamine from ethylene dichloride. Diethylene triamine used curing agent in epoxy resins for applications such as epoxy adhesives and other thermosets. When it reacts with epoxide groups, it undergoes N-alkylation, resulting in the formation of crosslinks within the material [64,65].

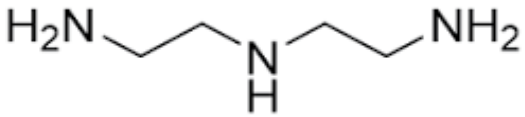


**Fig.2.10:** Structures of Diethylene Triamine (DETA)

## ❖ Vinyl Ester Resin

Vinyl Ester (VE) matrix systems are quite similar to conventional unsaturated polyester (UP) systems. They both use a base oligomer and reactive monomer that undergo a free-radical cross-linking cure mechanism to produce the final thermoset polymer network. Similar to UP systems, both vinyl ester (VE) oligomers and reactive monomers possess unsaturation sites that facilitate the formation of covalent bonds. Vinyl ester oligomers are created by reacting an unsaturated carboxylic acid (such as methacrylic or acrylic acid) with a foundational epoxide compound. The commonly employed epoxide in commercial vinyl ester (VE) systems is the diglycidyl ether of bisphenol A (DGEBA) epoxy. Nevertheless, alternative epoxy chemistries like novolacs are utilized for specialized VE formulations. DGEBA epoxy contains only terminal epoxy functional groups, which undergo a reaction with the carboxylic acid, resulting in a molecule featuring terminal unsaturation, as depicted in Figure 11. This differs significantly from typical unsaturated polyester (UP) oligomers, where unsaturation is present at multiple locations within the molecule. The lower ester content and reduced unsaturation in vinyl ester (VE) oligomers contribute to enhanced chemical and hydrolysis resistance, distinguishing them from UP systems [66].

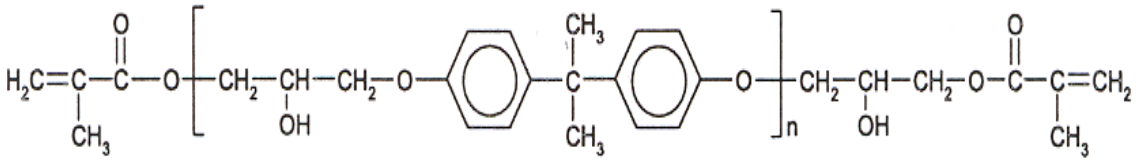

**Fig.2.11:** Structures of vinyl ester resin

- **Curing agents/crosslinkers for vinyl sster resin**

Vinyl ester resins undergo a curing process through a copolymerization reaction initiated by free radicals. The curing procedure begins with the introduction of a chemical initiator into the resin solution. This initiator decomposes under heat or radiation, generating the necessary free radicals for the curing process. The free radicals initiate the polymerization reaction by breaking the unsaturation (double carbon) bonds found in the end groups of the oligomer and the reactive monomer. Subsequently, these sites connect and form a three-dimensional crosslinked thermoset network. Because of their inherent instability, the organic peroxides utilized in curing vinyl ester (VE) resins are combined products that include a portion of the particular peroxide within a carrier medium. At room temperature, the decomposition rate of most peroxide initiators is insufficient for practical composite production. Therefore, an accelerator is employed to enhance the decomposition rate. The accelerator is introduced into the resin solution at relatively low concentrations (usually between 0.1 to 0.8%) before the peroxide initiator is added. Upon the addition of the initiator to the resin, the accelerator prompts the peroxide to decompose significantly faster. It's important to note that accelerators must never be directly mixed with peroxide initiators, as this could lead to a hazardous and explosive decomposition reaction. However, when combined correctly, accelerators can be employed to enhance the decomposition of peroxide to a suitable rate for fabricating materials at room temperature. Methyl

Ethyl Ketone Peroxides (MEKP) are likely the most extensively employed organic peroxide initiators for curing at room temperature. MEKP solutions manifest as transparent, colorless liquids and are typically utilized alongside metal salt cobalt octoate as accelerators [67].

## ➢ Pigments

Pigments can be described as solid particles that are mostly insoluble in the paint binder and solvents, capable of being dispersed within paint components to achieve desired paint properties. Within this broad pigment definition, two categories exist: true pigments and extender pigments. True pigments are utilized for color and opacity, while extenders are added to modify gloss and enhance economic aspects of paints. Pigments are further classified as inorganic and organic. Inorganic pigments encompass whites, extenders, and a variety of colors, both naturally occurring and synthetic. On the other hand, organic pigments are primarily synthetic in nature [68].

## • Rutile $TiO_2$ powder

Titanium dioxide stands out as the most commonly used white pigment due to its exceptional brightness and remarkably high refractive index, surpassed by only a few other substances. Ideally, the crystal size of titanium dioxide should be around 220 nm (measured using an electron microscope) to achieve optimal reflection of visible light. However, abnormal grain growth often occurs in titanium dioxide, particularly in its rutile phase. This abnormal grain growth results in a few crystallites deviating from the average crystal size and altering the physical properties of $TiO_2$. The purity of the pigment greatly influences its optical properties in the final product [69].

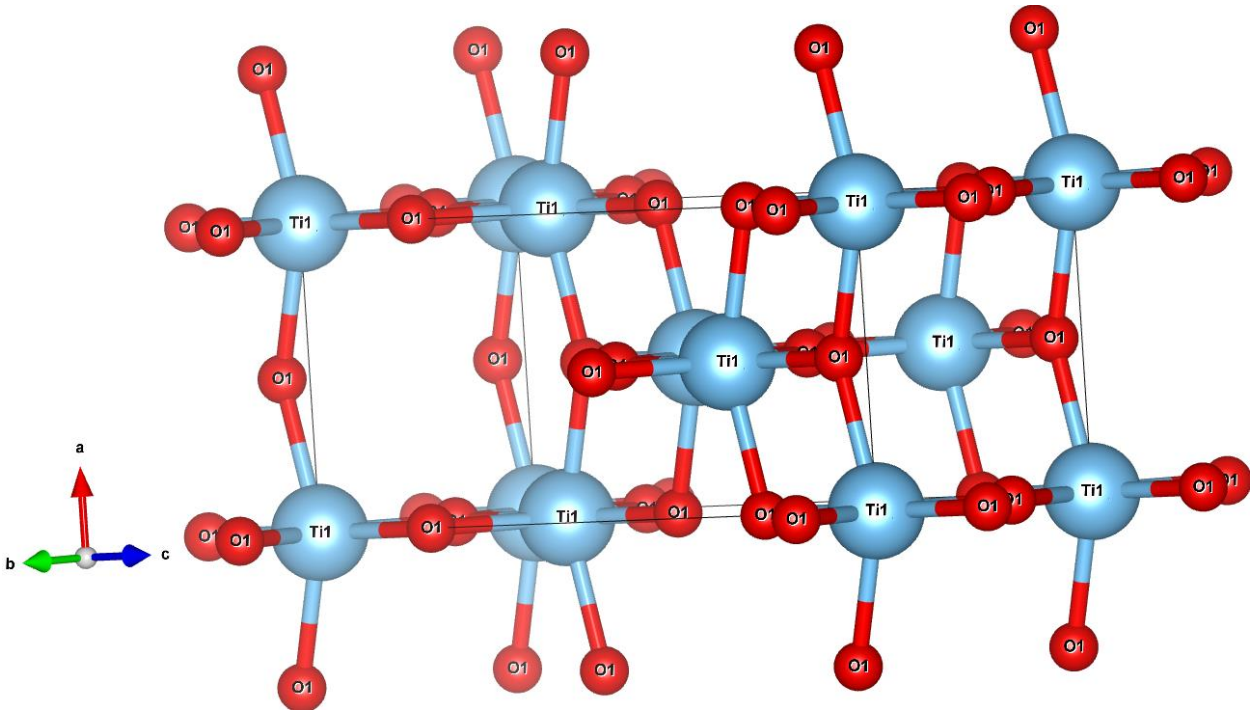


**Fig.2.12:** Structures of rutile $TiO_2$

## ➢ Additives

Aside from the major components, paint can include small amounts of various additives such as driers, plasticizers, flexibilizers, anti-skinning agents, wetting agents (e.g., BYK-204), air-releasing agents (e.g., BYK-530), slip agents (e.g., BYK-333), anti-settling agents, anti-fouling agents, and fungicides. These additives serve vital roles in paint formulations, each added for specific purposes. Typically, they are present in low concentrations, around 1-2% of the entire formulation. These additives contribute to package stability, ease of application, appearance, and corrosion resistance in the final coating [70].

## ➢ Extenders

$H_2Mg_3O_{12}Si_4$, commonly known as talc or soapstone, is an odorless mineral composed of a mixture of clay minerals and hydrated magnesium silicate. It stands out as an ordinary silicate mineral due to its exceptional softness, setting it apart

from nearly all other minerals. Talc is a natural mineral that forms soft sheets comprised of a layer of hydroxyl octahedral/magnesium-oxygen wedged between two layers of tetrahedral silica. The top surface of this sheet is referred to as the basal plane. Talc mineral lacks active ions and hydroxyl groups, rendering it inert and hydrophobic. It remains insoluble in weak acids, alkalis, and water. Possessing minimal chemical reactivity, it is non-flammable and displays amorphous properties along with bulk density. Upon reaching 900°C, talc loses its hydroxyl groups significantly, and at temperatures exceeding 1050°C, it undergoes re-crystallization into various forms. In the paint industry, talc is employed as a polishing and slipping agent [71].

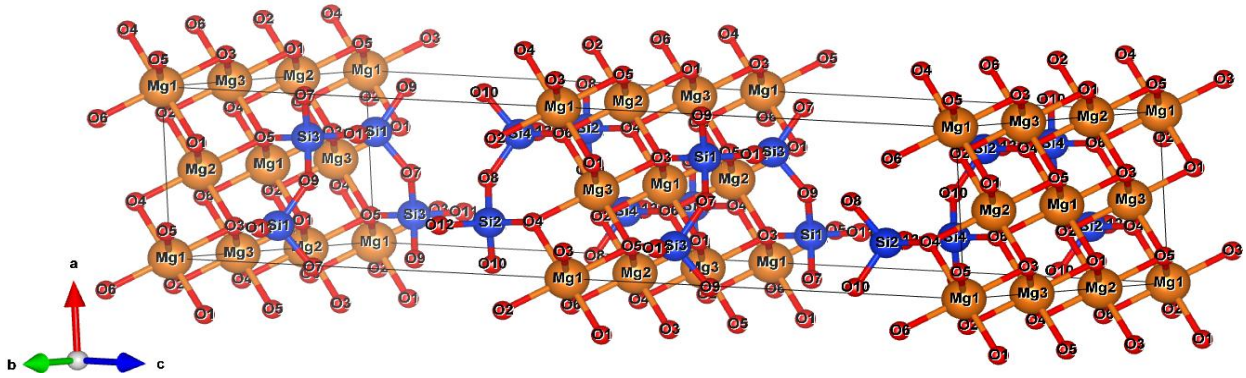


**Fig.2.13:** Structure of talc/soapstone

- **Quartz Silica**

Quartz is chemically composed of silicon dioxide ($SiO_2$), comprising 46.74% silicon and 53.26% oxygen by weight. It holds the distinction of being the most abundant mineral on Earth. Quartz adopts a three-dimensional structure consisting of silica tetrahedra. While predominantly crystalline in its arrangement, the degree of crystallization may vary. The macro-crystalline type is characterized by individual crystals visible to the naked eye. In contrast, the micro-crystalline or cryptocrystalline variety displays aggregates of crystals that are only observable

under high magnification. Transparent quartz tends to be macro-crystalline, while the cryptocrystalline variations appear translucent or mostly opaque [72].

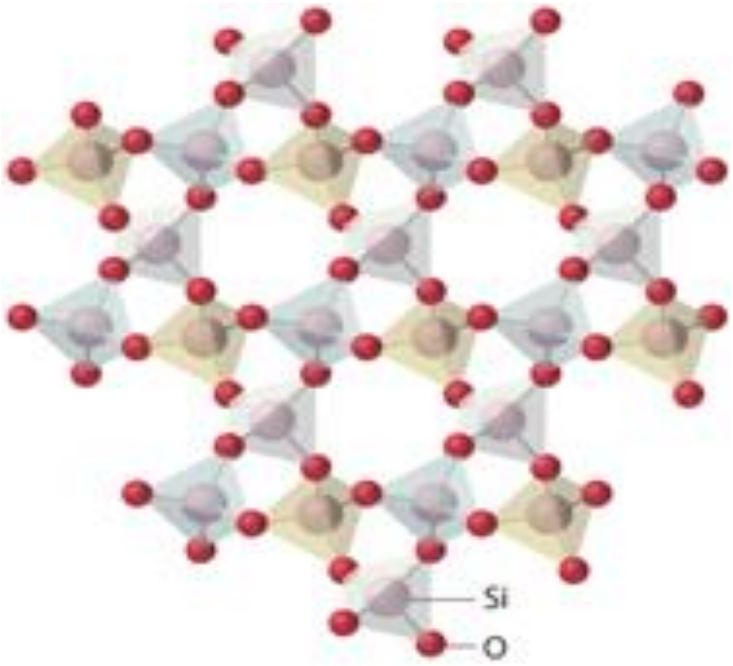


**Fig.2.14:** Structure of qurtz silica

- **Glass Flake**

An effective technique to enhance the performance of organic coatings in harsh environments involves reinforcing the polymer matrix with fillers. This reinforcement can yield improved corrosion protection through mechanisms like mechanical barrier formation due to inert salt precipitation or electrochemical protection through galvanic or passivation processes. Glass flake is a specific type of filler that has been employed in the coating industry for years to enhance the performance of epoxy coatings in highly corrosive settings. Previous researches have demonstrated that the incorporation of glass flakes into organic coatings enhances resistance against chemical ions, moisture, and gas diffusion. Glass flake particles with a high aspect ratio, signifying a large surface area and low thickness,

can align themselves within the polymer matrix parallel to the substrate. This arrangement creates a convoluted pathway for aggressive substances attempting to permeate the coatings, thereby extending the coating's lifespan.Apart from reducing coating permeability, glass flakes offer additional benefits compared to other fillers. These benefits encompass abrasion resistance, mechanical hardness, chemical inertness, and the absence of color transfer to the coating. These attributes often make glass flake a favored filler choice for developing coatings intended for extreme environments [73].

- **Solvent/Thinner**

The significance of the volatile component in a coating has often been overlooked, but it certainly has an influential role. This component actively dissolves the resin, decreasing the viscosity of the polymer to an appropriate consistency for application. It aids in effectively wetting the substrate and regulates the drying or setting rate of the coating film after application. Consequently, it profoundly impacts the durability of the coating. It's rare to employ a solitary solvent for a resin system. Typically, a combination of solvents, known as a solvent blend, is utilized [74].

## 2.2.7. Fillers (modifiers) for Improving the Corrosion Resistance of Polymeric Coatings

Solid particles, known as fillers, are incorporated into polymeric coatings to enhance properties and potentially reduce expenses. When choosing fillers for coatings, several factors need consideration, such as:

1. Purpose: Determine the intended function of the filler, whether it's for improved properties or cost reduction.
2. Compatibility: Ensure the chosen filler can blend well with the polymer matrix.

3. Particle Size and Distribution: Evaluate the size and uniformity of filler particles.
4. Aspect Ratio: Consider the length-to-width ratio for fillers like fibers or platelets.
5. Chemical Compatibility: Check for potential reactions between the filler and other components.
6. Surface Treatment: Assess if surface modifications are beneficial.
7. Reactivity: Evaluate potential interactions with other additives.
8. Thermal Stability: Consider the filler's resistance to high temperatures.
9. Characteristics of the coating
10. Easement of production and application of the coating to the substrate

## 2.2.8. Fillers (modifiers) which Influence Barrier Properties

Permeability of a coating refers to the ability of small molecules to diffuse through the coating. In coatings used to enhance corrosion resistance, it's essential that they restrict the passage of liquid or gaseous molecules. As most filler particles are solid and non-porous, small molecules are hindered from passing through and are compelled to take alternate paths around these particles. A coating with low permeability for small molecules tends to exhibit robust barrier properties. The shape of filler particles also plays a significant role in regulating permeability, as particle shape influences their alignment during film formation. For instance, platelet-shaped fillers like talc or mica tend to decrease permeability. Fillers capable of reducing permeability can enhance corrosion resistance by creating a barrier that impedes the diffusion of molecules responsible for corrosion, such as oxygen, water, salt, and acids. Furthermore, fillers with a high pH can also mitigate corrosion due to the accelerated corrosion rate in acidic environments.

## 2.2.9. Nanotechnology/Nanoparticle

Nanotechnology has become a rapidly growing field in the present era. In the global market, nanoparticle-based coating/paints are being extensively utilized. The incorporation of nanoparticles brings about notable changes in the attributes of protective coatings. Nanoparticles exhibit distinct properties compared to the same materials at macroscopic scales. These enhanced characteristics are closely linked to various physical factors like size, distribution, morphology, phase, and more. These unique nanoparticle properties are primarily a result of confinement within quantized nano-aggregates, a high surface-to-volume ratio, and a significant abundance of surface-reactive atoms/molecules.

## 2.2.10. Functionalized Nanoparticle

Nanoparticles (NPs), sized between 1-100 nm, possess unique chemical and physical properties, making them versatile materials. Advances in NP synthesis have led to diverse applications in fields like nanomedicine, biomedical science, and marine engineering. Despite their benefits, NPs exhibit drawbacks such as surface property limitations and interactions with host media and other species. Functionalization, achieved by adding specific chemical groups, can address these issues. This process enhances NPs properties and compatibility, preventing agglomeration and improving physical, chemical, and mechanical attributes. This functionalization expands possibilities for developing multifunctional tools in areas like anticorrosion and nanotechnology applications.

- **Application of Nanoparticles in Corrosion Mitigation**

  The improvement in the properties of the nanocomposites coatingsfor anticorrosion applications are described below:

- The inorganic constituents (nanoparticles) play a role in enhancing the scratch resistance and adhesion of metallic substrates.
- The organic component (nanoparticles) or active site enhances coating density and flexibility, while also promoting better compatibility with organic paint systems.
- To enhance UV-blocking capabilities and provide outstanding photo and thermal stability.
- To create coatings with anti-scratch and anti-abrasion properties.
- In a self-healing system, the coating's functionality is further restored by releasing self-healing agents after the initial repair, thereby forming a protective barrier coating within the defect.
- To create super-hydrophobic coatings.
- To formulate smart nanocapsules containing corrosion inhibitors for enhanced corrosion protection.

## 2.2.11. Nano Fillers

Incorporating a nano filler into an epoxy coating can prove advantageous for enhancing the coating's scratch resistance. This improvement leads to increased durability and overall performance of the coating. Nanofillers come in various types, including metals (such as gold, silver, platinum, zinc), semi-metals (like silica nanoparticles, layered silicates), and non-metals (organic) (including carbon nanotubes, nanofibers, and graphene). Fillers with at least one dimension equal to or smaller than 100 nm are categorized as nanoparticles. Nanofillers are commonly classified as: 0D nanoparticles: All dimensions are below 100 nm (e.g., spherical silica).1D nanoparticles: One dimension exceeds 100 nm while others remain below (e.g., Carbon nanotube, Halloysite nanotube). 2D nanoparticles: Two

dimensions exceed 100 nm, one remains below (e.g., graphene sheets). Nanomaterials represent a fascinating advancement in modern times. Among their key applications is the utilization of nanofillers to enhance polymer performance. Nanofillers can have a profound impact on the properties of incorporated polymers, including optical, electrical, mechanical, thermal, and fire retardant attributes, even when used in minimal quantities. The nanoparticles' minute size allows them to penetrate exceedingly small pores within the polymer matrix, ultimately bolstering the strength and longevity of coatings [75-78]. The incorporation of nanofillers into coatings remains a highly active and dynamic area of research. A diverse array of nanoparticles is utilized, including ZnO [79], $Ag_2O$ [80], $ZrO_2$ [81], clay [82], $SiO_2$ [83], $Fe_2O_3$ [84], $MoS_2$ [85], Zeolite [86], halloysite [87], CNT [88], and graphene [89,90]. A wide range of nanoparticles greatly enhances the barrier properties of coatings, effectively preventing the infiltration of corrosive agents such as water, oxygen, and chloride ions [91,92].

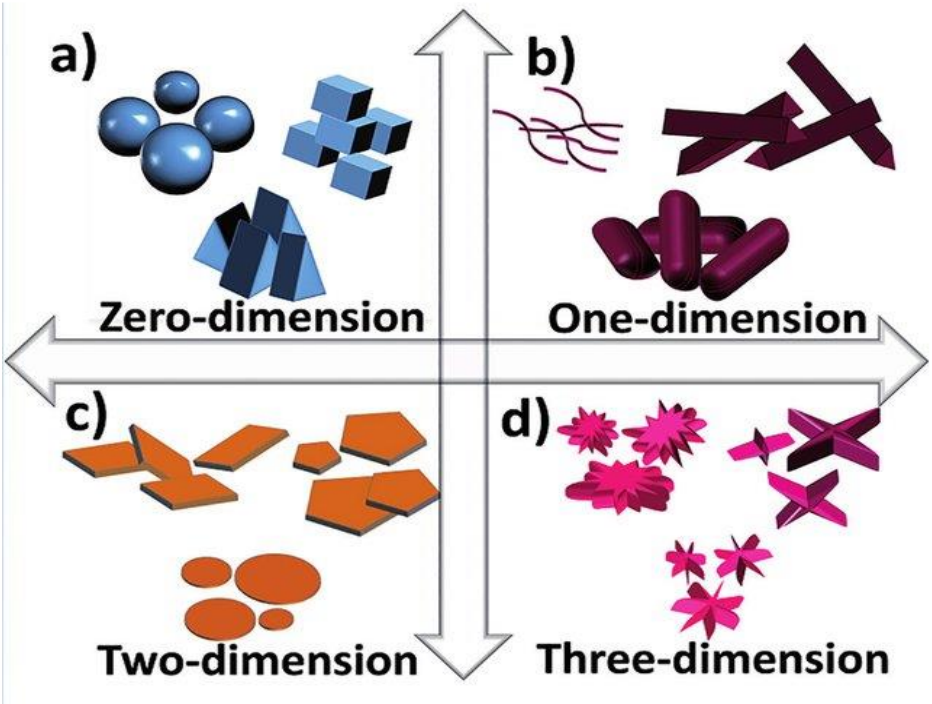


**Fig.2.15:** Different dimension of nano particles

## 2.2.12. Nano Organosilane Particles as Nano Ffiller (Selected Materials)

Fumed silica is a finely dispersed, amorphous form of silica. It is produced through high-temperature hydrolysis of silicon tetrachloride in an oxyhydrogen gas flame, give highly pure product. In the Aerosil (R972) manufacturing process, the primary particles that are created are nearly spherical and devoid of pores. This product exhibits a specific surface area (measured using the BET method) of 110 ± 20 $m^2g^{-1}$, with a primary particle size (PPS) of 12 nm and achieved by treating $SiO_2$ with dimethyl dichloro silane (DDS). Hydrophobic fumed silica is employed to enhance and sustain the flow characteristics of powders, thicken water-resistant systems, and develop anticorrosive coatings. The schematic chemical structures of these aforementioned organosilane-modified silica nanoparticles are depicted in Fig.2.16. It offers rheology control for intricate liquid systems and displays water resistance, facilitating hydrophobization of liquid systems. In coatings, it serves as an anti-settling agent, aids in pigment stabilization, and contributes to enhancing corrosion protection [93].

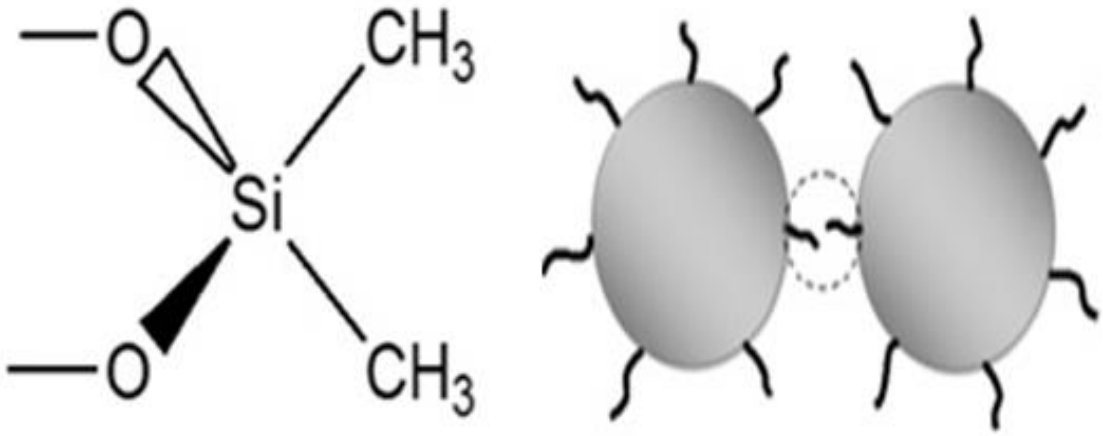


**Fig.2.16**: Schematic representation of organo silane-modified silica nanoparticles showing chemical structure and steric hindrance mechanism of R972

## 2.2.13. Polymer Nanocomposite Coatings

Composites are widely recognized materials in the field of engineering. There are untold natural (e.g., wood, bone) and commercial (e.g., concrete) composites. Polymer composites are crucial materials used in various applications. Conventional (micrometer scale) composites have inherent property limitations. Nanocomposites emerged in response to stringent requirements for modern advanced materials. Nanoscale fillers have significantly higher aspect ratios than micrometric fillers, resulting in much greater surface area-to-volume ratios in nanocomposite coatings compared to polymer microcomposites made from the same materials [94].

Nanocoatings typically contain at least one component in the nanoscale. Because of the extremely small particle sizes, they are highly effective at filling ultra-small spaces and preventing corrosive elements from diffusing into the substrate's surface. Furthermore, the high density of nanocoating grain boundaries improves adhesion properties, extending the coating's lifespan [95]. Nanocoatings also offer enhanced mechanical and electronic properties, making them stronger and harder [96]. Nanocoatings also exhibit self-healing properties [97], self-cleaning capabilities [98], and high scratch and wear resistance [99].

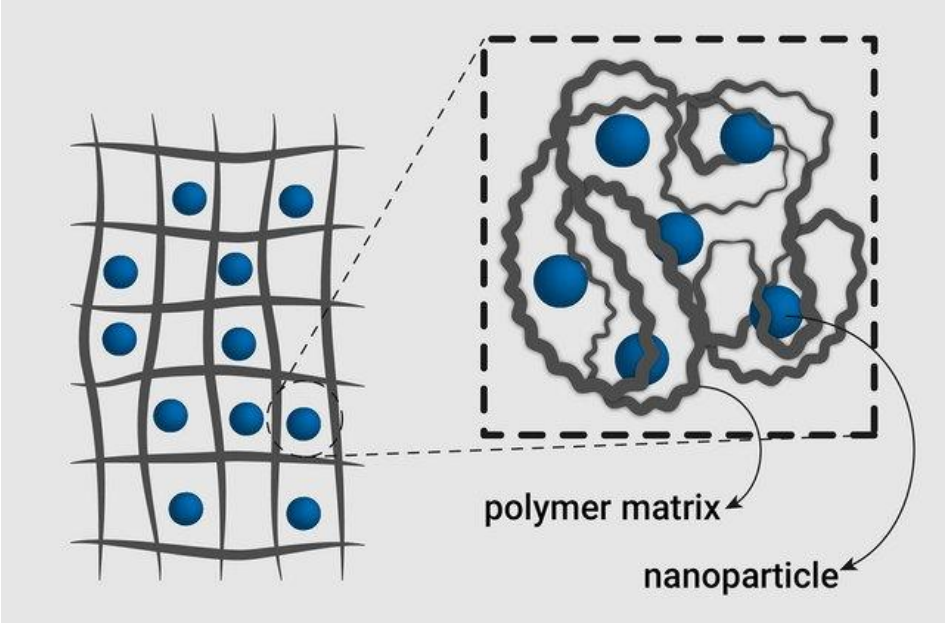


**Fig.2.17:** Distribution of nanoparticle in polymer matrix

A polymer nanocomposite is a solid material comprising at least two distinct phases. The primary or continuous phase is a polymer, while the secondary or dispersed phase is a nanofiller.

The morphology of the nanocomposite varies depending on the degree of interaction between the polymer and the nanofiller, and a well-exfoliated system yields the most favorable results, as shown in Fig.2.17.

Nanocomposites can be created through both complex and straightforward processes. Because nanocomposites consist of nanosized particles with substantial surface area, the interface between these particles plays a crucial role in determining the ultimate properties of the nanocomposites. Nanocomposites can be produced using processes similar to those employed for conventional polymer composites. The size, shape, and volume fraction of the nanoparticles are key factors that determine the properties of the nanocomposite.

Polymer nanocomposite coatings are created by adding nanoparticles to the polymer coating, leading to a substantial enhancement in the coating's mechanical properties [100,101]. Epoxy coatings modified with silicon dioxide nanoparticles exhibit notable improvements in impact strength, possibly attributed to two mechanisms.

i) The nanoparticles fill in pinholes and voids within the thin film coating, reinforcing the matrix by reducing the overall free volume and increasing crosslink density. Consequently, the cured nanocomposite coating exhibits reduced chain segmental motions and enhanced stiffness.

ii) Nanoparticles can help prevent the disaggregation of epoxy. In epoxy coating, the inclusion of nano $SiO_2$ increased Young's modulus by up to 20 times [102].

Incorporating nanofillers into polymer coatings can improve thermal stability by serving as excellent insulators and barriers to the mass transport of volatile products generated during decomposition [103]. The addition of nanofillers to the polymer coating alters its glass transition temperature ($T_g$), and in numerous instances, an increase in Tg has been documented [104-106].

In epoxy-based coatings, the incorporation of metal oxide nanoparticles significantly enhanced the corrosion resistance of coated steel [107].

Halloysite clay plays a significant role in this context. The addition of nanosilica into epoxy coatings reduced friction and wear at low concentrations. The dispersion of layered silicates as a reinforcing phase in polymer coatings is one of the most important types of nanocomposites [108-110].

### 2.2.13.1 Synthesis of Polymernanocomposite Coating

Developing successful polymer nanocomposite coatings presents two challenges.

a) The first challenge is ensuring chemical compatibility between the polymer matrix and the nanofiller at the nanoscale.

b) Uniform distribution of the nanofiller within the polymer matrix.

The quality of the polymer/nanofiller composite is significantly influenced by the interfacial interaction between the nanofiller and the polymer matrix, as well as the degree of nanofiller dispersion. These two critical features govern both the morphology of the polymer/nanofiller composite and its bulk properties, including strength, modulus, thermal stability, and more [111]. Enhancing the compatibility between the nanofiller and the polymer matrix can facilitate achieving a homogeneous dispersion of nanoparticles within the polymer matrix. In many cases, the van der Waals attraction between nanoparticles tends to promote the formation of clusters and agglomerates. Furthermore, when hydrophilic nanoparticles are combined with hydrophobic polymers, their lack of compatibility can lead to weak interfacial adhesion, ultimately resulting in inadequate dispersion and subpar material properties. To address these interfacial challenges, various synthesis methods have been developed to control the chemistry and morphology of polymer/nanofiller composites. There are three primary synthesis procedures for creating these composites: melt blending, solution blending, and in situ polymerization [112]. The solution blending technique typically results in superior dispersion of nanofillers within the polymer matrix when compared to melt blending, primarily because of its lower viscosity and intense agitation. However, it's worth noting that melt blending is a more cost-effective and environmentally friendly option, as mentioned in reference [113]. On the other hand, the in situ

polymerization method is highly versatile and is also likely to yield uniform dispersion, as suggested in reference [114].

**a) Solution blending**

Solution blending involves using a solvent to suspend the nanofiller, and in the case of layered nanofillers, this can lead to swelling of the layers, facilitating the exfoliation of the filler [115]. When this mixture is combined with the polymer, the polymer chains can intercalate and displace the solvent within the interlayers of the filler [116]. After the solvent is removed, typically by vaporization, the intercalated sheets reassemble to form a polymer/nanofiller composite. Achieving proper dispersion of the nanofiller usually requires strong agitation. In recent times, emulsifier stirring and ultrasonication are employed to enhance nanofiller dispersion. Despite the advantage of producing relatively uniform nanofiller dispersion, one drawback of the solution blending method is the use of large amounts of organic solvents. As a result, on an industrial scale, melt blending is often preferred for its economic and environmental advantages.

**b) Melt blending**

In the melt blending method, the desired quantity of nanofiller is combined with the polymer at a temperature above the polymer's softening point. One significant advantage of this approach is that it doesn't involve the use of solvents, making it a more cost-effective and environmentally friendly process. For thermoplastics, blending can be integrated into processing methods like extrusion and injection molding. Melt mixing can be executed as a batch process, for instance, in an internal mixer, or as a continuous process, such as in an extruder [117]. Key mixing parameters include residence time, shear, temperature, and pressure. While layered nanofillers can be effectively exfoliated and dispersed within the polymer

matrix using melt blending, it's worth noting that this method may sometimes lead to inadequate filler dispersion, particularly at high filler concentrations, resulting in aggregation [118]. As an alternative, in situ polymerization is often considered more effective in achieving uniform dispersion in such cases.

**c) In situ polymerization**

In situ polymerization can be done in different ways.

- ✓ In situ polymerization with nanoparticles or in situ nanoparticle synthesis with the polymer present.
- ✓ Nanoparticles and polymer are concurrently synthesized in situ.

The in situ polymerization technique is capable of producing intercalated and/or exfoliated structures, leading to enhanced thermal stability and mechanical properties, especially when using layered fillers, as noted in reference [119]. To further enhance the quality of the nanocomposite, ultrasonication can be employed in conjunction with in situ polymerization, as suggested in reference [120].

**d) Ultrasonication**

Ultrasonication is a commonly employed technique for achieving effective dispersion of nanofillers. It delivers a substantial amount of energy, disrupting both physical and chemical interactions. Consequently, ultrasonication finds widespread use in dispersing, emulsifying, crushing, and activating particles [121]. Moreover, ultrasound energy has the capability to break C─C bonds, resulting in the formation of radicals. These radicals can then bond to the surface of nanofillers in nanocomposite systems, thereby enhancing the interaction between the polymer and the filler [122]. Numerous studies have investigated the efficacy of ultrasonication in the preparation of nanocomposites [123-126] providing a body

of research in this area. In specific applications, high-power ultrasound has been successfully employed to disperse silica agglomerates in ethylene propylene diene monomer rubber (EPDM) [127].

### 2.2.14. Depositing Polymer Nanocomposite Coatings over Metal Substrates.

Nanocomposite coatings can be applied to metal substrates using mechanical, physical, or chemical methods [128]. Mechanical deposition includes spray, paint, spin coating, or dip coating. Physical methods involve bonding, condensation, or sputtering. Chemical deposition includes plating, sol-gel, etc. These techniques for thin film deposition on the substrate surface influence properties like uniformity, strength, fracture toughness, and ductility [129].

#### 2.2.14.1. Corrosion Resistance

The primary factors contributing to the high corrosion resistance of epoxy nanocomposite coatings are the crosslink density of the matrix and its barrier properties. However, with prolonged exposure to a corrosive environment, these coatings can develop holes and defects, which can allow corrosive substances to easily penetrate and compromise the coating's effectiveness [130]. The incorporation of layered nanofillers can introduce tortuous pathways for the movement of corrosive agents, unlike neat epoxy coatings, thereby enhancing corrosion resistance [131]. Epoxy coatings exhibit outstanding chemical resistance and strong adhesion to substrates. Nonetheless, they possess inherent brittleness and limited resistance to the initiation and propagation of cracks [132]. The incorporation of nanofillers can mitigate the brittle nature of epoxy, thereby preventing or delaying the formation of cracks. Polymer nanocomposite coatings

offer multiple avenues for reducing corrosion. They create a more effective protective barrier compared to neat polymers, enhance the electrical conductivity of the film, and promote oxygen reduction on the polymer's surface, reducing corrosion reactions on the metal surface, as illustrated in Fig.2.18.

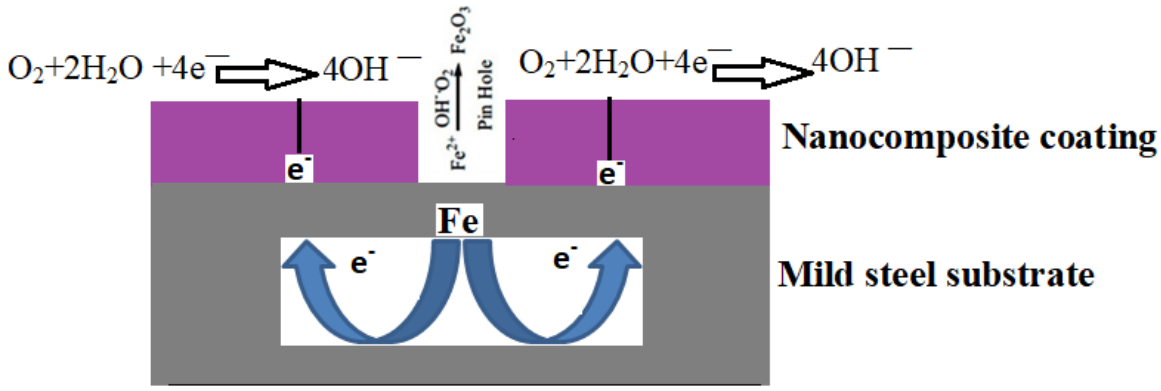


**Fig.2.18:** Corrosion prevention by creating an oxygen deficiency on the metal surface

Electrochemical impedance spectroscopy (EIS) is a commonly employed technique for studying corrosion resistance. It is an electrochemical method that involves the use of three electrodes: a working electrode, a reference electrode, and a counter electrode. EIS measures the electrical impedance of a system over a range of frequencies to analyze its electrochemical behavior and provide insights into corrosion processes and resistance. The instrument used for electrochemical impedance spectroscopy (EIS) can measure impedance across a wide range of frequencies by applying an alternating current (AC) voltage with specific amplitude to the circuit. These measurements are then recorded as a function of immersion time, allowing researchers to track how impedance changes over time and gain insights into the corrosion behavior of the system. In corrosion studies using electrochemical impedance spectroscopy (EIS), resistance directly reflects the corrosion resistance of the coating, while capacitance indicates the water

uptake of the coating. Interestingly, the results demonstrate that there exists an optimal concentration of nanoclay that yields the highest corrosion resistance. Beyond this optimal concentration, corrosion resistance starts to decline, possibly because of increased agglomeration of the clay particles, as discussed in reference [133].

### 2.2.14.2. Barrier Properties

The corrosion resistance of a coating is influenced by its barrier properties, and the permeability of moisture or oxygen through polymers depends on factors such as:

a) The structural characteristics and polarity of the polymer chains are key factors influencing the permeability of moisture or oxygen through polymers.

b) Intermolecular interactions, such as hydrogen bonding, also play a significant role in determining the permeability of moisture or oxygen through polymers.

c) Molecular weight and polydispersity, which refers to the distribution of molecular weights within a polymer sample, are additional factors that can affect the permeability of moisture or oxygen through polymers.

d) The degree of crosslinking or branching in the polymer structure is another crucial factor that can influence the permeability of moisture or oxygen through polymers.

e) The method of synthesis used to create the polymer can also impact its barrier properties and, consequently, its resistance to the permeation of moisture or oxygen.

f) The crystallinity of a polymer, which refers to the degree of molecular order and packing in its structure, can significantly affect its barrier properties and resistance to the permeation of moisture or oxygen.

Polymer nanocomposites are known for their excellent barrier properties [134]. These nanocomposites, which incorporate nanofillers like clays, graphene, carbon nanotubes, chitosan, etc [135-137], exhibit enhanced barrier properties. The dispersion of nanofillers in the polymer matrix impacts the coating's barrier properties in two main ways.

### 2.2.14.3. Mechanisms of Corrosion Protection by Coating

The application of organic coatings on metals is one of the oldest methods of corrosion control, dating back to ancient times. While surface coatings can only provide temporary protection against corrosion, choosing the right paint can significantly slow down the corrosion process. This can extend the structural integrity and lifespan of steel structures over time, making them durable and reliable. The three main methods for controlling corrosion on ferrous substrates using coatings are barrier protection, cathodic protection, and inhibitive protection. Barrier protection offers strong resistance to the penetration of water, ions, and oxygen through the paint film to reach the substrate. Barrier coatings have the additional capability of serving as ionic filters [138]. While water may seem to pass through most paint films relatively easily, the same cannot be said for ions, which face greater resistance and limitations in permeating these coatings. Water that manages to penetrate the coating is typically relatively ion-free, resulting in high electrical resistance. This high resistance hinders the corrosion process at the interface between the paint and the substrate. Consequently, when formulating barrier coatings, it's essential to design them in a way that resists the transmission

of ionic species, in addition to preventing oxygen permeation. Whether providing protection through resistance inhibition or oxygen deprivation as shown in Fig.2.19 the fundamental requirements of a barrier system are as follows: the coating should be impermeable to ionic substances and, if feasible, to oxygen. Furthermore, it should retain adhesion to the metal even under wet service conditions. Impermeability to ionic solutions and oxygen is considered more practical and crucial in preventing corrosion beneath barrier films. These factors are believed to be rate-determining for corrosion under such films. In contrast, the permeability of the film to water is generally thought to have a more direct impact on the loss of adhesion, ultimately leading to corrosion. It's worth noting that corrosion under a barrier film typically initiates only after adhesion has been compromised. Therefore, if adhesion can be maintained under wet service conditions, it ensures effective protection, as discussed in reference [139].

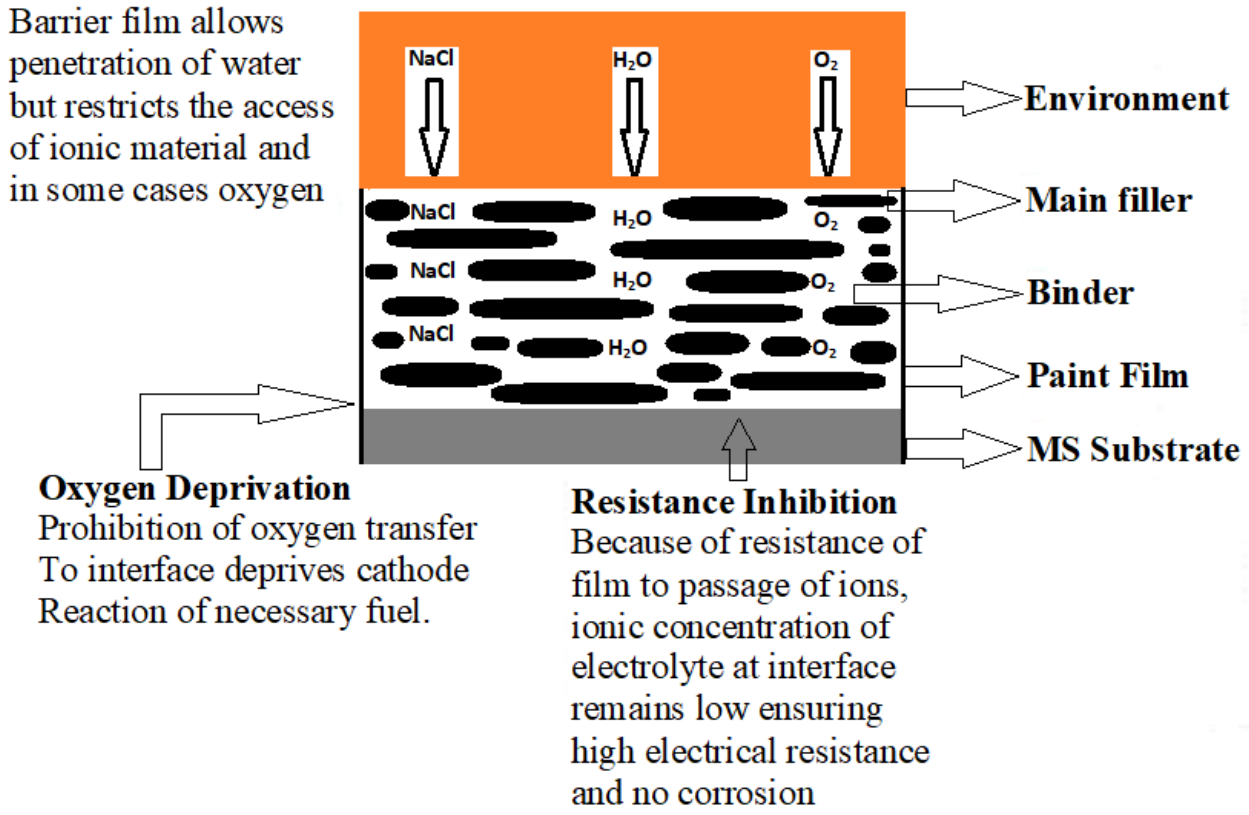


**Fig.2.19:** Corrosion protection by Barrier coating

## 2.2.15. Enhance Mechanical as well as Wear Properties of Coating

Nanocomposites exhibit significantly improved mechanical properties, including stiffness and strength, when compared to microcomposites [140,141]. Proper dispersion and alignment of nanoparticles can notably enhance the stiffness of the polymer matrix. Figure 11 illustrates a comparison of the modulus of an injection-molded composite based on nylon 6 filled with nano organoclay (MMT platelets) and micro glass fibers. In the comparison, the modulus of the nanocomposite is twice that of the microcomposite, despite the fact that the microcomposite contains more than three times the mass of glass fibers compared to MMT platelets. Additionally, when the platelets are aligned within the plane of the sample, this reinforcement effect is observed uniformly in all directions within the plane. In contrast, fibers reinforce only along a single axis in the direction of their alignment, as indicated in references [142-143].

Moreover, the nanocomposite exhibits a significantly superior surface finish compared to the microcomposite, attributed to the nanometer size of the clay platelets. Various properties of nanocomposites are influenced by the size and geometry of nanoparticles, including Young's and shear moduli, thermal expansion coefficient, as indicated in references [144-150,152]. The interface between nanoparticles and the matrix is of utmost importance, and the development of mechanical properties relies on proper interfacial adhesion [144, 145, 147, and 151].

# CHAPTER-3

# Research Objectives
# &
# Plan of the Work

## 3.1. Research Objectives

The objective of this study is to focus on the combination of polymers with nano fillers in the form of composite polymer based nanofiller which enhances the corrosion resistance of polymer and this is considered to be one of the most efficient polymeric coating materials and majority of the cases these fillers addition of unnecessary of pigments.

- Life of conventional organic coating and lining used for pipeline and structure is 5 to 15 years because of low physical & chemical property
- To develop and characterized nanocomposite organic coating of much higher physical and chemical resistance properties and thereby increasing life of pipeline structures substantially

There is need to develop better coating material by using nano fillers. Nanotechnology applications in coatings have shown remarkable growth in recent years. This is the result of two main factors:

1) Increased availability of nano-scale materials, such as various types of nanoparticles, and

2) Advancements in processes that can control coating structure at the nanoscale. Our focus should be out of this organo silane (silica) is selected for nano filler which will give a lot of efforts and improve coating technologies mostly like corrosion resistant because of greater surface activity with well dispersion of nanoparticales, in the resin through containing cross linking agent with lot of linkage group and gives three dimensional network rigid structures with desirable properties. It has remarkable physical properties including extreme scratch resistance, ultra high gloss, very high water and chemical resistance, extreme UV resistance, remarkable flexibility and cleaning properties. Different formed of silica is also economically and environmentally eco friend which is easily available

and industrial affordable. Quartz silica used as conventional filler which is used for comparative study of both composite coatings.

## 3.2. Plan of the Work

### 3.2.1. Development of Epoxy based Composite Coatings through Solution Blending Route and their Characterizations

(i) Quartz silica conventional filler based epoxy composite coating

(ii) Organo silane nano filler based composite coating

(iii) Quartz silica conventional filler and 160A glass flake based epoxy composite coating

(iv) Organo silane nano filler and 160A glass flake based epoxy composite coating

(v) Quartz silica conventional filler and 160N glass flake and based epoxy composite coating

(vi) Organo silane nano filler and 160N glass flake based epoxy composite coating.

### 3.2.2. Development of Polyurethane based Composite Coatings through Solution Blending Route and their Characterizations

(i) Quartz silica conventional filler based polyurethane composite coating

(ii) Organo silane nano filler based polyurethane composite coating

### 3.2.3. Development of Coal Tar Epoxy based Composite Coatings through Solution Blending Route and their Characterizations

(i) Quartz silica conventional filler based coal tar epoxy composite coating

(ii) Organo silane nano filler based coal tar epoxy composite coating

### 3.2.4. Development of Coal Tar Epoxy based Composite Coatings through Solution Blending Route and their Characterizations

(i) Quartz silica conventional filler and 160A glass flake based vinyl ester composite coating

(ii) Organo silane nano filler and 160A glass flake based vinyl ester composite coating

(iii) Quartz silica conventional filler and 160N glass flake and based vinyl ester composite coating

(vi) Organo silane nano filler and 160N glass flake based vinyl ester composite coating.

## 3.3. Characterizations

### 3.3.1. Techniques of Characterization

So, following characterizations technique to be carried out:

- FTIR of each film analysis to be carried out before and after salt spray of each film
- XRD of cured each composite film
- Particle size determination by Transmissioin Electron Microscope (TEM) of each nanocomposite film
- Morphology study by Scanning Electron Microscope (SEM) of each composite film
- Thermal (TGA-DTA) study of each composite film

### 3.3.2. Physico-Mechanical Testing

Following test to be carried out as per ASTM method:

- To determinate DFT (Dry Film Thickness) of each coated MS panel

- Coating holiday test of all coated MS substrate
- Determination of cross linking density of all composite films
- Adhesion test
    - Pull off (Before and after of salt spray of each coated panel)
- Flexibility test of each coated tin panel
- Hardness test
    - Scratch Hardness of each coated MS panel
    - Pencil Hardness of each coated MS panel
- Falling ball impact test of each coated MS panel
- Abrasion resistance of each coated MS panel
- Gloss meter to measure the specular reflection angle of a coated surface of MS panel
- Water permeability test of each composite film
- Chemical resistance test of each composite film

### 3.3.3. Corrosion Studies

Corrosion Studies of all composite coatings to be carried out following method:

- Potentiodynamic Polarization (PD) study of uncoated and coated MS rod
- To evaluate corrosion inhibition efficiency after PD studies
- To calculate porosity of each composite coating after PD studies
- Electro Impedance Spectroscopy (EIS) study uncoated and coated MS rod
- To determinate charge transfer resistance (Rct) after EIS studies
- Salt Spray Chamber (SSC) test will be carry out 2200 hours for each sample of cured panel and film
- Cathodic disbondment (CD) study of each coated panel
- Optical images analysis before and after corrosion studies of all composite coated MS rod

# Flow Chat of Plan of the Work


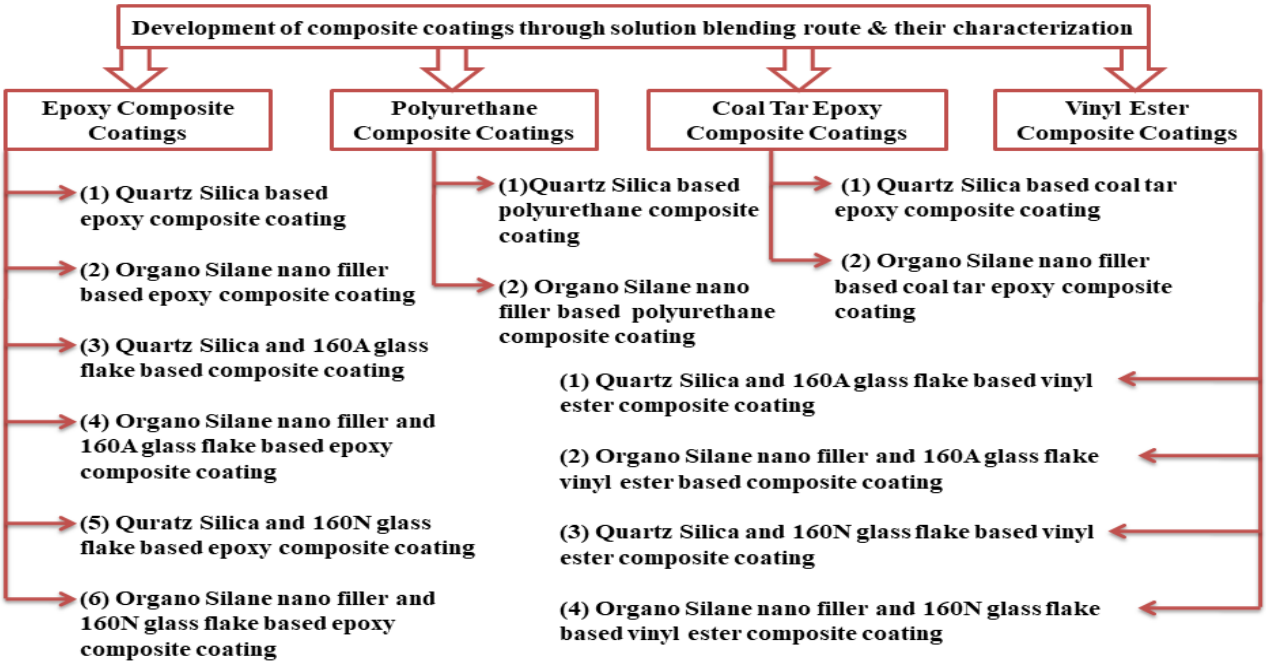


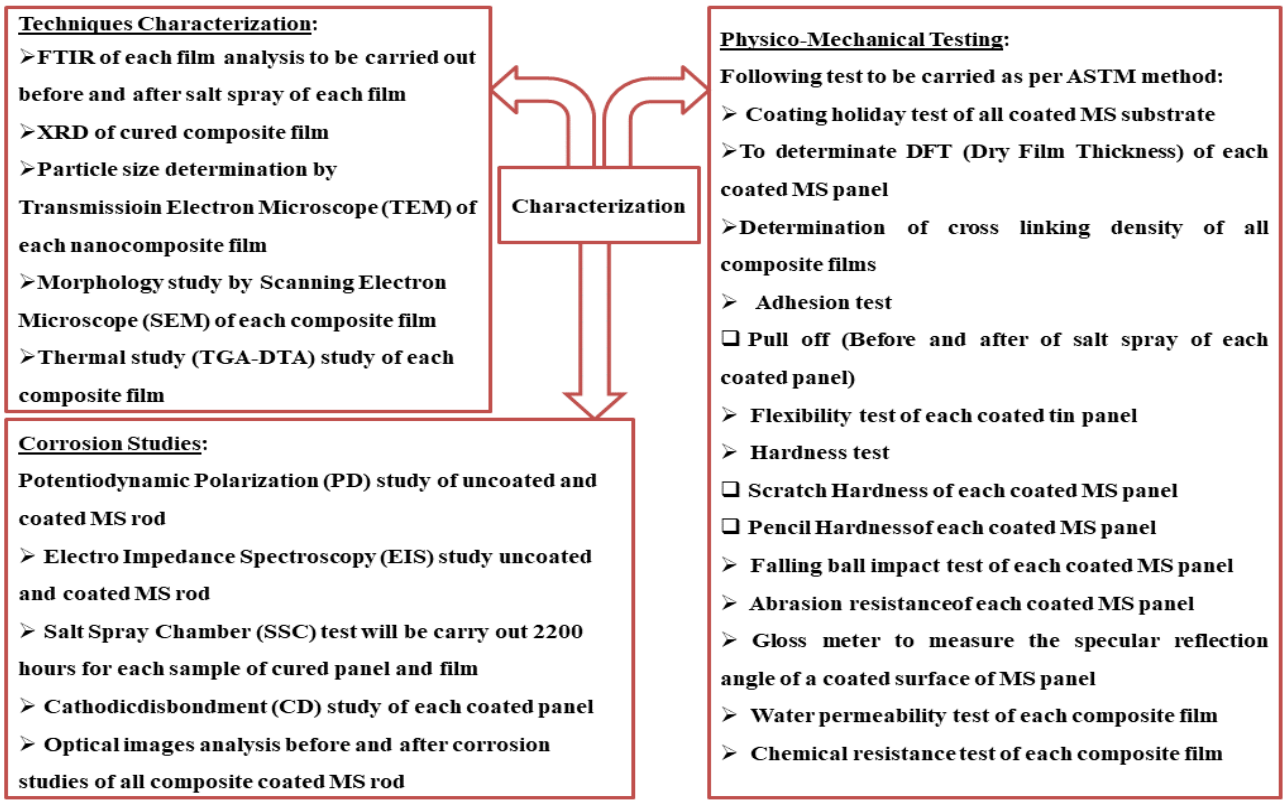

# CHAPTER- 4

# Experimental

## 4.1. Materials

Epoxy resin trade name YD-128 (Aditya Birla, India), castor oil polyol resin trade name Jagropol-115 (k2P Chem, India) for polyurethane (PU), coal tar free (Vijoy Solvent and Thinner, India), vinyl ester resin (Ruia Chemical, India) are used as resin in the study, phenalkamine (Cardolite, India), methylene diphenyl diisocyante (MDI) (Labdhi Chem, India), diethelene tri amine (DETA) (Meru Chem, India) and MEK peroxide as catalyst (Sigma Aldrich, Netherlands), as accelerator (Sigma Aldrich, Germany), Co octate as promoter (Sigma Aldrich, Germany) are used for the curing of epoxy, castor polyol, cal tar free epoxy and vinyl ester resin. BYK-204, (Anti-Terra, South Korea) is used as wetting agent, BYK-530 is used as air releasing deformer and BYK-333 is used as slip agent. Resin based cured composite coatings were formulated by using different formed of $SiO_2$ used as main filler, rutile $TiO_2$ (Sigma Aldrich, Germany) powder used as main pigment and soap stone powder (P.S. Chemical, India) as extender. The size of soap stone particles formulation was within 40-70 micron. Conventional silica named as qurtz silica (Galaxy Global India) powder is used for study. Aerosil972 (EVONIK, Germany) is organo silane used as $SiO_2$ nano particles. Glass flakes (NSG Group, Japan) of RCF-160N and RCF-160N where surface treated by amino group and acryloyl group respectively. And thickness of the both glass flake particle is 3.0 to 7.0 micron. Xylene (Moksha Chem, India), methyl isobutyl ketone (MIBK) (Sigma Aldrich, Germany) and Styrene (Sigma Aldrich, Netherlands) act as solvent.

## 4.2. Samples Preparation

### (1) Conventional filler based epoxy composite coating (EP1)

Materials: 0.20gm of BYK-204, 0.10gm of BYK-333, 0.10gm of BYK-530, 3gm of rutile $TiO_2$, 25gm of soap stone/talc, 5gm of xylene, 5gm of methyl isobutyl

ketone (MIBK) 10gm of quartz silica conventional filler was slowly introduce into the 40gm of epoxy resin.

Corresponding hardener mixed by 3:1 vol/vol of base, 27.36 gm of phenalkamine added in to grinding mixture and mixed well together for curing.

**(2) Nano filler based epoxy composite coating (EP2)**

Materials: Additives are 0.20gm of BYK-204, 0.10gm of BYK-333, 0.10gm of BYK-530, 3gm of rutile $TiO_2$, 25gm of soap stone/talc extender, 10gm of xylene, 10gm of MIBK and 6gm of organo silane (EVONIK, Germany) nano filler was slowly introduce into the 40gm of epoxy resin.

Corresponding hardener mixed by 3:1 vol/vol of base, 27.36gm of phenalkamine added in to grinding mixture and mixed well together for curing.

**(3) Conventional filler with 160A glass flake based epoxy composite coating (EP3)**

Materials: 0.50gm of BYK-204, 0.10gm of BYK-333, 0.10gm of BYK-530, 5gm of rutile $TiO_2$, 17gm of soap stone/talc powder, 10gm of 160A glass flake, 10gm of xylene, 10gm of MIBK and quartz silica was 10gm slowly introduce into the 50gm of epoxy resin.

Corresponding hardener mixed by 3:1 vol/vol of base, 34.21gm of phenalkamine added in to grinding mixture and mixed well together for curing.

**(4) Nano filler with 160A glass flake based epoxy composite coating (EP4)**

Materials:0.50gm of BYK-204, 0.10gm of BYK-333, 0.10gm of BYK-530, 5gm of rutile $TiO_2$, 17gm of soap stone/talc powder, 10gm of 160A glass flake, 15gm of

xylene, 15gm of MIBK and nano organo silane was 7gm slowly introduce into the 50gm of epoxy resin.

Corresponding hardener mixed by 3:1 vol/vol of base, 34.21 gm of phenalkamine added in to grinding mixture and mixed well together for curing.

**(5) Conventional filler with 160N glass flake based epoxy composite coating (EP5)**

Materials: 0.50gm of BYK-204, 0.10gm of BYK-333, 0.10gm of BYK-530, 5gm of rutile $TiO_2$, 17gm of soap stone/talc powder, 10gm of 160N glass flake, 10gm of xylene, 10gm of MIBK and quartz silica was 10gm slowly introduce into the 50gm of epoxy resin.

Corresponding hardener mixed by 3:1 vol/vol of base, 34.21gm of phenalkamine added in to grinding mixture and mixed well together for curing.

**(6) Nano filler with 160N glass flake based epoxy composite coating (EP6)**

Materials: 0.50gm of BYK-204, 0.10gm of BYK-333, 0.10gm of BYK-530, 5gm of rutile $TiO_2$, 17gm of soap stone/talc powder, 10gm of 160N glass flake, 15gm of xylene, 15gm of MIBK and nano organo silane was 7gm slowly introduce into the 50gm of epoxy resin.

Corresponding hardener mixed by 3:1 vol/vol of base, 34.21 gm of phenalkamine added in to grinding mixture and mixed well together for curing.

**(7) Conventional filler based polyurethane composite coating (PU1)**

Materials: 0.30gm of BYK-333, 0.40gm of BYK-530, 5gm of rutile $TiO_2$, 17gm of soap stone/talc powder, 10gm of xylene, quartz silica was 10gm slowly introduce into the 50gm of castor oil polyol resin.

Corresponding hardener mixed by 3:1 vol/vol of base, 22gm of MDI added in to grinding mixture and mixed well together for curing.

(8) **Nano filler based polyurethane composite coating (PU2)**

Materials: 0.30gm of BYK-333, 0.40gm of BYK-530, 5gm of rutile $TiO_2$, 17gm of soap stone/talc powder, 10gm of xylene, nano organo silane was 10gm slowly introduce into the 50gm of castor oil polyol resin.

Corresponding hardener mixed by 3:1 vol/vol of base, 22gm of MDI added in to grinding mixture and mixed well together for curing.

**(9) Conventional filler based coal tar epoxy composite coating (CTEP1)**

Materials: 15gm of soap stone/talc powder, 18.35gm of high build epoxy, 10gm of xylene and quartz silica was 6.5gm slowly introduce into the 60gm of dehydrated coal tar.

Corresponding hardener mixed by 4:1 vol/vol of base, 2gm of DETA added in to grinding mixture and mixed well together for curing.

**(10) Nano filler based coal tar epoxy composite coating (CTEP2)**

Materials: 15gm of soap stone/talc powder, 18.35gm of high build epoxy, 10gm of xylene and nano organo silane was 6.5gm slowly introduce into the 60gm of dehydrated coal tar.

Corresponding hardener mixed by 4:1 vol/vol of base, 2gm of DETA added in to grinding mixture and mixed well together for curing.

**(11) Conventional filler with 160A glass flake based vinyl ester composite coating (VE1)**

Materials: 10gm of rutile $TiO_2$, 10gm of 160A glass flake, 10gm of styrene and quartz silica was 10gm slowly introduce into the 40gm of vinyl ester resin.

1.6gm of MEK peroxide as catalyst and 0.1gm of Co Octate as promoter added slowly into grinding mixture and mixed well together for curing.

**(12) Nano filler with 160A glass flake based vinyl ester composite coating (VE2)**

Materials: 10gm of rutile $TiO_2$, 10gm of 160A glass flake, 5gm of styrene and nano organo silane was 5gm slowly introduce into the 40gm of vinyl ester resin.

1.6gm of MEK peroxide as catalyst and 0.1gm of Co Octate as promoter added slowly into grinding mixture and mixed well together for curing.

**(13) Conventional filler with 160N glass flake based vinyl ester composite coating (VE3)**

Materials: 10gm of rutile $TiO_2$, 10gm of 160N glass flake, 10gm of styrene and quartz silica was 10gm slowly introduce into the 40gm of vinyl ester resin.

1.6gm of MEK peroxide as catalyst and 0.1gm of Co Octate as promoter added slowly into grinding mixture and mixed well together for curing.

**(14) Nano filler with 160N glass flake based vinyl ester composite coating (VE4)**

Materials: 10gm of rutile $TiO_2$, 10gm of 160N glass flake, 5gm of styrene and nano organo silane was 5gm slowly introduce into the 40gm of vinyl ester resin.

1.6gm of MEK peroxide as catalyst and 0.1gm of Co Octate as promoter added slowly into grinding mixture and mixed well together for curing.

### 4.2.1. Experimental procedure of Polymer Nanocomposite Coatings

Developing successful polymer nanocomposite coatings presents two challenges.

i) One of the challenges in developing successful polymer nanocomposite coatings is ensuring chemical compatibility between the polymer matrix and the organo silane nano filler at the nano scale.

ii) Another challenge is achieving a homogeneous dispersion of the nano filler within the polymer matrix.

Solution blending involves suspending the nano filler in a solvent. When mixed with the polymer, the polymer chains can intercalate and displace the solvent within the interlayer of the filler. Upon solvent removal through vaporization, the intercalated particles reassemble resulting in polymer nano filler composite. Achieving a uniform dispersion of the nano filler necessitates strong agitation. The interfacial interaction between the nano filler and polymer matrix as well as the quality of nano filler dispersion, will profoundly impact the quality of the polymer/nano filler composite.

Method of all samples preparation was solution blending technique. Mixtures of resins are very viscous and high volume solid so mixing processes have to be carried out quickly. Solution blending method followed for developing of composite materials. There is no need of heating the mass. The mixture will be subjected to high speed mixer 4000-6000 RPM for 2.5 to 3 hours at 40-50$^{O}$C. Good dispersion will be achieved by mechanical stirring with high speed continuously. Composite based all samples are prepared with different code names.

After optimization of nano filler in resin, weight percentage of resin, extenders, additives, solvents and both type of fillers were varied. The Pigment Volume Concentration (PVC) of the formulation was 100%.

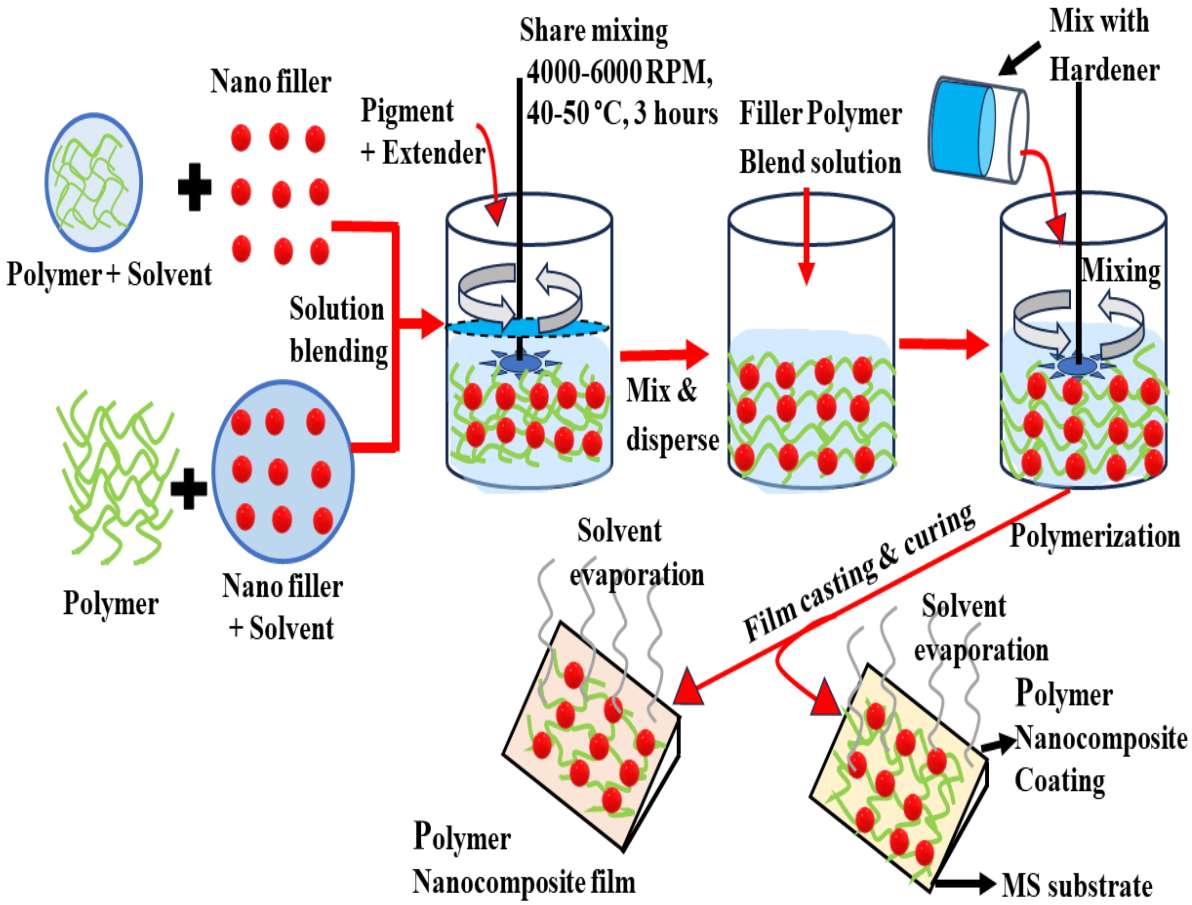


**Fig.4.1:** Flow chart of solution blending procedure

**Table.4.1.** Formulation of different chemical compositions of epoxy, polyurethane and coal tar epoxy composite coatings

| **Pigment Volume Concentration (PVC) %** | | | | | | | | | | | |
|---|---|---|---|---|---|---|---|---|---|---|---|
| **Samples code name** | **Resin (%)** | **BYK-204 (%)** | **BYK-530 (%)** | **BYK-333 (%)** | **Rutile $TiO_2$ (%)** | **Soap stone (%)** | **Glass flake (%)** | **Qurtz silica (%)** | **Nano organo silane (%)** | **Xylene (%)** | **MIBK (%)** |
| (1) EP1 | 51.36 | 0.2 | 0.1 | 0.1 | 6.14 | 32 | × | 10 | × | 5 | 5 |
| (2) EP2 | 51.36 | 0.2 | 0.1 | 0.1 | 6.14 | 32 | × | × | 6 | 10 | 10 |
| (3) EP3 | 56.14 | 0.5 | 0.1 | 0.1 | 5.5 | 17 | 11,(160A) | 10 | × | 10 | 10 |
| (4) EP4 | 56.14 | 0.5 | 0.1 | 0.1 | 5.5 | 17 | 11,(160A) | × | 7 | 15 | 15 |
| (5) EP5 | 56.14 | 0.5 | 0.1 | 0.1 | 5.5 | 17 | 11,(160N) | 10 | × | 10 | 10 |
| (6) EP6 | 56.14 | 0.5 | 0.1 | 0.1 | 5.5 | 17 | 11,(160N) | × | 7 | 15 | 15 |
| (7) PU1 | 60 | × | 0.1 | 0.1 | 5.5 | 18 | × | 10 | × | 10 | × |
| (8) PU2 | 60 | × | 0.1 | 0.1 | 5.5 | 18 | × | × | 10 | 15 | × |
| (9) CTEP1 | 75 | × | × | × | × | 15 | × | 10 | × | 10 | × |
| (10) CTEP2 | 75 | × | × | × | × | 15 | × | × | 10 | 15 | × |

**Table.4.2.** Formulation of different chemical compositions of vinyl ester composite coatings

| **Pigment Volume Concentration (PVC) %** | | | | | | |
|---|---|---|---|---|---|---|
| **Samples code name** | **Vinyl Ester Resin** | **Rutile $TiO_2$ (%)** | **Glass flake (160A/160N) (%)** | **Qurtz silica (%)** | **Nano organo silane partcle (%)** | **Styrene (%)** |
| (11) VE1 | 65 | 10 | 15,(160A) | 10 | × | 10 |
| (12) VE2 | 65 | 10 | 15,(160A) | × | 5 | 10 |
| (13) VE3 | 65 | 10 | 15,(160N) | 10 | × | 10 |
| (14) VE4 | 65 | 10 | 15,(160N) | × | 5 | 10 |

## 4.3. Preparation of the Mild Steel (MS) coated panels and rods

MS panels (6″ × 2″), (6″ × 4″), (5″ × 2½″) and MS rods of size (8 mm × 6″) were de-greased, sand blasted and cleaned, prior to coating. Both conventional silica and nano silica containing grinding mixture base with hardener mixed well together for 5 mints. The mixture was sprayed using spray painting gun onto the MS panels and rod substrates to develop uniformly coated samples achieve uniform coating thickness is 200±10 micron on MS specimen as per ASTM standard.

## 4.4. Prepation of composite film

The preparation of both conventional and nano silica based grinding mixture base films were prepared by using spray painting gun on the hard plastics substrate and then cured films were kept for 24 hrs at room temperature in order to achieve uniform film thickness of 200±10 micron according to ASTM standard. Again after putting over from the substrate films and coated panel were post cured at $60^{O}C$ for 2 hrs over hot oven. Then both the composite films and different size of coated panels were allowed to stabilize for 15 days at $28\pm5^{O}C$ within desiccators and 50% relative humidity, before any experiment was carried out.

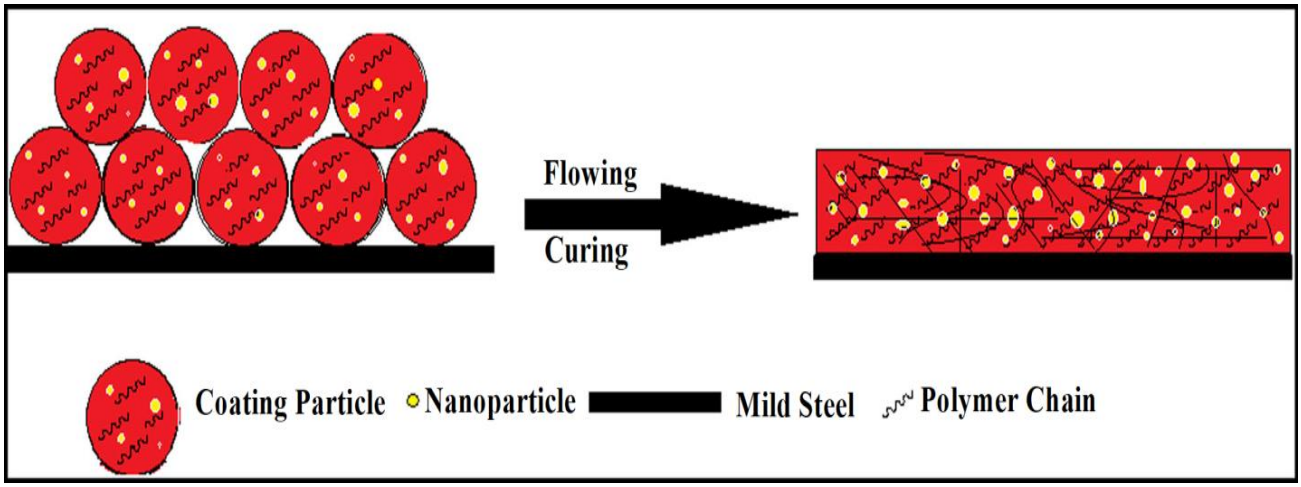


**Fig.4.2:** Schematic image of nanocomposite coating on MS substrate

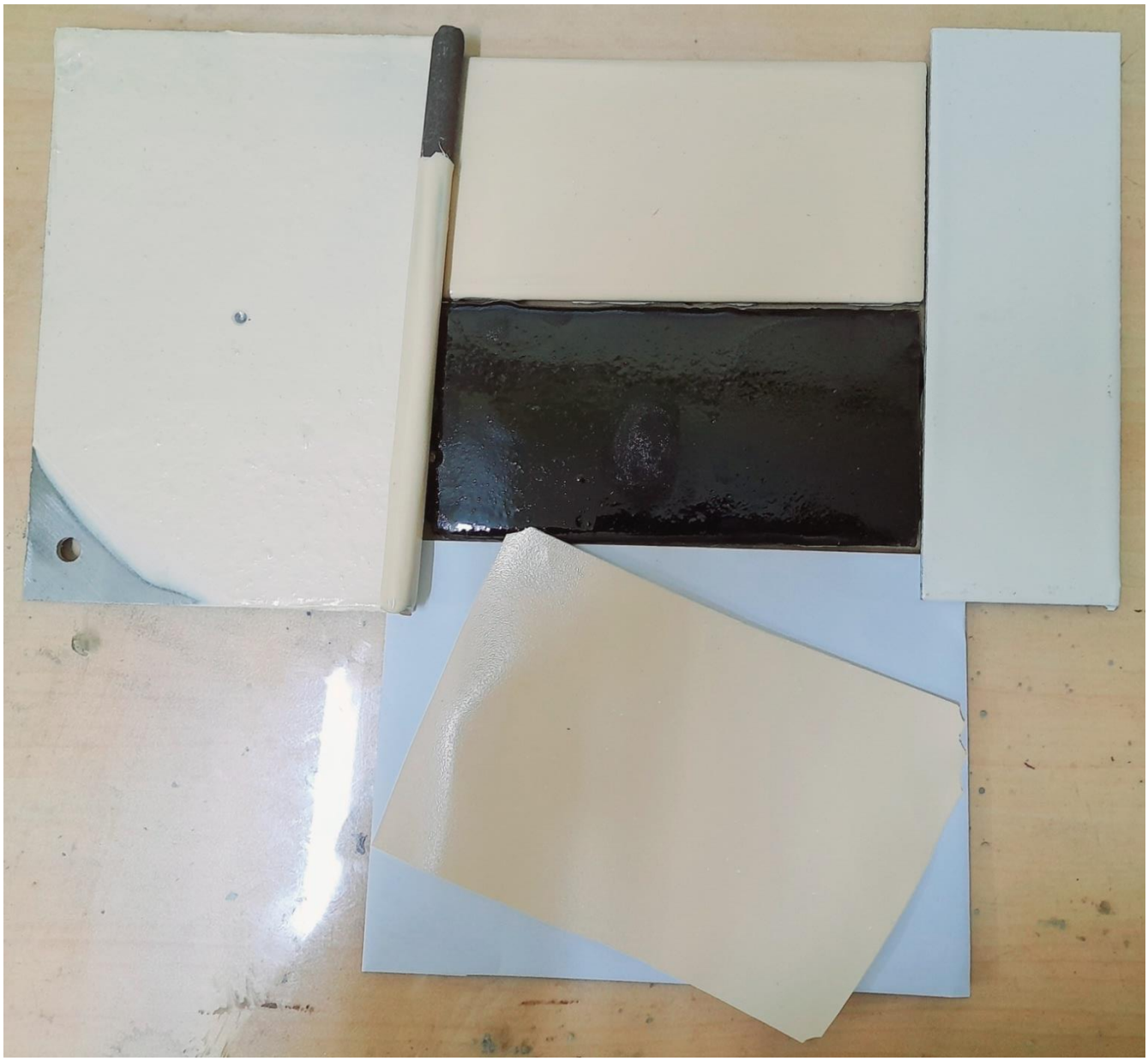

**Fig.4.3:** Image of different size of coated panels and rod

## 4.5. Characterization Technique (Instruments Details) of Composite Films

(i) Fourier Transform Infrared Spectroscopy (FTIR) studies recorded by IR Prestige in the range between 400 and 4500 $cm^{-1}$. This experiment was done in the School of Material Science, Jadavpur University, Kolkata.

(ii) The powder, X-ray diffraction (XRD) patterns in conventional composite films, organo silane particles and also nano particles embedded composite coating were noted using Panaytical Netherland (X'pert Pro). This study is conducted in the Metallurgical & Material Enggineering Department, Jadavpur University, Kolkata.

(iii) Thermal analysis of TGA-DTA studies done by PerkinElmer (x86) in nitrogen atmosphere at 10.00°C/min. Thermal analysis done in the Metallurgical & Material Enggineering Department, Jadavpur University, Kolkata.

## 4.6. Morphology Study

(i) Transmission electron microscopy (TEM) images were taken by JEM-2100, 200KV, jeol. This study done in the NEHU, SAIF, Shilong.

(ii) Scanning Electron Microscope (SEM)images taken by FEI Quanta 200 F SEM, Netherland, Analysis of this experiment done in the Chemistry Department, IIT Delhi.

(iii) Scanning Electron Microscope (SEM)(INSPECT F50, GERMANY) images taken by Department of Physics, Jadavpur University, Kolkata.

(iv) Optical images were taken before and after corrosion of coating surface on rod by Leica (Model name/no: DM4 B) optical microscope in the Department of Metallurgical & Material Enggineering, Jadavpur University, Kolkata.

## 4.7. Physico-Mechanical Testing

(i) Holiday test (Model name/no: HD-830, Caltech Engineering) was carried out cured panels and rods with an approved high voltage holiday detector, preferably equipped with an audio visual signaling device to indicate any faults, holes, damaged or conductive particles in the protective coating as per ASTM D-5162.

(ii) As per ASTM D-1400 standard a dry film thickness gauge (Model name/no: Elecoat M) used to measure the dry film thickness (DFT).

(iii) As per ASTM-D6824 method percentage of cross link density of both types of composite coatings has evaluated.

The crosslink density (%) of water was calculated by universal technique. where $W_2$ is before absorption film weight and $W_1$ is the film weight after solvent absorption for 72hours:

$$\%\ \text{Crosslink density} = \frac{W_1 - W_2}{W_2} \times 100$$

(iv) Adhesion behaviors test was evaluated on coated MS panels as per ASTM D-4541 and ASTM D-3359. Here “Pull off” and “Cross-cut” methods are used for adhesion testing. “Pull off” test was studied before and after Salt Spray Chamber (SSC) test of 2200 hrs of MS coated panel. In this study, the test dolly was bonded to the coating using an appropriate adhesive. The test is done by Caltech Pull Off tester machine.

(v) The flexibility of the coatings was carried out with regard to the ‘crack resistance’ and these experiments were performed on coated MS panel by standard Conical Mandrel tester as per ASTM D-4145.

(vi) The pencil hardness test was studied on coated MS panels using pencils 6B to 6H range, as per ASTM D-3363.

(vii) Scratch hardness (Model name/no-SHT-01) of the coated MS panels was carried out as per ASTM D-3363 method.

(viii) Falling ball impact (Model name/no: Globe Tex) test was performed by impact tester dropping a 0.9 kg weight from a maximum height of 50.8 cm and from 6.35 cm on MS coated panels. When fallings the ball was dropped onto a MS coated surface of panel i.e. 'intrusion' and on the back side of uncoated panel with reference to the coated surface i.e. 'extrusion' as per ASTM D-2794.

(ix) Using Taber Abraser (Model name/no: 5153) for 1000 Cycles as per ASTM D-4060 for resistance of abrasion was studied.

(x) The measurements was covering the specular illustration of the specimens of paint for gloss meter (Model name/no: Gloss-11) geometry of $60^{O}$ on a flat, homogeneous and clean surface as per ASTM D-523.

Above all Physico-Mechanical testings was done in the Aglow lab (NABL Certified), Kolkata.

## 4.8. Studies of Corrosion (PD and EIS) on Coatings

AC impedance measurements are evaluated on epoxy-nano and conventional $SiO_2$ composite coatings over the steel surface along with the corrosion resistance. Potentiodynamic polarization (PD) and electro impedance spectroscopy (EIS) experiments were done by Autolab electrochemical workstation. The PD test is performed in 3.5% Nacl solution using a standard three-electrode system. For this study, Pt and 3.5M Ag/AgCl were used as counter electrode and reference electrode respectively and nano/micro silica based epoxy composite coated rod

was used as a working electrode. PD was done at scan rate of 1mV in the potential range 1.0 V to −1.0 V vs Ag/AgCl. EIS has been measured in a frequency range of 0.01 Hz to 100 kHz at 10mV amplitude. Nova 2.1 (FRA software) was used to analyze the impedance spectrum. All potentials are measured with respect to Ag/AgCl electrode. This experiment done in the SSS National Institute of Bio Energy, Punjab, India.

Corrosion of uncoated MS rod, anti corrosion properties of both nano and micro silica composites were compared by using the above mentioned technique. PD and impedance measurements were conducted at different phases like (initial 1, 7, 15 and 30) days of time interval. This test was conducted based on ASTM standard B 117.4.

## (a) Corrosion Inhibition Efficiency (%)

The linear segments of the anodic and cathodic curves were extrapolated to determine the corrosion current densities ($I_{corr}$) and corrosion potential ($E_{corr}$). The corrosion inhibition efficiency was calculated from the measured $I_{corr}$ values using the following equation:

$$\% \text{ Corrosion Inhibition Efficiency} = \frac{I^{o}_{corr} - I_{corr}}{I^{o}_{corr}} \times 100$$

Where, $I^{o}_{corr}$ is the corrosion current density of the uncoated sample and $I_{corr}$ is the corrosion current density of the coated sample

### (b) Charge transfer resistance (Rct in %)

A 10 mV AC perturbation was applied to a metal/coating system in the frequency range of $10^{-2}$ to $10^{5}$ Hz during EIS measurements with the open-circuit potential. The protection efficiency was calculated using the charge transfer resistance (Rct) values:

$$\%\ \text{Rct} = \frac{Rct - Rct^{o}}{Rct} \times 100$$

Where, *Rct* and $Rct^{o}$ are the charge transfer resistance of coated and uncoated samples.

### (c) Porosity Measurement

Porosity in polymer coatings on mild steel was determined from potentiodynamic polarization measurements using a specific relationship, which assesses the coating's suitability to protect the underlying metal against corrosion:

$$\text{P} = \frac{R_{P(Uncoated)}}{R_{P(Coated)}} \times 10^{-\frac{(\Delta E_{corr})}{b_a}}$$

Where, P is the total porosity, $R_{P\ (Uncoated)}$ and $R_{P\ (Coated)}$ are the polarization resistance of uncoated and coated MS, $\Delta E_{corr}$ is the difference between corrosion potential and $b_a$ is the anodic Tafel slope for uncoated MS.

## 4.9. Salt Spray Chamber (SSC) Experiments

In the salt spray chamber (SSC) test, both panels with coating were scratched in the centre and they were exposed to fog where 5% sodium chloride solution at $P^{H}$ 7.2 was atomized by use of compressed air in order to create a continuous fog for 2200

hours. This test was conducted based on ASTM standard B 117.1. This corrosion studies done in the Aglow lab (NABL Certified), Kolkata.

## 4.10. Cathodic Disbondment (CD) Experiments

As per ASTM standard B 117.1, MS Coated panels were subjected to CD (Model name: CD-405S) test at −1.5V and at 30±20$^{O}$C for 28 days. The two individual cells are made having electrolyte with a concentration 3.5% Nacl solution for CD test. At the centre of each cell a hole of 6 mm diameter was drilled to remove the coating material up to the base metal substrate acting as a cathode. To measure the continuous potential for 28 days, platinum electrode used as anode and reference calomel electrode is immersed in each cell for testing. This corrosion studies conducted in the Aglow lab (NABL Certified), Kolkata.

## 4.11. Water and Chemical Resistance Behaviors

The degree of water absorption i.e. water swell evaluated by preserving of film with in water. The swell (%) of water was calculated by universal technique. where $W_b$ is before absorption film weight and $W_a$ is the film weight after water absorption for 30 days:

$$\%\ \text{Swell} = \frac{W_a - W_b}{W_b} \times 100$$

By using in acids (5% HCl and 5% $H_2SO_4$) and alkali (5% NaOH) immersion test for 65 days the chemical resistance prominency of the cured composite coatings were studied.

# CHAPTER-5

# Result and Discussion

# 5(A)

# EPOXY BASED COMPOSITE COATINGS

## 5.(A). Characterization

## 5(A). 1. FTIR spectroscopy

First, qurartz silica and organo silane nano particle have studied on IR beam. The glass flake based epoxy composite coating system proffers a very compact and rigid structure than epoxy composite coating. As result, the different intensities of the band of the different functional group are not irradiated to the IR beam during its channel or the structure is so rigid that the vibration of normal stretching and bending are too much repressed. The free volume porosity of such composite coating is very less.

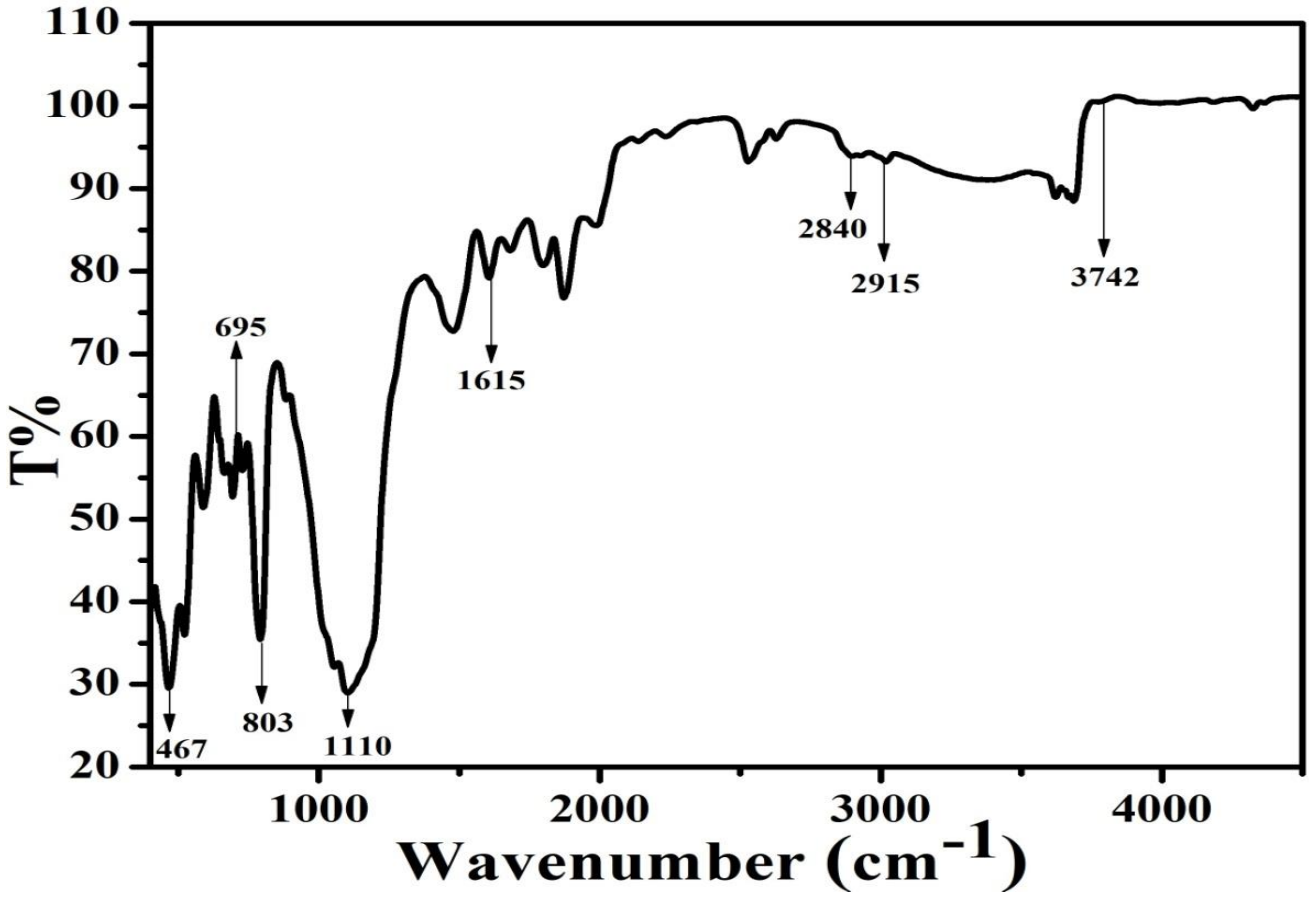


**Fig.5(A).1:** FTIR spectroscopy of quartz silica particles

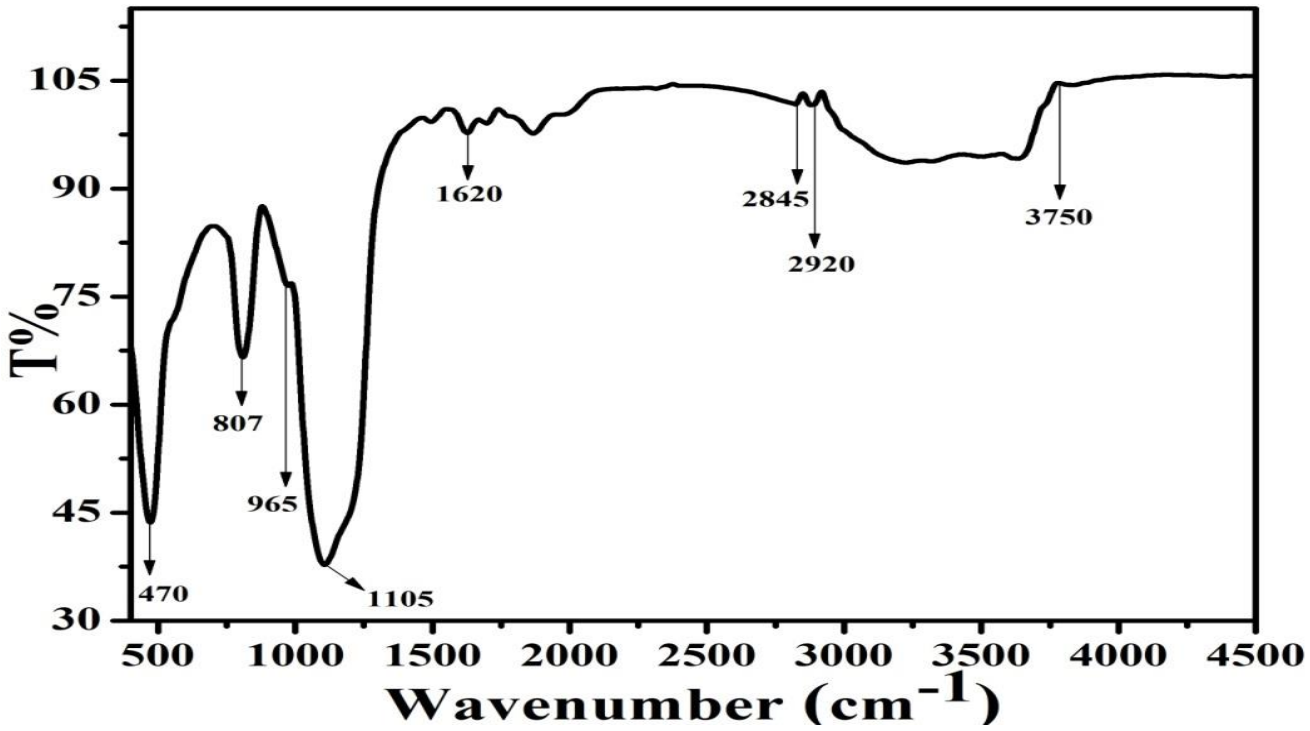


**Fig.5(A).2:** FTIR spectroscopy of organo silane nano particles

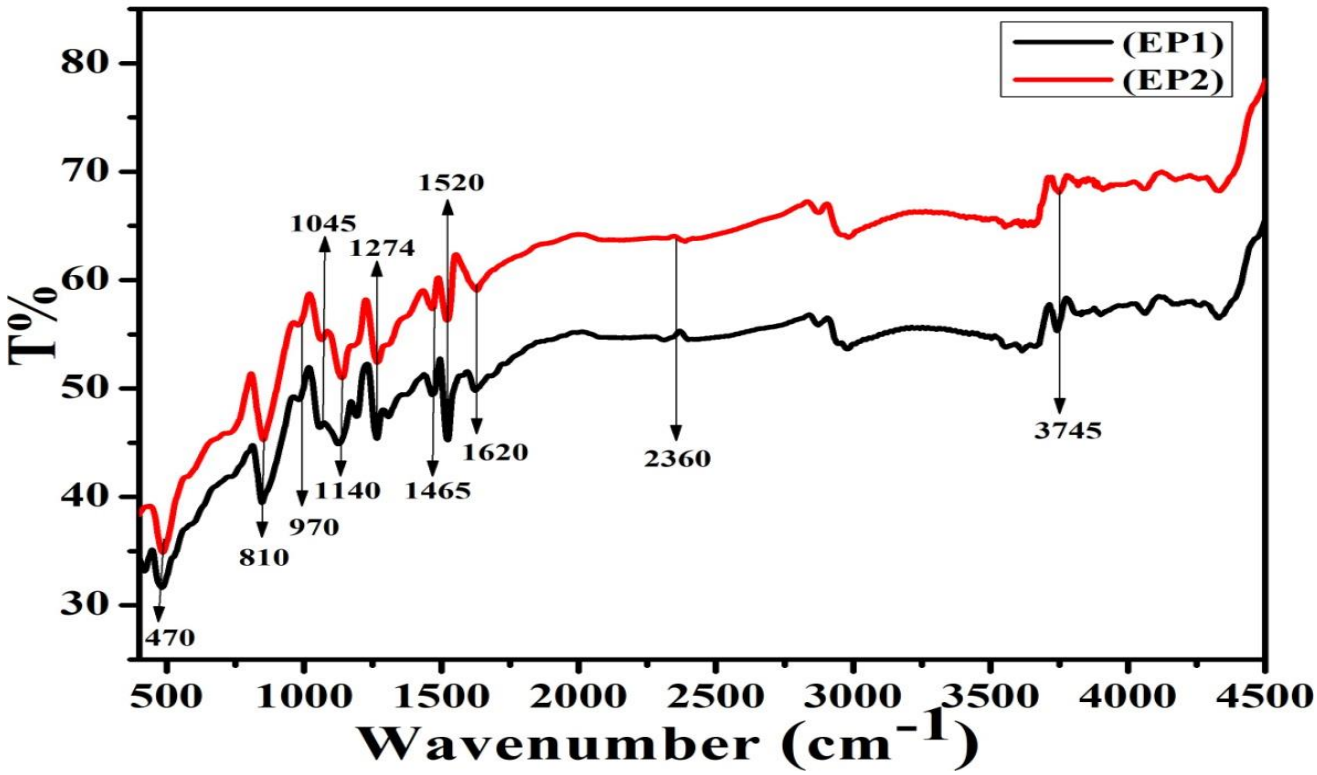


**Fig.5(A).3:** FTIR spectroscopy of composite of EP1and EP2

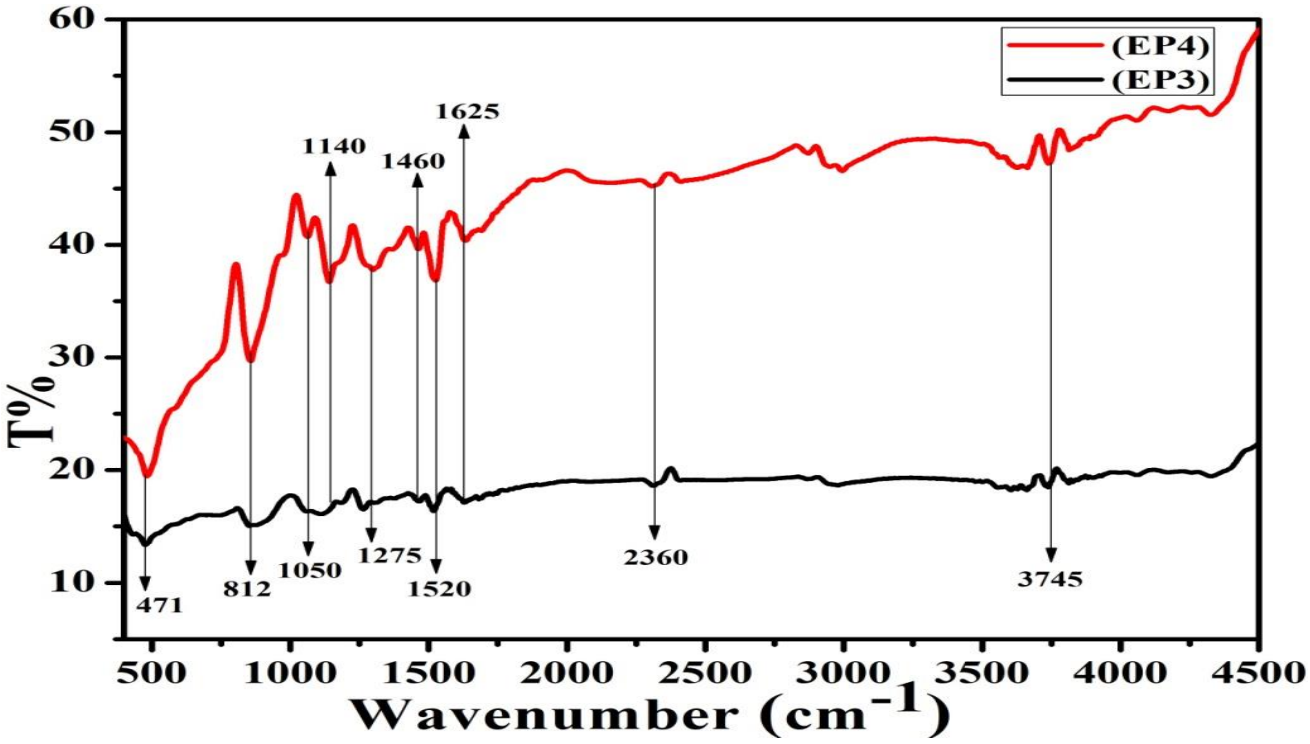


**Fig.5(A).4:** FTIR spectroscopy of composite of EP3and EP4

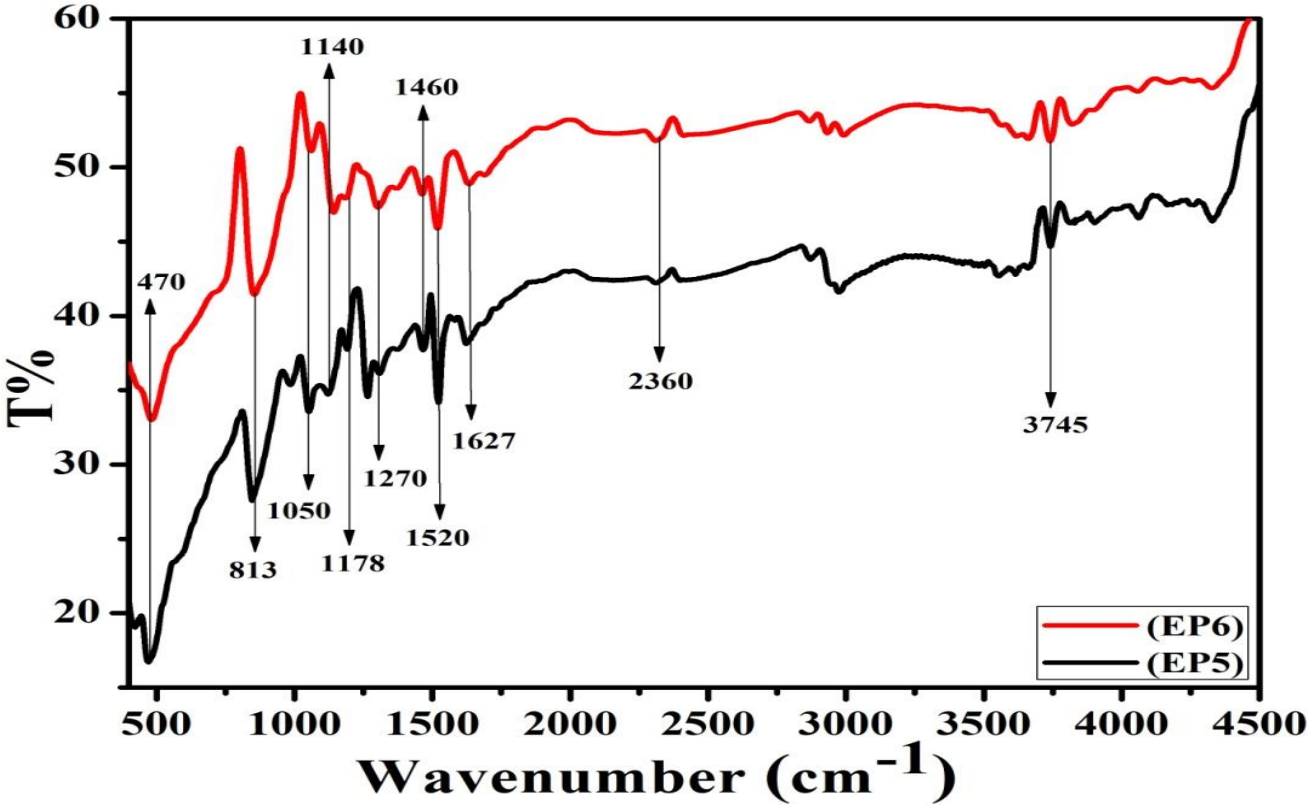


**Fig.5(A).5:** FTIR spectroscopy of composite of EP5and EP6

**Table. 5(A).1:** Characteristic bands obtained from FTIR spectra of quartz silica, nano organo silane and developed epoxy composite coating

| **Wavenumber ($cm^{-1}$)** | **Assignments** |
|---|---|
| 3743 | Free SiOH |
| 3090─3600 | OH of H—OH, Et—OH and Si—OH/N—H of primary and secondary amines |
| 2855─2995 | C—H of $CH_2$, $CH_3$/CH aromatic and aliphatic |
| 2849 | Symmetrical stretching of CH |
| 2360 | Steric effect of higher amine |
| 1722 | C═O |
| 1662 | N—H of primary amines |
| 1617 | H—O—H bending |
| 1585 | —C═C— aliphatic linkage |
| 1510 ─1615 | For benzene ring |
| 1460 | —C═C—for aromatic backbone |
| 1278 | Aliphatic —C─N— stretching |
| 1240 | —C—O—C— epoxide group |
| 1185 | Si—O—Si of ≡Si—O—Si≡/C—C—O—C |
| 1103 | Asym. Si—O—Si Stretching |
| 1038 | C—O—C of ethers |
| 968 | —C—O— stretching vibration of Si─OH bond |
| 803 | $SiO_4$ tetrahedron ring |
| 695 | Si—O—Si Stretching |
| 466 | O—Si—O |

FTIR studies were carried out to find out to what prolong these free OH group has interacted with the modification of nano organosiliane composite. Fig.5(A).1 and Fig.5(A).2 show the FTIR spectra of transmittance quartz silica, nano organo

silane particle. Fig.5(A).3 to Fig.5(A).5 display various type of developed composite coatings respectively. The band assignments of attribute peaks which have also given in Table.5(A).1 From Fig. the actual characteristics peaks are observed in the region 2855─3000cm$^{-1}$ [1,4,5] where CH─ stretching band are noticeable. Observed bands make sure alkyl group from the organo siliane particle in the surface of nano composite coating. Moreover, the intensity of the peaks increases from nano composite compare conventional composite ones when the number of methyl groups surrounding a Si atom increases more instance. It has seen that at band 3745cm$^{-1}$ maximum level of free SiOH belongs in nano organosiliane powder and nano composite coating [2,3].

The comparative FTIR studies are recorded from IR spectra data for each cured film after 2200hrs salt spray test and evaluated the degradation pattern of different composite coating system.

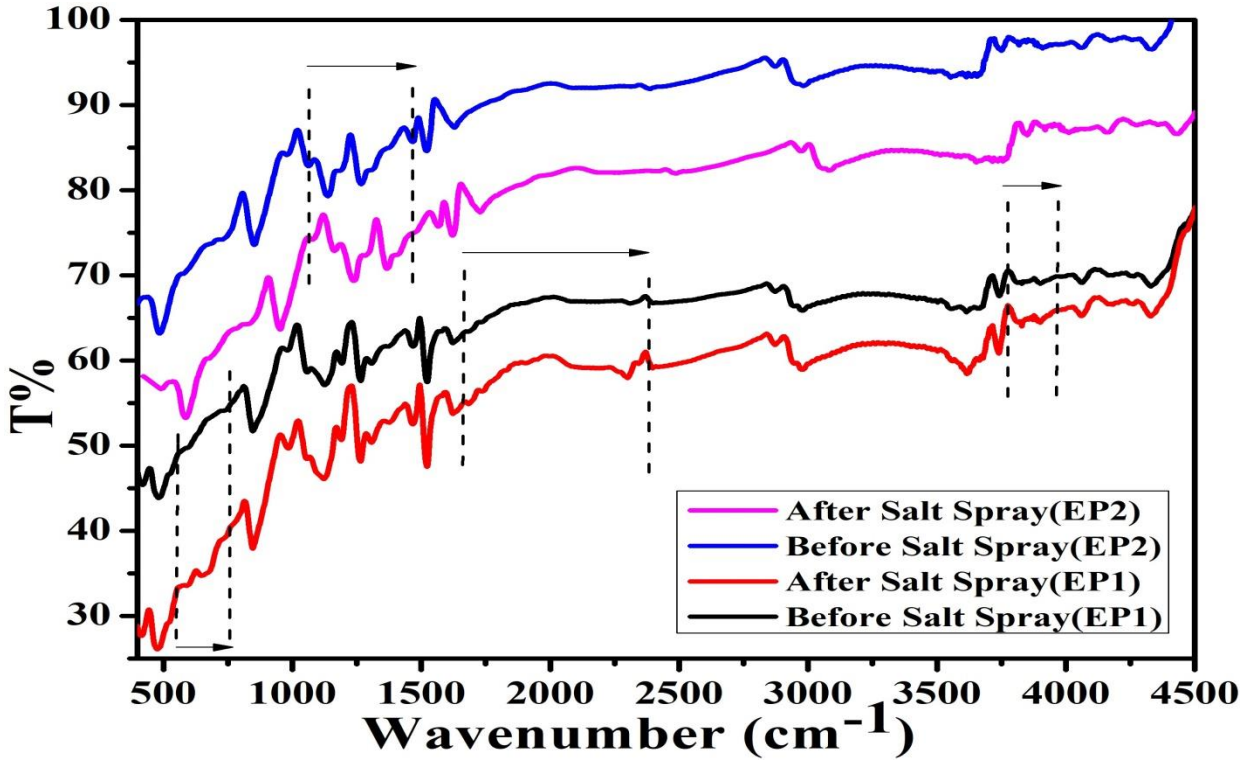


**Fig.5(A).6:** FTIR spectroscopy of composite of EP1 and EP2 before and after 2200hrs salt spray test

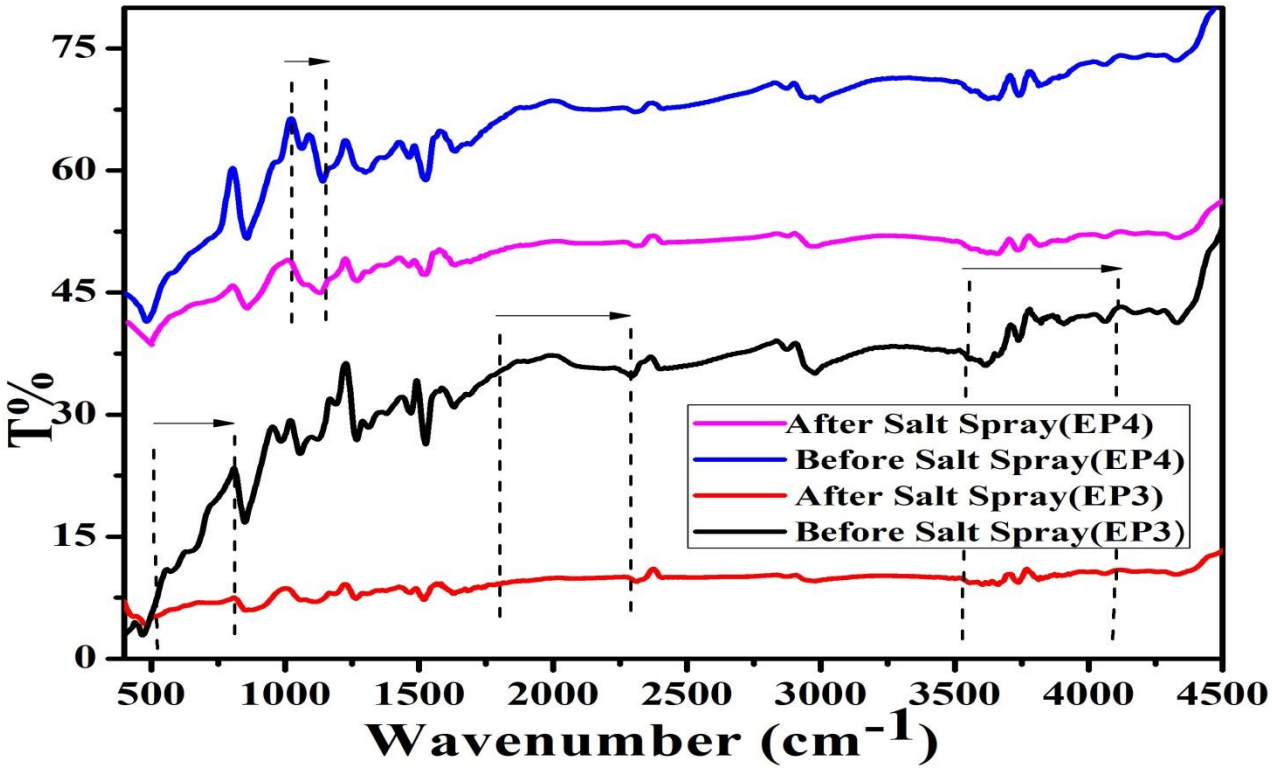


**Fig.5(A).7:** FTIR spectroscopy of EP3 and EP4 before and after 2200hrs salt spray test

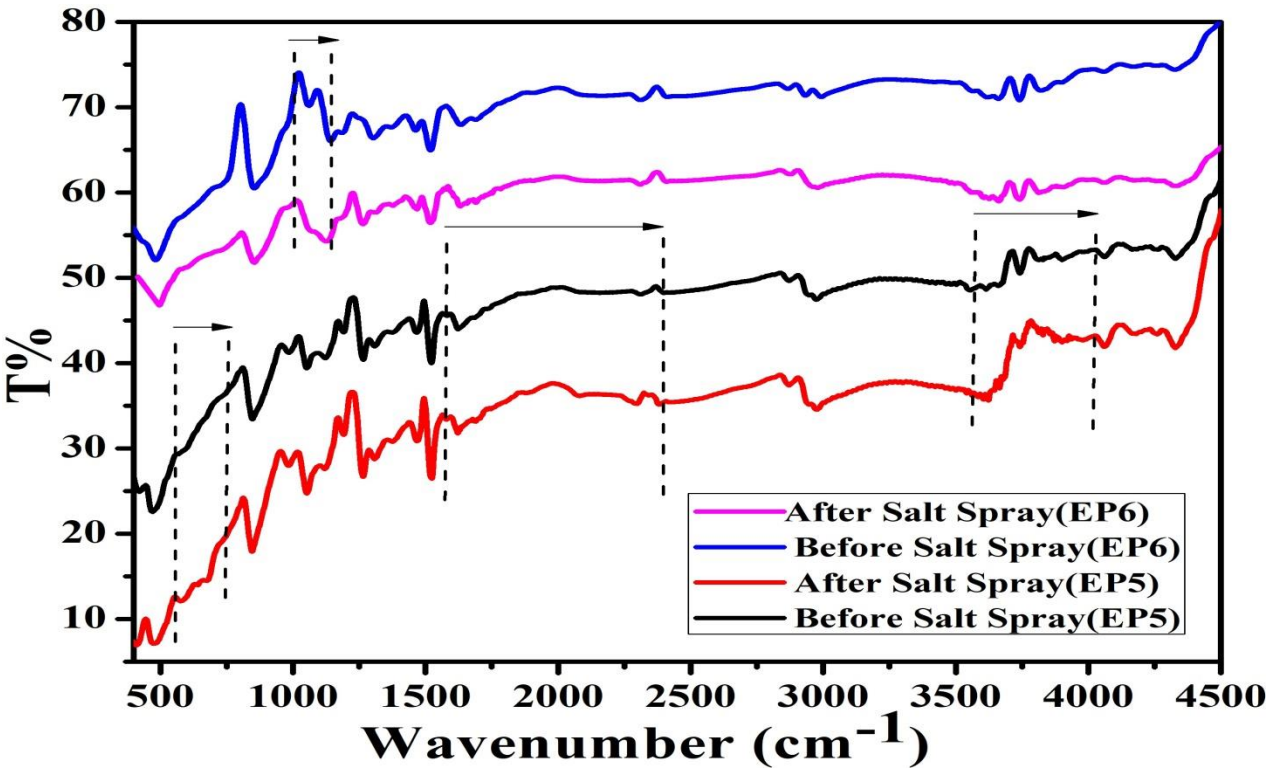


**Fig.5(A).8:** FTIR spectroscopy of EP5 and EP6 before and after 2200hrs salt spray test

In the salt spray chamber presence of saline water (5% Nacl solution) composite coating may be degrade mainly the functional group like ester, alkyl, amides and ethers etc are split and also new functional groups are generated. After 2200hrs of salt spray studied FTIR spectra recorded in Fig.5(A).6 to Fig.5(A).8 the relative transmittance of salt sprayed composite coatings are very closer to unprocessed one in case of epoxy nanocomposite coatings. Additional very weak bands are (i) 1058 to 1470 $cm^{-1}$ for EP2 (ii) 1018 to 1145 $cm^{-1}$ for EP4 and (iii) 1005 to 1138 $cm^{-1}$ for EP6 observed respectively in resin degradation of epoxy nanocomposite coatings. So, it can be concluded that there is no significant interaction between the glass flake epoxy nanocomposite coating and the salt spray, indicating limited resin degradation and offering a high level of resistance against corrosion. But in case of epoxy conventional coatings additional vibrational bond observed at (i) 3775 to 3963$cm^{-1}$ (ii) 1667 to 2336$cm^{-1}$ (iii) 543 to 750$cm^{-1}$ for EP1 coating, (i) 3554 to 4110$cm^{-1}$ (ii) 1801 to 2283 $cm^{-1}$ (iii) 509 to 810$cm^{-1}$ for EP3 coating and (i) 3568 to 4030$cm^{-1}$ (ii) 1580 to 2391$cm^{-1}$ (iii) 550 to 750$cm^{-1}$ for EP5 coating of resin degradation occurs from less instance band observed C—C and C—H stretching for alkynes in this region [6]. These generated peaks suggested that corrosion occurs in salt spray medium.

## 5.(A).2. XRD Patterns Analysis

The XRD peaks of quartz silica and organo silane nano particles are presented in Fig.5(A).9 and Fig.5(A).10. A broad pattern obtained at 2θ=22.21 (JCPDS No: 84-1286 and COD ID: 1010921) compared to the presence of $SiO_2$ crystalline particle it correlate that particles are amorphous in nature [5] different form of silica. In composites quarta silica, pigment of rutile $TiO_2$ and and extender of talc peaks are observed at different angles of 2θ values at ( *h k l* ) planes (Card No: 21-1276) and (COD ID: 10-00036) respectively values observed in Fig.5(A).11 to Fig.5(A).13.

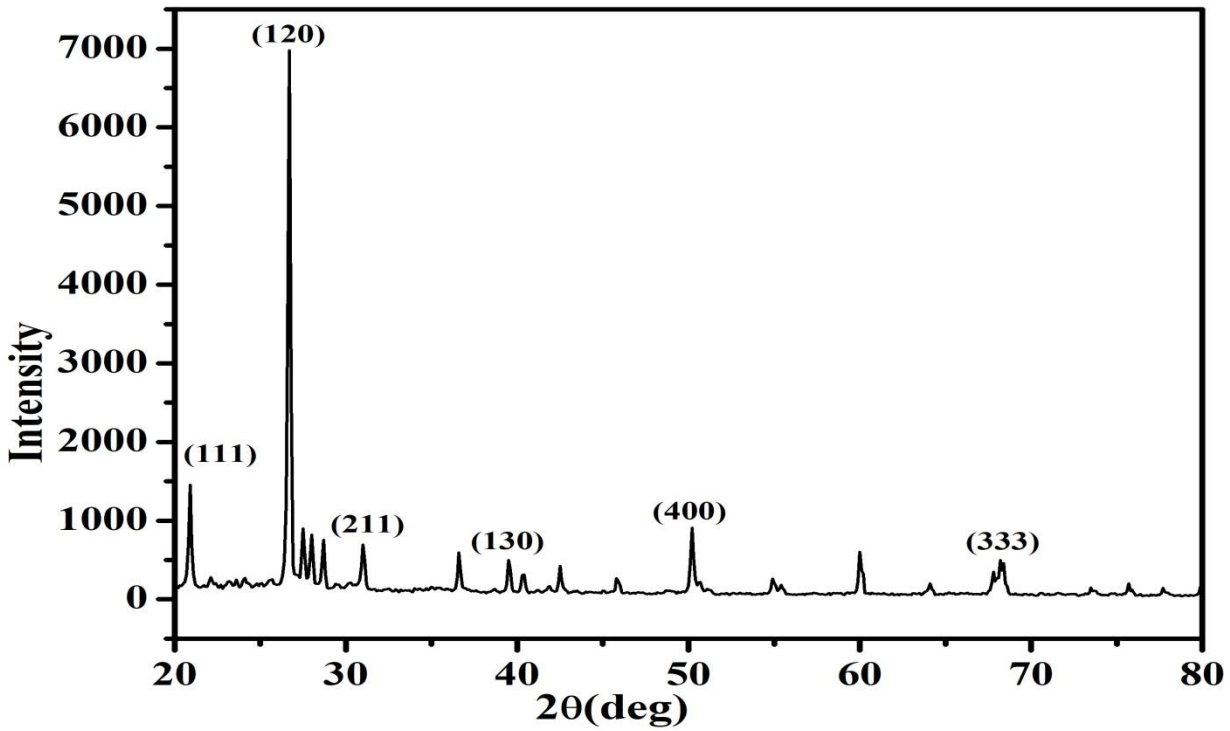


**Fig.5(A).9:** XRD pattern quartz silica particle

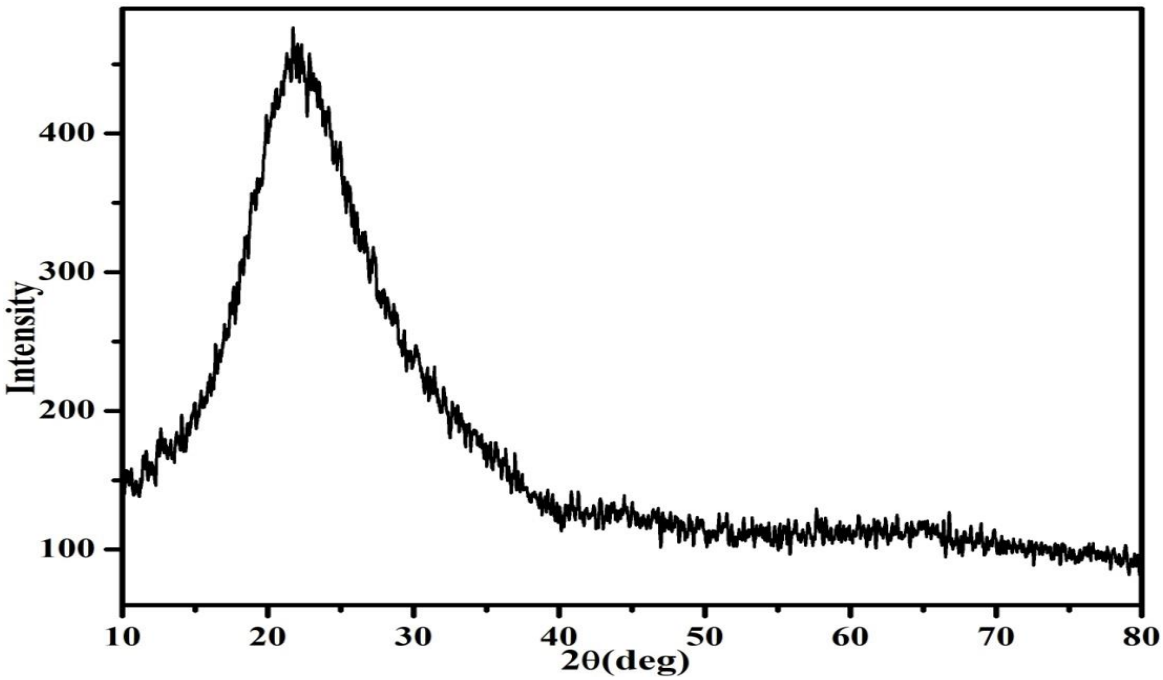


**Fig.5(A).10:** XRD pattern of organo silane nano particle

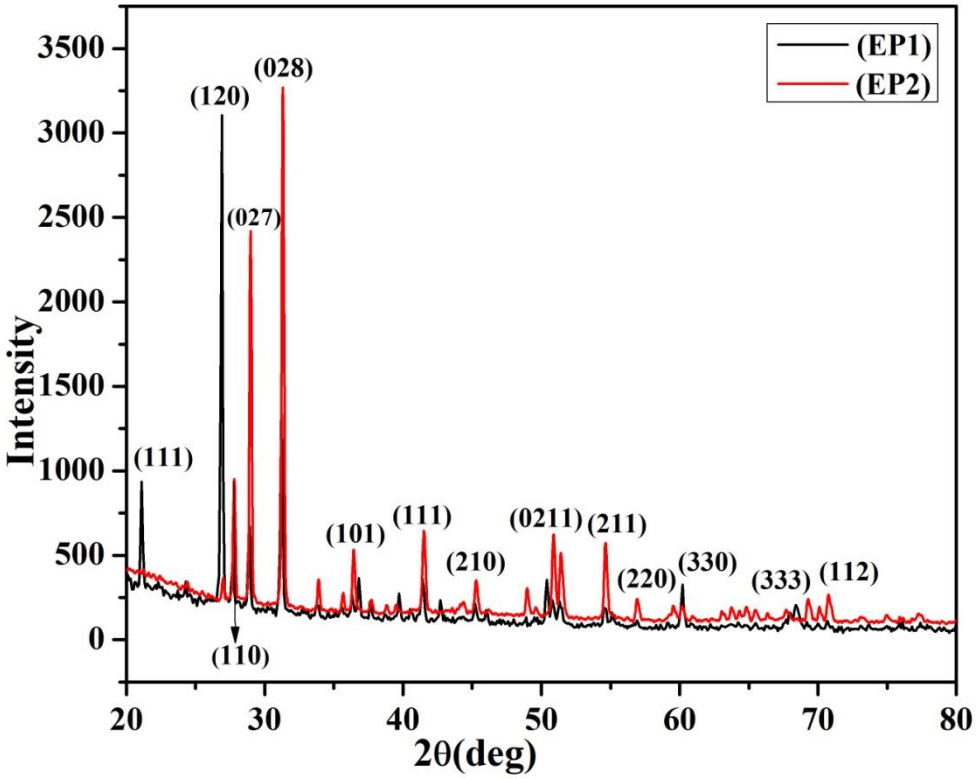


**Fig.5(A).11:** XRD pattern of epoxy composite coating of EP1 and EP2

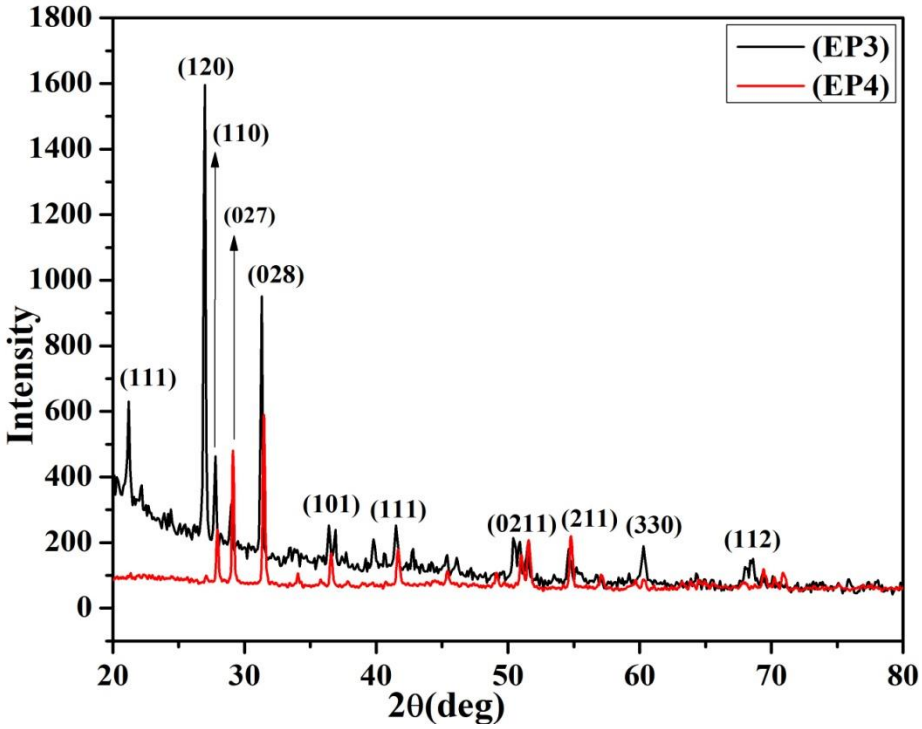


**Fig.5(A).12:** XRD pattern of epoxy composite coating of EP3 and EP4

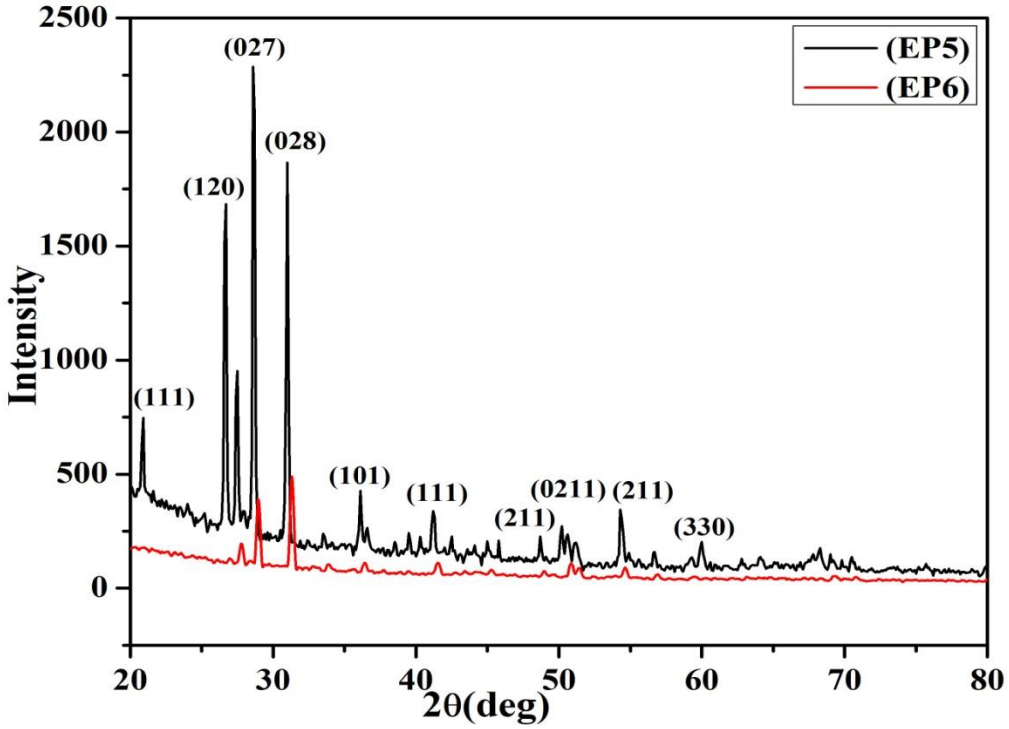


**Fig.5(A).13:** XRD pattern of epoxy composite coating of EP5 and E6

From Fig.5(A).11 to Fig.5(A).13, at different angles of 2θ values at ( *h k l* ) planes observed 20.90 *(1 1 1)*, 27.03 *(1 2 0)*, 31.02 *(2 1 1)* 39.40 *(130)* and 68.32 *( 3 3 3 )* for quartz silica, 27.76 *( 1 1 0 )*, 36.4 *( 1 0 1 )*, 41.4 *( 1 1 1 )*, 54.25 *( 2 1 1 )*, 56.6 *( 2 2 0 )* and 69.01 *( 1 1 2 )* for $TiO_2$ pigment, 29.06 *( 0 2 7 )*, 31.21 *( 0 2 8 )*, 51.2 *( 0 2 11 )* and 60.2 *( 3 3 0 )* for extender respectively. Now it is confirmed that all composition are fully embedded in epoxy matix but glass flake based nanocomposite developed more dense structure at curing time so, x ray beam cannot passed properly.

## 5.(A).3. Morphology Study

### 5.(A).3. 1. Scanning Electron Microscope (SEM)

For better corrosion performance of resultant nano coating it is very important to good wetting necessary of particles in nano sized in composite. All micrograophs

are depicted in Fig.5(A).14**,** at two different magnifications SEM images of conventional composite in (a) and (b) for EP1, (e) and (f) for EP3, (m) and (n) for EP5 where some particles are observed at micro level on the surface of coating and also micrographs also show heterogeneous dispersion of silica particles within the polymer matrix. The size distributions from 1μm to 10μm range, the particles are cluster form. From the SEM images of (c) and (d) for EP2, (g) and (h) for EP4, (o) and (p) for EP6, it is evident that the silica particle is fully wetted by the epoxy resin during composite formation. The micrographs also show uniform dispersion of silica particles within the polymer matrix. However, in epoxy filled of nano $SiO_2$, there are larger agglomerates and aggregates observed. Here at two different magnifications of images 1μm to 10μm used for both coatings observation.

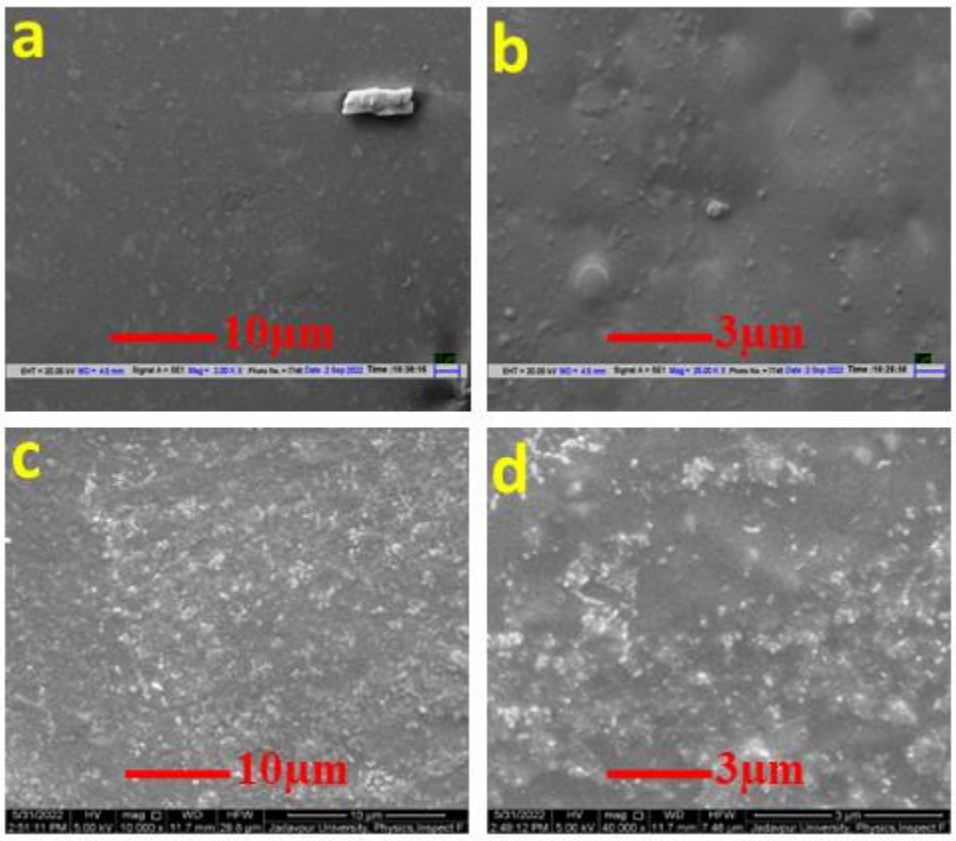

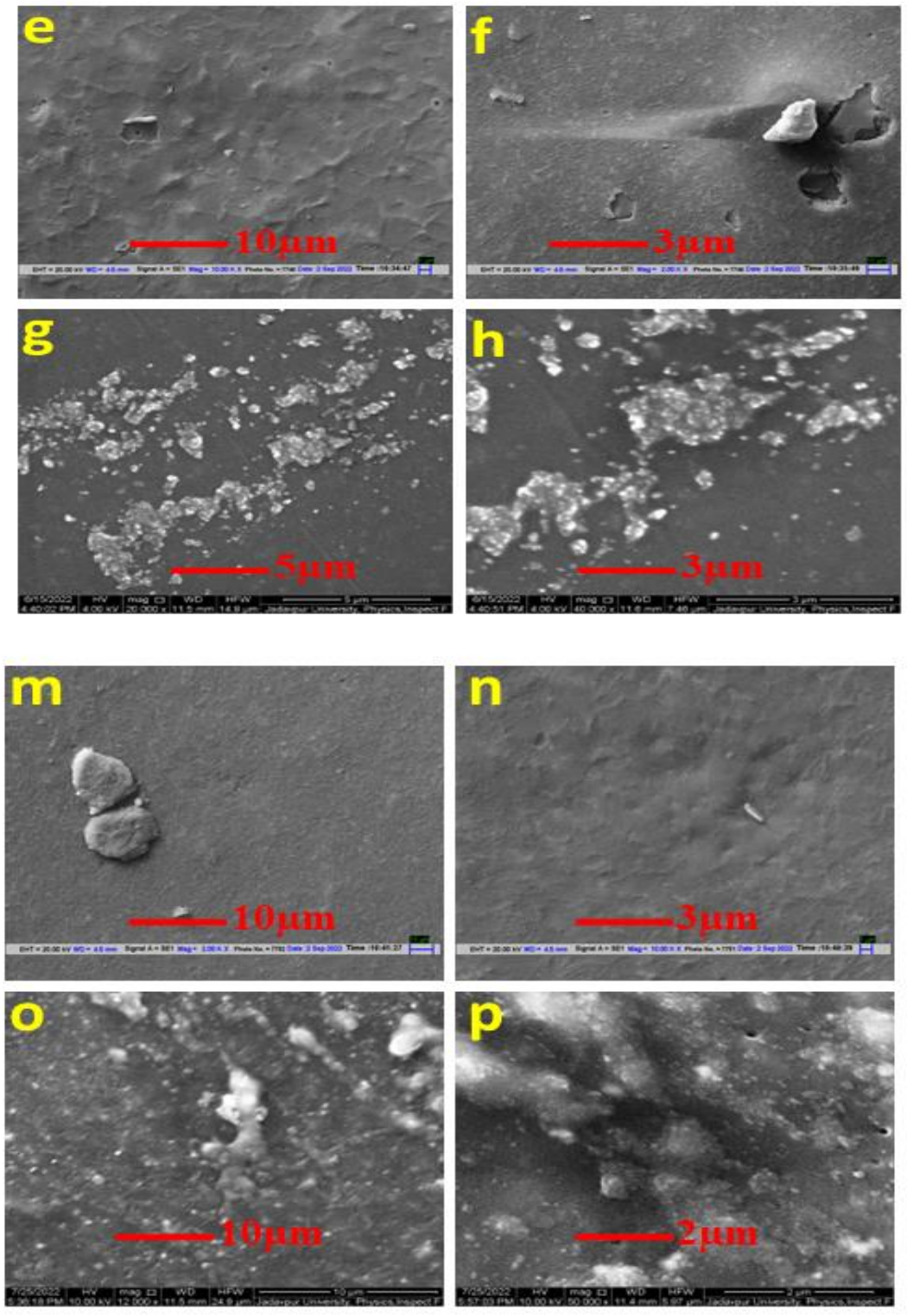


**Fig.5(A).14:** SEM images of conventional composite in (a) and (b) for EP1, (e) and (f) for EP3, (m) and (n) for EP5 and SEM images of dispersed nano silica in (c) and (d) for EP2, (g) and (h) for EP4, (o) and (p) for EP6 in the epoxy matrix.

## 5.(A).3.2. Transmission Electron Microscope (TEM)

The micrographs in Fig. 5(A).15 clearly show that organo-silane treated silica nanoparticles maintain their even distribution even at high concentrations of $SiO_2$ nano filler, resulting in particle sizes of less than 20 nm. The surface treatment of nanoparticles enhances steric hindrance between them, as schematically illustrated in Fig. 2.16. This treatment also improves their wet ability and compatibility within the polymeric matrix [8].

The improved dispersion and reduced aggregation observed in coatings containing SiO2 nanoparticles can be attributed to the higher concentration of methyl groups on the surface of these SiO2 nanoparticles, making them more hydrophobic.

TEM analyses have confirmed that surface-modified $SiO_2$ nanoparticles exhibit significantly improved dispersion within the epoxy matrix compared to untreated SiO2 nanoparticles. The purpose of TEM analysis is to assess the morphology and the extent of dispersion of surface-treated $SiO_2$ nanoparticles, which plays a crucial role in influencing the corrosion performance of the resulting nanocoatings. The use of Image J software indicates that the detected organosilane particle size is less than 20 nm. The size of the silica particles depicted in Fig. 5(A).15 to Fig. 5(A).17 falls within the range of 50 nm and exhibits a spherical shape, with even distribution within the epoxy matrix.

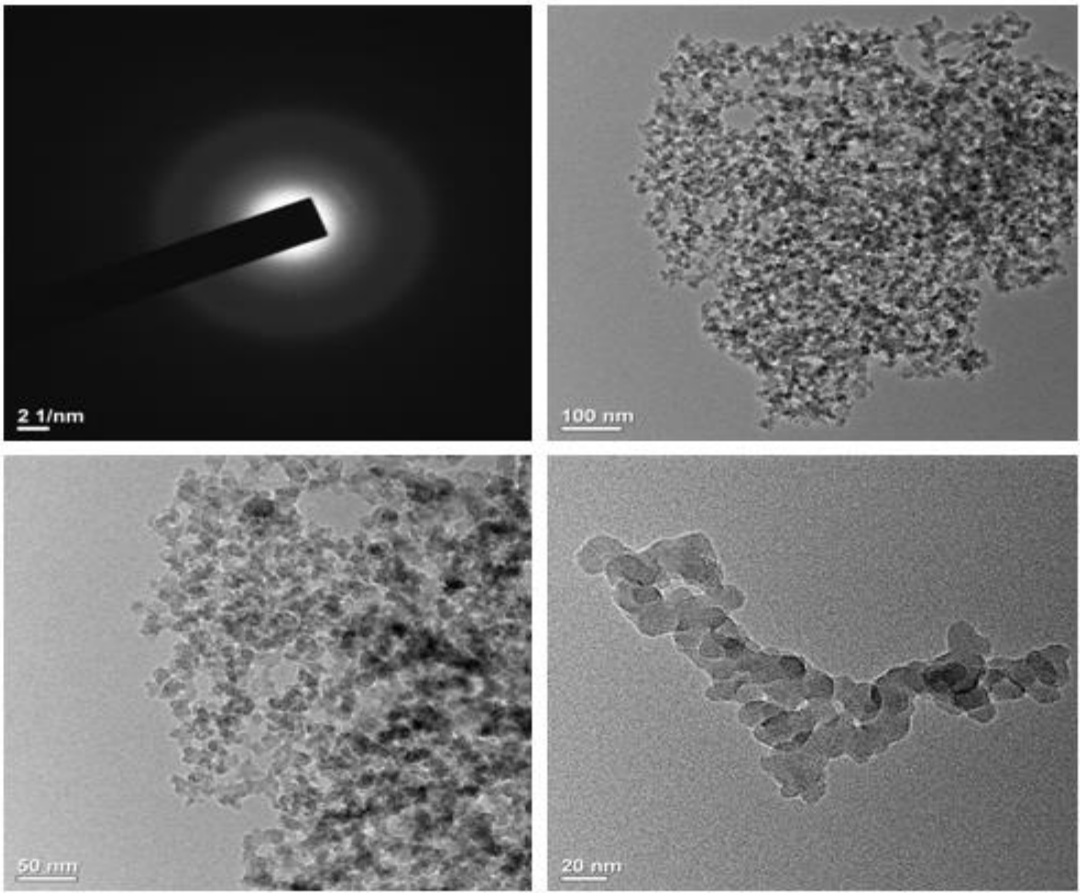


**Fig.5(A).15:** Transmission electron images of nano organosilane (R972) particle

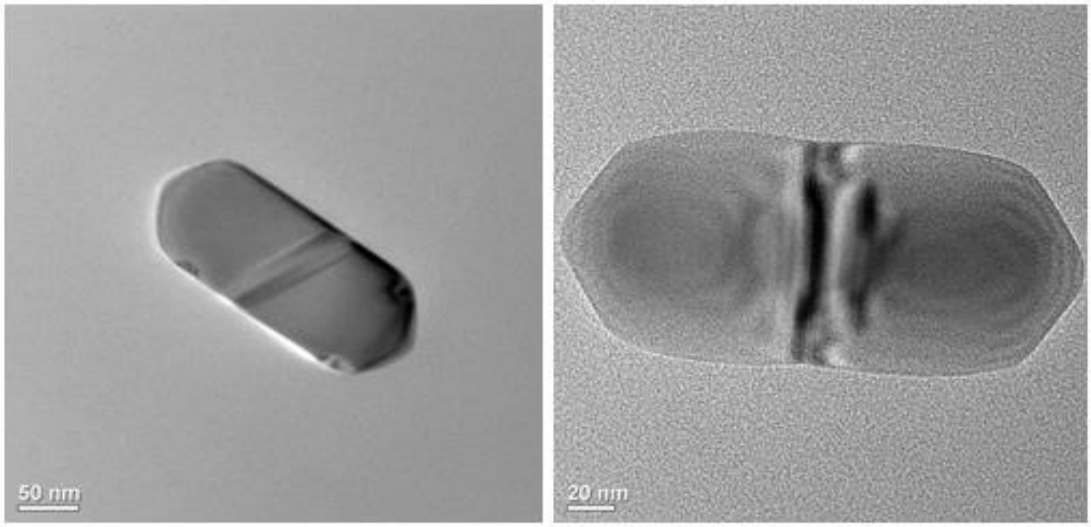


**Fig.5(A).16:** Transmission electron images of epoxy nano composite coating of EP2

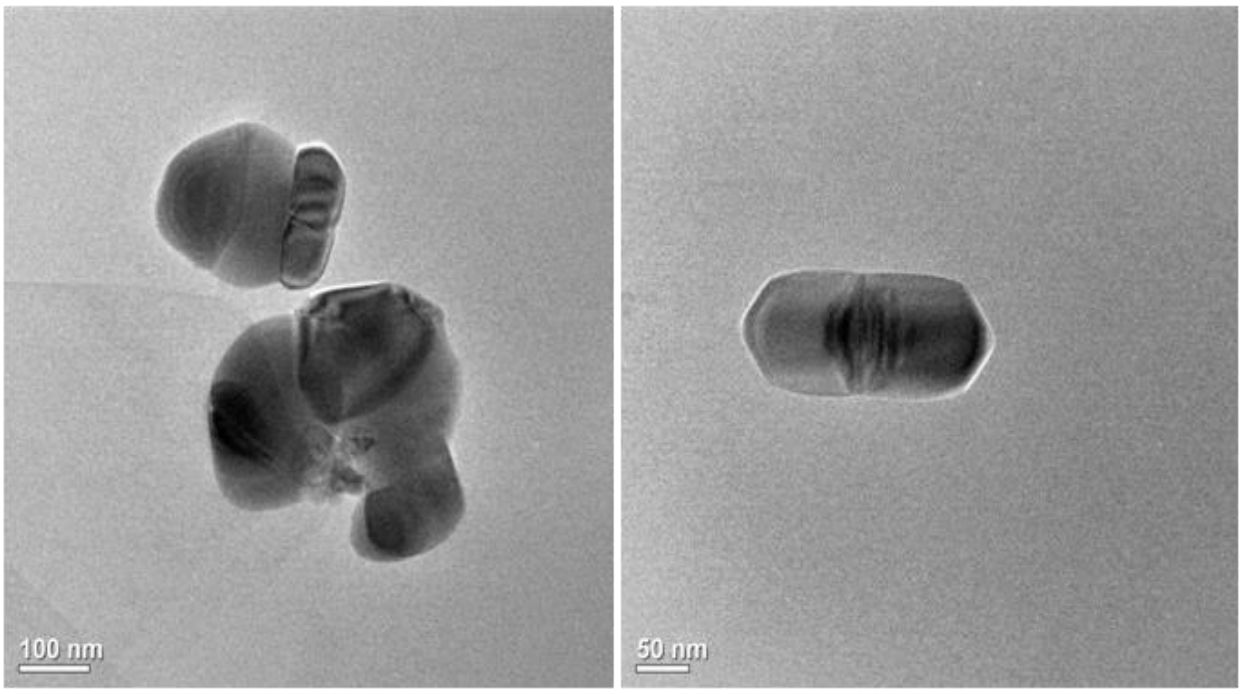


**Fig.5(A).17:** Transmission electron images of epoxy nano composite coating of EP4

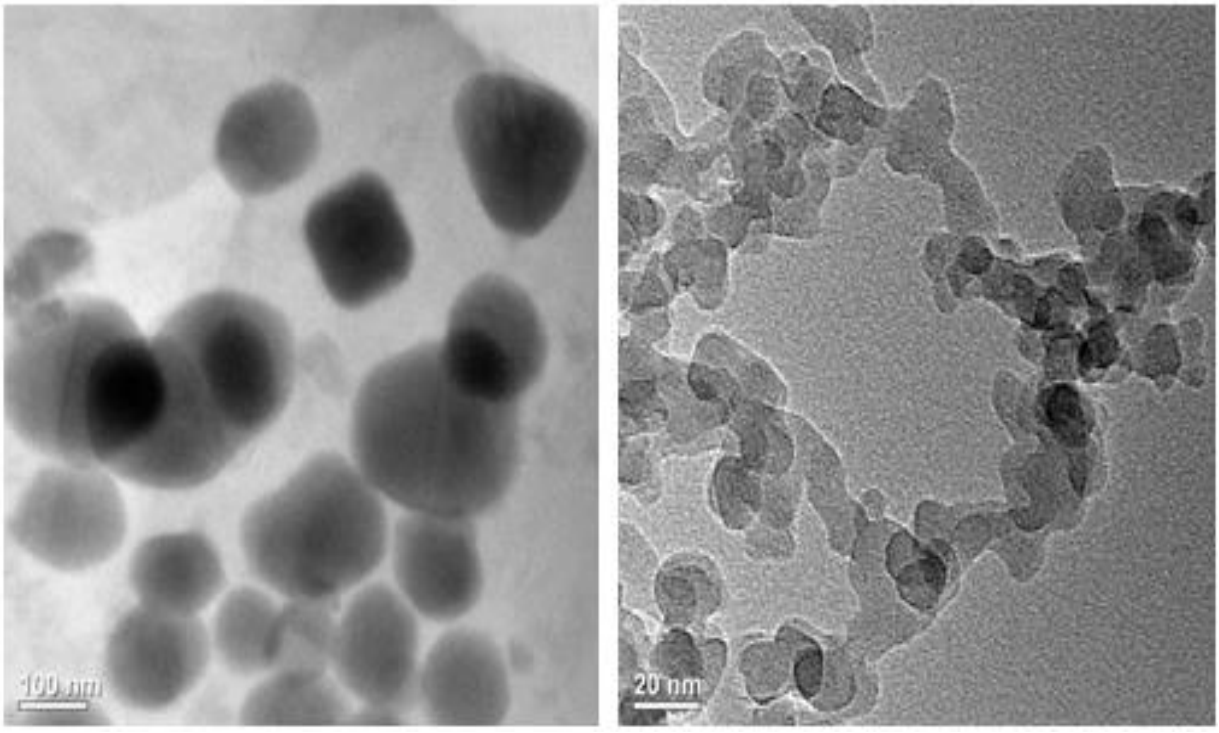


**Fig.5(A). 18:** Transmission electron images of epoxy nano composite coating of EP6

## 5.(A).4. Thermal Analysis (TGA-DTA)

Thermal stability of all silica based epoxy composite film was studied by TGA-DTA method in Fig.5(A).19 to Fig.5(A).21. From thermograms firstly it has observed degrade long aliphatic chain in phenalkamine at lower temperature and secondly degrade of crosslinked epoxy polymer at higher tempreature.

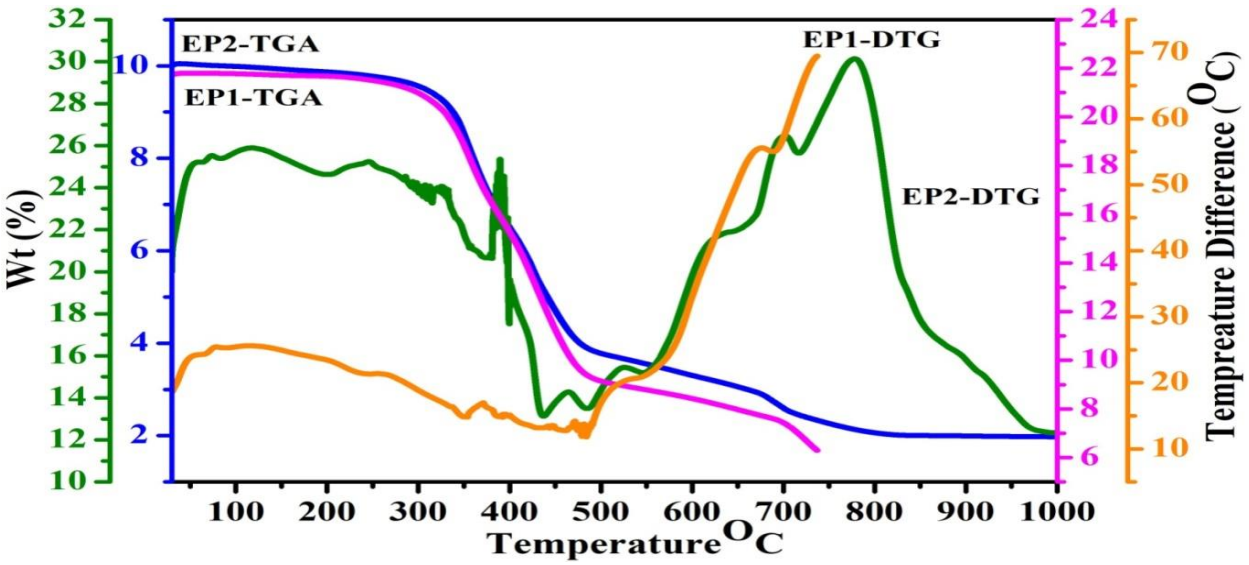


**Fig.5(A).19**: TGA-DTA thermogram for EP1and EP2 epoxy composite film

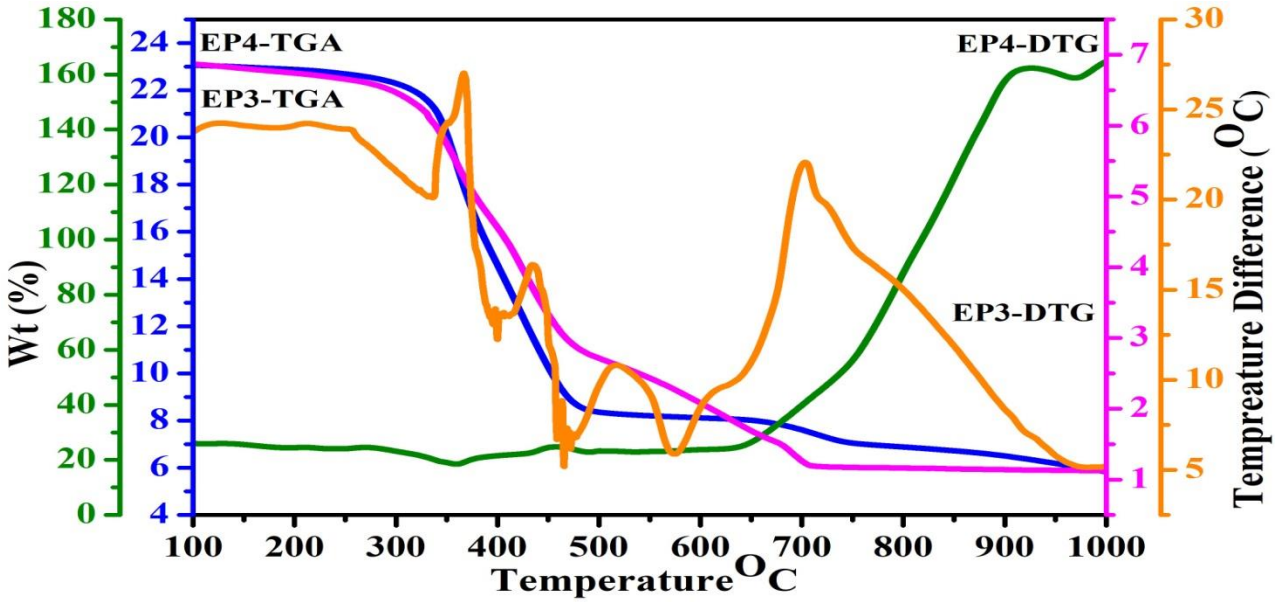


**Fig.5(A).20**: TGA-DTA thermogram for EP3 and EP4 epoxy composite film

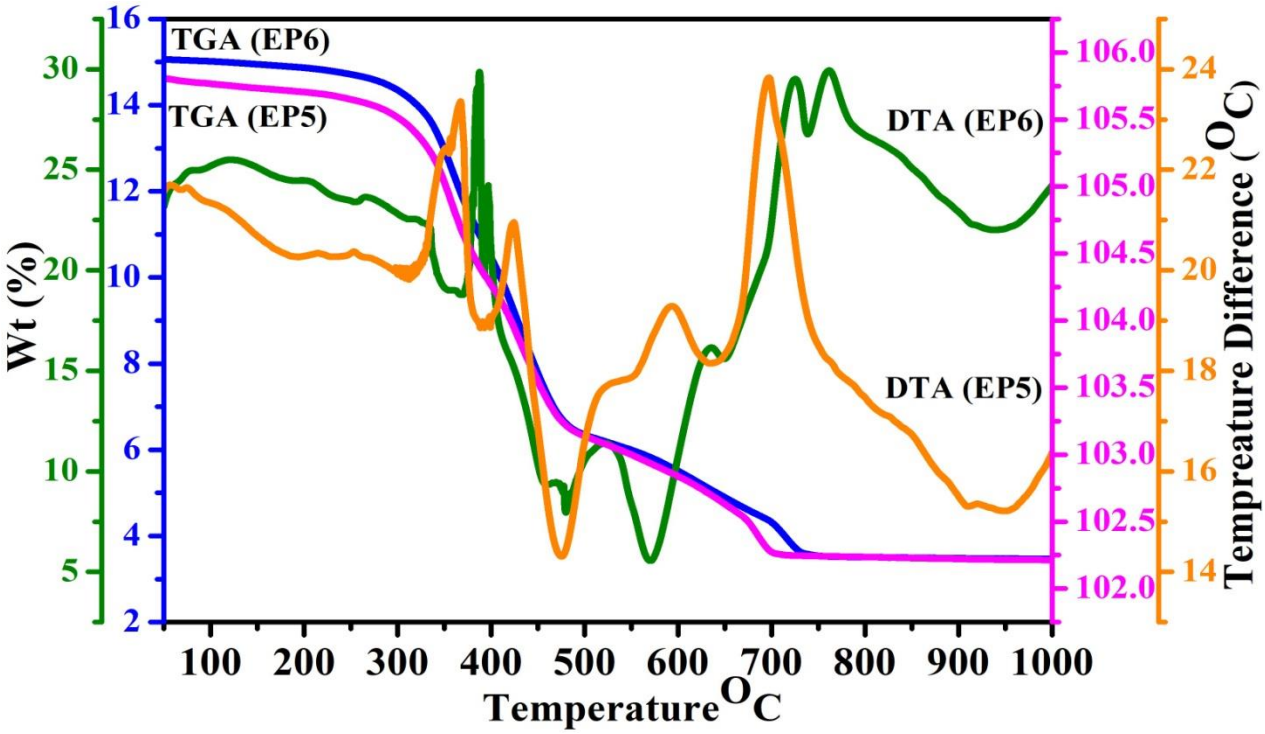


**Fig.5(A).21:** TGA-DTA thermogram for EP5 and EP6 epoxy composite film

At initial stage, when all samples are heated above 200-250$^{O}$C epoxy-amine linkges are broken and further heated at 300$^{O}$C the reaction of Mannich Bridge clevagee noticed. Above 450$^{O}$C composite coating of conventional one decomposes to amines, phenolic and benzene derivatives. Further degradation for cured nano composite coating happened near at well above 750$^{O}$C.

Glass transition temperature decreased to 310$^{O}$C compared to quartz silica particles. Weight loss observed up to 760$^{O}$C. At 400$^{O}$C organic part of epoxy disintegrated with 26.7% weight loss for EP5 compared EP3 than EP1. At, 460$^{O}$C nano particle $SiO_2$ in composite remained with 38.4% residue for EP6 compared EP4 than EP. DTA diagram predicted endothermic reaction occurred at 400 to 600$^{O}$C for solvent evaporation. Exothermic reaction occurred 350 to 800 $^{O}$C due to binder disintegration in composite coating.

Moreover, less thermal stability of conventional cured composite coating than that of nano composite coating and it perhaps attribute to exsistance of more long lenghted hydrophobic units in composition which influence interactions at the polymer and nano filler interfaces in the matrix.

## 5 (A). 5. Physico-Mechanical Properties

After holiday (electrical insulation) test, no audio visual sound, any spark pinhole break and presence of conductive particles observed from any coated panel. Here, with regard to the mixing ability of the formation viscosity play significant role, it is observed that with the addition of nano organo silane resulted increases viscosity as compared to addition of conventional qurtz silica due to the silica nano particles have interfacial interaction with high surface area for contact with the polymer chains in composite matrix. The others mechanical behaviors like DFT (Dry Film Thickness), flexibility in Fig.5(A).19, scratch hardness, pencil hardness, adhesion, and fallings ball impact in Fig.5(A).20 and abrasion resistance of composite coatings were studied and evaluated and the results are provide below. DFT of every composite coating is 200±10 micron. It is seen by flexible nature follows EP2 > EP6 > EP4 > EP3 > EP5 > EP1. Nano composite coating shows better results of scratch and pencil hardness than conventional silica due to hardness and cross linking density are proportional of the coating of composite. Falling ball impact test shows good because dispersion of nano fillers are uniformed which give more cross link elastomeric rigid structure. The cross-linking density of composite thermosets was studied by % swelling method in xylene. EP2 has better crosslink than others because of longer lengthed hydrophobic chains on the surface of nano filler, extremely enhances the interactions at the polymer interfacial segments [6-8].

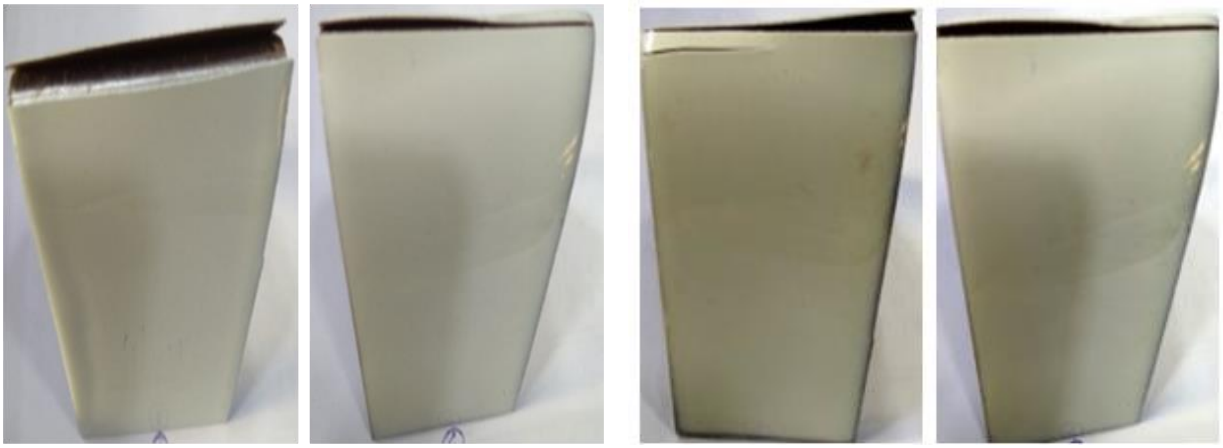

EP1 EP2 EP3 EP4

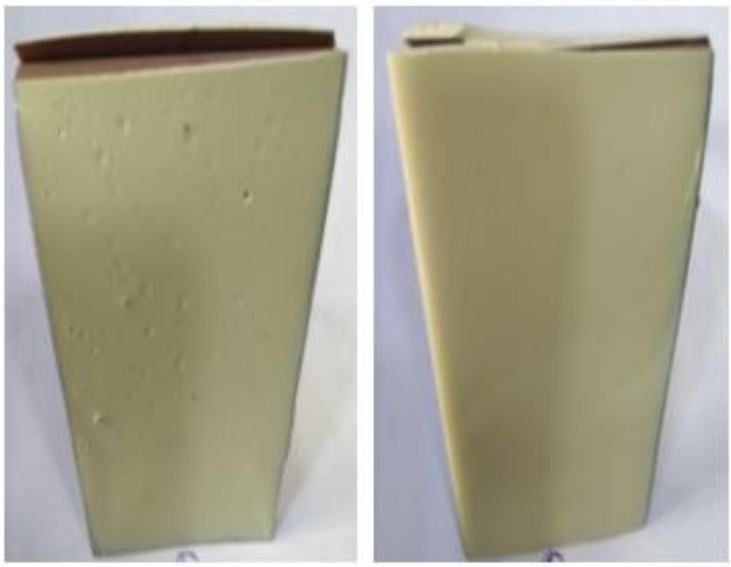

EP5 EP6

**Fig.5 (A).22:** Images of flexibility test of coated epoxy composite coating on MS panel

**Table. 5(A).2:** Result of scratch hardnes and pencil hardness of coated epoxy composite coating on MS panel

| Coating code Name | 500 gm Weight | 1000 gm Weight | 1500 gm Weight | Hardness (6B to 6H) |
|---|---|---|---|---|
| EP1 | Passed | Passed | Failed | Failed at 2H |
| EP2 | Passed | Passed | Passed | Passed |
| EP3 | Passed | Passed | Failed | Passed |
| EP4 | Passed | Passed | Passed | Passed |
| EP5 | Passed | Passed | Passed | Passed |
| EP6 | Passed | Passed | Passed | Passed |

In the epoxy composite coating incorporated nano silica remarkably improve abrasion resistance with the minor weight loss than dispersion of silica micro particles in polymer matrix. It is calculated of all composite coatings, weight loss from wear index data 7.8 mg/1000cycles for conventional composite coating. Since in nano silica composite coating, it is observed 2.1 mg/1000cycles which indicate uniform distribution of nano particles in polymer chains give more tough three dimensional network structure.

The adhesion properties of before and after salt spary test nanocomposite coatings shows excellent than conventional coatings due to distribution of nano particle increases more crosslink density in polymer matrix.

EP1 EP2 EP3 EP4

EP5 EP6

**Fig. 5 (A). 23:** Images of falling ball impact test of epoxy composite coating on MS panel

**Table. 5(A).3:** Result of Physico-Mechanical testing of epoxy composite coating

| Coating code name | Cross link Density (%) | Adhesion Property ($N/mm^2$) | | Impact Test (KG.M) | | Abrasion Test (mg/cycles) | Gloss |
|---|---|---|---|---|---|---|---|
| | | Before Salt Spray | After 2200 hrs Salt Spray Test | Instrusion | Extrusion | | At $60^O$ angle |
| EP1 | 85 | 23.5 | 7.8 | >1.3 | >1.5 | 7.8 | 90 |

| | | | | | | | |
|---|---|---|---|---|---|---|---|
| EP2 | 97 | 43.7 | 29.8 | >0.7 | >0.9 | 3.8 | 123 |
| EP3 | 87 | 33.8 | 23.6 | >0.9 | >0.7 | 6.2 | 111 |
| EP4 | 95.8 | 45.3 | 32.3 | >0.3 | >0.4 | 2.1 | 147 |
| EP5 | 83.65 | 32.5 | 16.2 | >0.6 | >0.8 | 4.7 | 105 |
| EP6 | 96.20 | 44.2 | 36.1 | >0.2 | >0.2 | 2.3 | 152 |

## 5.(A).6. Corrosion Studies

### 5(A).6.1. Tafel curves analysis of the uncoated rod and various composite epoxy coatings

Uncoated MS rod and various epoxy composite coatings were immersed in 3.5 wt% Nacl solution. Polarization curves were studied at periodic time (initial, 1, 7, 15, and 30 days). Electrochemical parameters measured included corrosion potential ($E_{corr}$), cathode Tafel slope ($\beta_c$), anode Tafel slope ($\beta_a$), corrosion current ($I_{corr}$), polarization resistance ($R_p$), and corrosion current density ($J_{corr}$). Fig.5(A).24 for uncoated MS rod and Fig.5(A).25 to Fig.5(A).30 depicted for Tafel curves of developed epoxy composite coatings.

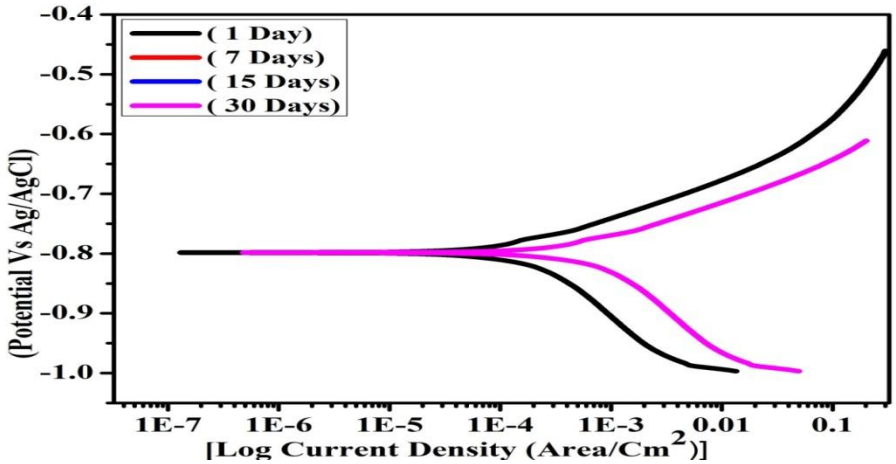


**Fig.5(A).24:** Tafel curves for uncoated MS rod after (1, 7, 15, and 30) days of immersion in 3.5 wt% Nacl aqueous solution

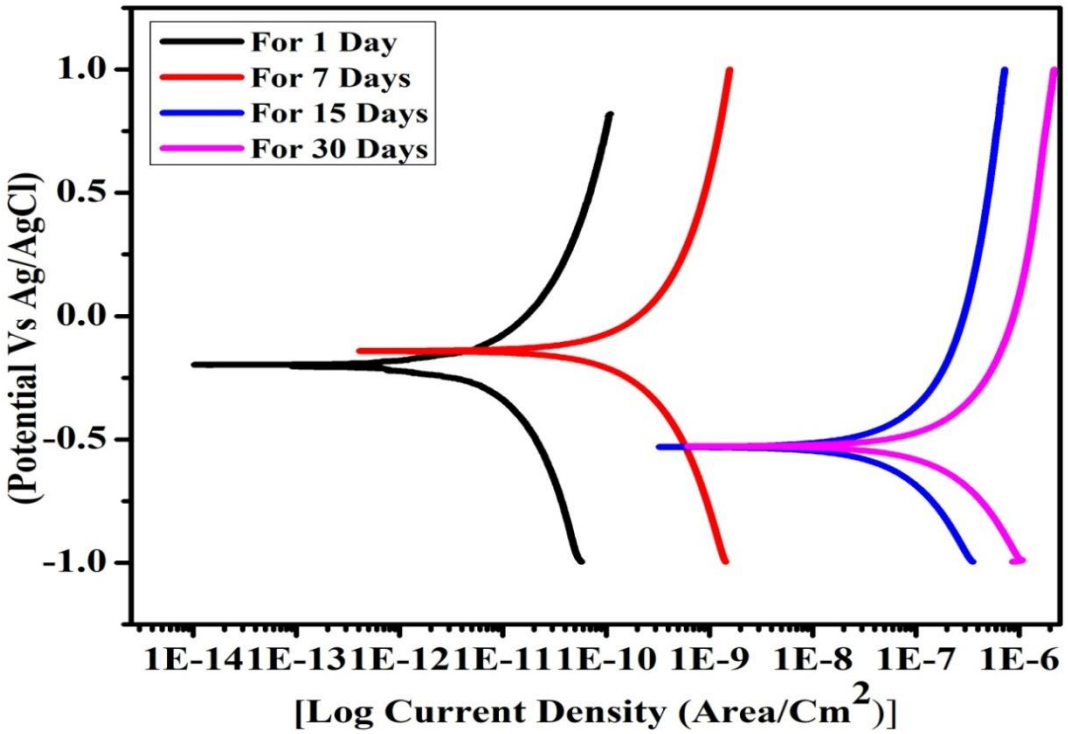


**Fig.5(A).25:** Tafel curves for epoxy composite coating EP1 after (1, 7, 15, and 30) days of immersion in 3.5 wt% Nacl aqueous solution

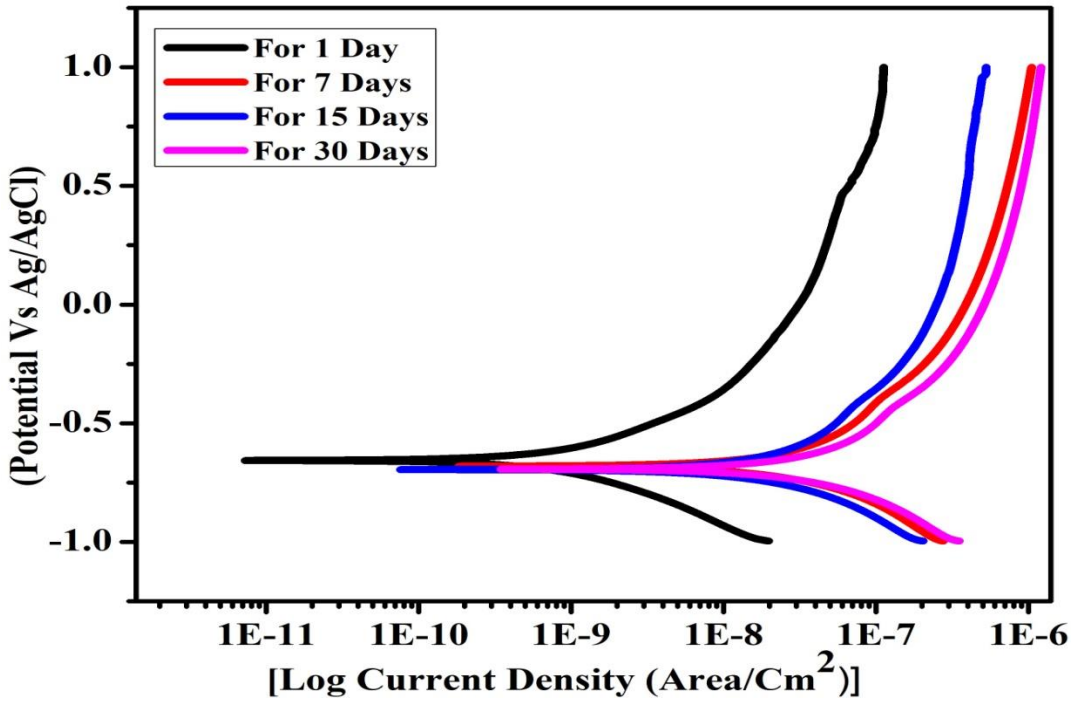


**Fig.5(A).26:** Tafel curves for epoxy composite coating EP2 after (1, 7, 15, and 30) days of immersion in 3.5 wt% Nacl aqueous solution

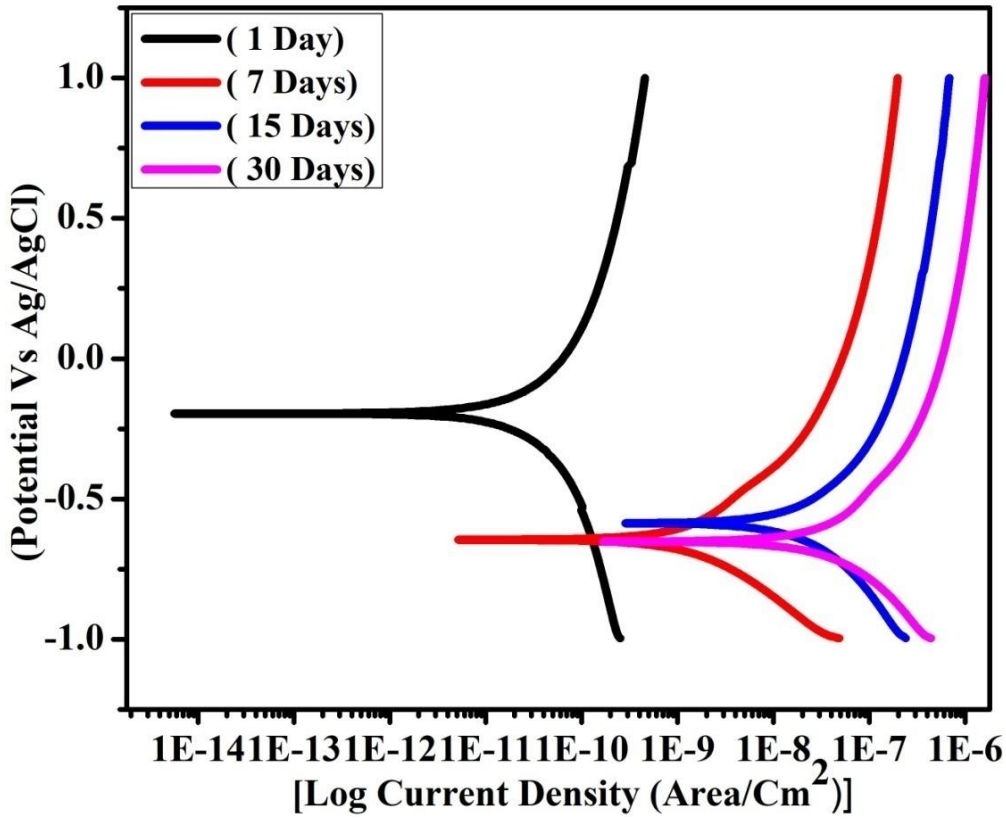


**Fig.5(A).27:** Tafel curves for epoxy composite coating EP3 after (1, 7, 15, and 30) days of immersion in a 3.5 wt% Nacl aqueous solution

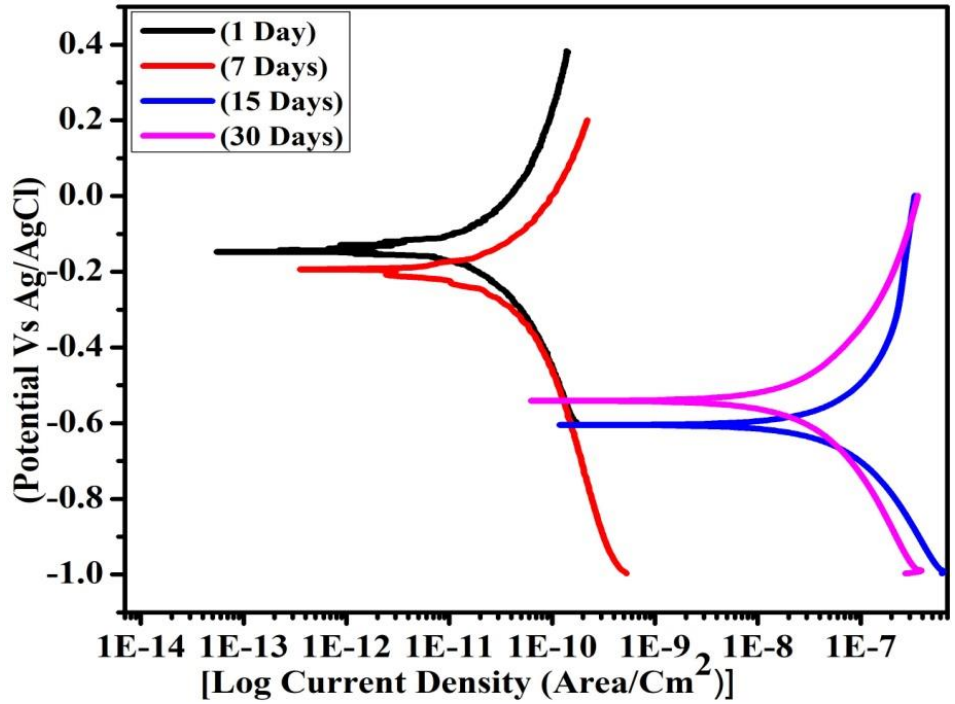


**Fig.5(A).28**: Tafel curves for epoxy composite coating EP4 after (1, 7, 15, and 30) days of immersion in a 3.5 wt% Nacl aqueous solution

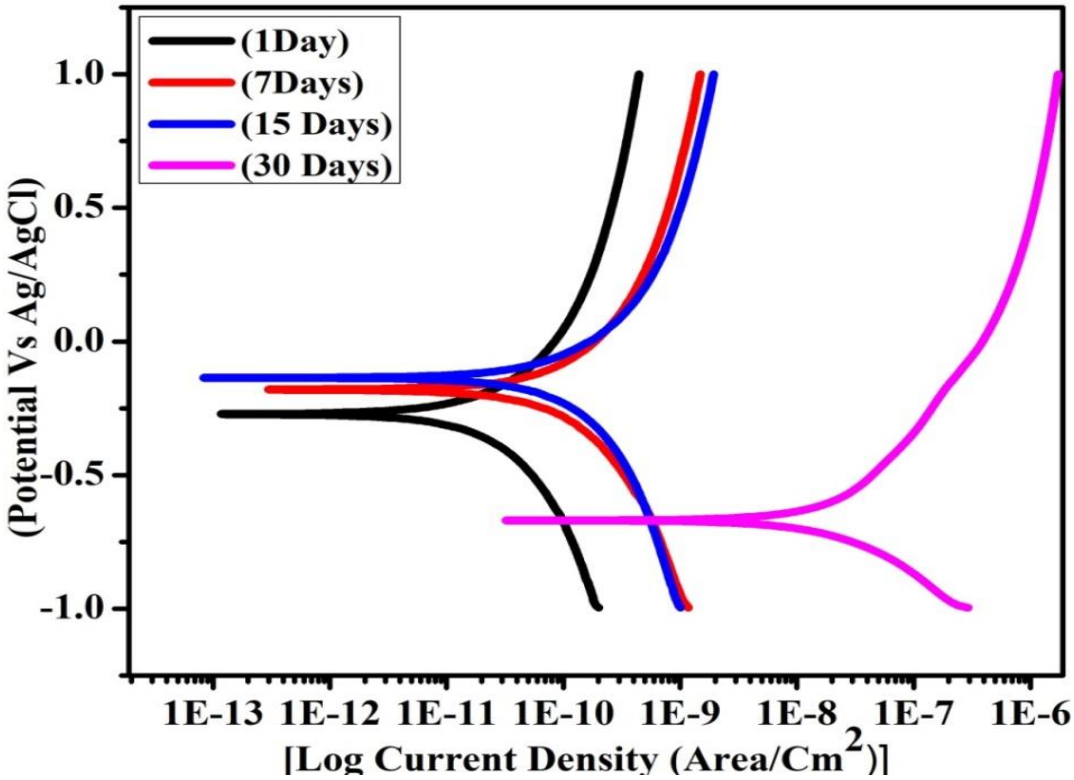


**Fig.5(A).29:** Tafel curves of epoxy composite coating of EP5 after (1, 2, 15 and 30) days immersions in 3.5 wt% Nacl aqueous solution

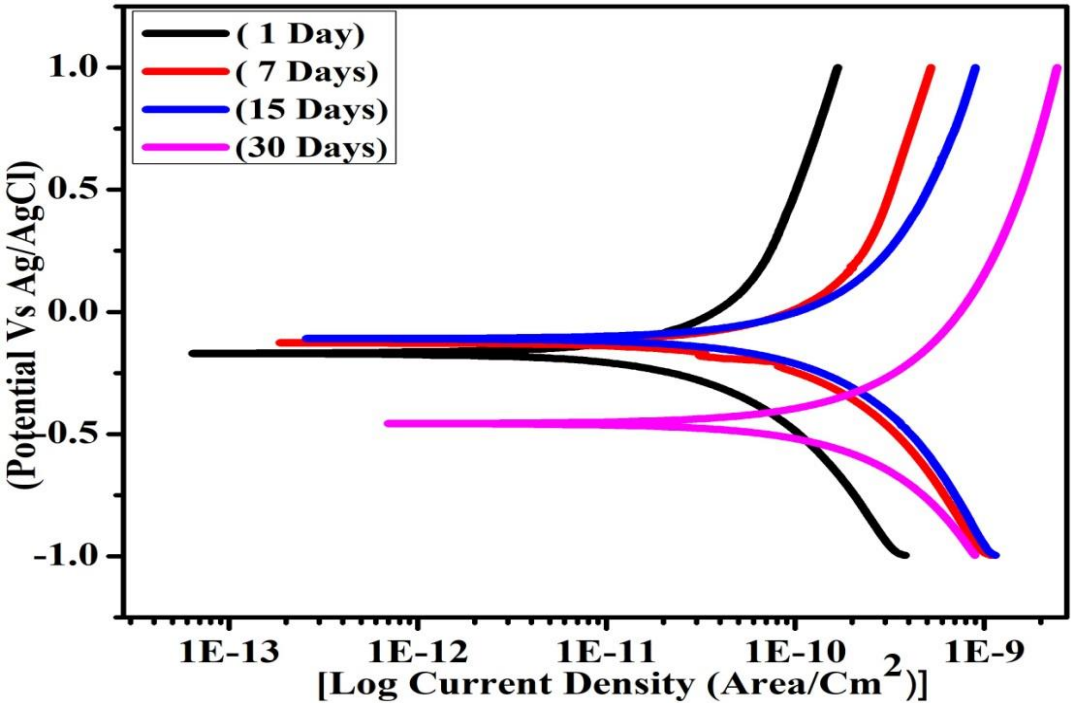


**Fig.5(A).30:**Tafel curves of epoxy nano composite coating of EP6 after (1, 7, 15 and 30) days immersions in 3.5 wt% Nacl aqueous solution

**Table.5(A).4:** Electrochemical parameters after soaking for periodic time intervals (1, 7, 15 and 30) days of polarization measurements of uncoated MS rod

| Samples Name | Day(s) | $-E_{corr}$ (V vs SCE) | $J_{corr}$ ($A/cm^2$) | $I_{corr}$ ($mA\ cm^{-2}$) | Corrosion rate (mm/year) | $R_p$($\Omega\ cm^2$) | βa ($mV\ dec^{-1}$) | βc ($mV\ dec^{-1}$) |
|---|---|---|---|---|---|---|---|---|
| Uncoated MS rod | 1 | ─0.805 | 7.38E-05 | 2.00E-05 | 0.85773 | 617.1 | 0.053 | 0.62 |
| | 7 | ─0.910 | 4.63E-05 | 1.25E-05 | 0.8721 | 177.66 | 0.400 | 0.005 |
| | 15 | × | × | × | × | × | × | × |
| | 30 | × | × | × | × | × | × | × |

**Table.5(A).5:** Electrochemical parameters after soaking for periodic time intervals (1, 7, 15 and 30) days of polarization measurements of EP1 and EP2

| Samples code name | Day (S) | $-E_{corr}$ (V vs SCE) | $J_{corr}$ ($A/cm^2$) | $I_{corr}$ ($mA\ cm^{-2}$) | Corrosion rate (mm/year) | $R_p$($\Omega\ cm^2$) | βa ($mV\ dec^{-1}$) | βc ($mV\ dec^{-1}$) |
|---|---|---|---|---|---|---|---|---|
| EP1 | 1 | ─0.403 | 3.16E-12 | 6.57E-11 | 3.67E-08 | 9.07E+08 | 0.268 | 0.281 |
| | 7 | ─0.310 | 6.87E-11 | 1.42E-09 | 7.98E-07 | 4.59E+07 | 0.264 | 0.352 |
| | 15 | ─0.580 | 6.42E-08 | 5.03E-07 | 0.00028 | 1.10E+05 | 0.262 | 0.247 |
| | 30 | ─0.594 | 8.16E-08 | 1.69E-06 | 0.00094 | 30446 | 0.294 | 0.290 |
| EP2 | 1 | ─0.517 | 2.3E-10 | 1.19E-08 | 2.17E-06 | 4.27E+06 | 0.178 | 0.181 |
| | 7 | ─0.568 | 1.82E-08 | 4.07E-07 | 0.00021 | 3.88E+05 | 0.263 | 0.227 |
| | 15 | ─0.590 | 1.27E-08 | 2.76E-07 | 0.00014 | 3.98E+05 | 0.257 | 0.203 |
| | 30 | ─0.590 | 2.01E-08 | 4.73E-07 | 0.00024 | 108392 | 0.235 | 0.196 |

**Table.5(A).6.** Electrochemical parameters after soaking for periodic time intervals (1, 7, 15 and 30) days of polarization measurements of EP3 and EP4

| Samples code name | Day (S) | $-E_{corr}$ (V vs SCE) | $J_{corr}$ ($A/cm^2$) | $I_{corr}$ ($mA\ cm^{-2}$) | Corrosion rate (mm/year) | $R_p$($\Omega\ cm^2$) | βa ($mV\ dec^{-1}$) | βc ($mV\ dec^{-1}$) |
|---|---|---|---|---|---|---|---|---|
| EP3 | 1 | −0.194 | 1.40E-11 | 2.94E-10 | 1.62E-07 | 2.11E+08 | 0.283 | 0.288 |
| | 7 | −0.664 | 7.56E-10 | 1.58E-08 | 8.78E-06 | 2.33E+06 | 0.189 | 0.155 |
| | 15 | −0.584 | 8.04E-09 | 1.68E-07 | 9.34E-05 | 2.17E+05 | 0.174 | 0.163 |
| | 30 | −0.677 | 8.03E-09 | 4.24E-07 | 0.0002349 | 1.04E+04 | 0.215 | 0.192 |
| EP4 | 1 | −0.134 | 5.83E-13 | 1.01E-10 | 6.43E-09 | 3.14E+08 | 0.124 | 1334 |
| | 7 | −0.205 | 1.32E-11 | 2.44E-10 | 1.54E-07 | 1.73E+08 | 0.181 | 0.211 |
| | 15 | −0.605 | 1.89E-08 | 3.49E-07 | 0.0002203 | 78315 | 0.132 | 0.120 |
| | 30 | −0.539 | 2.02E-08 | 3.49E-08 | 9.34E-05 | 1.62E+05 | 0.110 | 0.111 |

**Table.5(A).7.** Electrochemical parameters after soaking for periodic time intervals (1, 7, 15 and 30) days of polarization measurements of EP5 and EP6

| Samples code Name | Day(s) | $-E_{corr}$ (V vs SCE) | $J_{corr}$ ($A/cm^2$) | $I_{corr}$ ($mA\ cm^{-2}$) | Corrosion rate (mm/year) | $R_p$($\Omega\ cm^2$) | βa ($mV\ dec^{-1}$) | βc ($mV\ dec^{-1}$) |
|---|---|---|---|---|---|---|---|---|
| EP5 | 1 | −0.269 | 1.19E-11 | 2.44E-10 | 1.39E-07 | 2.63E+08 | 0.268 | 0.332 |
| | 7 | −0.201 | 7.00E-11 | 1.43E-09 | 8.13E-07 | 6.68E+07 | 0.415 | 0.468 |
| | 15 | −0.159 | 6.52E-11 | 1.33E-09 | 7.58E-07 | 5.90E+07 | 0.318 | 0.422 |
| | 30 | −0.699 | 1.01E-08 | 2.06E-07 | 0.00011748 | 2.09E+05 | 0.235 | 0.173 |
| EP6 | 1 | −0.166 | 1.18E-11 | 2.80E-10 | 1.37E-07 | 2.33E+08 | 0.328 | 0.277 |
| | 7 | −0.134 | 5.08E-11 | 1.20E-09 | 5.90E-07 | 7.58E+07 | 0.486 | 0.369 |
| | 15 | −0.115 | 5.62E-11 | 1.32E-09 | 6.53E-07 | 6.17E+07 | 0.408 | 0.352 |
| | 30 | −0.416 | 1.02E-10 | 1.51E-09 | 1.18E-06 | 4.62E+07 | 0.403 | 0.403 |

From the table, electrochemical parameters of various composite coatings are put forward. The higher $E_{corr}$, lower $I_{corr}$, and higher Rp values revealed better corrosion resistive properties. Thus we can say that corrosion potential ($E_{corr}$) of EP6 is higher than that of others composite. Meanwhile, the corrosion current ($J_{corr}$) of EP6 > EP4 > EP2 coatings is the lowest. Interestingly, the corrosion potential first increased and then decreased in EP6 coating and also corrosion current to be inversely related. Moreover, EP6 coating has the largest $E_{corr}$(─0.4169) than EP4 and EP2, the smallest $J_{corr}$(1.0231E-10 A/cm$^2$) for 30 days compared to EP5. In term of polarization resistance, EP6 is 4.6214E+07Ωcm$^2$ which is about $2.2032\times10^2$ more than that of EP5, EP4 is 1.6257E+05Ωcm$^2$ i.e about 15.63 times more than EP3 and EP2 is 108392Ωcm$^2$ which is about 3.56 more than that of EP1 Nano composite coating possesses the superior corrosion resistance properties over conventional composite coating.

## 5(A).6.2. Analysis of EIS results of uncoated MS rod and various composite epoxy coatings

Corrosion prevention performance EIS experiment was done by immersion in 3.5% Nacl aqueous solution for (initial 1, 7, 15 and 30) days with a stable OCP, to investigate the corrosion resistance properties of the composite epoxy coatings [9,10]. In the Nyquist diagram, the arc radius of the capacitor impedance is directly proportional to the corrosion resistance of the coating. This means that as the impedance arc's value increases, the corrosion resistance also improves [11].

Compared with Fig.5(A).31 for uncoated, it can be seen from Fig.5(A).32, 34 and 36, that after immersion of initial period after 1 day the EP1 other than EP3 and EP5 composite coatings reveal initial behavior is dominated by the coating capacitance at higher frequency immersion and coating resistance at lower

frequency with a resistive component greater than $6\times10^7$ MΩcm$^2$. After 30 days of immersion, the arc radius of the semicircle in the EIS spectrum which was initially immersed at the end of the 15 day curve decreases. This reduction in arc radius is attributed to a decrease in the resistance of the coating. This decrease occurs because water and ions are able to penetrate the small pores and channels within the coating matrix, ultimately reaching the outer edges of the metal substrate (MS). In the impedance spectrums the presences of semi circle frequencies reduce which indicate that electrochemical reaction occurred between composite coating and MS surface was progressing [12-13].

It can be seen from Fig.5(A). 33, 35 and 37, Nyquist plot of organo silane composite coating has different result than conventional coating. Initial 1 day of immersion time of EP6 the resistance values reached $4\times10^7$ MΩcm$^2$ and after 30 days immersion values exceeded $9\times10^6$ MΩcm$^2$, which is illustrated by semicircles. It has different curve consisting of different semicircles for EP6 after 30 days immersion compared to EP4 and EP2. After 30 days immersion of EP6 exposure to the electrolyte solution shows good corrosion behavior as compared to conventional one due to agglomeration behaviors of nanoparticles in composite epoxy coating [14-16].

It can be clearly seen that after soaking for 30 days to the electrolyte solution, in case of conventional epoxy composite coatings the arc radius of the coating initially increases and there after it decreases indicating that it has the worse corrosion resistance capacitor. Interestingly, EP6 composite coating shows highest impedance arc radius. Nyquist diagram reveals that well dispersion of nano silica truly increases the performance of corrosion protection on metal substrate.

From the Nqquist diagram Ru (solution resistance), Rp (coating resistance), Rct (charge transfer resistance) C.P.E (constant phase element), $Y_o$ (admittance nature of coating) and N (capacitive nature of coating) are derived and tabulated in table.8. These are used to evaluate the equivalent circuit. We use one time constant from electrochemical behavior and another for corrosion mechanism for the given coating shown in Fig.5(A).44. Our studies show that the metal corrosion rate with the coating are inversely related to Rct or charge transfer resistance and barrier properties for the coating. Therefore in order to improve the corrosion resistance we have to have higher Rp and Rct value for the given coating [18-20]. From values in Table.4(A).8 to Table.4(A).11 we can see that EP6 has the much better corrosion resistance properties than EP5 for immersion for a time interval, in 3.5 weight % Nacl aqueous solution.

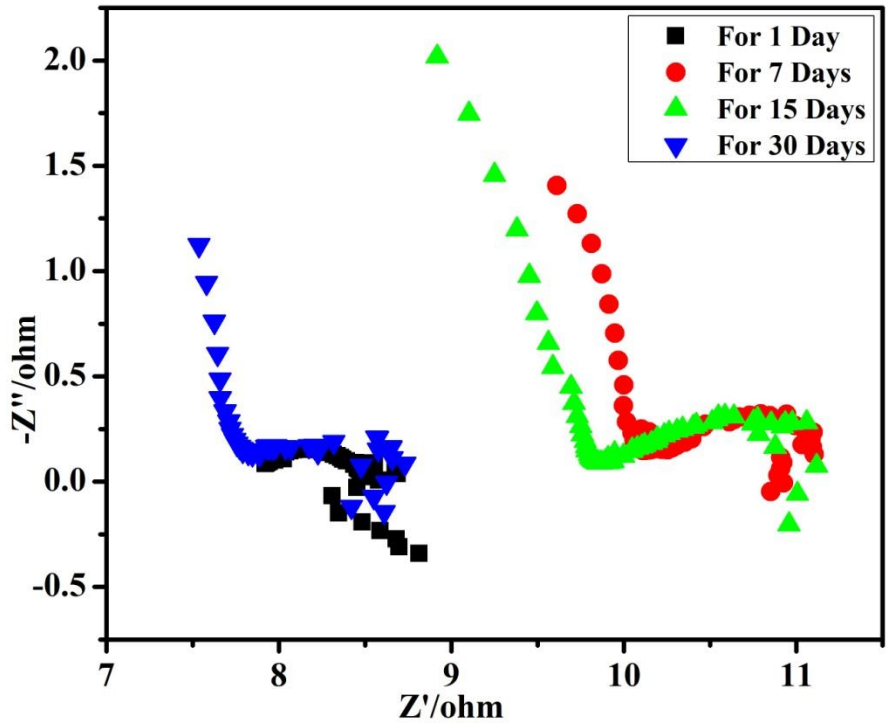


**Fig.5(A).31:** Nyquist plot of uncoated MS rod after soaking for 3.5 weight% Nacl aqueous solution for (1, 7, 15 and 30) days

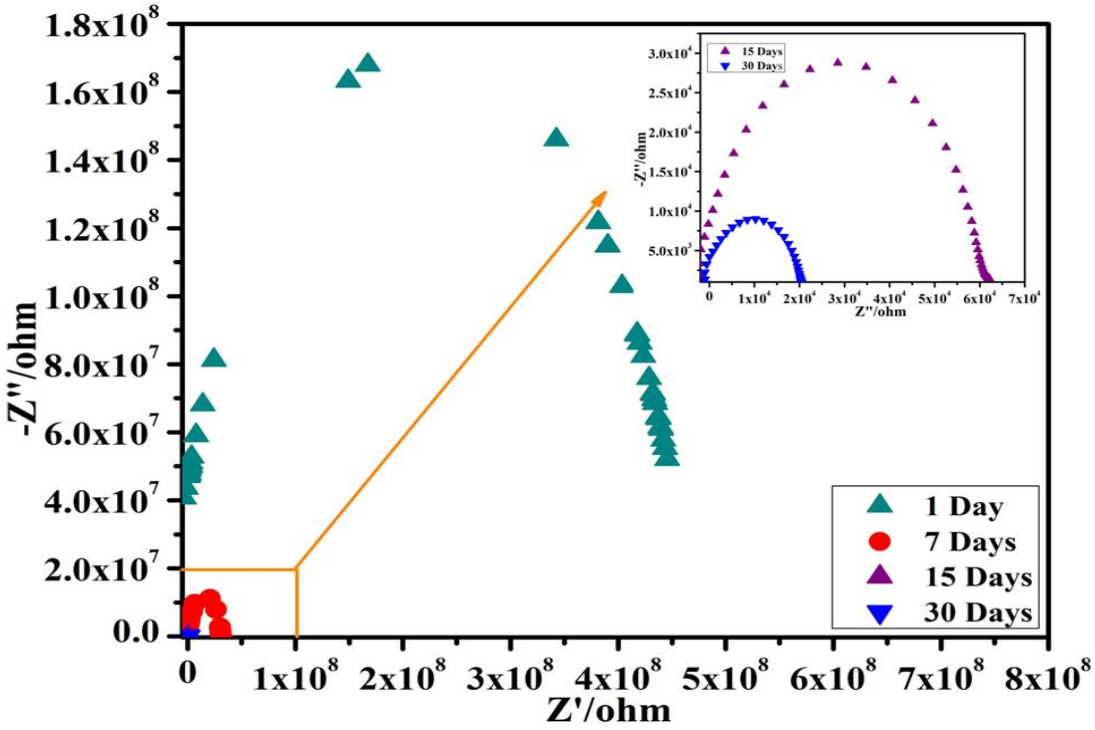


**Fig.5(A).32:** Nyquist plot of EP1 after immersion in a 3.5% weight Nacl aqueous solution for (1, 7, 15, and 30) days

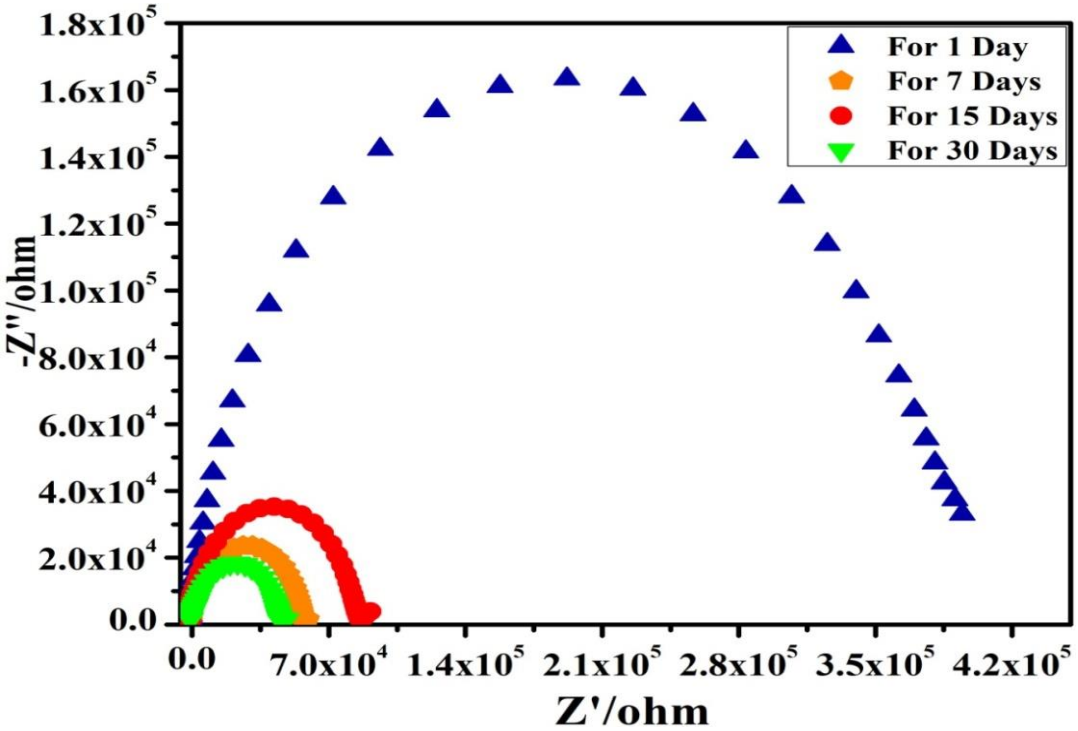


**Fig.5(A).33.** Nyquist plot of EP2 after immersion in a 3.5% weight Nacl aqueous solution for (1, 7, 15, and 30) days

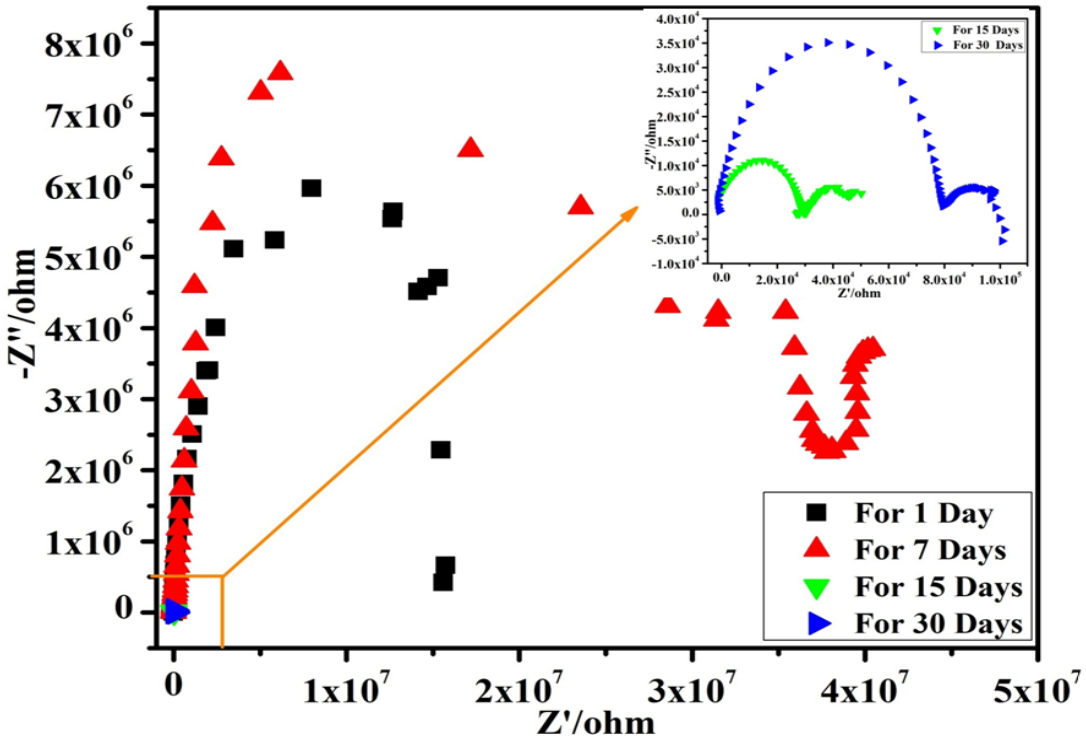


**Fig.5.(A).34:** Nyquist plot of EP3 after immersion in a 3.5% weight Nacl aqueous solution for (1, 7, 15, and 30) days

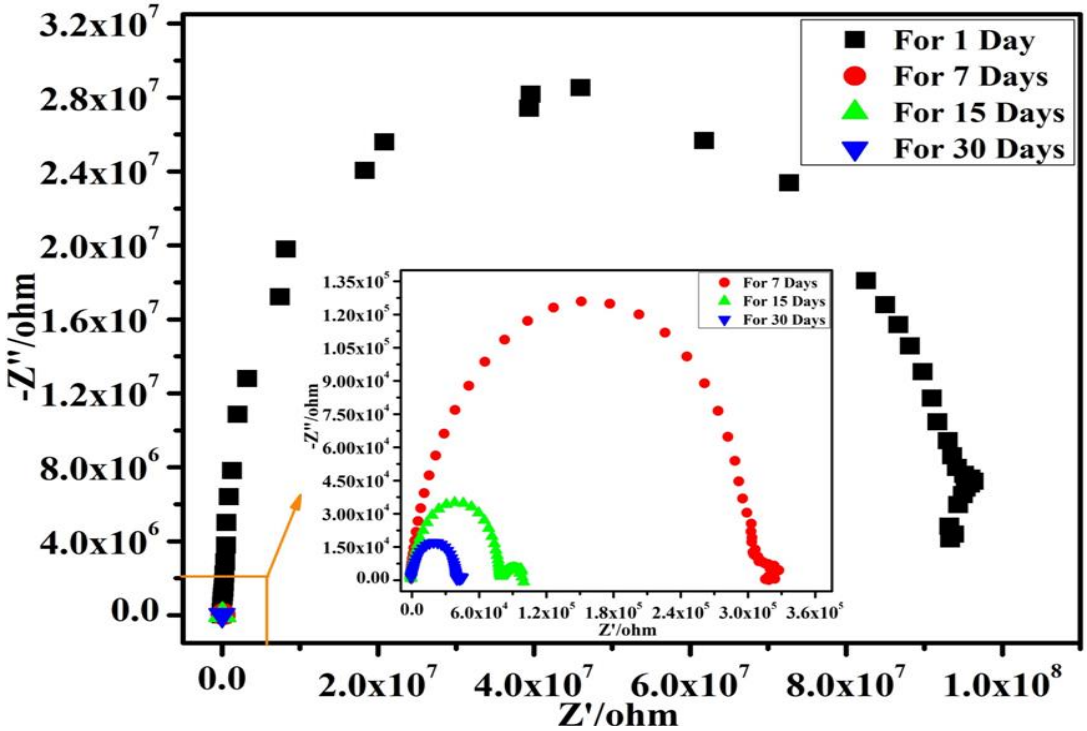


**Fig.5(A).35:** Nyquist plot of EP4 after immersion in a 3.5% weight Nacl aqueous solution for (1, 7, 15, and 30) days

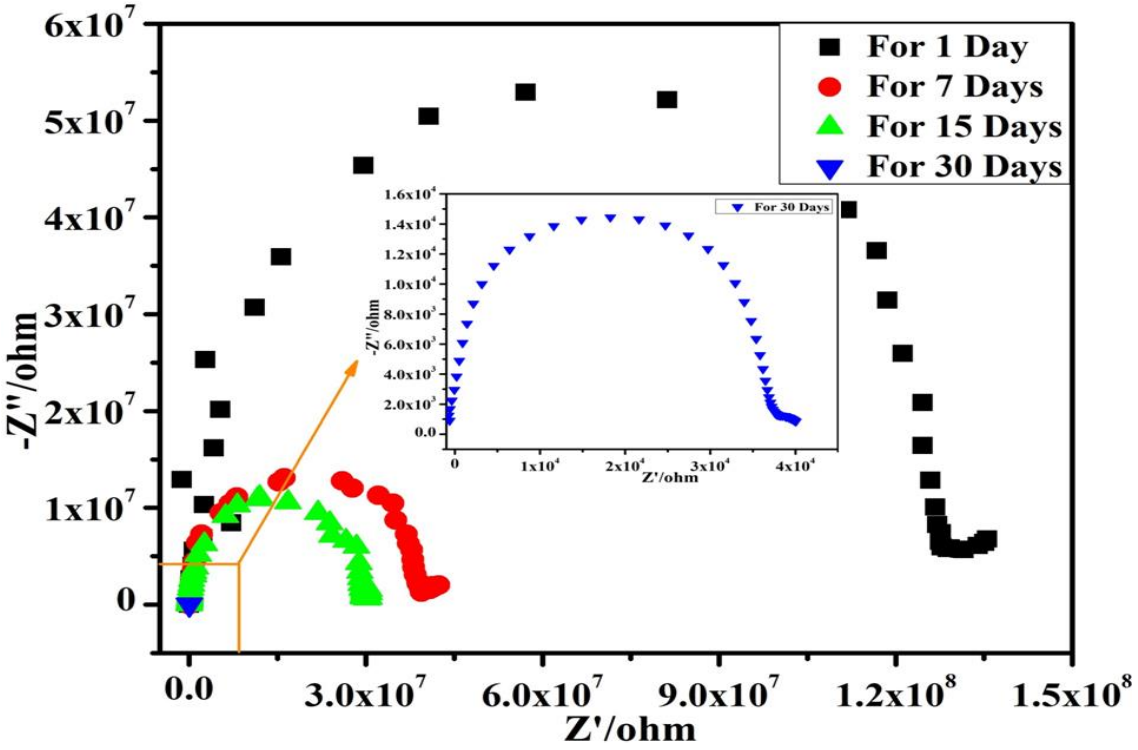


**Fig.5(A).36:** Nyquist plot of EP5 after immersion in a 3.5% weight Nacl aqueous solution for (1, 7, 15, and 30) days

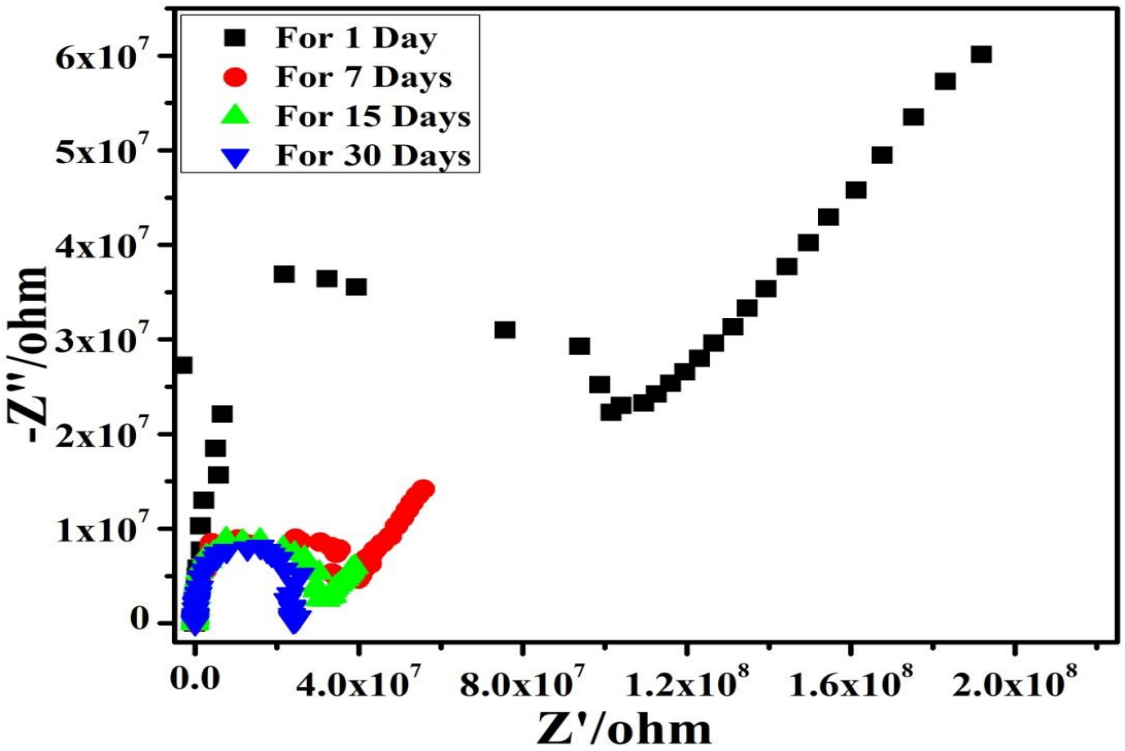


**Fig.5(A).37:** Nyquist plot of EP6 after immersion in a 3.5% weight Nacl aqueous solution for (1, 7, 15, and 30) days

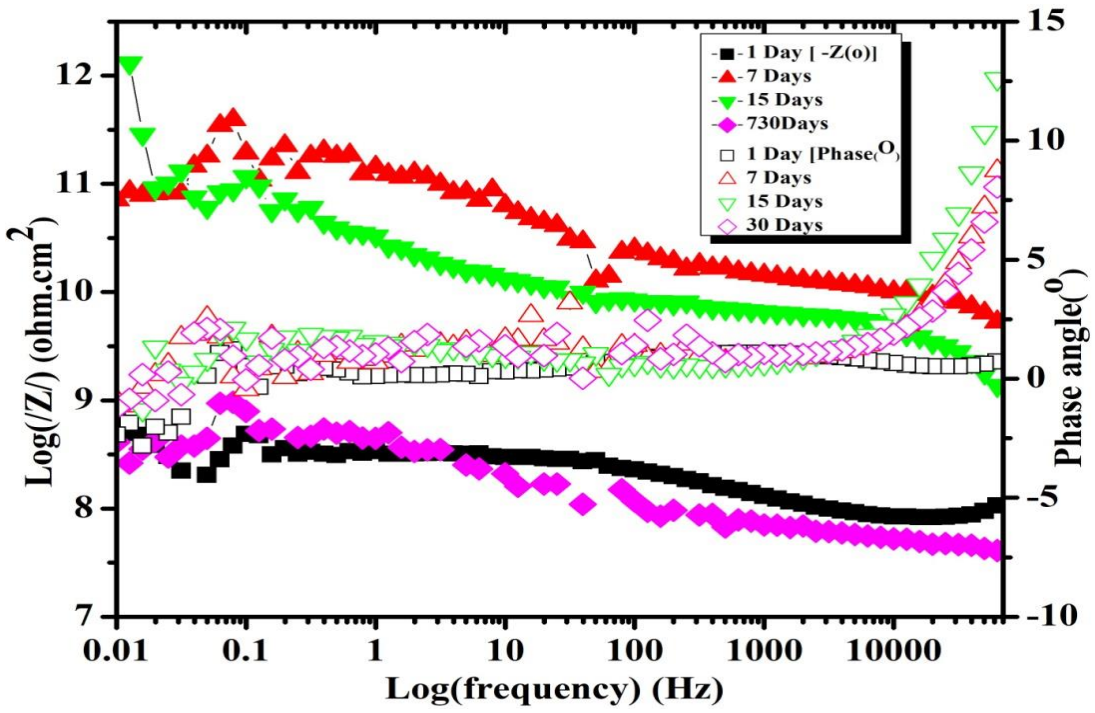


**Fig.5(A).38**: Bode plot of uncoated MS rod after soaking for 3.5 weight% Nacl aqueous solution for (1, 7, 15 and 30) days

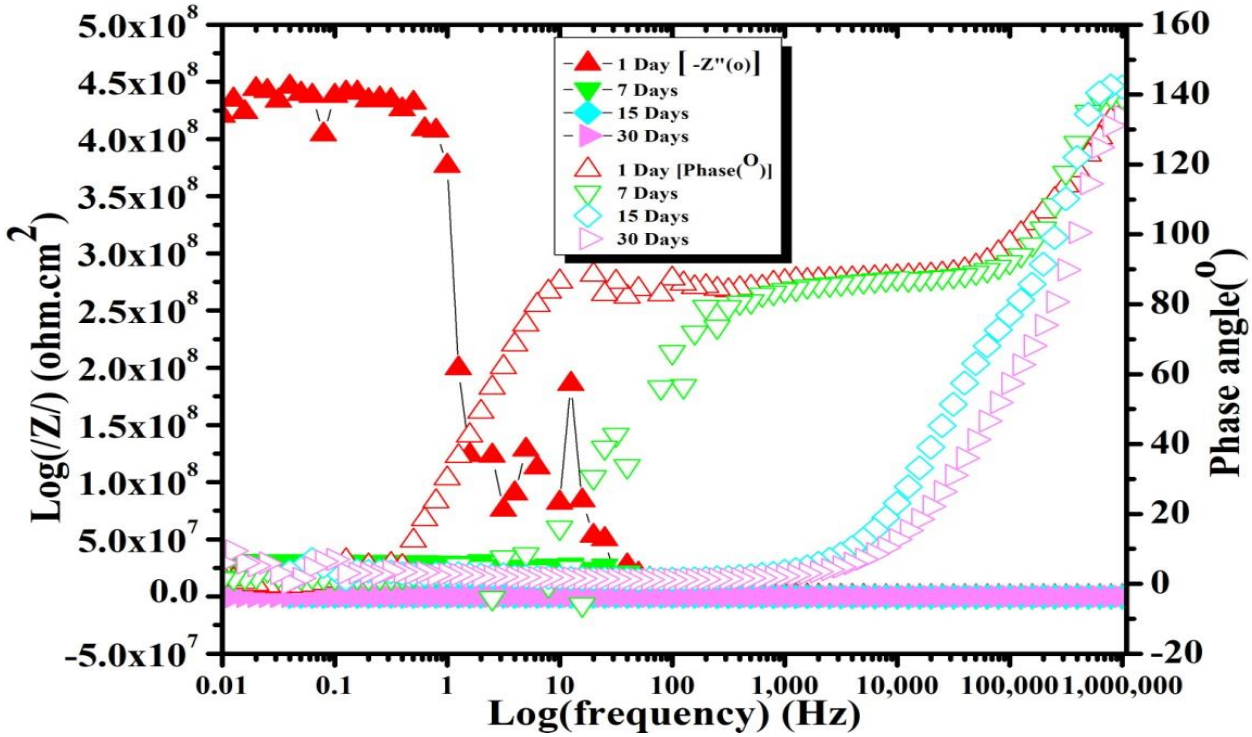


**Fig.5(A).39**: Bode plot of EP1 after soaking in a 3.5% weight Nacl aqueous solution for (1, 7, 15, and 30) days

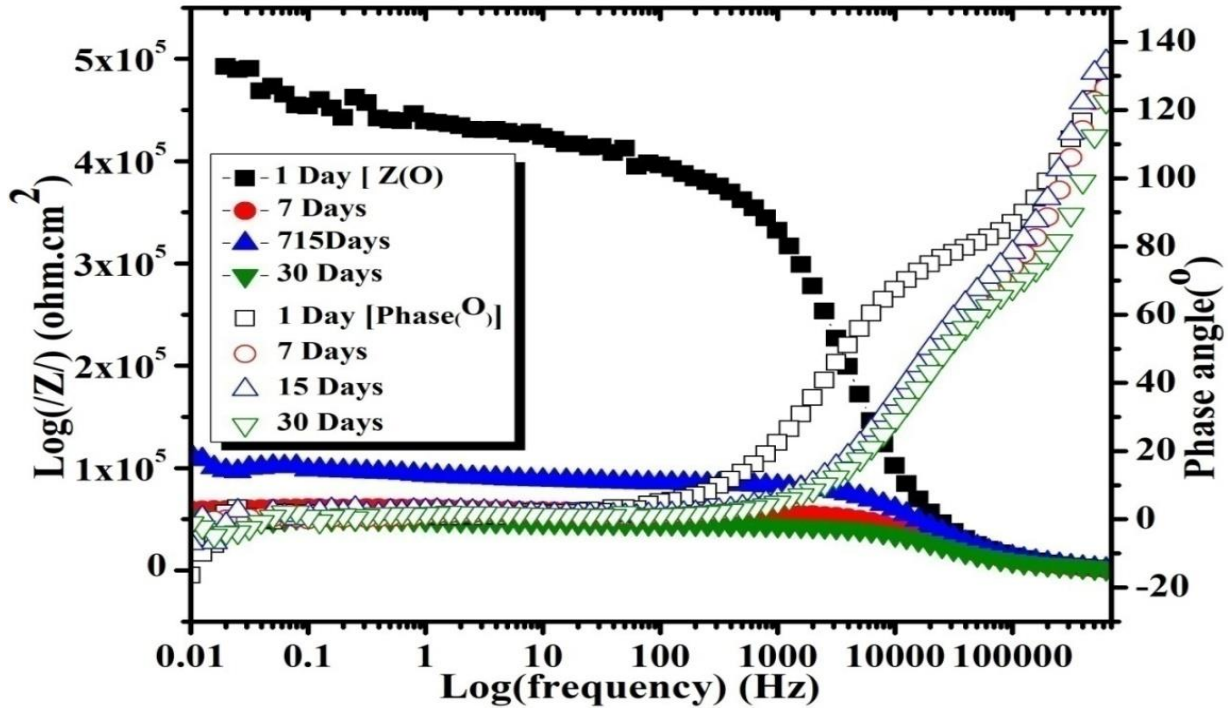


**Fig.5(A).40:** Bode plot of EP2 after soaking in a 3.5% weight Nacl aqueous solution for (1, 7, 15, and 30) days

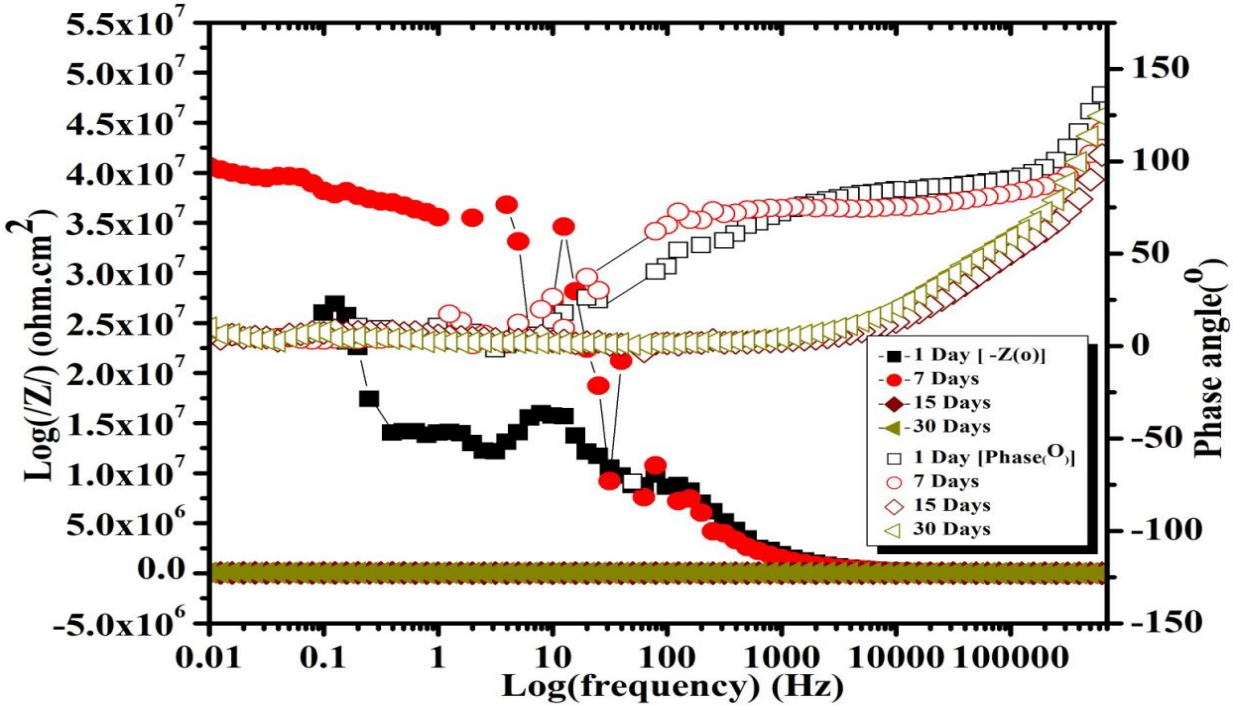


**Fig.5(A).41:** Bode plot of EP3 after soaking in a 3.5% weight Nacl aqueous solution for (1, 7, 15, and 30) days

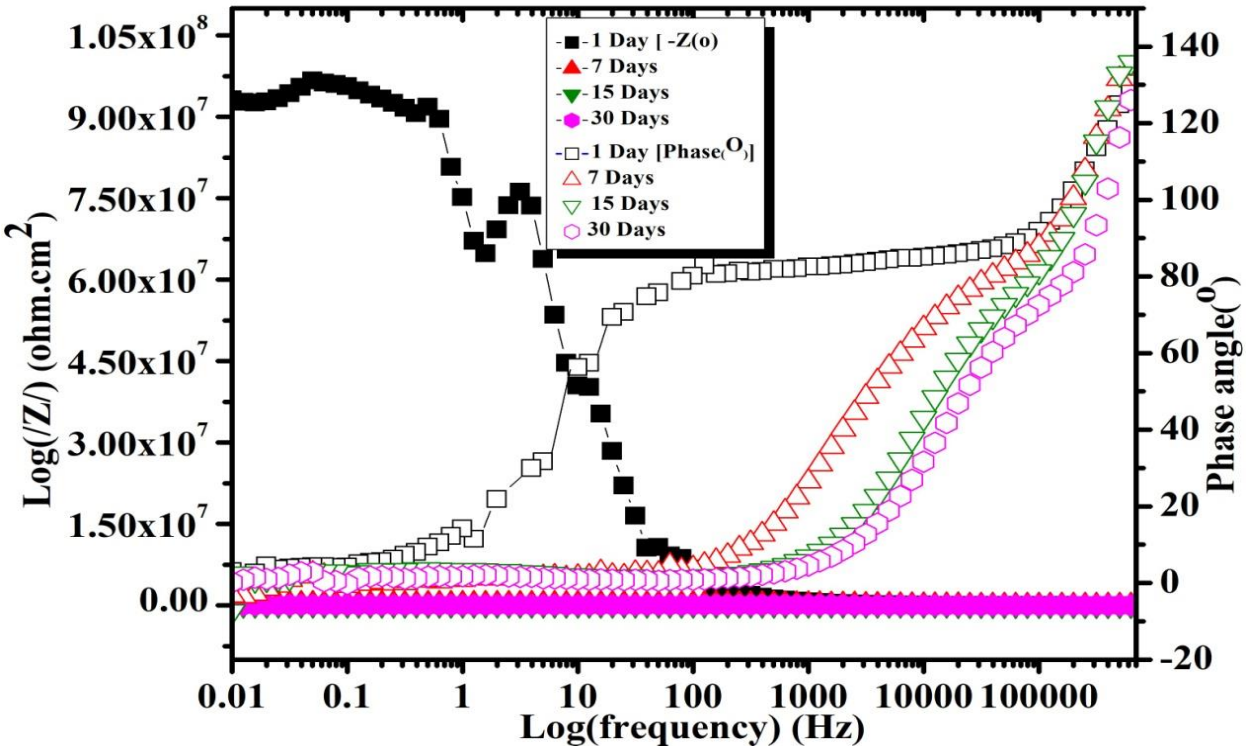


**Fig.5(A).42:** Bode plot of EP4 after soaking in a 3.5% weight Nacl aqueous solution for (1, 7, 15, and 30) days

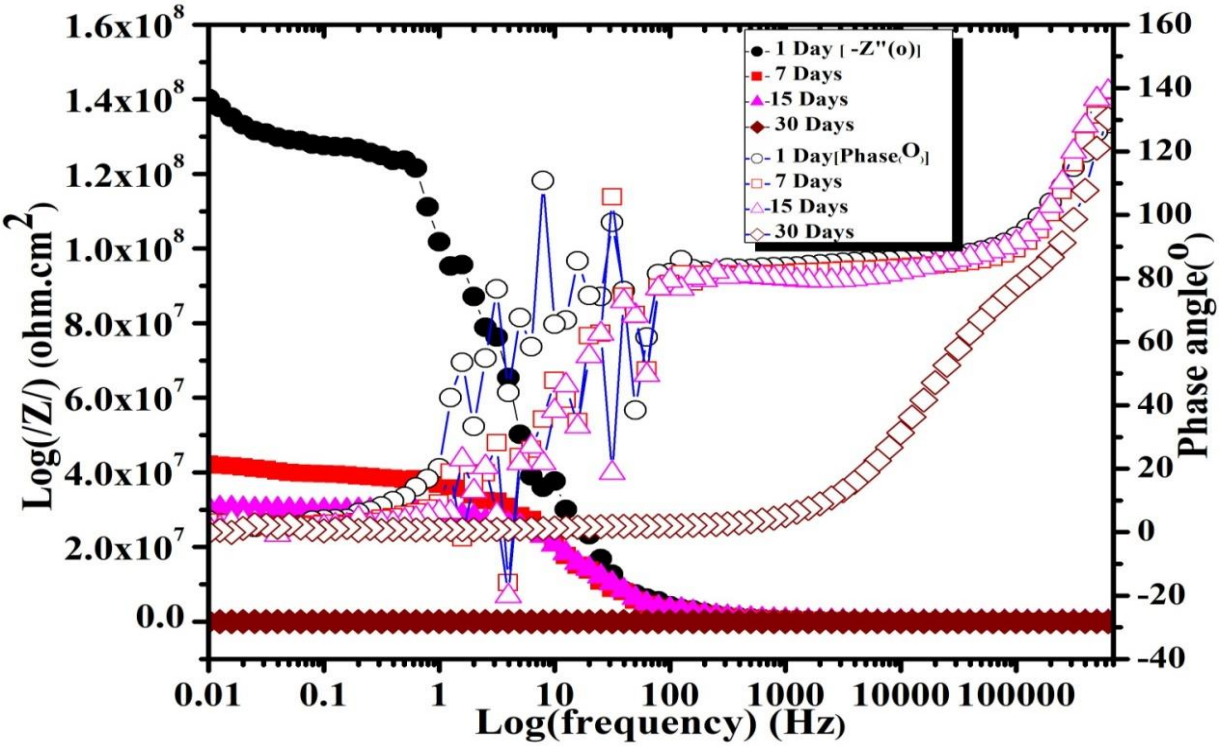


**Fig.5(A).43:** Bode plot of EP5 after soaking in a 3.5% weight Nacl aqueous solution for (1, 7, 15, and 30) days

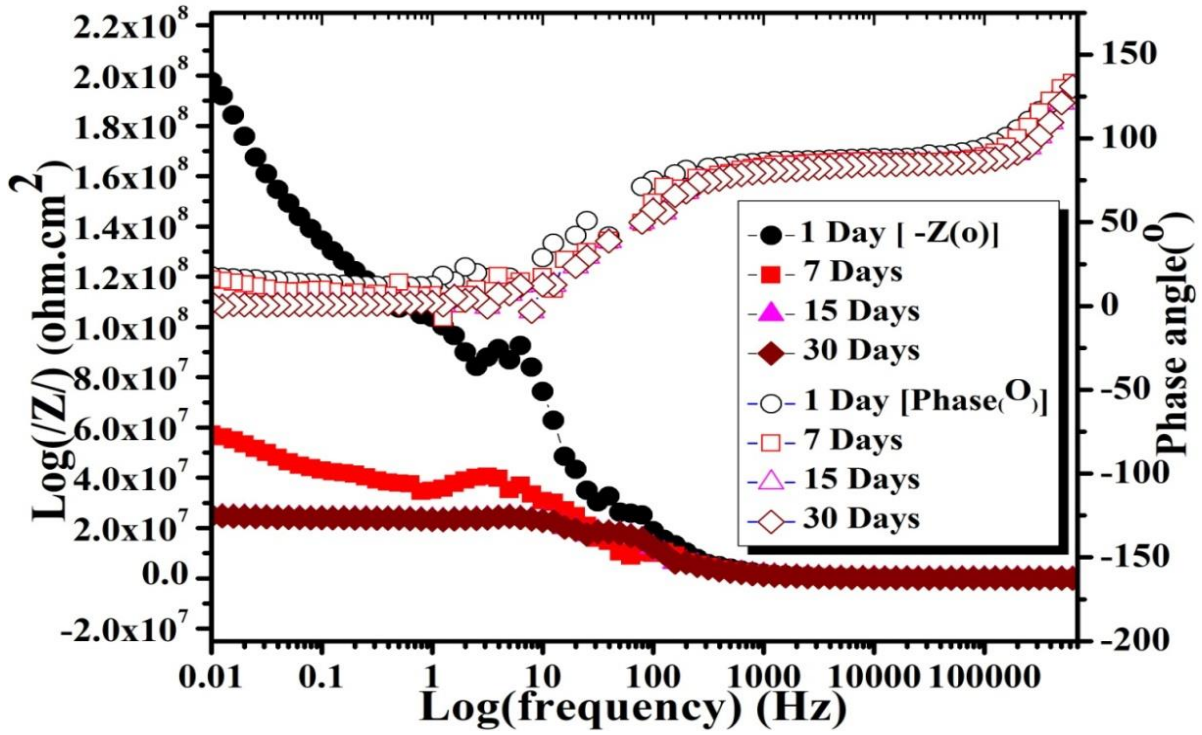


**Fig.5(A).43:** Bode plot of EP5 after soaking in a 3.5% weight Nacl aqueous solution for (1, 7, 15, and 30) days

Bode plot suggests that impedance modulus increased at lower frequency for better corrosion resistance. Bode plots of conventional and nano composite coatings with altered time immersion intervals (initial 1, 7, 15, and 30 days) are shown in Fig.5(A).38 to Fig.5(A).44 compared with Fig.5(A).39 for uncoated MS rod. We use impedance modulus at frequencies which are lowest ($|Z|_f$ = 0.01Hz) and analyze the corrosion resistance properties of composite coatings. The impedance modulus value ($|Z|_f$ = 0.01Hz) decreases in the order 1day > 7 days > 15 days > 30 days, for conventional coating, which indicates less corrosion protection. Meanwhile, compared with conventional coationg, nano coating composite shows better corrosion protection ability after 15 days. This suggests that the corrosive environment has affected the MS substrate due to the excessive mobilization of nanoparticles in the composite coating matrix. However, in the case of coatings

with organo silane nanocomposites, mobilization is observed only after 30 days of immersion. This observation indicates that the corrosion mediums are unable to penetrate these coatings effectively. It reveals that the nanoparticles are well-dispersed within the nanocomposite, effectively enhancing the epoxy matrix and thus improving the corrosion barrier properties of the coatings through a "labyrinth effect," which restricts the permeation of corrosive ions [14].

**Table.5(A).8:** Fitting results of uncoated MS rod

| **Sample name** | **Day** | **C.P.E ($Y_o$)** | **Rp.(Ω)** | **C.P.E (N)** |
|---|---|---|---|---|
| Uncoated MS rod | 1 | 0.00035 | 0.517 | 0.503 |
| | 7 | 0.00065 | 0.821 | 0.521 |
| | 15 | × | × | × |
| | 30 | × | × | × |

**Table.5(A).9:** Fitting results of EP1 and EP2

| **Samples code name** | **Day (s)** | **C.P.E ($Y_o$)** | **Rp.(Ω)** | **C.P.E (N)** |
|---|---|---|---|---|
| EP1 | 1 | 2.67E−11F | 4.38E+08 | 0.917 |
| | 7 | 1.27E−10F | 3.07E+07 | 0.835 |
| | 15 | 1.01E−10F | 650022 | 0.872 |
| | 30 | 1.27E−10F | 22751 | 0.853 |
| EP2 | 1 | 1.67E−10F | 4.24E+05 | 0.895 |
| | 7 | 1.83E−10F | 68746 | 0.879 |
| | 15 | 1.69E−10F | 90590 | 0.864 |
| | 30 | 1.97E−10F | 60783 | 0.910 |

**Table.5(A).10:** Fitting results of EP3 and EP4

| Samples code name | Day (s) | C.P.E ($Y_o$) | Rp.(Ω) | C.P.E (N) |
|---|---|---|---|---|
| EP3 | 1 | 1.02E-10F | 9.80E+07 | 0.870 |
| | 7 | 2.63E-10F | 3.20E+05 | 0.854 |
| | 15 | 1.99E-10F | 83069 | 0.903 |
| | 30 | 2.46-10F | 41587 | 0.882 |
| EP4 | 1 | 6.71E-10F | 1.51E+07 | 1.106 |
| | 7 | 1.54E-10F | 3.90E+07 | 0.778 |
| | 15 | 9.17E-11F | 33039 | 0.776 |
| | 30 | 1.32E-10F | 44921 | 0.707 |

**Table.5(A).11:** Fitting results of EP5 and EP6

| Samples code name | Day (s) | C.P.E ($Y_o$) | Rp.(Ω) | C.P.E (N) |
|---|---|---|---|---|
| EP5 | 1 | 9.70E-10F | 1.29E+08 | 0.947 |
| | 7 | 5.40E-10F | 3.98E+07 | 0.913 |
| | 15 | 4.85E-10F | 2.98E+07 | 0.926 |
| | 30 | 2.60E-10F | 38853 | 0.887 |
| EP6 | 1 | 6.68E-11F | 1.03E+08 | 1.05 |
| | 7 | 3.81E-10F | 4.58E+07 | 0.793 |
| | 15 | 1.23E-10F | 3.21E+07 | 0.922 |
| | 30 | 1.99E-10F | 2.53E+07 | 1.024 |

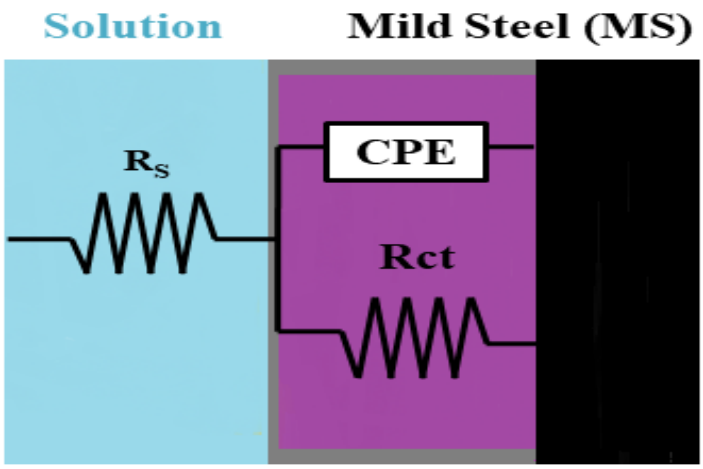


**(a)**

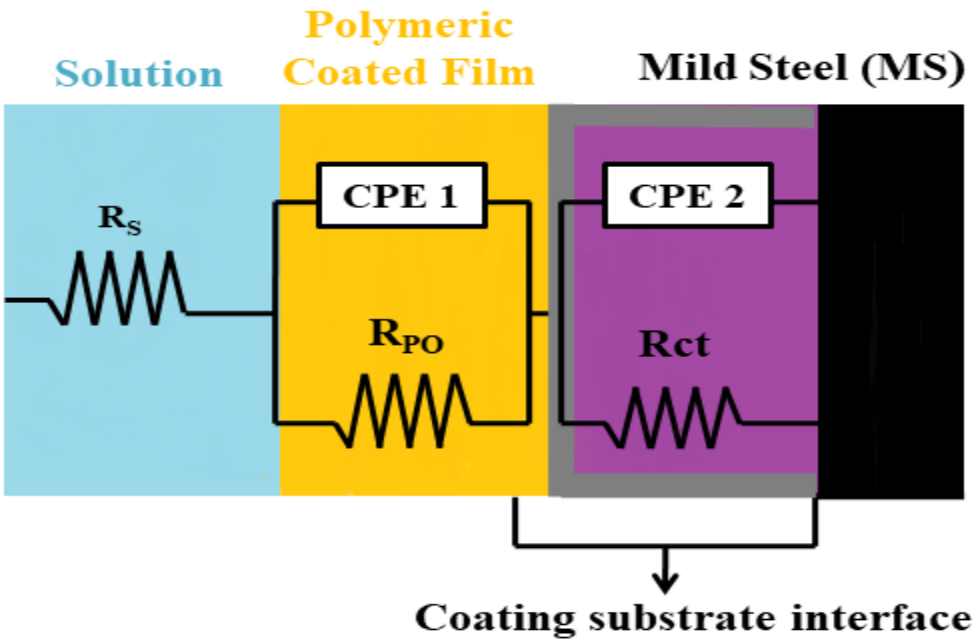


**(b)**

**Fig.5(A).44:** The equivalent electrical circuit models used to simulate EIS measurements of coatings at various immersion stages: (a) for one time constant and (b) for two time constant

**Table.5(B).12:** Inhibition efficiency of developed epoxy composite coating from electrochemical parameter after corrosion studies

| **Coating code Name** | **% Corrosion Inhibition Efficiency=** $\frac{I^{o}_{corr} - I_{corr}}{I^{o}_{corr}} \times 100$ | **% Rct =** $\frac{Rct - Rct^{o}}{Rct} \times 100$ | $P = \frac{R_{P(Uncoated)}}{R_{P(Coated)}} \times 10^{-\frac{(\Delta E_{corr})}{b_a}}$ |
|---|---|---|---|
| EP1 | 98.70 | 98.83 | $P= 45.78\times10^{-7}$ |
| EP2 | 99.61 | 99.20 | $P=38.69\times10^{-10}$ |
| EP3 | 99.18 | 99.30 | $P=20.23\times10^{-7}$ |
| EP4 | 99.92 | 99.78 | $P=10.26\times10^{-12}$ |
| EP5 | 99.84 | 99.86 | $P=26.59\times10^{-8}$ |
| EP6 | 99.90 | 99.96 | $P=23.48\times10^{-14}$ |

From electrochemical parameter it has been seen, EP6>EP4>EP2>EP5>EP3>EP1 increasing order for corrosion inhibition efficiency, EP6>EP5>EP4>EP3>EP2>EP1 increasing order for charge transfer resistance and EP6>EP4>EP2>EP5>EP3>EP1 increasing order for porosity measurement of different type of composite coatingsre respectively. It has suggested that nano filler embedded coating best results in corrosion inhibition efficiency and charge transfer resistance due to dense structure formed when cured with hydrophobic nano silica particle.

## 5(A).7. Surface Analysis of Coatings (Optical Images)

Optical images with different magnifications are taken before and after corrosion test of coatings on MS rod of electrochemical experiments. Fig.5(A).45 to

Fig.5(A).50 in the below depicted before and after corrosion of conventional and nano silica based composite coatings. After corrosion study it has been seen that most pits are observed over the surface of coating EP1. Some pin holes are noticeable glass flakes (160A and 160N) with conventional silica based epoxy composite coatings of EP3 and EP5 respectively. It revealed that swelling has occurred in Nacl medium of conventional epoxy coatings. Damages observed at the metal-coating interface uptake electrolyte that implies the weak resistance nature of conventional composite coatings. There are no such pits and damages observed after corrosion study of nano epoxy composite coatings in EP2, EP4 and EP6 respectively. Presence of nano organosiliane at metal/coating interface prevented the penetration of corrosion ions on MS substrate.

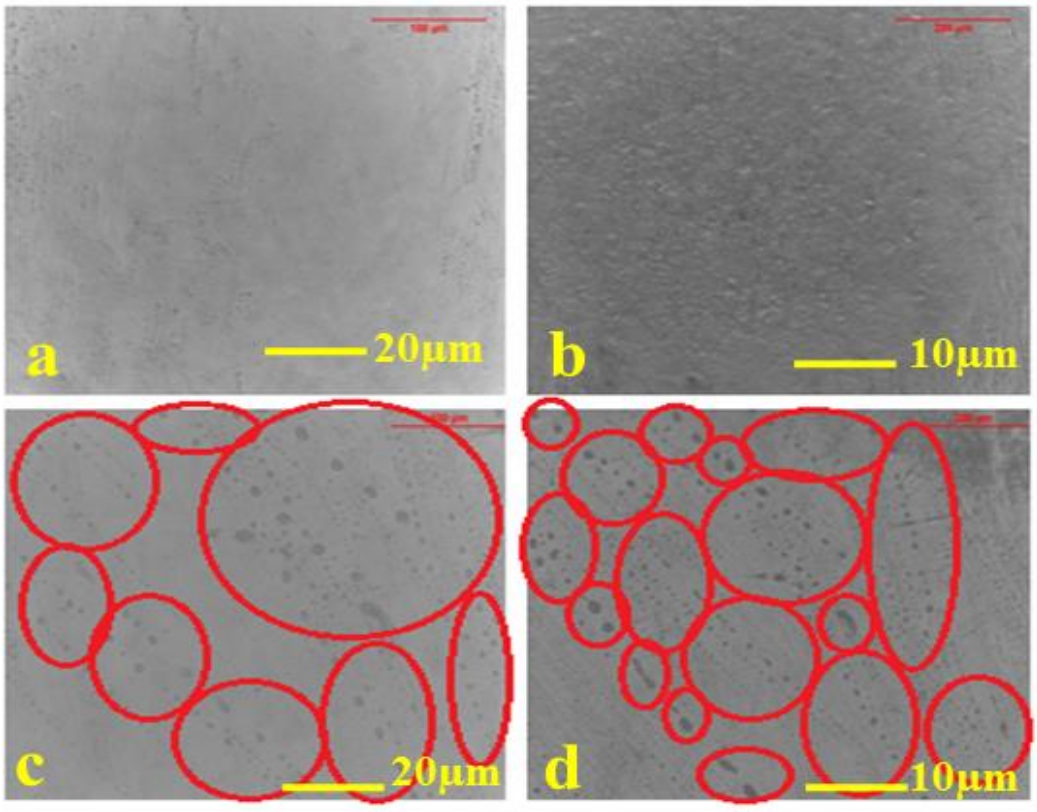


**Fig.5(A).45:** Image shows studies at different magnifications (a) and (b) before corrosion and after corrosion (c) and (d) of EP1

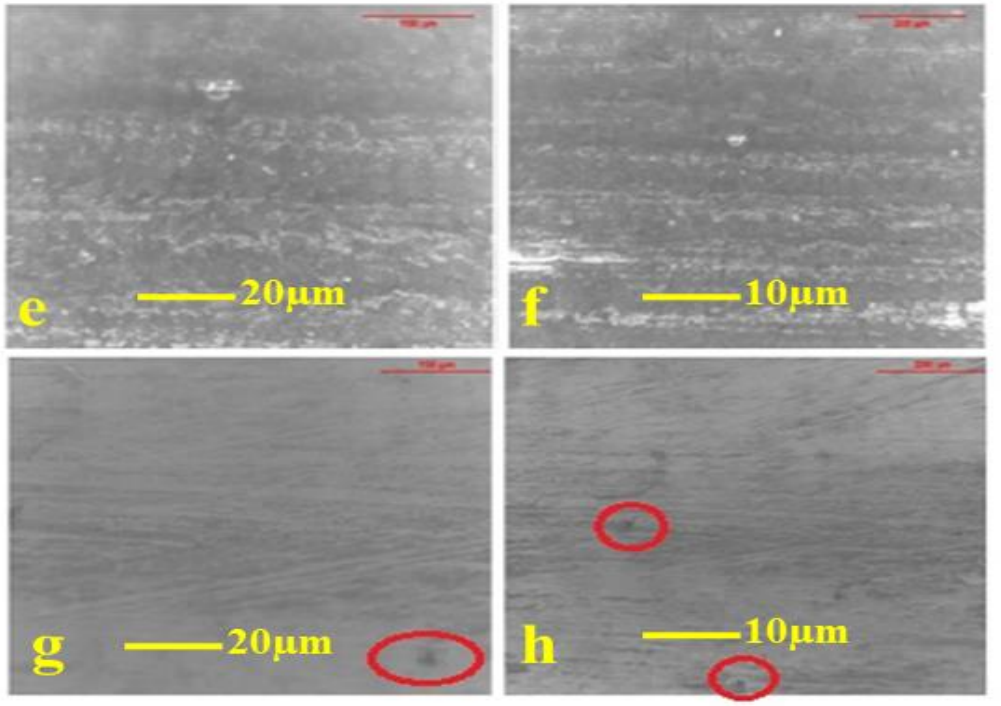


**Fig.5(A).46:** Image shows studies at different magnifications (e) and (f) before corrosion and after corrosion (g) and (h) of EP2

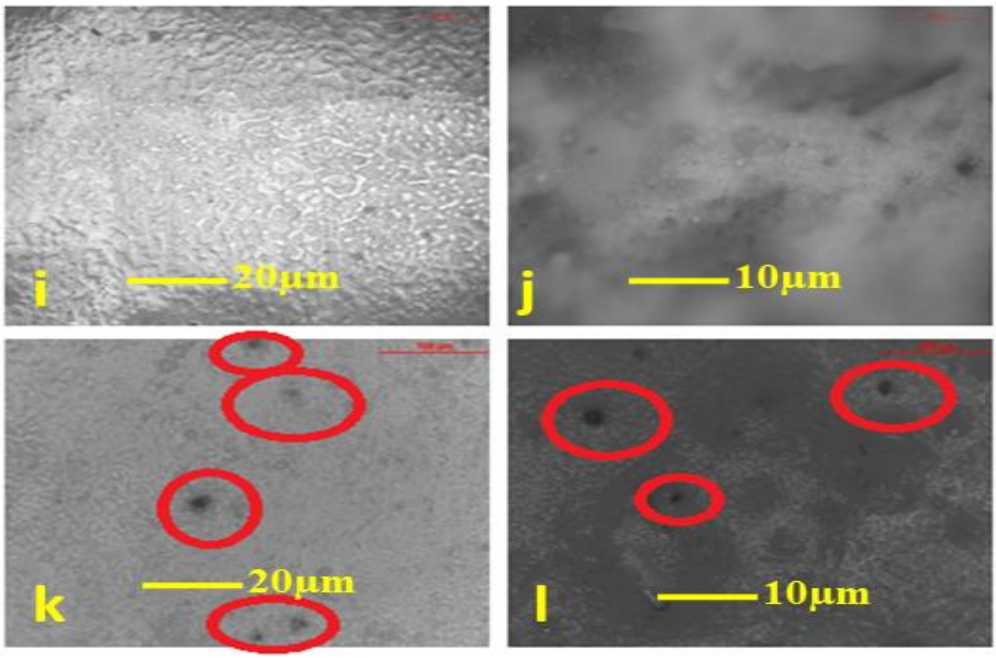


**Fig.5(A).47:** Image shows studies at different magnifications (i) and (j) before corrosion and after corrosion (k) and (l) of EP3

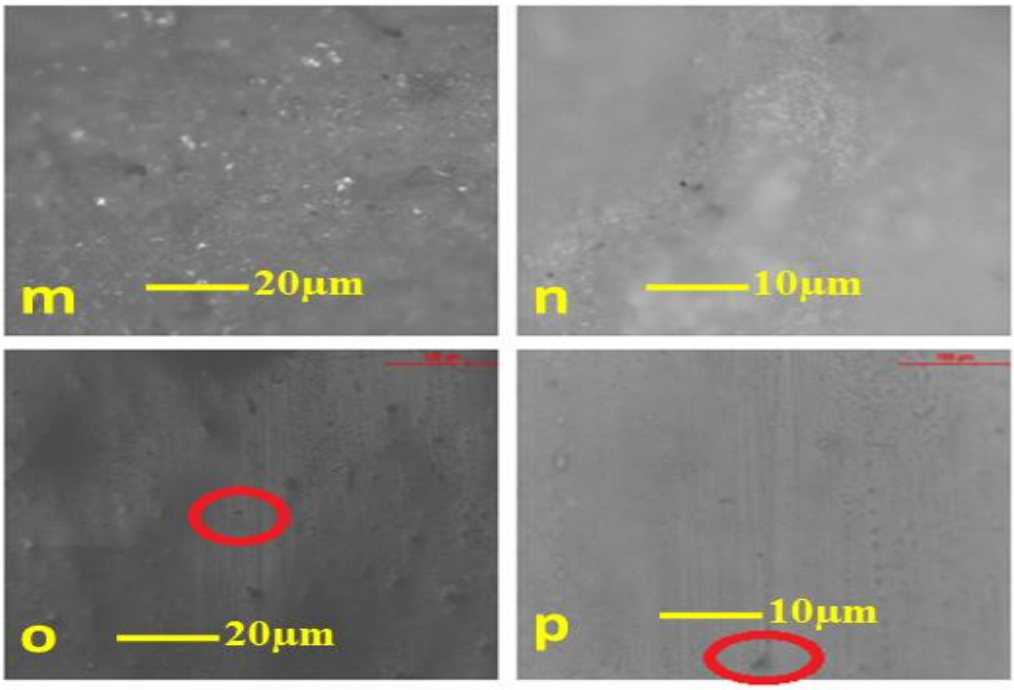


**Fig.5(A).48:** Image shows studies at different magnifications (m) and (n) before corrosion and after corrosion (o) and (p) of EP4

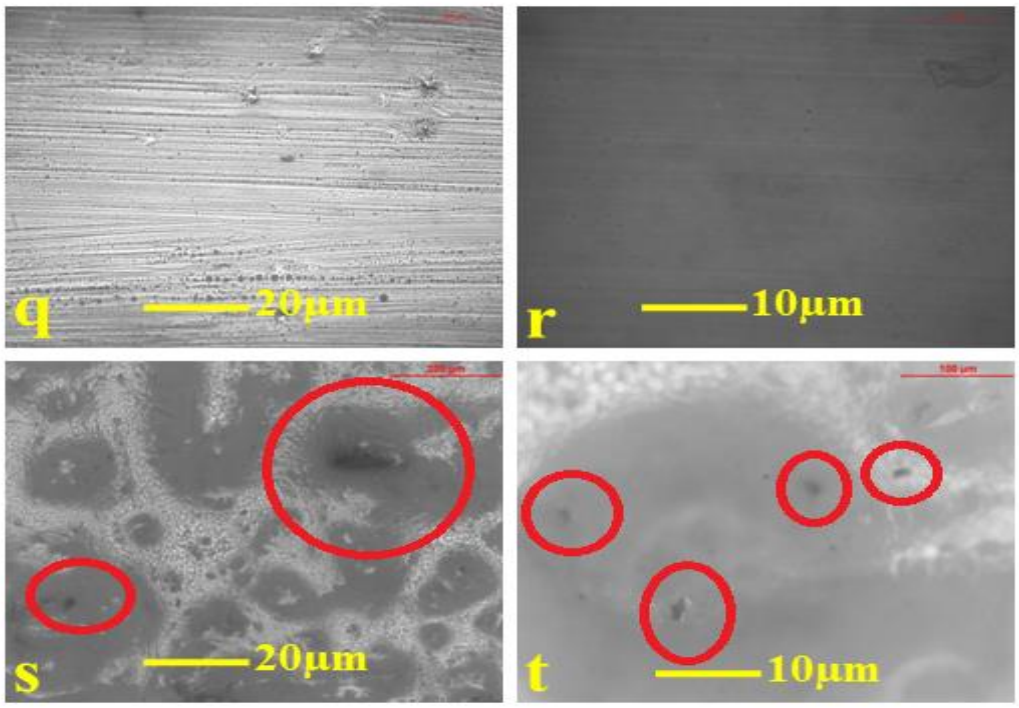


**Fig.5(A).49:** Image shows studies at different magnifications (q) and (r) before corrosion and after corrosion (s) and (t) of EP5

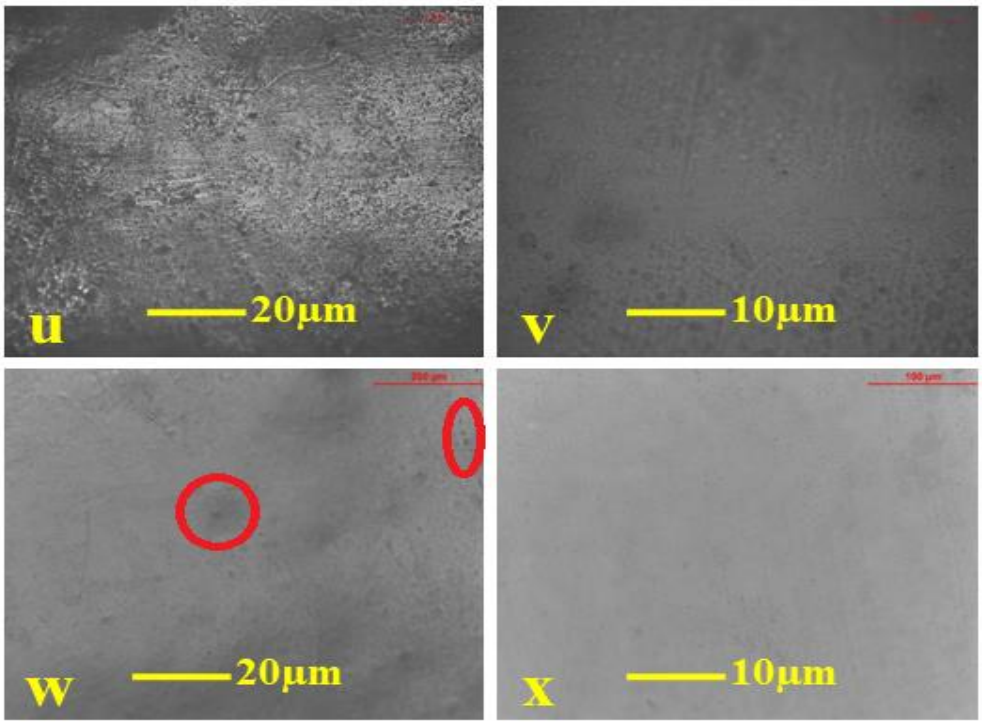


**Fig.5(A).50:** Image shows studies at different magnifications (u) and (v) before corrosion and after corrosion (w) and (x) of EP6

## 5(A).8. Salt Spray Chamber (SSC) Study

In salt spray chamber test is carried out to completion for 2200 hours of continuous fog on coated panels. From Fig.5(A).51 results indicate corrosion and blister formation occurred only in micron silica based epoxy and not in nano silica epoxy composite coating. But in case of micro silica with 160N and 160A glass flake based epoxy composite coatings (EP5 and EP3) showed less corrosion and blister formation compared to EP1 coating and also nano silica with 160N and 160A glass flake based epoxy composite coatings (EP4 and EP6) showed very less corrosion and blister observed compared to EP2 coating This indicates nano silica embedded epoxy is having much better corrosion resistant properties than conventional silica based epoxy coating.

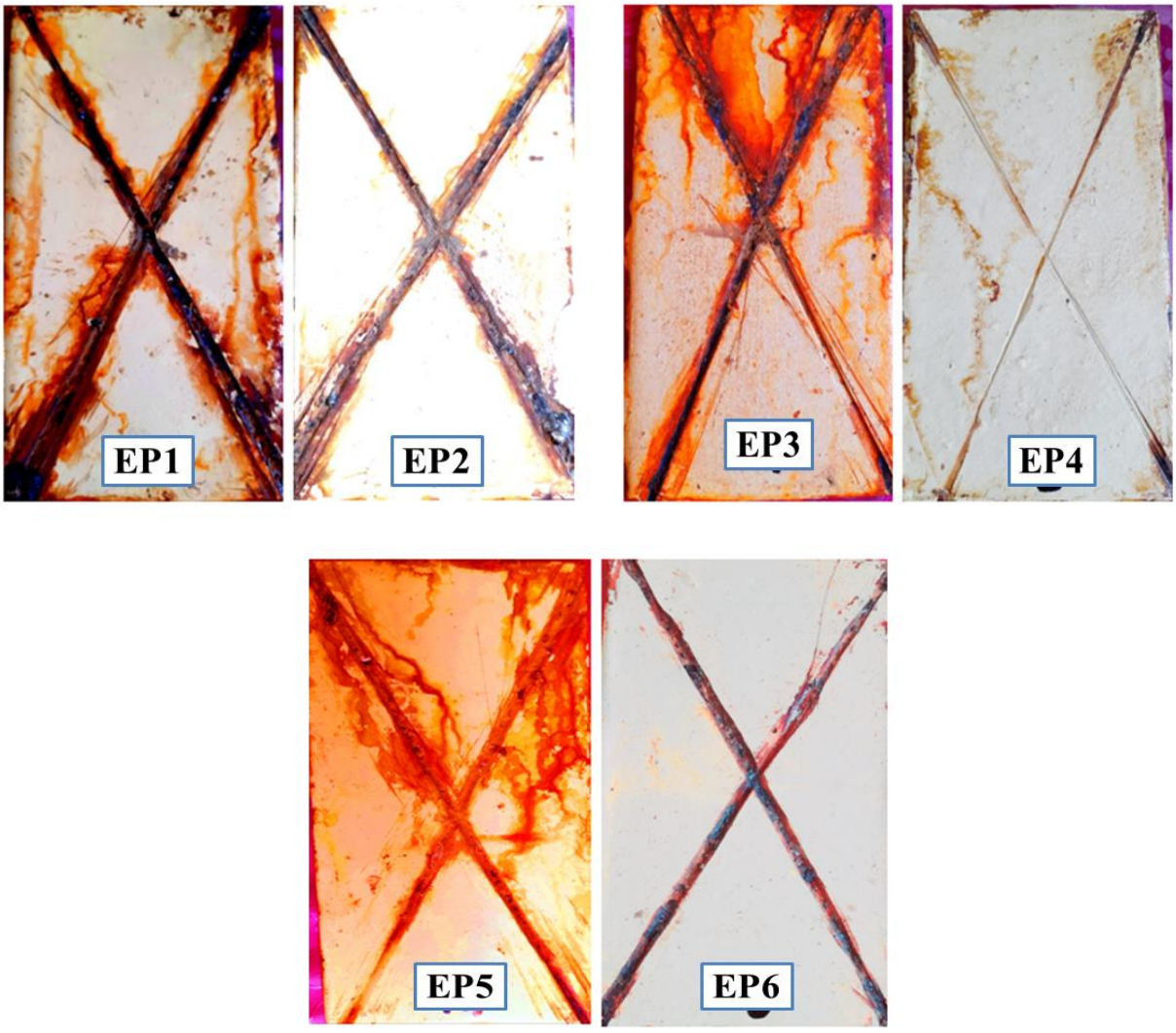


**Fig.5(A).51:** Images of the epoxy coated panel after 2200 hours expose in 5% Nacl solution salt spray

## 5(A).9. Cathodic Disbondment Study

After completion of experiment phenopthalein indicator was poured in drilled hole at the centre of each cell. There was change of violet colour observed which indicates violet colour zone has been corroded shown and shown in Fig.5(A).52. Here temperature plays major role in disbonding of coating. Here temperature plays important role, which is directly proportional to disbondment (mm/day).

Moreover, following an increase of the current, greater expansion will be observed at higher temperatures. At high vapour pressure porosity of coating increases as a result there will be increase in the permeation of electrolyte through the coating. This results in the chemical attack and thermal expansion of the metal substrate. Moreover, at elevated temperatures dissolution of interface oxides will be accelerated. Result shows epoxy nano composite sample has much lesser cathodic disbondment area than conventional one which indicates that nano embedded nano composite sample has better corrosion resistant properties.

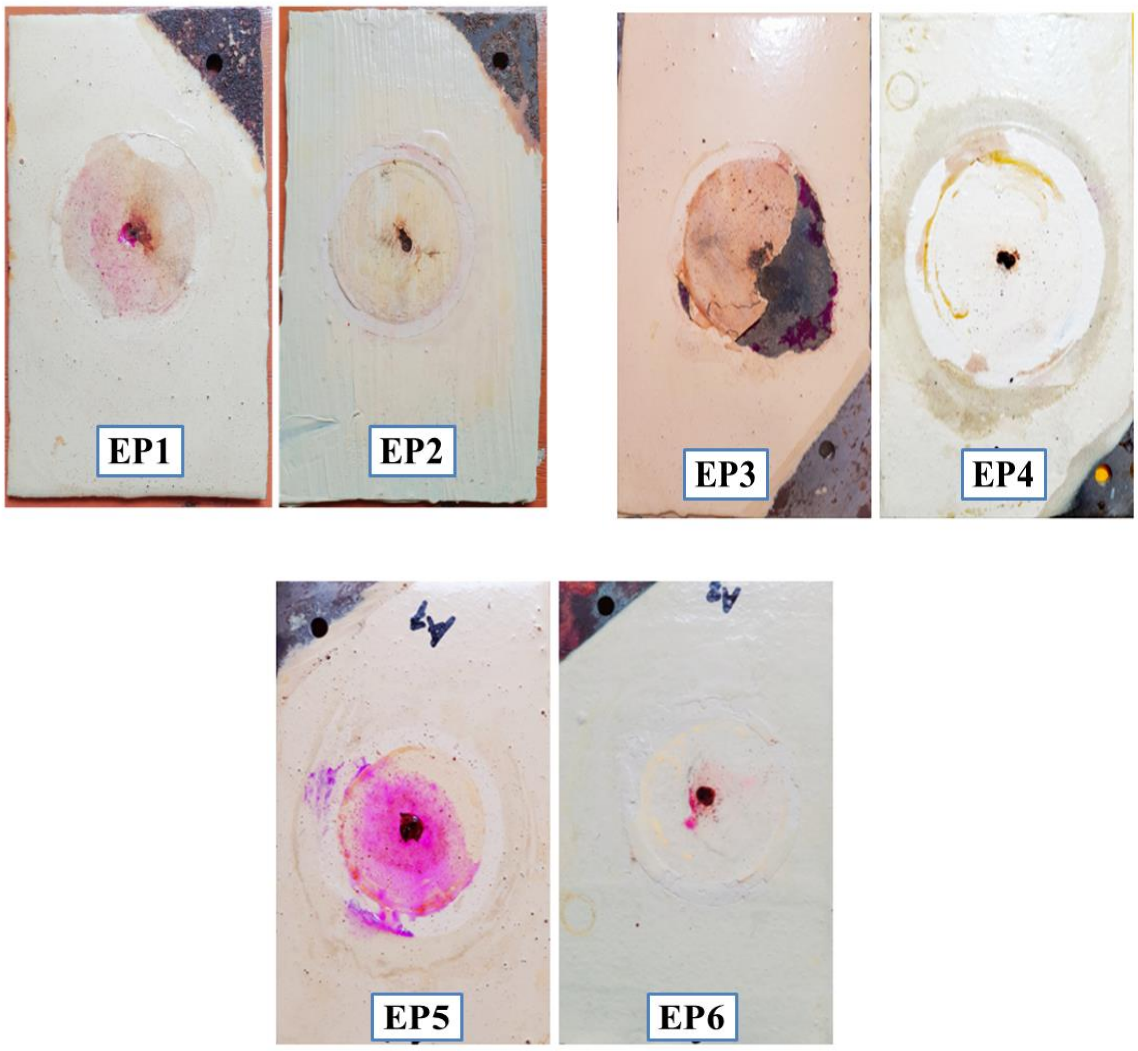


**Fig5(A).52:** Images of MS Coated panels after cathodic disbond test for 3.5% Nacl solution 28 days

**Table.5(A). 13.** Cathodic disbondment results on epoxy based composite coatings

| Samples code name | Voltage (V) | Current (mA) | Temp ($^{O}$C) | Duration (Days) | Disbondment area (mm)/Remarks |
|---|---|---|---|---|---|
| EP1 | ─1.5 | 40─95 | 30-45 | 28 | 6 ─ 13.2 |
| EP2 | ─1.5 | 40─95 | 30-45 | 28 | 6 ─ 9.5 |
| EP3 | ─1.5 | 40─95 | 30-45 | 28 | Partially delamination and 1/3 th area of coating comes out |
| EP4 | ─1.5 | 40─95 | 30-45 | 28 | 6─8.7 |
| EP5 | ─1.5 | 40─95 | 30-45 | 28 | 6─9.3 |
| EP6 | ─1.5 | 40─95 | 30-45 | 28 | 6─7.3 |

## 5.(A).10. Water and Chemical Resistance Study

The degree of water absorption has been evaluated by using formula of % swell test for 65 days. The nano filler based cured film (EP6>EP4>EP2) showed excellent water resistant than conventional cured film (EP5>EP3>EP1).

As result, absorption of water EP5, EP3 and EP1 are 15.14%, 20.8% and 34.2% respectively and where as EP6, EP4 and EP2 are 2.53%, 5.4% and 9.3% respectively.

The resistance behaviors of chemicals of the cured films were studied by in solution of acids (5% HCl and 5% $H_2SO_4$) and alkali (5% NaOH) immersed continue for 65 days.

These studies exposed that the films, acid and alkali immersion test showed damages and weight loss in acid medium is 15-25% and loss of gloss in alkali of conventional cured film. On the other hand small damages and weight loss in acid (3-8%) and little loss of gloss in alkali of nano filler based cured film observed.

Nano composite coatings show better water and chemical resistance than conventional composite coating due to nano particles completely wetted by epoxy and adduct of aliphatic chain from phenalkamine give cured highly crosslink density rigid molecule structure presence of hydrophobic groups of nano organosiliane, etc.

## 5.(A).11. Conclusions

In summary, we have tested the organo silane epoxy nanocomposite material by simple method and successfully showed excellent result in all experiments. Nano composite material's superior corrosion properties than conventional coating have been confirmed by TEM, XRD, SEM and TGA-DTA studies. The most noticeable thing is that the organo silane nano filler with glass flkae embedded polymeric coating exhibits the lowest lowest corrosion current density, resistance to corrosion as well as more positive corrosion potential and excellent polarization resistance when compared to conventional silica based epoxy coating. Even salt spray chamber test shows better corrosion resistance for nano composite epoxy compared to conventional epoxy. Nano composite coating shows much lower cathodic disbondment properties and hence much better corrosion resistance properties. Also, it has been observed that resin can consume 6.5 to 7 wt% of nanoparticles by optimization**.** With view above epoxy nanocomposite coating should be used for corrosion mitigation in the practical applications.

# 5(B)

# POLYURETHANE BASED COMPOSITE COATINGS

## 5(B).1. FTIR spectroscopy

The PU composite coating system proffers a rigid structure. As result, the different intensities of the band of the different functional group are not properly irradiated to the IR beam during its channel or the structure is so rigid that the vibration of normal stretching and bending are too much repressed. The free volume porosity of such composite coating is very less.

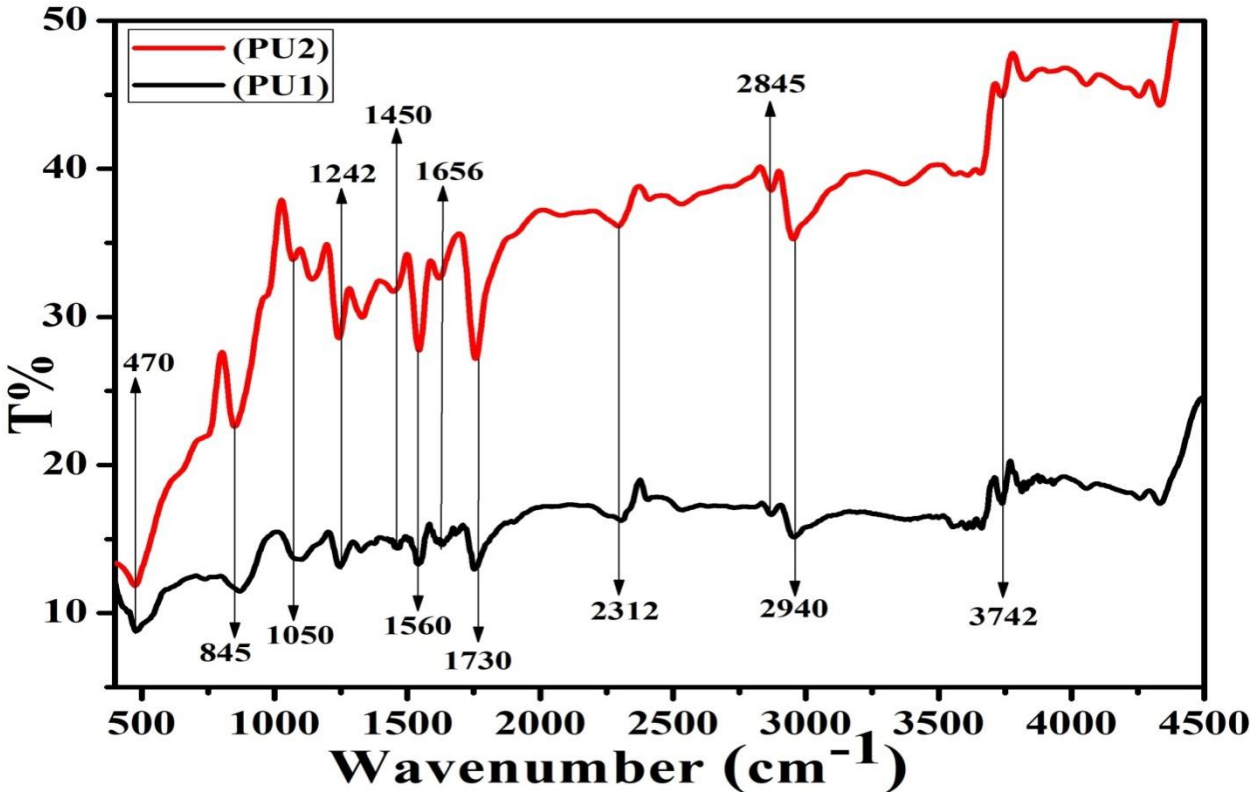


**Fig.5(B).1:** FTIR spectroscopy of composite coatings for PU1 and PU2

The comparative FTIR studies are recorded from IR spectra data for each cured film and evaluated the band pattern of different composite coatings system in Fig.5(A).2 compared with organo siliane nano particles. The assignments for characteristics peaks are given Table.5(B).1. Most observable region are main distinguishable peaks of C─H stretching band (2800─4000cm$^{-1}$) appear. These peaks are mainly associated to urethane linkage (NHCOO) in a polyurethane film

is hydrogen bonded to each other with distinguished functional groups and the nano organo siliane doped on the surface of composite coating. Moreover, the intensity of the peak nanocomposite coating (PU2) increasesess than conventional composite coating (PU1) for embedded organo siliane nanoparticle due to number of methyl groups surrounding Si atom increases intensifies more [21,22].

**Table.5(B).1:** Characteristics peaks from FTIR spectra for PU composite coatings

| **Wavenumber ($cm^{-1}$)** | **Assignments** |
|---|---|
| 3800─4400 | OH of H—OH, Et—OH and Si—OH/N—H of primary and secondary amines |
| 3742-3748 | Free SiOH |
| 2935 | C—H of $CH_2$, $CH_3$/CH aromatic and aliphatic |
| 2920 | Asym.CH stretching |
| 2845 | Symmetrical stretching of CH |
| 2312 | Isocynate |
| 1726 | C═O |
| 1656 | N—H of primary amines |
| 1620 | H—O—H bending |
| 1560 | Polymerized urethanes |
| 1450 | $CH_3$— stretching |
| 1386 | $CH_2$— stretching |
| 1242 | —C—O—C— group |
| 1180 | Si—O—Si of ≡Si—O—Si≡/C—C—O—C |
| 1105 | Asym. Si—O—Si Stretching |
| 1045 | C—O—C of ethers |
| 965 | —C—O— stretching vibration of Si─OH bond |
| 807 | $SiO_4$ tetrahedron ring |
| 470 | O—Si—O |

Polyurethane coating is formed by reacting isocyanates with hydroxyl-containing compounds such as polyethers, polyesters, castor oils, polyhydric alcohols, and so

on. Polymerization of polyurethane takes place when di or poly functional isocyanates react with hydroxyl-terminated compounds. Fig.5(B).1 displays the FTIR spectra of the polyurethane coating in its as prepared state.

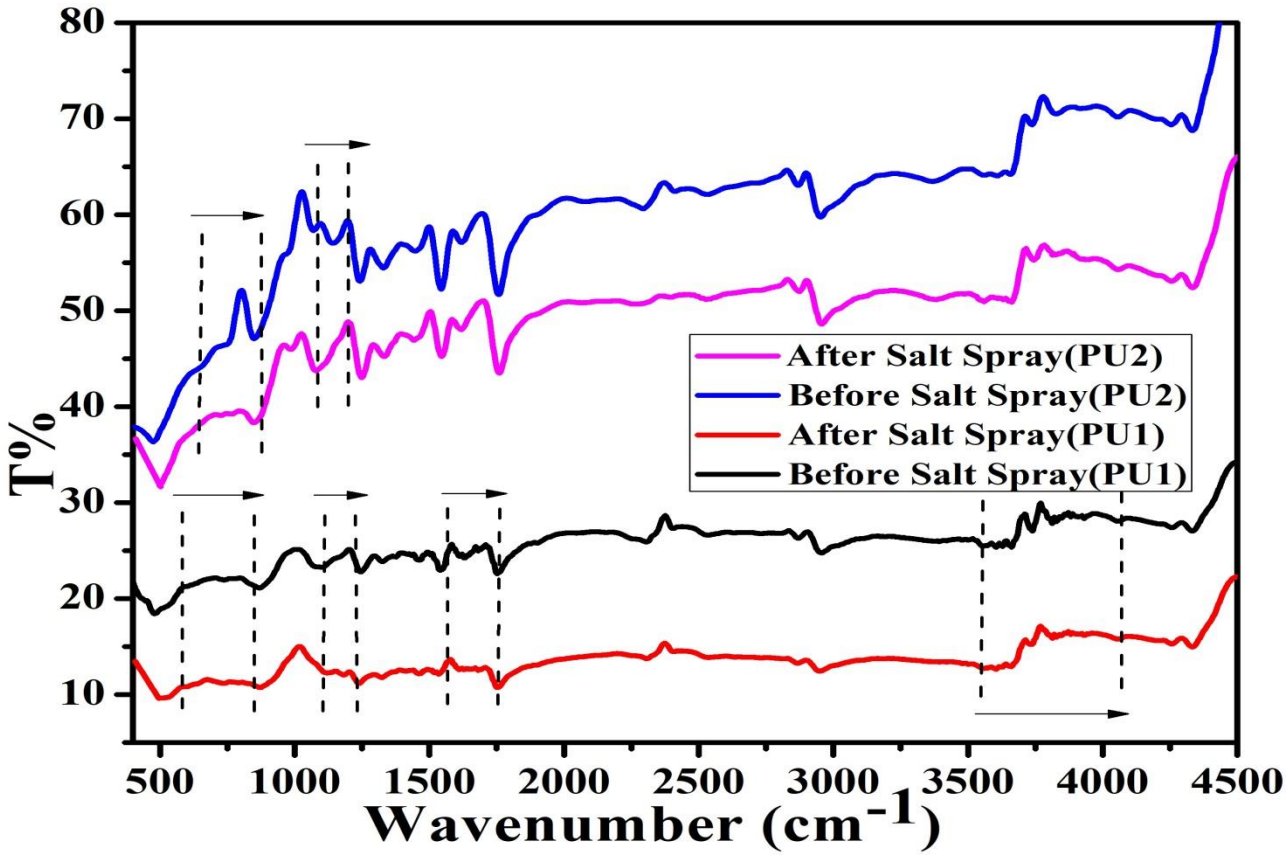


**Fig.5(B).2:** FTIR spectroscopy of polyurethane composite coatings of PU1 and PU2 after 2200hrs salt spary test

After 2200 hours of salt spray exposure, the FTIR spectra of composite coatings recorded in Fig.5(B).2 showed that the relative transmittance of the salt-sprayed nano-composite coating closely resembles that of the unprocessed one. Additional very weak bands (i) 1078 to 1191cm$^{-1}$ and (ii) 649 to 870cm$^{-1}$ are observed in resin degradation of nanocomposite coating of PU2. The presence of such a peak indicates an interaction between the polyurethane coating and the salt spray, suggesting slow corrosion resistance against salt spray. But in case of conventional composite coating of PU1, additional bands (i) 3554 to 4056cm$^{-1}$ (ii) 1560 to

1761cm$^{-1}$ (iii) 1111 to 1332cm$^{-1}$ and (iv) 583 to 844cm$^{-1}$ are observed in resin degradation which signify corrosion occurred in between polyurethane and salt spray [6].

## 5(B).2. XRD Patterns Analysis

The XRD peaks of organo siliane particles and composite coating of cured film seen in Fig.5 (B).3. A broad pattern obtained at 2θ = 22.21 compared to the presence of $SiO_2$ crystalline particle it correlate that particles are amorphous in nature [17]. In composite, pigments broad peaks are observed at angles of 2θ values and (*hkl*) planes are 20.90 *(1 1 1)*, 27.03 *(1 2 0)*, 31.02 *(2 1 1)* 39.40 *(130)* and 68.32 *( 3 3 3 )* for quartz silica (Card No: 1010921), 27.7 (*110*), 36.2 *(101)*, 41.4 *(111)*, 44.5 *(210)* 54.3 *(211)* and 56.6 (*200*) for rtile $TiO_2$ respectively (Card No: 21-1276) and additives of soap stone powder observed at angles of 2θ values and (*hkl*) planes are 29.4 *(027)*, 31.29 *(028)*, 51.2 *(0211)* and 60.2 *(330)* respectively (Card No: 10-0036). Now it can say that all composition are fully embedded in PU matrix but PU2 nanocomposite showed more intense peak due to more amorphous nature of organo silane nano filler.

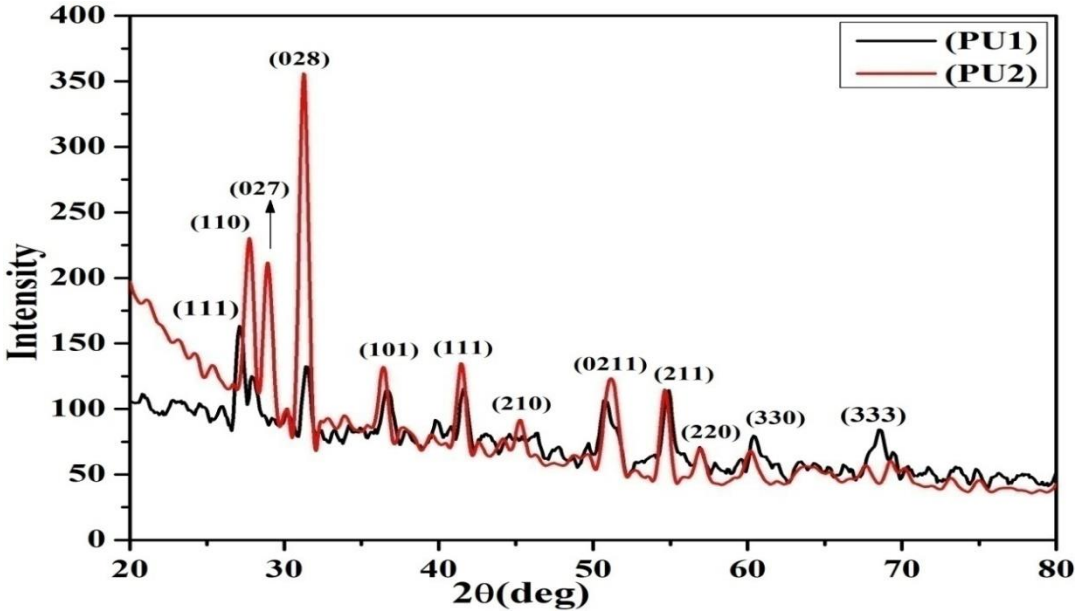


**Fig.5 (B).3:** XRD pattern of organo silane nano particles embedded PU composite

## 5(B). 3. Morphology Study

### 5(B). 3.1. Scanning Electron Microscope (SEM)

For better corrosion performance of resultant nano coating it is very important to good wetting necessary of particles in nano sized in composite. Fig.5(B).4 shows at two different magnifications SEM images of PU1 in (a) where some particles are observed at micro level and SEM micrographs of dispersed nano silica of PU2 in (b). SEM images displays the silica nano particles are homogeneously dispersed in the polymer matrix and agglomeration occurred during the formation of composite coating. Here at two different magnifications of images 3µm and 10 µm used for both coating observation.

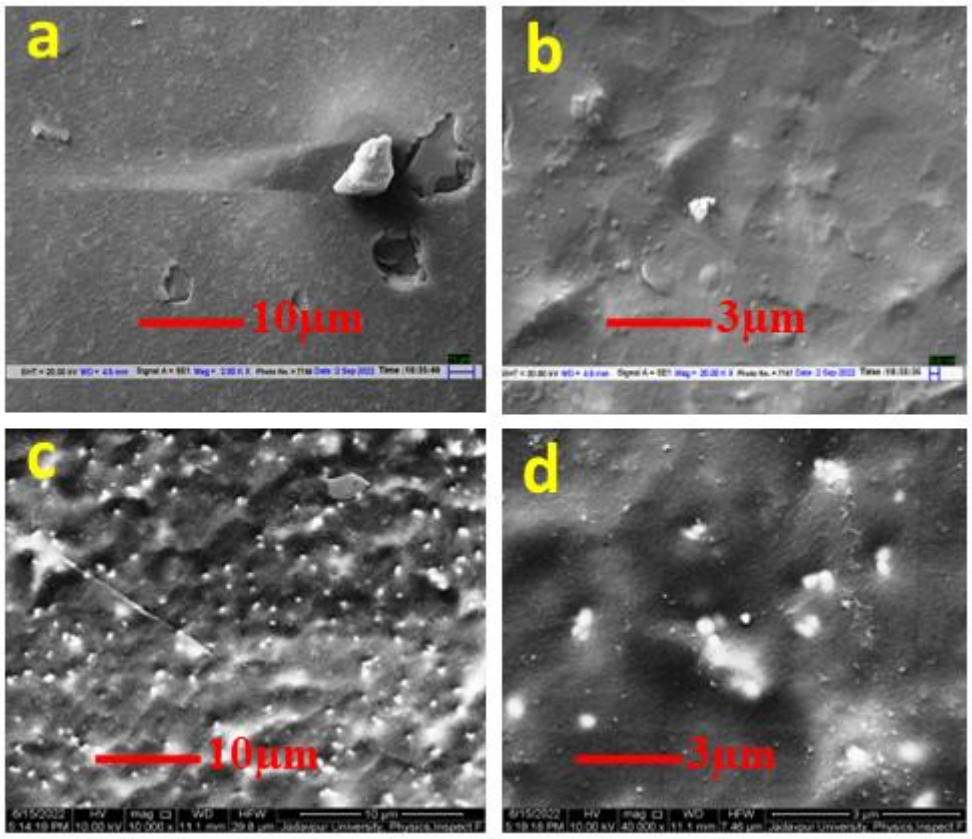


**Fig.5(B).4:** SEM images of (a) & (b) for PU1 and (c) & (d) for PU2 composite film

## 5(B). 3.1. Transmission Electron Microscope (TEM)

TEM studies determine degree of dispersion tread $SiO_2$ nono filler in the morphology which will truly get into better corrosion performance of the nano composite coating. Used of Image J software organo silane particle size is less than 20nm detected. Fig.5(B).5 shows TEM images of nano organo silane embedded PU composite coating.

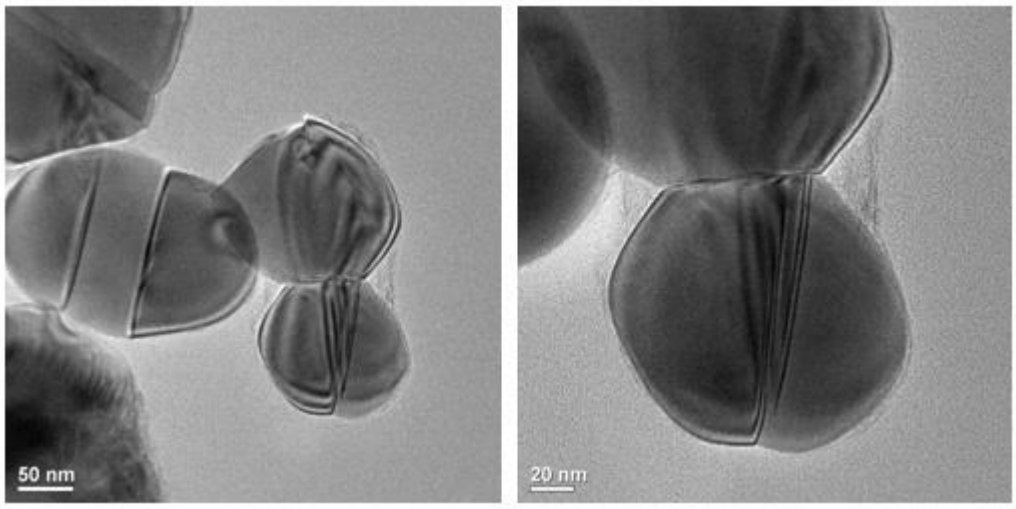


**Fig. 5 (B).5:** Transmission electron image of organo silane nano PU composite

## 5(B).4. Thermal Analysis (TGA-DTA)

The thermal stabilities of the PU composite films were assessed using TGA-DTA analysis, as depicted in the Fig. 5(A).6. The TGA-DTA curves displayed two distinct stages of mass loss. These stages were attributed to the decomposition of MDI present in the pre-polymer and the ester groups found in the polyol. The first stage involved the decomposition of MDI with the breakage of urethane bonds, resulting in an 8% mass loss occurring between 200 and 350°C for PU1. The second stage entailed ester decomposition, leading to an 11% mass loss between 350 and 535°C for PU2. Notably, for the nano PU2 sample, the film fully degraded

at a higher temperature range of 750-760°C, indicating a significant difference in mass loss compared to the NCO/OH ratios [23-25].

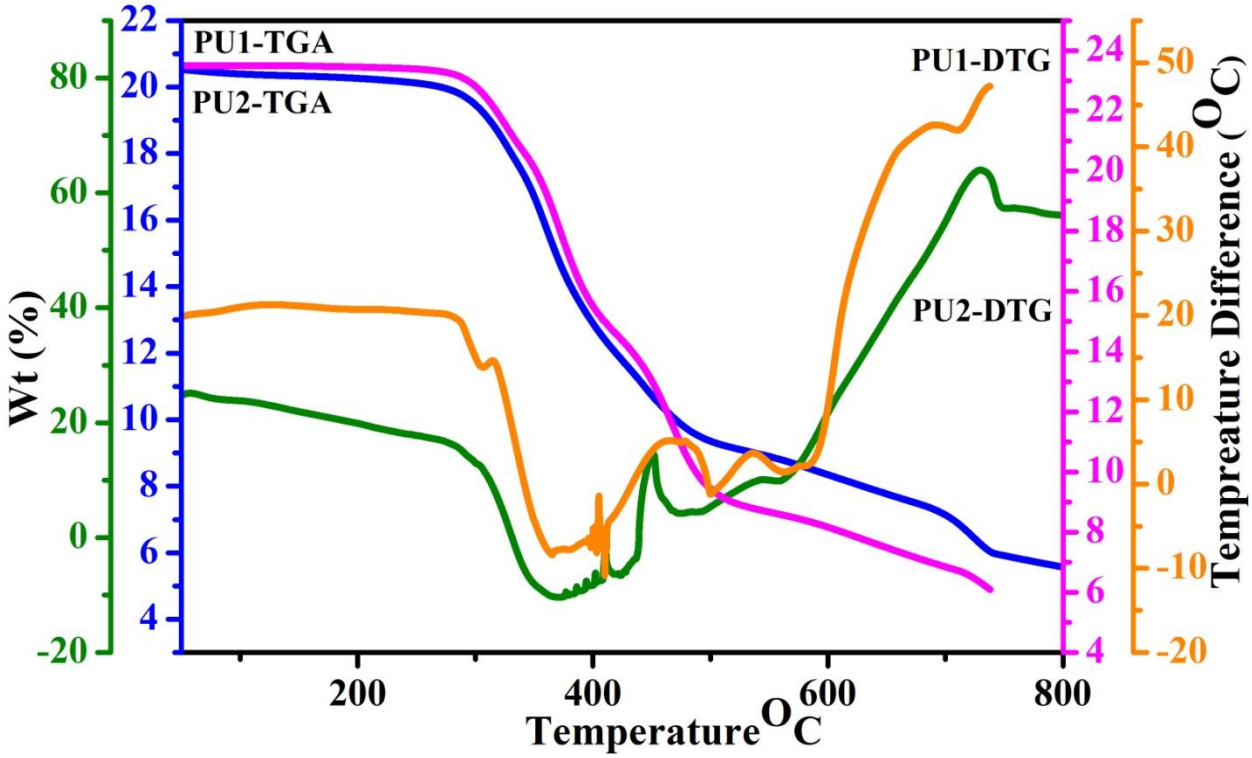


**Fig. 5(A).6**: TGA-DTA thermogram for PU1 and PU2 composite film

DTA diagram predicted endothermic reaction occurred at 250 to 350$^{O}$C for solvent evaporation. Exothermic reaction occurred 450 to 780$^{O}$C due to binder disintegration in composite coating.

## 5(B).5. Physico-Mechanical Properties

In the regard of mixing ability and formation viscosity, the addition of nano organo silane increases viscosity more than conventional quartz silica. This is because silica nanoparticles have a higher surface area for interaction with polymer chains in the composite matrix. After holiday (electrical insulation) test, no audio visual sound, any spark pinhole break and presence of conductive particles observed. Various mechanical properties such as DFT, flexibility, scratch hardness, pencil

hardness, adhesion, falling ball impact, and abrasion resistance were evaluated for composite coatings. Both types of coatings have a DFT of 200±10 microns. PU2 is more flexible than PU1, and PU2 also exhibits better scratch and pencil hardness due to higher hardness and cross-linking density. There were no cracks observed after the falling ball impact test, indicating a uniform dispersion of nano fillers and a strong cross-linked elastomeric structure. PU2 has a superior cross-link density compared to PU1, attributed to longer hydrophobic chains on the surface of nanoparticles, enhancing interactions within the polymer segments.

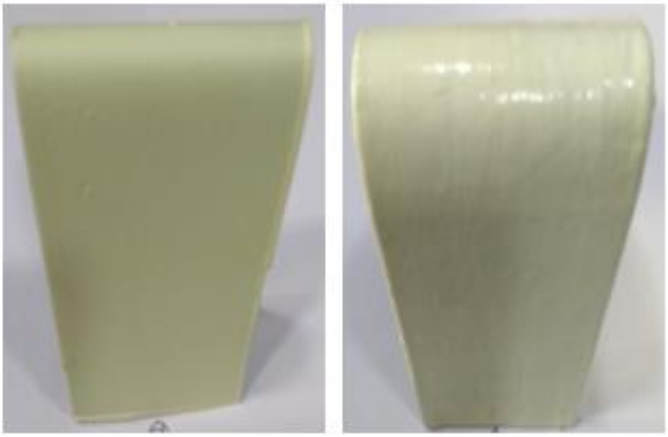

PU1 PU2

**Fig. 5(B).7:** Images of flexibility coated PU composite on MS panel

**Table. 5(B).2:** Result of scratch hardnes and pencil hardness of PU composite coating on MS panel

| **Sample code Name** | **500 gm Weight** | **1000 gm Weight** | **1500 gm Weight** | **Hardness (6B to 6H)** |
|---|---|---|---|---|
| PU1 | Passed | Passed | Failed | Failed at 3H |
| PU2 | Passed | Passed | Passed | Passed |

In PU composite coatings, incorporating nano silica significantly improves abrasion resistance with minimal weight loss compared to silica micro particles.

Nano silica coatings exhibit 2.1 mg/1000 cycles weight loss, indicating uniform distribution for a stronger network. Adhesion properties in nanocomposite coatings are superior, thanks to increased crosslink density due to nano-particle distribution, especially after a salt spray test. At 60$^{o}$ angel PU2 displays better gloss than PU1 i.e. PU2 of nano silica particles has high refractive index than conventional of PU1.

PU1 PU2

**Fig.5 (B).8:** Images of falling ball impact test of PU composite coating on MS panel

**Table. 5(B).3:** Result of Physico-Mechanical testing of PUcomposite coating

| **Coating code name** | **Cross link Density (%)** | **Adhesion Property (N/mm$^2$)** | | **Impact Test (KG.M)** | | **Abrasion Test (mg/cycles)** | **Gloss** |
|---|---|---|---|---|---|---|---|
| | | **Before Salt Spray** | **After 2200 hrs Salt Spray Test** | **Instrusion** | **Extrusion** | | **At 60$^{O}$ angle** |
| PU1 | 87 | 29.5 | 18.8 | >0.5 | >0.7 | 7.8 | 102 |
| PU2 | 92 | 43.7 | 34 | >0.4 | >0.3 | 3.8 | 143 |

## 5.(B).6 Corrosion Studies

## 5 (B).6.1. Tafel curves analysis of the various composite PU coatings

Various composite PU coatings of PU1and PU2, polarization curves were studied for periodic time intervals (initial, 1, 7, 15 and 30 days) by immersion in 3.5 wt% Nacl solution and have been depicted in Fig.5(B).9 and Fig.5(B).10 polarization curves, corrosion potential ($E_{corr}$), cathode Tafel slope ($\beta_c$), anode Tafel slope ($\beta_a$), corrosion current ($I_{corr}$), polarization resistance ($R_p$) and corrosion current density ($J_{corr}$) are calculated.

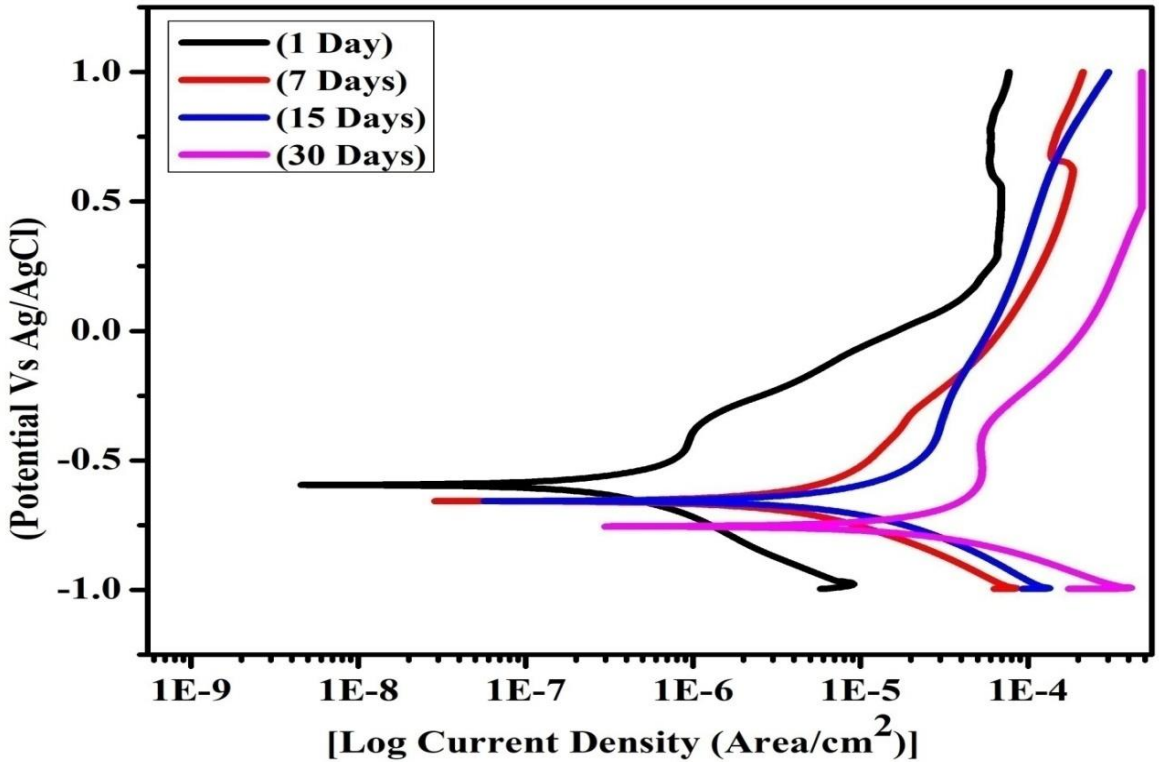


**Fig.5(B).9:** Tafel curves of PU1 after (1, 2, 15 and 30) days immersions in 3.5 wt% Nacl aqueous solution

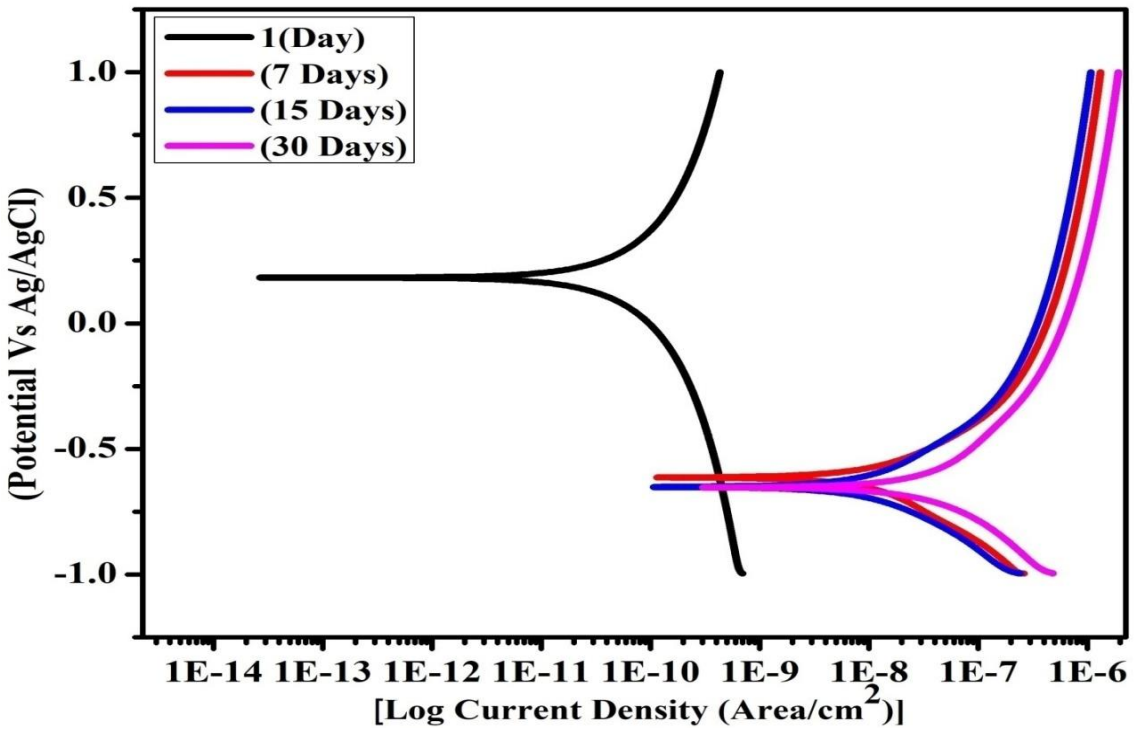


**Fig.5 (B).10:** Tafel curves of PU2 composite coating after (1, 2, 15 and 30) days immersions in 3.5 wt% Nacl aqueous solution

**Table.5(B).4:** Electrochemical parameters after soaking for different time (1, 7, 15 and 30) day intervals of polarization measurements for PU1 and PU2 composite coating

| Samples code Name | Day(s) | $-E_{corr}$ (V vs SCE) | $J_{corr}$ (A/cm$^2$) | $I_{corr}$ (mA cm$^{-2}$) | Corrosion rate (mm/year) | $R_p$(Ω cm$^2$) | βa (mV dec$^{-1}$) | βc (mV dec$^{-1}$) |
|---|---|---|---|---|---|---|---|---|
| PU1 | 1 | −0.594 | 2.28E-07 | 4.74E-06 | 0.00265 | 8153.90 | 0.158 | 0.204 |
| | 7 | −0.651 | 2.94E-06 | 6.16E-05 | 0.03426 | 748.26 | 0.224 | 0.200 |
| | 15 | −0.632 | 6.90E-06 | 0.00014 | 0.08017 | 368.63 | 0.228 | 0.263 |
| | 30 | −0.746 | 1.66E-05 | 0.00034 | 0.19345 | 119.71 | 0.235 | 0.161 |
| PU2 | 1 | (+)0.182 | 2.56E-11 | 6.12E-10 | 2.97E-07 | 1.10E+08 | 0.308 | 0.313 |
| | 7 | −0.612 | 8.43E-09 | 2.01E-07 | 9.79E-05 | 2.06E+05 | 0.190 | 0.236 |
| | 15 | −0.651 | 6.27E-09 | 1.50E-07 | 7.29E-05 | 2.63E+05 | 0.191 | 0.173 |
| | 30 | −0.653 | 1.87E-08 | 4.48E-07 | 0.00021 | 93929 | 0.211 | 0.179 |

In Table 5(B**)**.4, electrochemical parameters of various composite coatings are given. From the table it is found that PU2 sample given higher $E_{corr}$, lower $I_{corr}$, and higher Rp values as compared to PU1. This suggests that PU2 composite coating gives better corrosion resistive properties as compare to PU1. Meanwhile, the corrosion current ($J_{corr}$) of PU2 coating is also the lowest. Interestingly, the corrosion potential first increased and then decreased in PU1 coating and also corrosion current to be inversely related. Moreover, PU2 coating has the largest $E_{corr}$(−0.65351) and the smallest $J_{corr}$(1.8767E-08A/$cm^2$) for 30 days compared to PU1. In term of polarization resistance of PU2 is 93929Ω$cm^2$ whereas PU1 is 119.71Ω $cm^2$. From this study it is found that nano composite coating possesses the superior corrosion resistance properties over the conventional composite coating.

## 5 (B).6.2. Analysis of EIS results of various composite PU coating

Fig.5(B).11 and Fig.5(B).12 shows EIS, Bode and Nyquist plot of samples PU1 and PU2 after immersed in 3.5% Nacl aqueous solution for (initial 1, 7, 15 and 30) day(s). After the initial 1 day, the Nyquist diagram PU2 shows large arc radius than PU1. Fig.5(B).13 and Fig.5(B).14 While Bode diagrams in shows impedance behavior of composite coating of PU2 is $2\times10^3$ times greater than PU1. This time PU2 coating show better protective barrier with large impedance and matrix is most shielding wall. After immersion of 7 days for PU1 coating exhibit decreases arc radius than 1 day as well as in Bode diagrams the impedance at low frequency gradually decline with time interval. It could be say that the electrolyte solution was penetrating through the composite coatings. Over the 15 days Nyquist diagram exhibit two times constant. In Bode plot the diagonal, capacitive nature in the high frequency region shifted to the low frequency direction. It has observed that the nature of capacitance increased gradually and the protective nature decline of PU1

coating. But in case of PU2 after 7days immersion arc radius of Nyquist plot same as 1 day's diagram and Bode diagram follows same impedance due to agglomeration behaviors of nanoparticles in composite PU coating [20,21]. Interestingly, after 15 days PU2 composite coating shows highest impedance arc radius as well as high frequency in Bode plot. Nyquist diagram reveals that well dispersion of nano silica truly increases the performance of corrosion protection on metal substrate.

With the immersion testing progress on, after 30 days in case of PU1 composite coating the capacitance arc of Nyquist plot follows same as 15 days diagram with two times constant. In Bode diagrams the impedance at low frequency be disposed loss steadily, which introducing the penetration of electrolyte solution in the composite coating has nearly reached at saturation. In Nyquist diagram arc radius is reduced indicating the corrosion could be started in PU2 coating. Now, two plot forms are seen in the high and low frequency region which convey resistance and delimination nature of coatings PU2 and PU1 respectively [26,27].

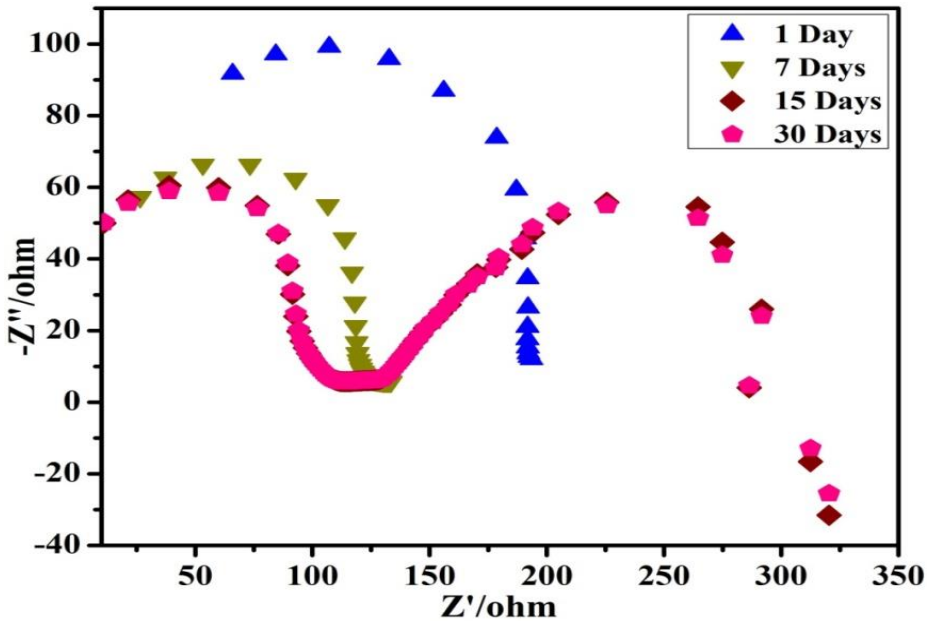


**Fig.5(B).11:** Nyquist plot of PU1 after soaking for 3.5 weight% Nacl aqueous solution for (1, 7, 15 and 30) days

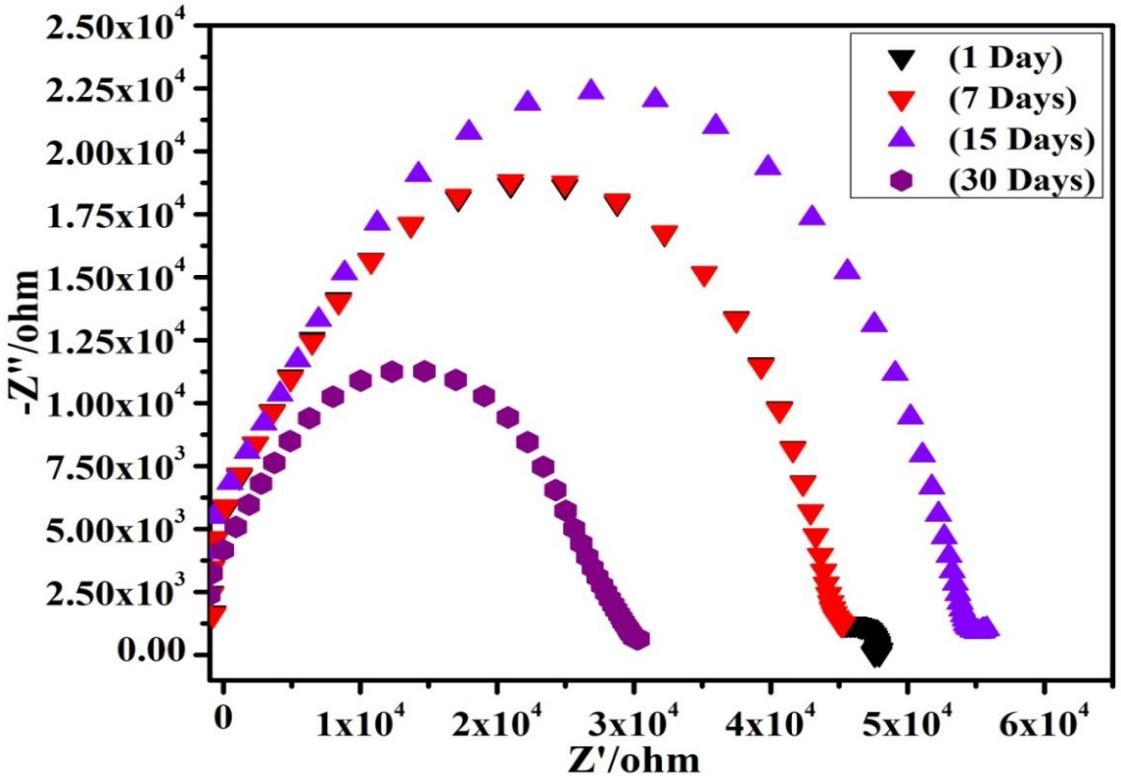


**Fig.5(B).12:** Nyquist plot of PU2 after soaking for 3.5 weight% Nacl aqueous solution for (1, 7, 15 and 30) days

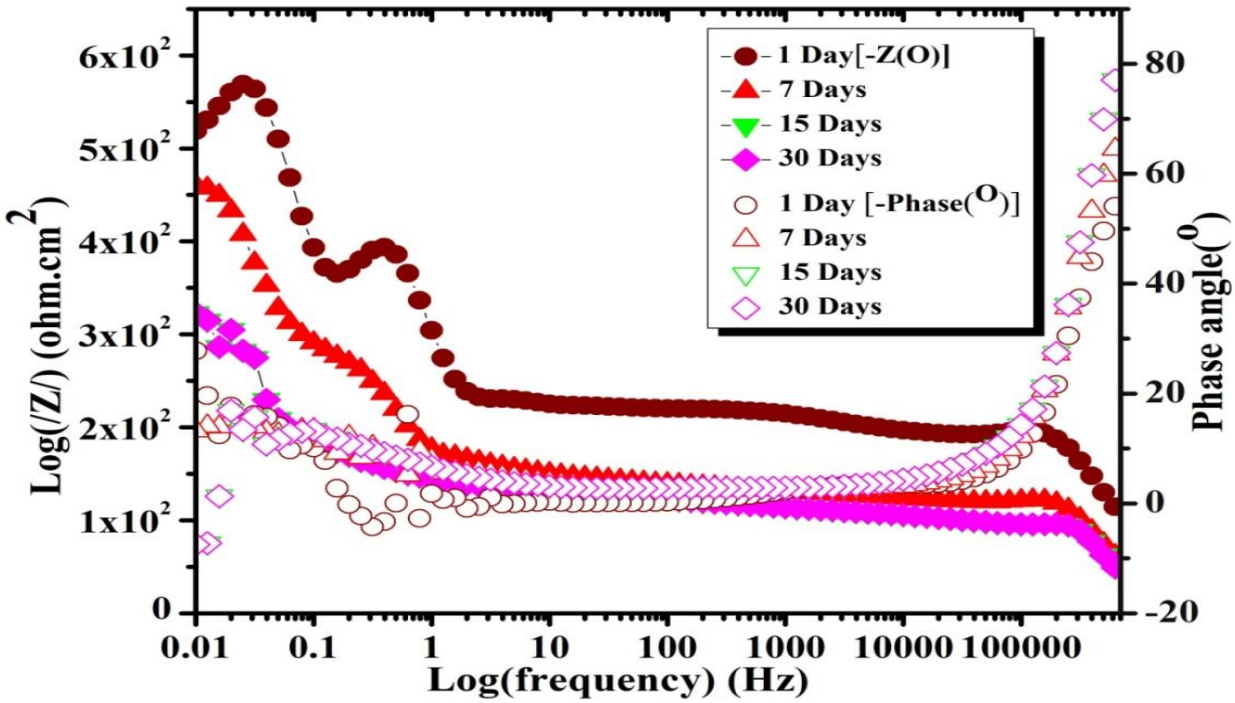


**Fig.5(B).13:** Bode plot of PU1 after soaking for 3.5 weight% Nacl aqueous solution for (1, 7, 15 and 30) days

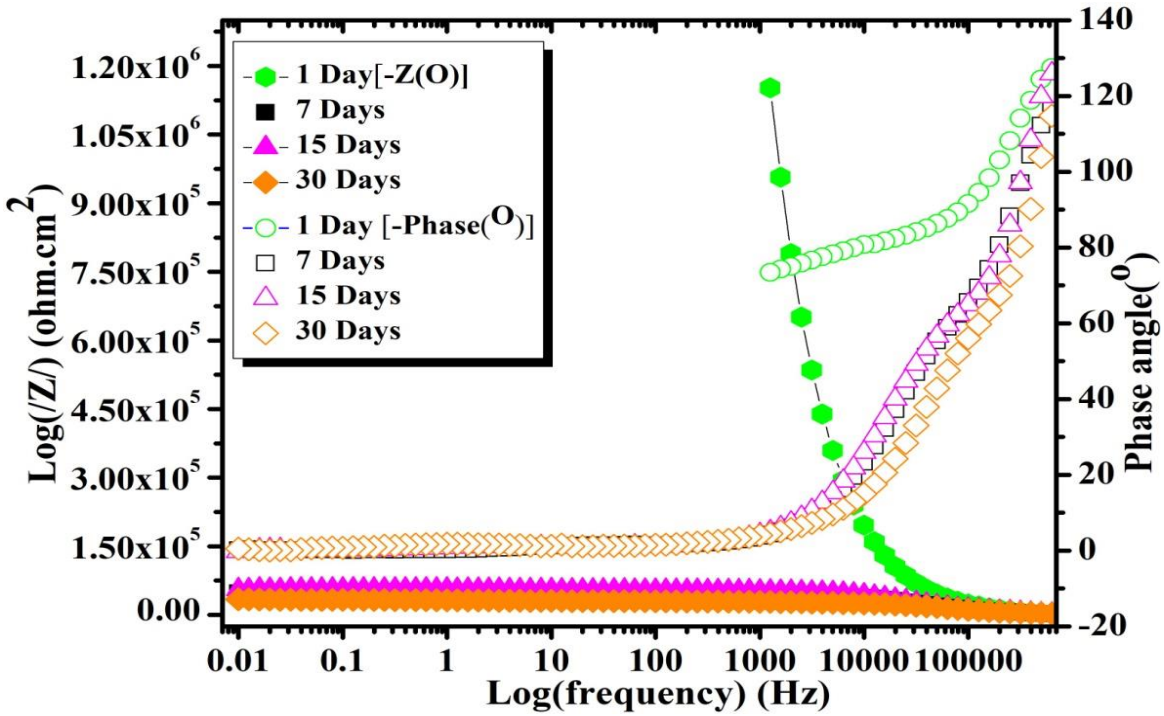


**Fig.5(B).14:** Bode plot of PU2 after soaking for 3.5 weight% Nacl aqueous solution for (1, 7, 15 and 30) days

From the Nquist diagram,solution resistance(Ru), polarization resistance (Rp),charge transfer resistance(Rct),constant phase element(C.P.E),admittance nature of coating($Y_o$)and capacitive nature of coating(N)are derived and tabulated in table.8. These are used to evaluate the equivalent circuit. Nyquist plots shows one time constant and two times constant from electrochemical behavior and the equivalent circuit has been depicted in Fig.5(B).15. From this study it isfound that the metal corrosion rate with the coating are inversely related to Rct or charge transfer resistance and barrier properties for the coating. Therefore in order to improve the corrosion resistance we have to have higher Rp and Rct value for the given coating [20-22]. From values in table.8.we can see that PU2 has the much better corrosion resistance properties than PU1for immersion for a time interval, in 3.5 weight % Nacl aqueous solution.

**Table.5(B).5:** Fitting results of PU1 and PU2

| **Samples name** | **Day(s)** | **C.P.E ($Y_o$)** | **Rp.R(Ω)** | **C.P.E (N)** |
|---|---|---|---|---|
| PU1 | 1 | 2.4029E-09F | 166.63 | 1.1476 |
| | 7 | 3.9278E-09F | 119.77 | 1.126 |
| | 15 | 2.321E-08F | 83.13 | 0.813 |
| | 30 | 1.764E-05 | 34.53 | 0.541 |
| PU2 | 1 | 2.3489E-10F | 8.051E+07 | 0.89832 |
| | 7 | 1.3589E-10F | 57242 | 0.84937 |
| | 15 | 1.3351E-10F | 58380 | 0.83721 |
| | 30 | 1.1831E-10F | 32883 | 0.78725 |

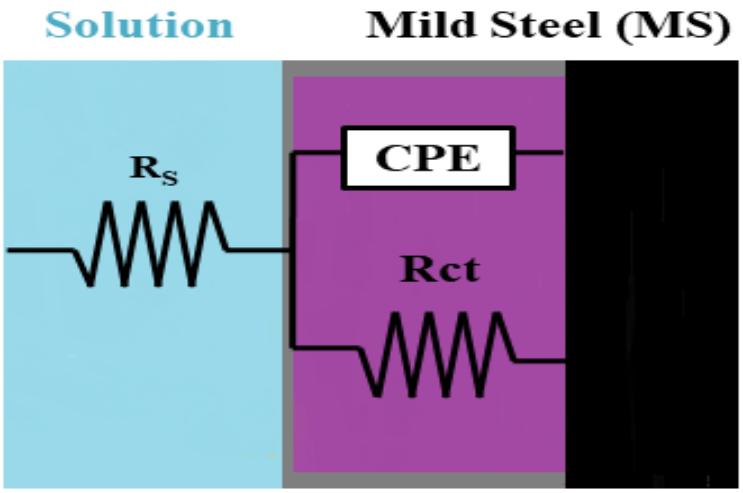


**(a)**

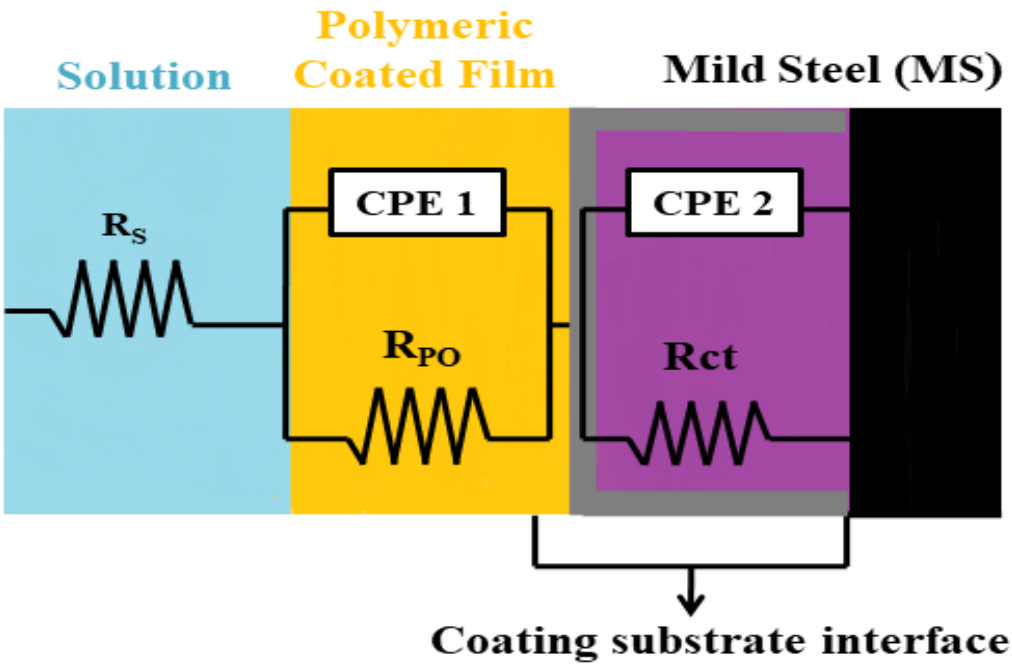


**(b)**

**Fig.5(B).15:** The equivalent electrical circuit models used to simulate EIS measurements of coatings at various immersion stages: (a) for one time constant and (b) for two time constant

**Table.5(B).6:** Inhibition efficiency of developed PU from electrochemical parameter after corrosion studies

| **Coating code Name** | **% Corrosion Inhibition Efficiency=** $\frac{I^{o}_{corr}-I_{corr}}{I^{o}_{corr}} \times 100$ | **%  Rct =** $\frac{Rct-Rct^{o}}{Rct} \times 100$ | **P =** $\frac{R_{P(Uncoated)}}{R_{P(Coated)}} \times 10^{-\frac{(\Delta E_{corr})}{b_a}}$ |
|---|---|---|---|
| PU1 | 69.70 | 75.62 | $P=23.74\times10^{-3}$ |
| PU2 | 99.89 | 99.94 | $P=87.24\times10^{-10}$ |

From Table.5(B).6, electrochemical parameter, it has been seen, PU2>PU1> increasing order for corrosion inhibition efficiency, PU2>PU1 increasing order for charge transfer resistance and PU2>PU1 increasing order for porosity measurement of different type of composite coatings respectively. It has suggested that nano filler embedded PU coating best results in corrosion inhibition efficiency and charge transfer resistance due to dense structure formed when cured with hydrophobic nano silica particle compared to conventional one [27].

## 5.(B).7. Surface Analysis of Coatings (Optical Images)

Optical images with different magnifications are taken before and after corrosion test of coatings on MS rod of electrochemical experiments. In Fig.5(B).14 (a) & (b) show images before corrosion of PU1 coating with different magnification. After corrosion study it has been seen that most pits with degradation are observed over the surface of PU1 coating in Fig.5(B).14 (c) & (d). It revealed that swelling has occurred in Nacl medium of conventional coating of PU1. Damages observed

at the metal-coating interface uptake electrolyte that implies the weak resistance nature of PU1coating. Fig.5(B).15 (p) & (q) show images before corrosion of PU2 coating. There are no such holes and damages observed after corrosion study of PU2 coating in Fig.5(B).15 (r) & (s). Presence of nano organosiliane at metal/coating interface prevented the penetration of corrosion ions on MS substrate.

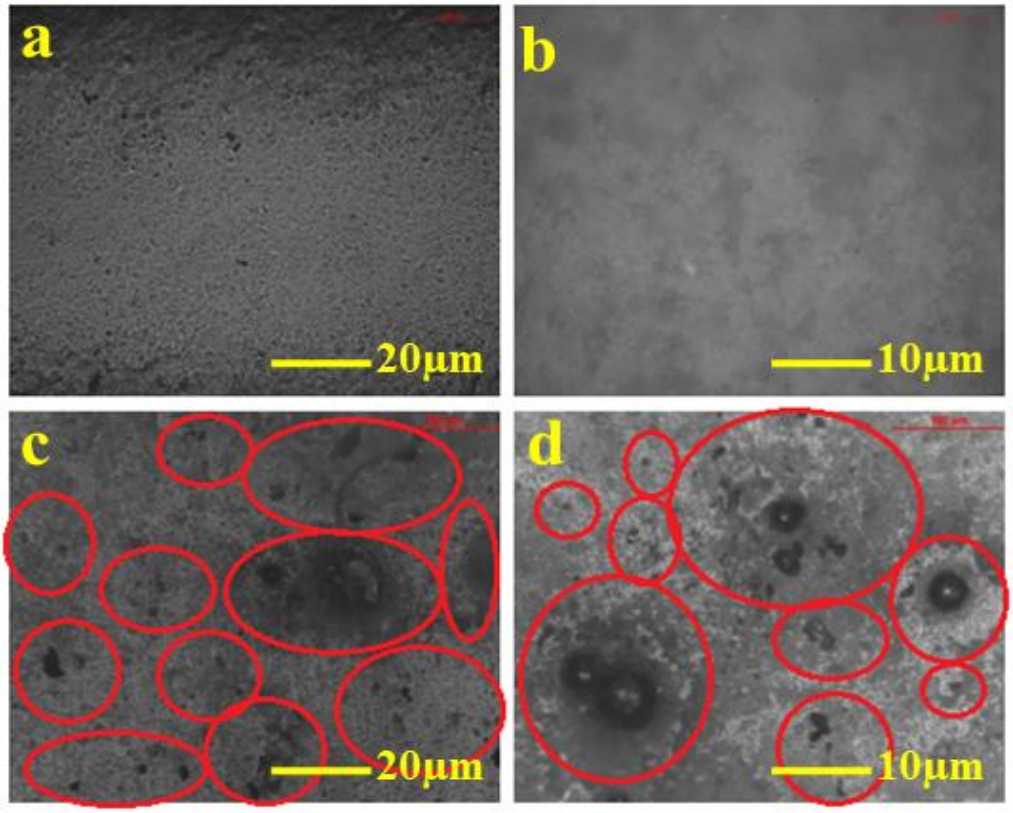


**Fig.5 (B).14**. Image shows studies at different magnifications (m) before corrosion and (n) after corrosion of PU1

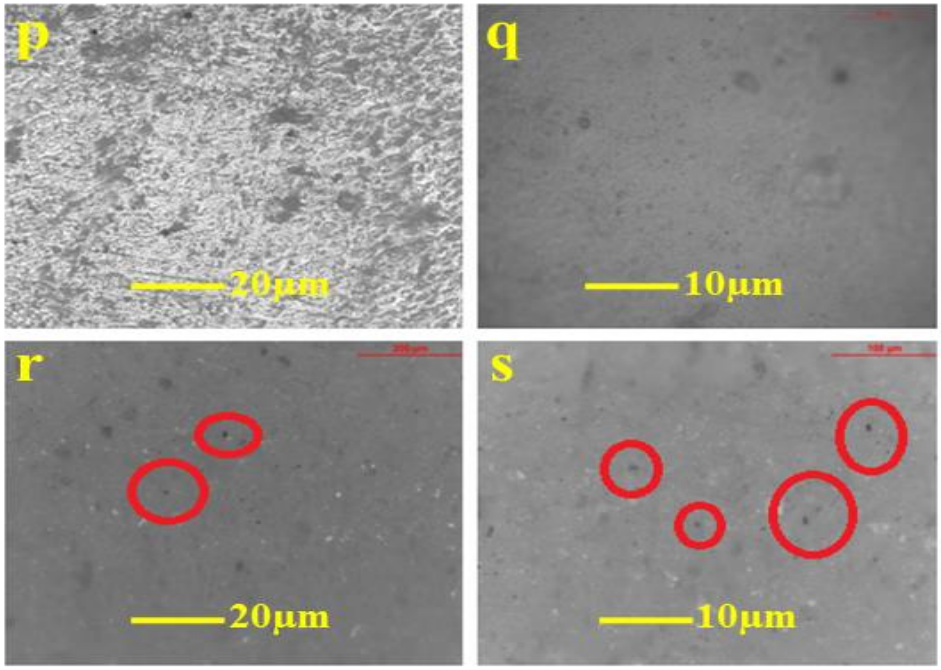


**Fig.5(B.)15**. Image shows studies at different magnifications (o) before corrosion and (p) after corrosion of PU2

## 5.(B). 8. Salt Spray Study

Salt spray chamber test is carried out for 2200 hours incontinuous fog on coated panels. From, Fig.5(B).16 it is indicated, that corrosion and blister formation occurred only in micron silica based epoxy and not in nano silica composite epoxy coating. This indicated nano silica embedded PU1 having much better corrosion resistant properties than conventional silica based PU2 coating.

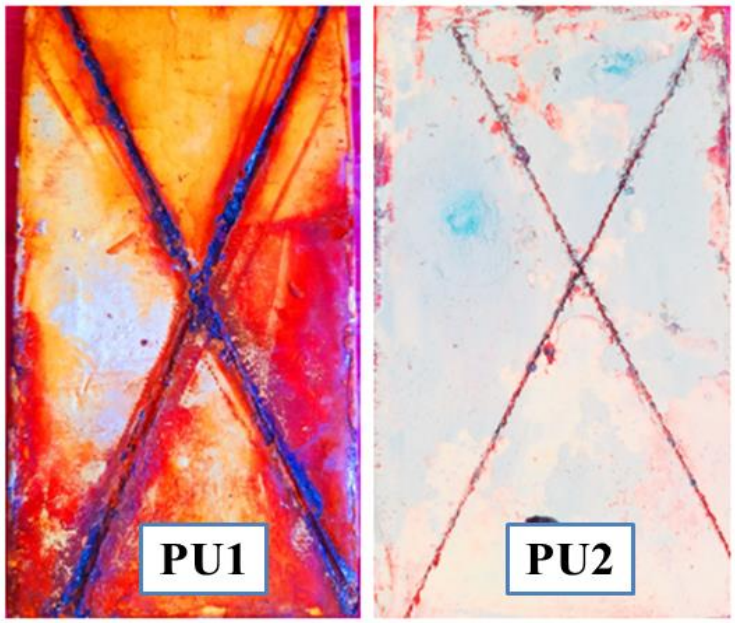


**Fig.5(B).16:**Images of the PU composite coated panel after 2200 hours expose in 5% Nacl solution salt spray

## 5(B).9. Cathodic Disbondment Study

After completion of experiment phenopthalein indicator was poured in drilled hole at the centre of each cell. There was change of violet colour,which indicates violet colour zone has been corroded shown and givenin Fig.5(B).17. Here temperature plays major role in disbonding of coatingwhich is directly proportional to disbondment (mm/day). Moreover, following an increase of the current, greater expansion will be observed at higher temperatures [28,29]. At high vapour pressure porosity of coating increases as a result there will be increase in the permeation of electrolyte through the coating. This results in the chemical attack and thermal expansion of the metal substrate. Moreover, at elevated temperatures dissolution of interface oxides will be accelerated. Result shows epoxy composite PU2 sample has much lesser cathodic disbondment area than PU1which again suggestedthat nano embedded PU2 sample has better corrosion resistant properties than PU1.

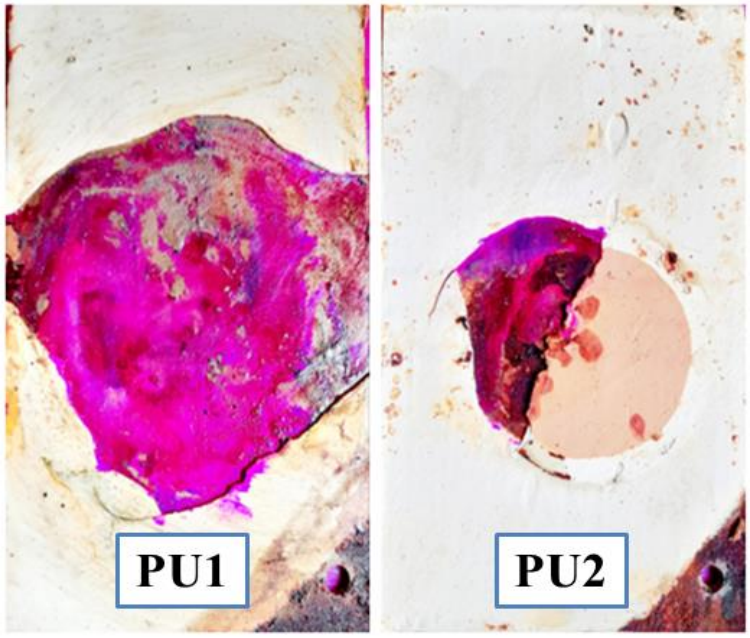


**Fig.5 (B).17**: Images of MS Coated panels after cathodic disbond test for 3.5% Nacl solution 28 days

**Table.5 (B).7:** Cathodic disbondment result for PUcomposite coating

| Sample | Voltage (V) | Current (mA) | Temp ($^{O}$C) | Duration (Days) | Disbondment area (mm) |
|---|---|---|---|---|---|
| PU1 | −1.5 | 40−95 | 30-45 | 28 | Less delamination |
| PU2 | −1.5 | 40−95 | 30-45 | 28 | Fully delamination |

## 5.(B). 10. Water and Chemical Resistance Study

The degree of water absorption has been evaluated by using formula of % swell test for 65 days. The nano filler based cured film PU2 showed excellent water resistant than conventional cured film PU1. As result, absorption of water PU1 is 25.32% and where as PU2 is 6.23%. The resistance behaviors of chemicals of the

cured films were studied by in solution of acids (5% HCl and 5% $H_2SO_4$) and alkali (5% NaOH) immersed continue for 65 days. These studies exposed that the films, acid and alkali immersion test showed damages and weight loss in acid medium is 20-30% and loss of gloss in alkali of PU1. On the other hand small damages and weight loss in acid (8-17%) and little loss of gloss in alkali of PU2 observed. PU2 shows better water and chemical resistance than PU1 due to nano particles completely wetted by polyurethane and adduct of MDI give cured highly crosslink density rigid molecule structure presence of hydrophobic groups of nano organo silane, etc.

## 5.(B). 11. Conclusions

Developed composite materials have been confirmed by FTIR, XRD, TEM, XRD, SEM, and TGA-DTA studies. The most noticeable thing is that the nano organosilane embedded polymeric coating exhibits the lowest lowest corrosion current density, resistance to corrosion as well as more positive corrosion potential and excellent polarization resistance when compared to conventional silica based PU coating. Even salt spray chamber test shows better corrosion resistance for nano filler compared to conventional filler. Nano composite coating shows much lower cathodic disbondment properties and hence much better corrosion resistance properties. Importantly, the composite coating with nano composite material displays excellent wear resistance and thermal behaviors than conventional one. Nano base composite coating has low water absorption and high chemical resistance than conventional one. Also, it has been observed that resin can consume 6.5-10wt% of nanoparticles by optimized. With view above nano composite PU coating should be used for corrosion mitigation in the practical applications.

# 5(C)

# COAL TAR-EPOXY BASED COMPOSITE COATINGS

## 5 (C).1. FTIR Spectroscopy

Fig. 3. Shows C─H stretching bands are observable in regions (2850 to 3200 $cm^{-1}$). These bands are very closely associated to alkyl groups of the organo silane particle inthe nanocomposite surface.

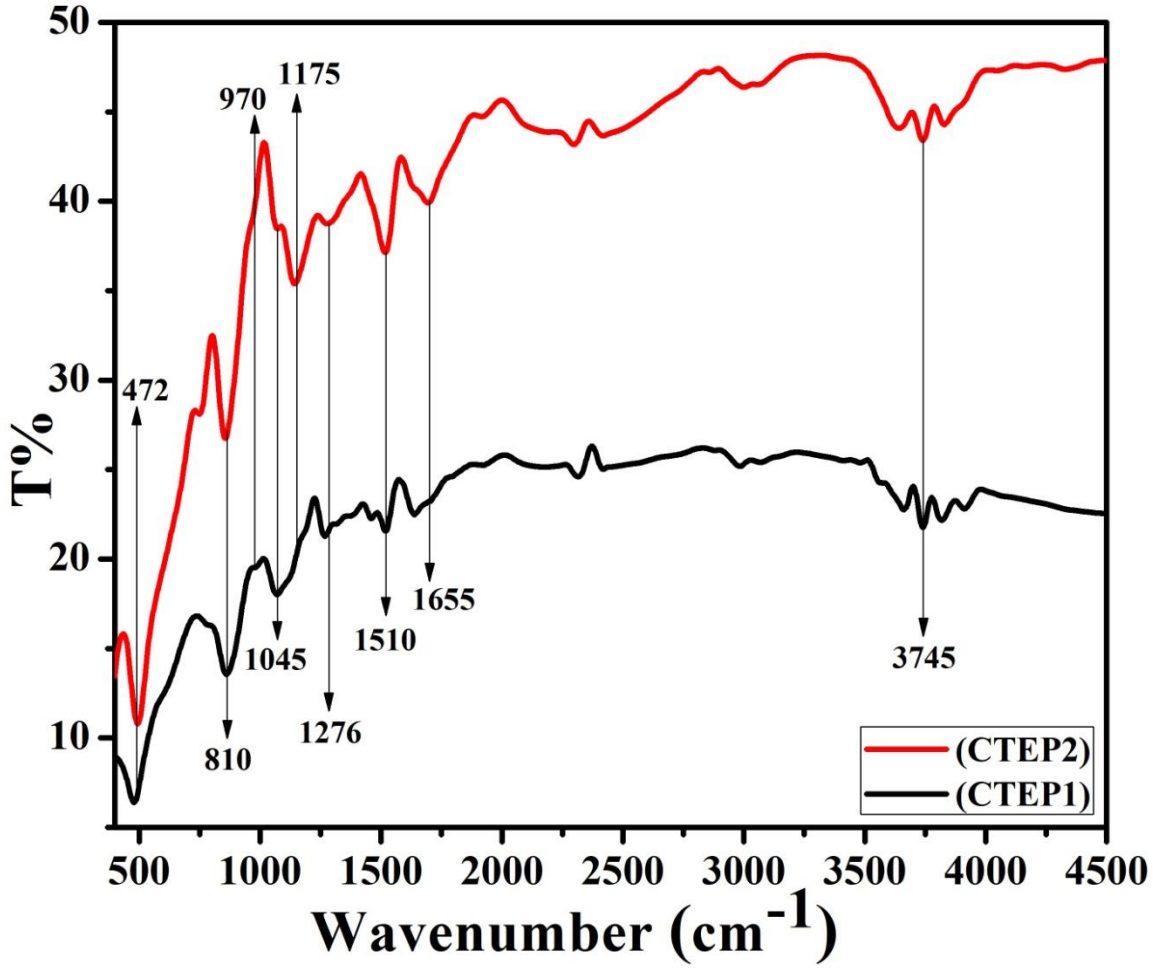


**Fig.5(C).1**: FTIR spectroscopy of composite coatings of CTEP1 and CTEP2

Two type coatings structure revel a peak at 1276$cm^{-1}$ which suggested aliphatic ─C─N─ stretching. At 1510 to 1615$cm^{-1}$ for benzene ring and 1460$cm^{-1}$ for aromatic backbone bands are confirmed. Transmission peaks are confirmed at 2855 to 2995$cm^{-1}$ make sure aliphatic and aromatic ─CH─ linkages respectively. Cured films of coal tar epoxy composite undergo stretching vibration ─C─O─C─ oxirane

ring at 1045 $cm^{-1}$, ─C─O─ at 1175$cm^{-1}$ and also ─N─H─ of primary amine at 1655$cm^{-1}$[30,31]. The IR spectrum DETA indicate characteristics peaks are at 2850$cm^{-1}$ for alkyl group, 1460 $cm^{-1}$ for aromatic ─C═C─ and 1276$cm^{-1}$ for aliphatic ─C─N─ stretch and 3745 $cm^{-1}$ confirmed that free SiOH group of organo siliane based nanocomposite coating [30-32].

**Fig.5(C).1:** Characteristic bands obtained from FTIR spectra of developed coal tar epoxy composite coating

| **Wavenumber ($cm^{-1}$)** | **Assignments** |
|---|---|
| 3743 | Free SiOH |
| 3090─3600 | OH of H—OH, Et—OH and Si—OH/N—H of primary and secondary amines |
| 2855─2995 | C—H of $CH_2$, $CH_3$/CH aromatic and aliphatic |
| 2849 | Symmetrical stretching of CH |
| 1655 | N—H of primary amines |
| 1510 ─1615 | For benzene ring |
| 1460 | —C═C—for aromatic backbone |
| 1276 | Aliphatic —C─N— stretching |
| 1175 | Si—O—Si of ≡Si—O—Si≡/C—C—O—C |
| 1103 | Asym. Si—O—Si Stretching |
| 1045 | C—O—C of ethers |
| 970 | —C—O— stretching vibration of Si─OH bond |
| 810 | $SiO_4$ tetrahedron ring |
| 472 | O—Si—O |

Coal tar epoxy is a three-component system consisting of coal tar, epoxy resin, and polyamide resin. After 2200 hours of continuous fog of salt spray chamber, the FTIR spectra of composite coatings recorded in Fig.5(C).3, show that the relative transmittance of the salt-sprayed nano-composite coating closely resembles that of the unprocessed one.

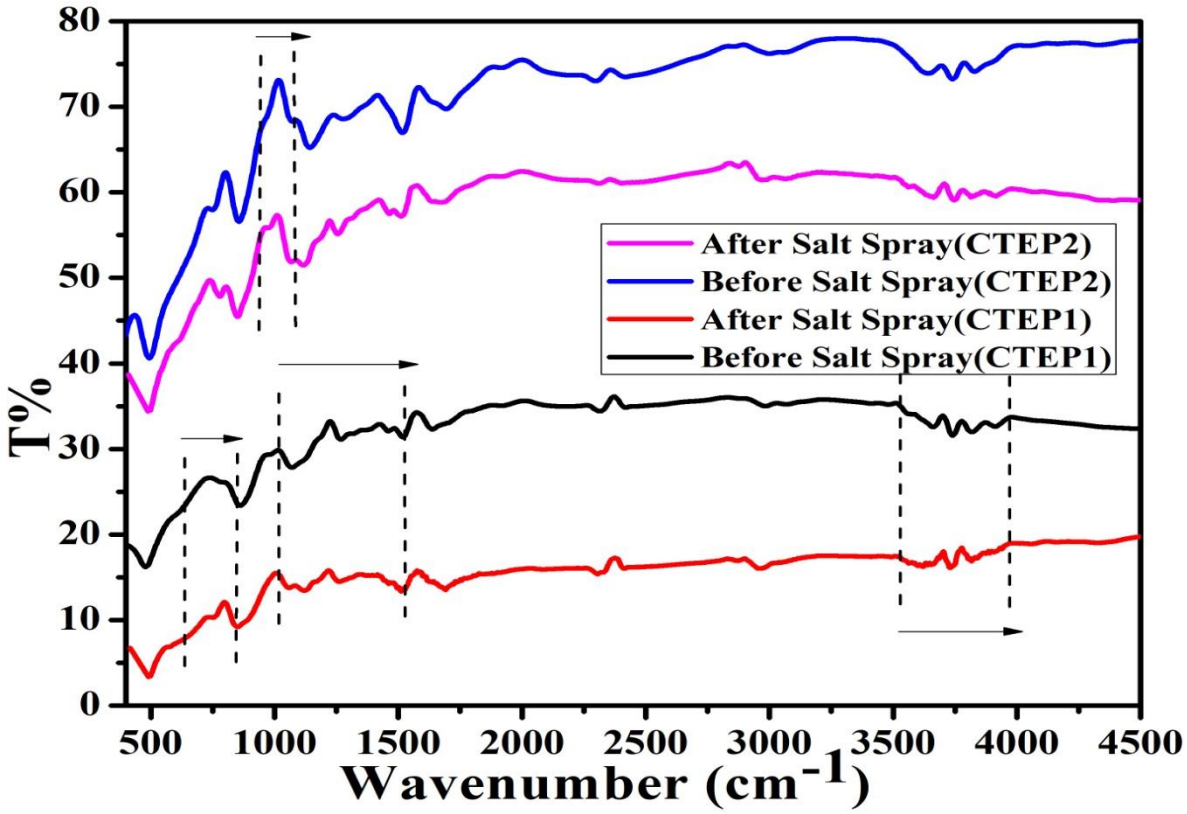


**Fig.5(C).2:** FTIR spectroscopy of composite coatings of CTEP1 and CTEP2 after 2200hrs salt spary test

Additional very weak band (i) 944 to 1085cm$^{-1}$ is observed in resin degradation of nanocomposite coating of CTEP2. From the FTIR spectrum, it is evident that the relative transmittances of samples before and after the salt spray test are very similar. This suggests that in this case, the resin system is not degraded in the presence of salt spray. In the case of the conventional composite coating of CTEP1, additional bands are (i) 3528 to 8970cm$^{-1}$ (ii) 1018 to 1527cm$^{-1}$ (iii) 636 to 844cm$^{-1}$ observed. The changes observed in the transmittance spectra can be attributed to the interaction between the conventional coating and salt spray, resulting in the formation of new C-H bonding [6].

## 5(C).2. XRD Patterns Analysis

The XRD peaks of organo siliane particles and composite coating of cured film seen in Fig.5(C).3. A broad pattern obtained at 2θ = 22.23 compared to the presence of $SiO_2$ crystalline particle it correlate that particles are amorphous in nature. At different angles of 2θ values at ( *h k l* ) planes observed 20.90 *(1 1 1)*, 27.03 *(1 2 0)*, 31.02 *(2 1 1)* 39.40 *(130)* and 68.32 *( 3 3 3 )* for quartz silica, 27.76 *( 1 1 0 )*, 36.4 *( 1 0 1 )*, 41.4 *( 1 1 1 )*, 54.25 *( 2 1 1 )*, 56.6 *( 2 2 0 )* and 69.01 *( 1 1 2 )* for $TiO_2$ pigment, 29.06 *( 0 2 7 )*, 31.21 *( 0 2 8 )*, 51.2 *( 0 2 11 )* and 60.2 *( 3 3 0 )* for extender respectively. Now it is confirmed that all composition are fully embedded in cured coal tar epoxy matrix but nanocomposite film showed more intense peaks than conventional one due to more amorphous in nature.

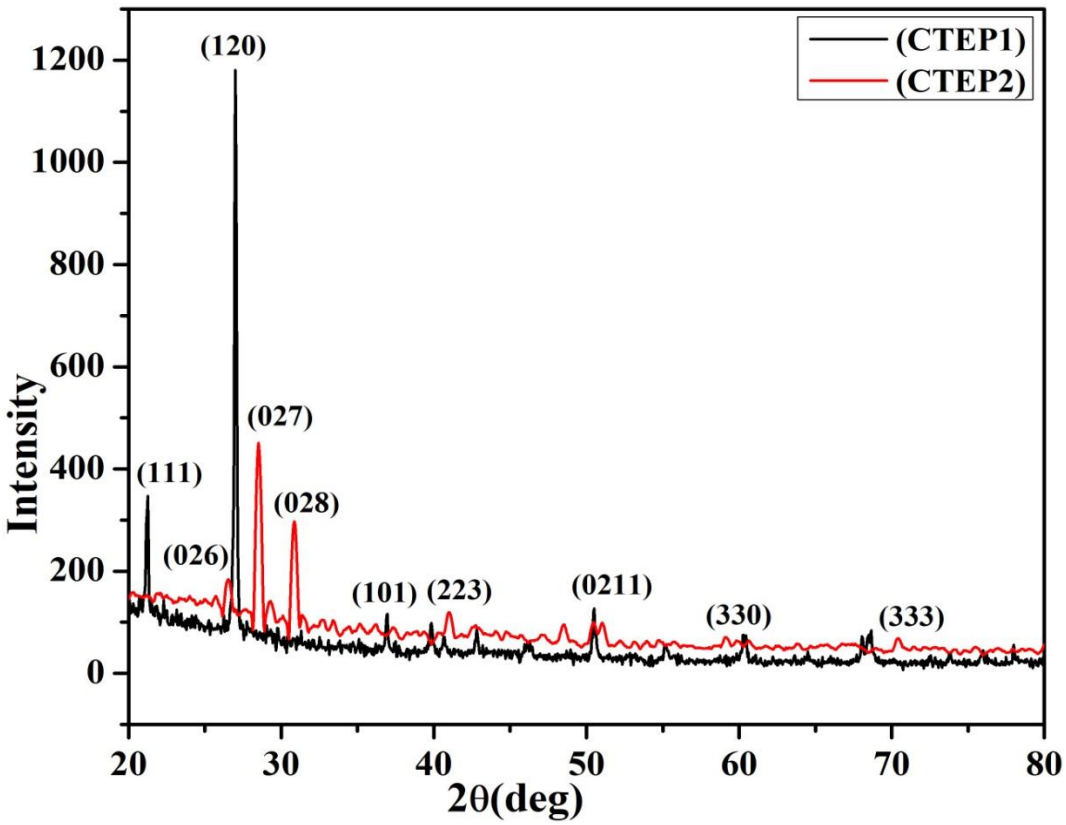


**Fig.5(C).3:** XRD pattern of Coal Tar Epoxy nano composite of CTEP2 coating

## 5(C).3. Morphology Study

### 5(C).3.1. Scanning Electron Microscope (SEM)

For better corrosion performance of resultant nano composite coating it is very important to good wetting necessary of particles in nano sized in composite. Fig. 5 shows at two different magnifications SEM images of CTEP1 in (a) & (b) where some particles are observed at micro level with pore and dispersed nano silica of CTEP2 in (c) & (d). SEM images displays the silica nano particles are dispersed with agglomeration in the polymer matrix during the formation of composite coating. Here at two different magnifications of images 5µm to 10 µm used for CTEP1 coating and 1µm to 300nm used for CTEP2 observation.

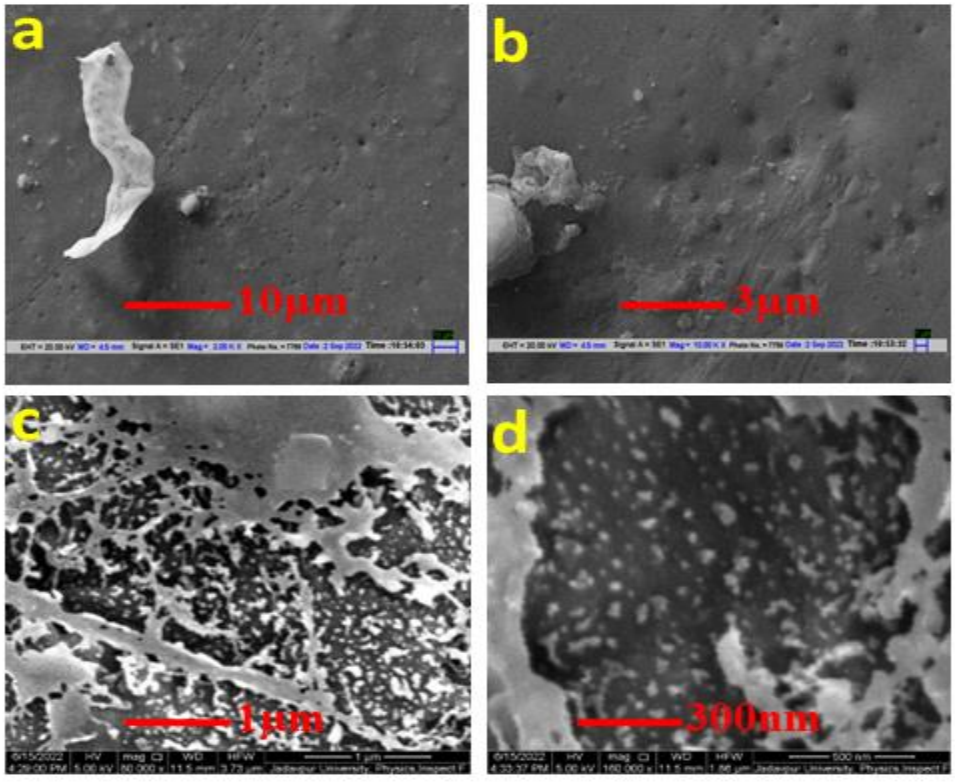


**Fig.5(C).4:** SEM images of (a) and (b) is CTEP1 and FESEM images of (c) and (d) are CTEP2

## 5(C).4. Thermal (TGA-DTA) Analysis

Thermal stability of all silica based coal tar epoxy composite film was studied by TGA-DTA method in Fig.5(C).5. From the thermograms, two distinct degradation processes can be observed. First, there is the degradation of the long aliphatic chain in DETA, which occurs at lower temperatures. Second, there is the degradation of the crosslinked epoxy polymer, which takes place at higher temperatures. During the initial heating stage, when all samples are heated above 200-350°C, the epoxy-amine linkages are broken. When heated further to around 500°C, the cleavage of Mannich Bridge reactions is observed. Above 350°C, the conventional composite coating decomposes into amines, phenolic compounds, and benzene derivatives. For the cured nano composite coating, further degradation occurs at much higher temperatures, typically well above 650°C.

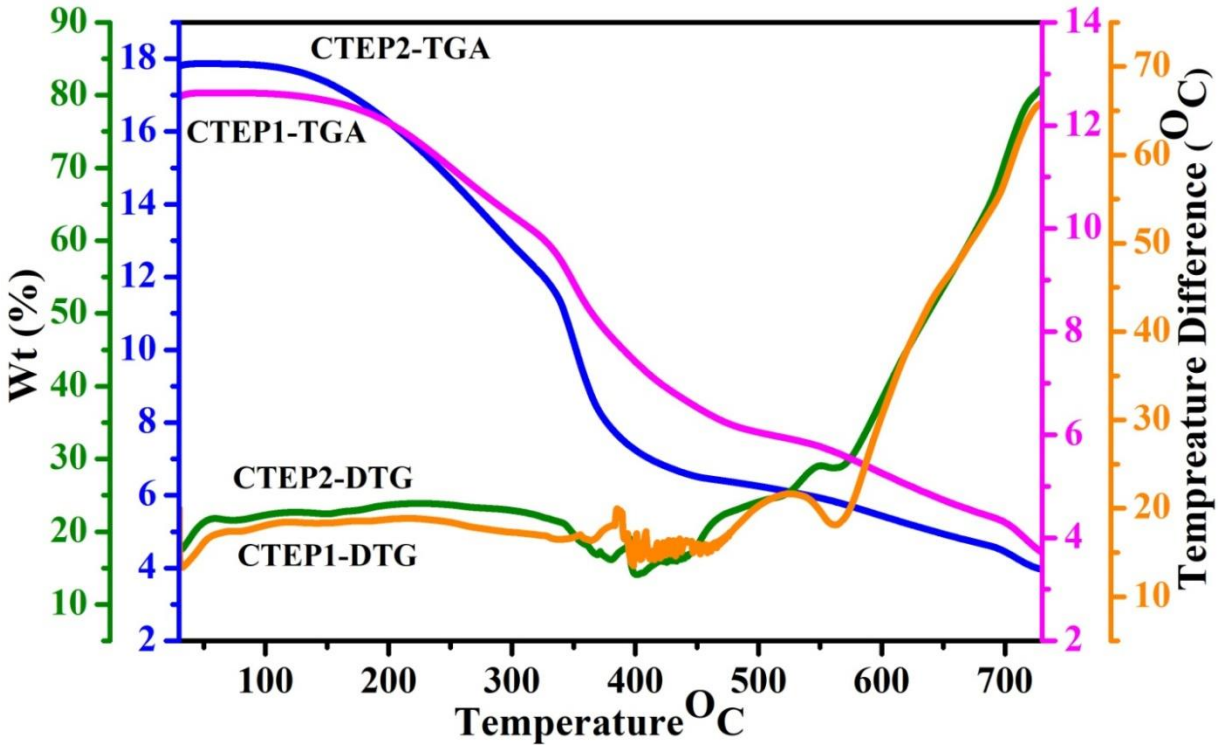


**Fig.5(C).5:** TGA-DTA thermogram curve of coal tar epoxy composite film

The glass transition temperature decreased to 210°C when compared to quartz silica particles. Weight loss was observed up to 700°C. At 400°C, the organic part of epoxy disintegrated, resulting in a 6.8% weight loss for CTEP2 compared to CTEP1. The DTA diagram indicated an endothermic reaction occurring at 350 to 450°C due to solvent evaporation and an exothermic reaction in the range of 500 to 650°C, attributed to binder disintegration in the composite coating.

The thermal stability of the conventional cured composite coating is lower than that of the nano composite coating. This difference in thermal stability is likely attributed to the presence of longer hydrophobic units in the composition, which influence the interfacial interactions at the polymer-nano filler interfaces in the matrix.

## 5(C).5. Physico-Mechanical Properties

In terms of mixing ability and formation viscosity, adding nano organo-silane increases viscosity more than conventional quartz silica due to the higher surface area of silica nanoparticles for interaction with polymer chains in the composite matrix. After an electrical insulation test, no issues such as audio visual disturbances, sparks, pinhole breaks, or the presence of conductive particles were observed. Various mechanical properties, including DFT, flexibility, scratch hardness, pencil hardness, adhesion, falling ball impact, and abrasion resistance, were evaluated for both types of coatings. Both coatings had a DFT of 200±10 microns. CTEP2 showed better flexibility and hardness compared to CTEP1, with no cracks observed after the falling ball impact test. CTEP2 also exhibited superior cross-link density, attributed to longer hydrophobic chains on nanoparticle surfaces, enhancing interactions within the polymer segments.

CTEP1 CTEP2

**Fig.5(C).6:** Images of flexibility coated coal tar epoxy composite on MS panel

**Table.5(C).2:** Result of scratch hardnes and pencil hardness of coal tar epoxy composite coating on MS panel

| **Sample code Name** | **500 gm Weight** | **1000 gm Weight** | **1500 gm Weight** | **Hardness (6B to 6H)** |
|---|---|---|---|---|
| CTEP1 | Passed | Passed | Failed | Failed at 1H |
| CTEP2 | Passed | Passed | Passed | Passed |

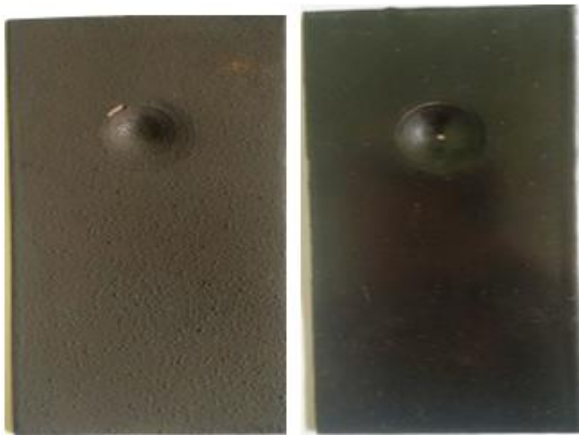

CTEP1 CTEP2

**Fig.5(C).7:** Images of falling ball impact test of coal tar epoxy composite coating on MS panel

In coal tar epoxy composite coatings, adding nano silica greatly enhances abrasion resistance with minimal weight loss compared to silica micro-particles. Nano silica coatings show only a 3.2 mg/1000 cycles weight loss, signifying uniform distribution for a stronger network. Adhesion properties in nanocomposite coatings are superior due to increased crosslink density from nano-particle distribution, particularly evident after a salt spray test. At a 60 degree angle, CTEP2 exhibits better gloss than CTEP1, indicating that CTEP2 with nano silica particles has a higher refractive index than the conventional CTEP1.

**Table.5(B).3:** Result of Physico-Mechanical testing of coal tar epoxy composite coating

| Coating code name | Cross link Density (%) | Adhesion Property ($N/mm^2$) | | Impact Test (KG.M) | | Abrasion Test (mg/cycles) | Gloss |
|---|---|---|---|---|---|---|---|
| | | Before Salt Spray | After 2200 hrs Salt Spray Test | Instrusion | Extrusion | | At $60^O$ angle |
| CTEP1 | 85 | 28.9 | 21.7 | >0.8 | >0.7 | 5.6 | 80 |
| CTEP2 | 97 | 41.3 | 36.6 | >0.4 | >0.5 | 3.2 | 115 |

## 5 (C). 6.Corrosion Studies

## 5 (C). 6.1. Tafel curves analysis of the various composite epoxy coatings

Various coal tar epoxy composite coatings, polarization curves studied for periodic time intervals (initial, 1, 7, 15 and 30 days), by immersion in 3.5 wt% Nacl solution depicted in Fig.5(C).8 and Fig.5(C).9. In the PD curve, corrosion potential ($E_{corr}$), cathode Tafel slope ($\beta_c$), anode Tafel slope ($\beta_a$), corrosion current ($I_{corr}$),

polarization resistance ($R_p$) and corrosion current density ($J_{corr}$) are used as electrochemical parameters.

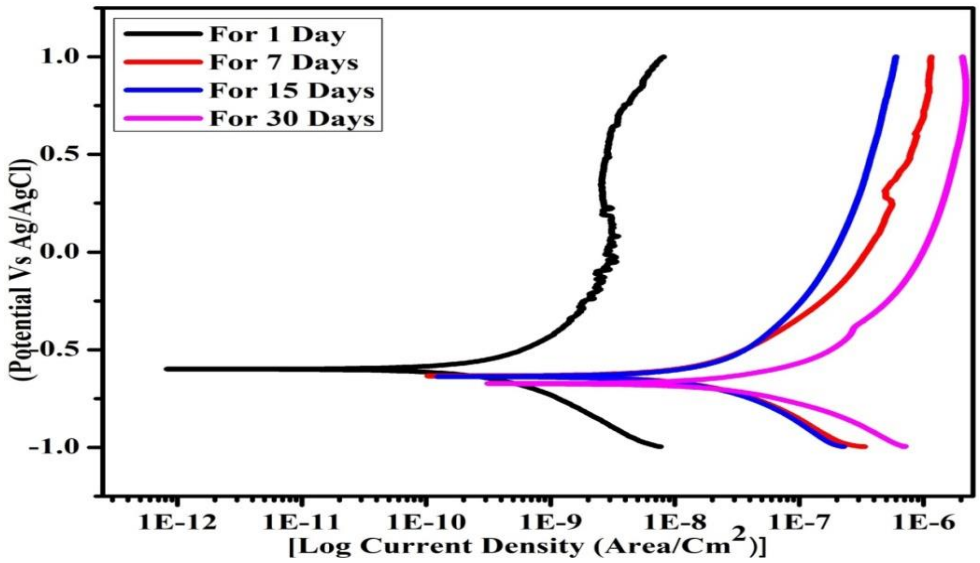


**Fig.5(C).8:** Tafel curves of composite coating of CTEP1 after (1, 7, 15 and 30) days immersions in 3.5 wt% Nacl aqueous solution

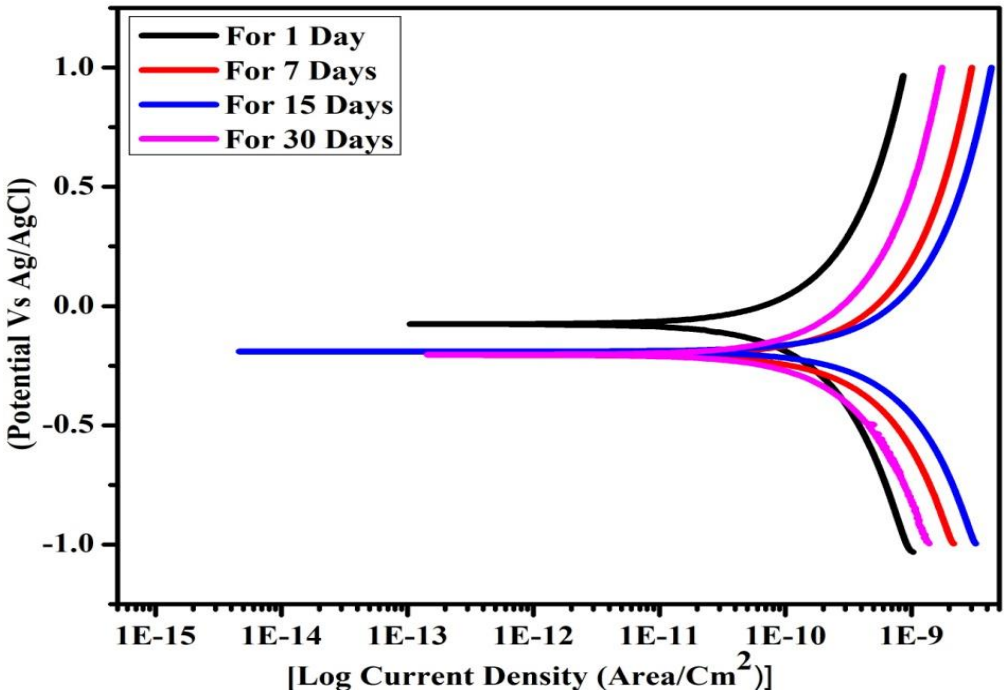


**Fig.5(C).9:** Tafel curves of composite coating of CTEP2 after (1, 7, 15 and 30) days immersions in 3.5 wt% Nacl aqueous solution

**Table.5(C).4.** Electrochemical parameters after soaking for different time intervals (1, 7, 15 and 30) day(s) of polarization measurements of CTEP1 and CTEP2

| Samples code Name | Day (s) | $-E_{corr}$ (V vs SCE) | $J_{corr}$ (A/cm$^2$) | $I_{corr}$ (mA cm$^{-2}$) | Corrosion rate (mm/year) | $R_p$(Ω cm$^2$) | βa (mV dec$^{-1}$) | βc (mV dec$^{-1}$) |
|---|---|---|---|---|---|---|---|---|
| CTEP1 | 1 | ─0.594 | 2.09E-10 | 4.26E-09 | 2.42E-06 | 1.07E+07 | 0.223 | 0.199 |
| | 7 | ─0.627 | 8.78E-09 | 1.78E-07 | 0.00010 | 2.25E+05 | 0.193 | 0.178 |
| | 15 | ─0.629 | 8.89E-09 | 1.81E-07 | 2.25E+05 | 2.19E+05 | 0.307 | 0.243 |
| | 30 | ─0.677 | 3.18E-08 | 6.49E-07 | 0.00037 | 70557 | 0.225 | 0.198 |
| CTEP2 | 1 | ─0.072 | 3.57E-11 | 8.18E-10 | 4.15-07 | 7.13E+07 | 0.264 | 0.272 |
| | 7 | ─0.202 | 9.47E-11 | 2.16E-09 | 1.10E-06 | 2.47E+07 | 0.237 | 0.225 |
| | 15 | ─0.188 | 8.20E-11 | 1.87E-08 | 9.53E-07 | 1.66E+07 | 0.139 | 0.147 |
| | 30 | ─0.201 | 3.08E-11 | 7.05E-6 | 3.58E-07 | 4.34E+07 | 0.142 | 0.139 |

In Table.5(C).5 electrochemical parameters of various composite coatings are put forward. The higher $E_{corr}$, lower $I_{corr}$, and higher Rp values show better corrosion resistive properties. Thus we can say that corrosion potential ($E_{corr}$) of CTEP2 is higher than that of CTEP1. Meanwhile, the corrosion current ($J_{corr}$) of CTEP2 coating is the lowest. Interestingly, the corrosion potential first increased and then decreased in CTEP1 coating and also corrosion current to be inversely related. Moreover, CTEP2 coating has the largest $E_{corr}$(─0.201) and the smallest $J_{corr}$(7.0584E-06 A/cm$^2$) for 30 days compared to CTEP1. In term of polarization resistance, CTEP2 is 4.3441E+07 Ωcm$^2$ where as 70557 Ωcm$^2$ for CTEP1. Say that, CTEP2 coating possesses the superior corrosion resistance properties over CTEP1.

## 5(C).6.2. Analysis of EIS results of various composite epoxy coatings

Nyquist and Bode plots of the coated MS rod after immersion (1,7,15 and 30) day(s) periodically of the corrosion studies are display in Fig.5(C).10 to

Fig.5(C).13. Nyquist plot revealed a huge semicircle and Bode plot indicate a capacitance behavior suggested the high corrosion resistance of the coating. The impedance $|Z|_{0.01}$ at low frequencies showed very large values $10^6$ and phase angle 130 for CTEP2 coating. A time const could be noticed from the impedance spectra exposed for the barrier characteristics of the coal tar epoxy coating [33,34]. After, 1 day to 30 days resulted data pronounced corrosion resistance behavior.

When an ionic path was generate in the coating a squeezed new semi circle appear of CTEP1 after 15 days in the Nyquist plot. That can be constitute by an electrical equivalent circuit including working electrode (W.E), charge transfer resistance and constant phase element (CPE) in series with a parallel combination of the coating. Whereas such phenomena does not occurred of CTEP2 coating.

From, Fig.5(C).11 of Nyquist and Bode plot in Fig.5(C).13 of nano composite coating (CTEP2) exhibited the impedance modulus $|Z|_{0.01}$ at low frequencies increased with corrosion time than 15 and 30 days and behaves like good protective barrier. But in case of conventional based composite coating (CTEP1) suffer degradation after corrosion time. It has assumed that the electrolyte penetration through the coating and constitute of a path to the MS coated surface and get degradation[35,37].

After 7 days, an extension in the second time constant of the impedance plots is observed, which is represented by the appearance of the second semi-circle in the Nyquist plot at lower frequencies. During this stage, the barrier properties of the conventional composite coating (CTEP1) gradually deteriorated, leading to substrate exposure to the solution. In this context, the first semi-circle in the impedance plot is associated with the barrier characteristics of the CTEP2 coating, while the second semi-circle characterizes the corrosion process occurring at the

interface between the substrate and the damaged area of the coating. This second semi-circle represents the charge transfer process between the substrate and the electrolyte solution. Under these conditions, the electrical equivalent circuit is depicted in Fig.5(C).13[38-40].

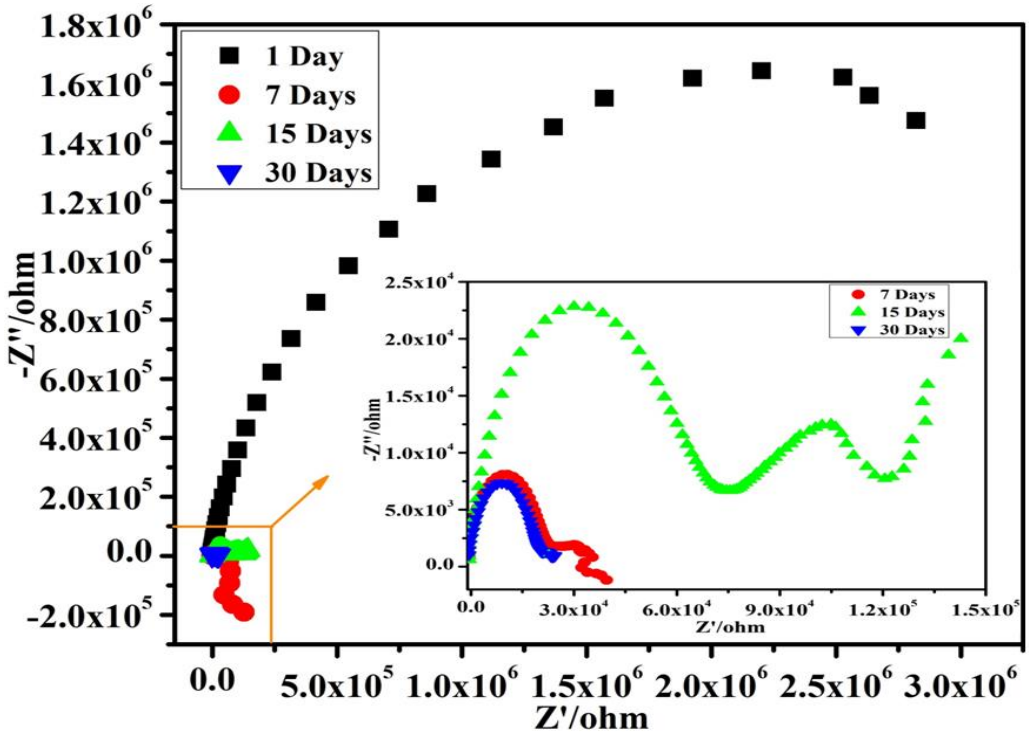


**Fig.5(C).10:** Nyquist plot of CTEP1 after soaking for 3.5 weight% Nacl aqueous solution for (1, 7, 15 and 30) days

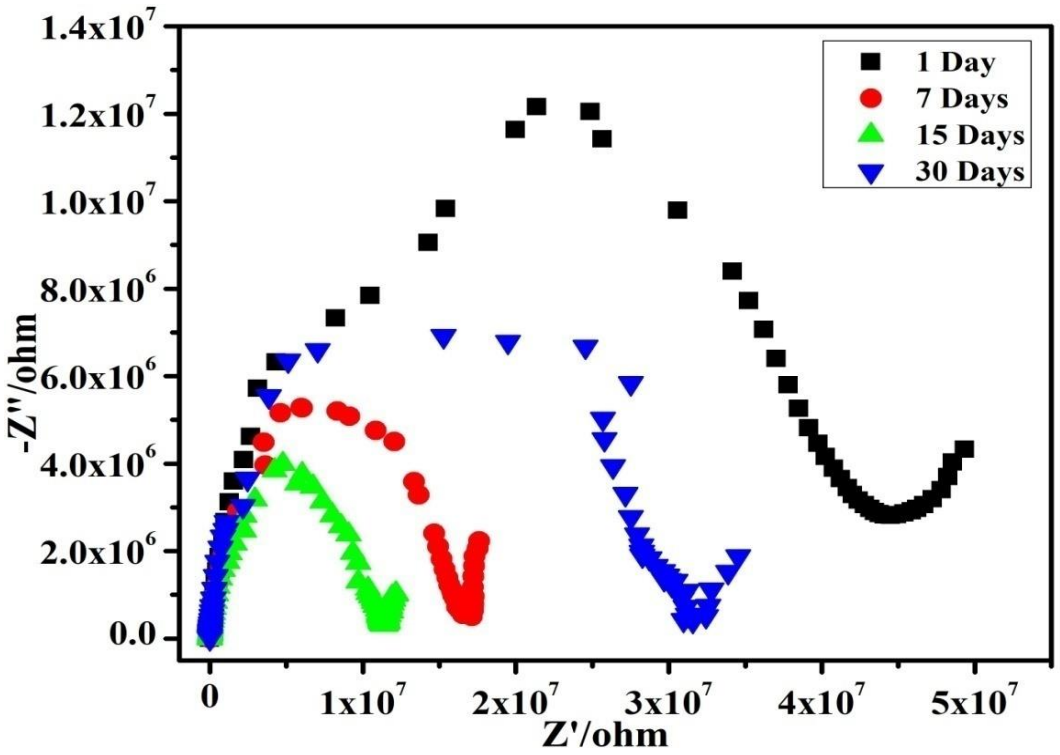


**Fig.5(C).10:** Nyquist plot of CTEP2 after soaking for 3.5 weight% Nacl aqueous solution for (1, 7, 15 and 30) days

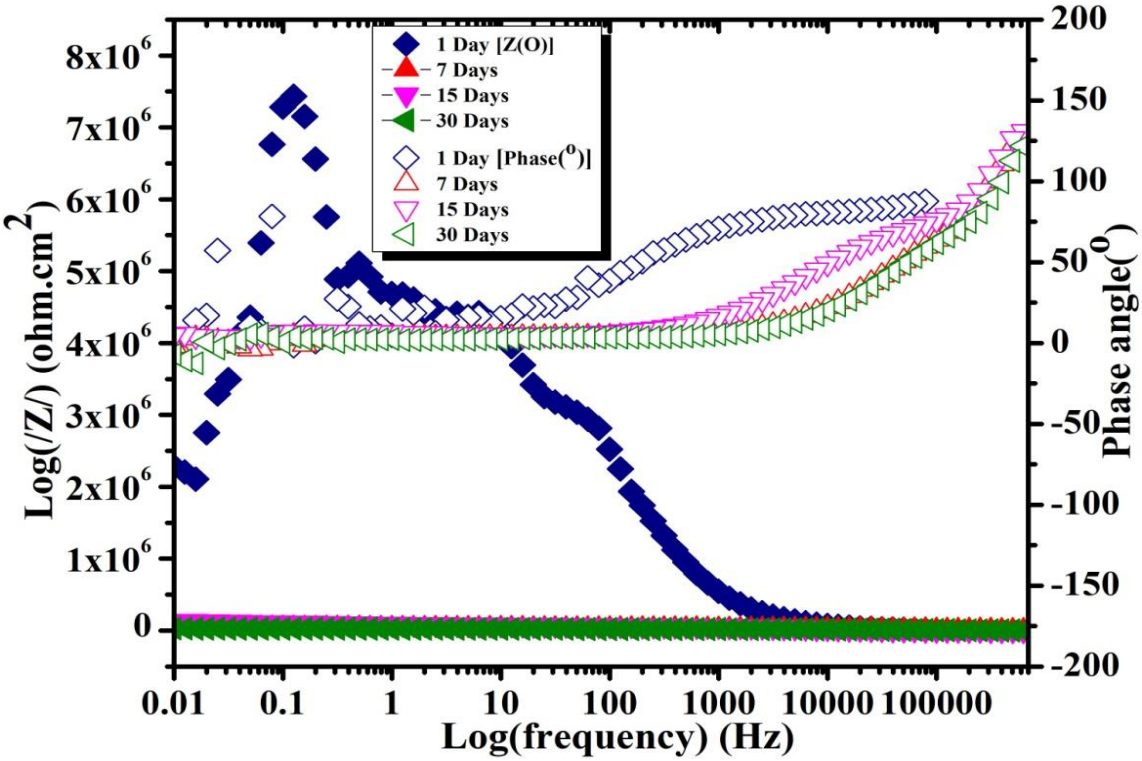


**Fig.5(C).11**: Bode plot of CTEP1 after soaking for 3.5 weight% Nacl aqueous solution for (1, 7, 15 and 30) days

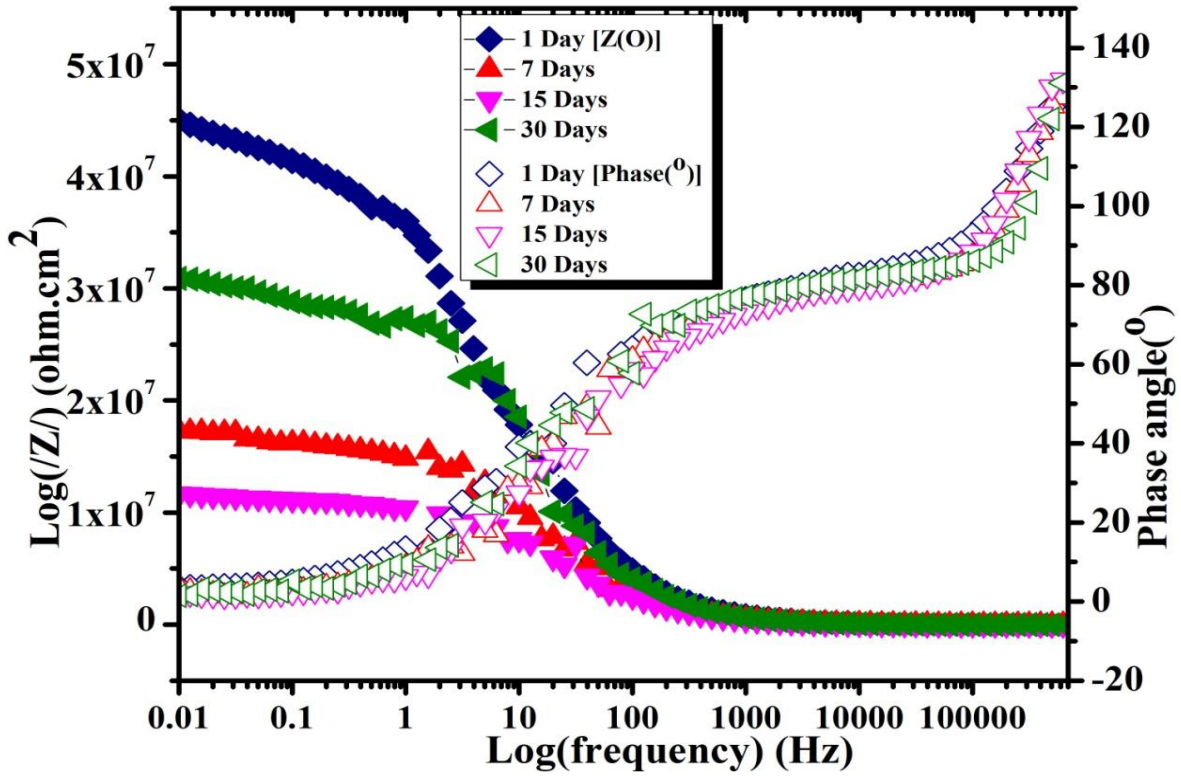


**Fig.5(C).12:** Bode plot of CTEP2 after soaking for 3.5 weight% Nacl aqueous solution for (1, 7, 15 and 30) days

**Table.5(C).5:** Fitting result

| Samples code name | Day(s) | C.P.E ($Y_o$) | $R_p(\Omega)$ | C.P.E (N) |
|---|---|---|---|---|
| CTEP1 | 1 | 4.57E-10F | 4.56E+06 | 0.717 |
| | 7 | 0.00038 | 1.64E+05 | 1.120 |
| | 15 | 6.42E-05F | 15543 | 0.240 |
| | 30 | 2.53E-10F | 21905 | 0.760 |
| CTEP2 | 1 | 1.03E-09F | 4.67E+07 | 0.676 |
| | 7 | 7.94E-10F | 1.74E+07 | 0.683 |
| | 15 | 4.17E-10F | 1.17E+07 | 0.762 |
| | 30 | 7.16E-11F | 3.48+07 | 0.851 |

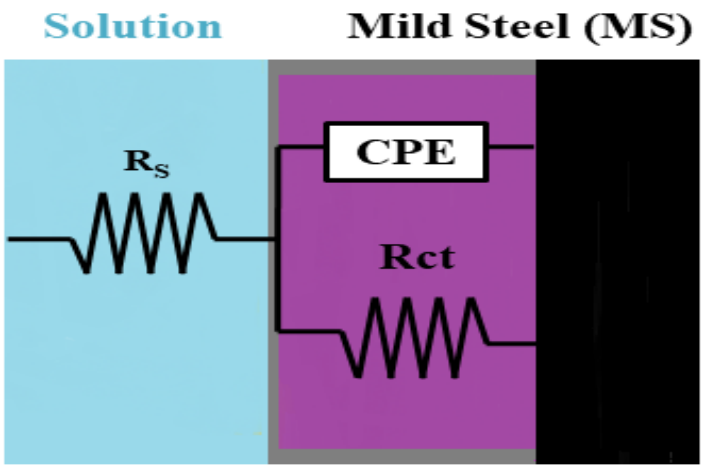


**(a)**

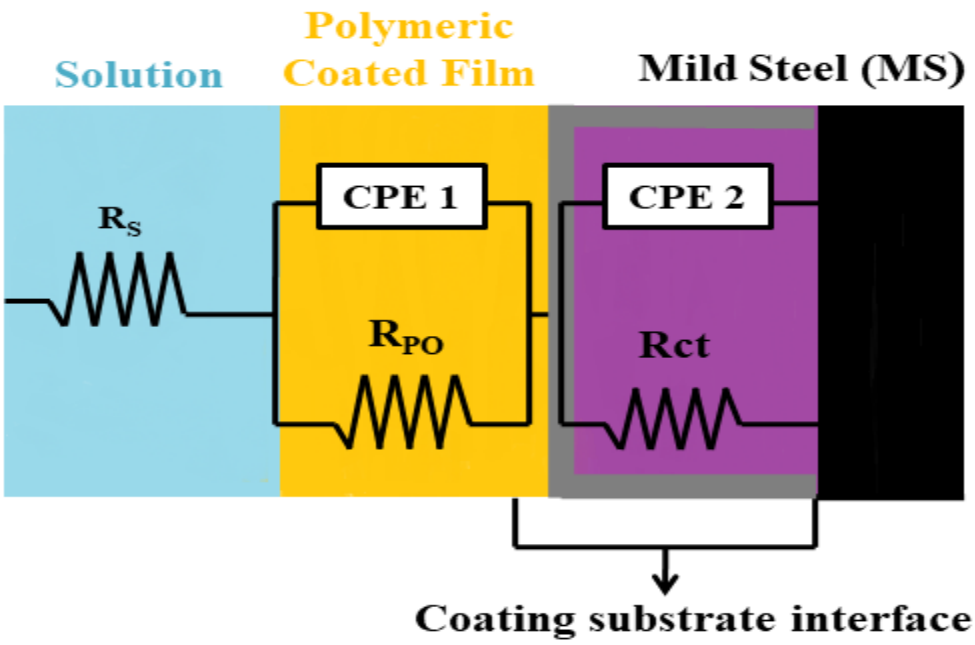


**(b)**

**Fig.5(C).13:** The equivalent electrical circuit models used to simulate EIS measurements of coatings at various immersion stages: (a) for one time constant and (b) for two time constant

**Table.5(C).6:** Inhibition efficiency of developed coal tar epoxy composite coating from electrochemical parameter after corrosion studies

| **Coating code Name** | **% Corrosion Inhibition Efficiency=** $\frac{I^{o}_{corr}-I_{corr}}{I^{o}_{corr}} \times 100$ | **%  Rct =** $\frac{Rct-Rct^{o}}{Rct} \times 100$ | **P =** $\frac{R_{P(Uncoated)}}{R_{P(Coated)}} \times 10^{-\frac{(\Delta E_{corr})}{b_a}}$ |
|---|---|---|---|
| CTEP1 | 84.30 | 97.54 | $P=78.96\times10^{-6}$ |
| CTEP2 | 99.85 | 99.87 | $P=71.92\times10^{-10}$ |

From Table.5(C).6, electrochemical parameter, it has been seen, CTEP2>CTEP1> increasing order for corrosion inhibition efficiency, CTEP2>CTEP1 increasing order for charge transfer resistance and CTEP2>CTEP1 increasing order for porosity measurement of different type of composite coatings respectively. It has suggested that nano filler embedded coal tar epoxy coating best results in corrosion inhibition efficiency and charge transfer resistance due to dense structure formed when cured with hydrophobic nano silica particle compared to conventional one [27].

## 5(C).7. Surface Analysis of Coatings (Optical Images)

Optical images at different magnifications (10 & 20µm) were captured before and after the corrosion studies of coatings on an MS rod in electrochemical experiments. After the corrosion study, it was observed that some pits with degradation appeared on the surface of the CTEP1 coating in Fig.5(C).14 (c) and (d). It was revealed that swelling occurred in the Nacl medium for the conventional coal tar epoxy coating of CTEP1. The damages observed at the metal-coating interface allowed the uptake of electrolyte, indicating the weak resistance nature of

the CTEP1 coating. Only three pits are observed after the corrosion study of the CTEP2 coating in Fig.5(C).14 (o) and (p). The presence of nano organo silane at the metal/coating interface effectively prevented the penetration of corrosion ions onto the MS substrate.

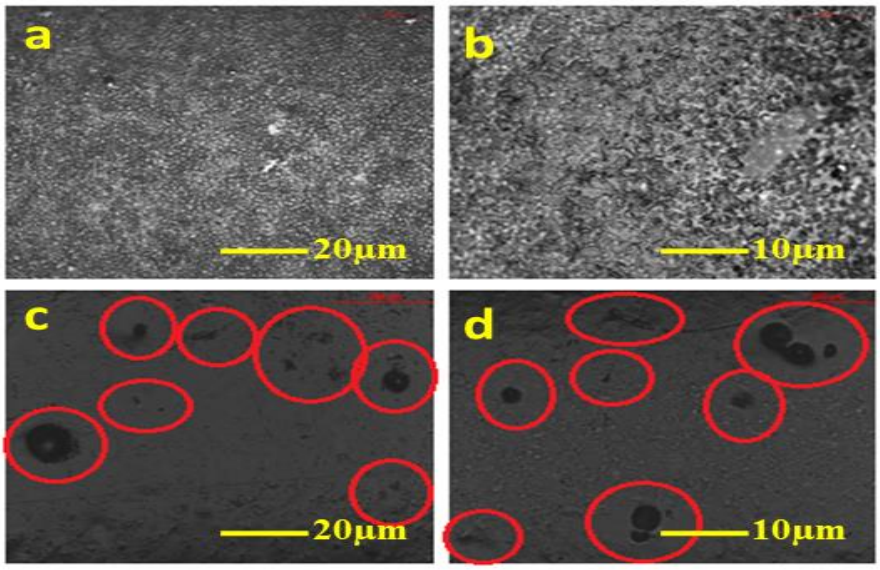


**Fig.5(C).14**: Image shows studies at different magnifications (a) & (b) before corrosion and (c) & (d) after corrosion of CTEP1

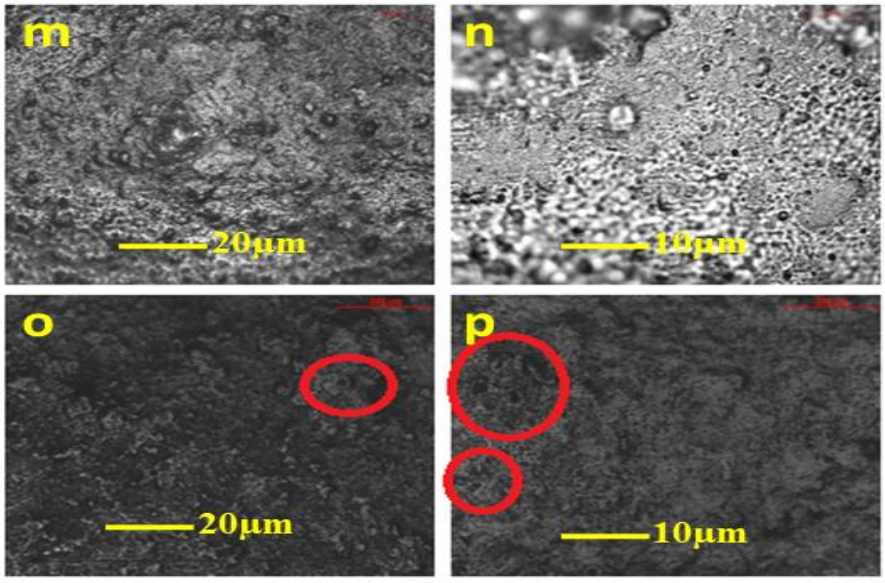


**Fig.5(C).15**: Image shows studies at different magnifications (m) & (n) before corrosion and (o) & (p) after corrosion of PU1

## 5 (C). 8. Salt Spray Study

In a salt spray chamber test, continuous fog exposure was conducted for 2200 hours on coated panels. The results, as depicted in Fig.5(C).16 indicate that corrosion and blister formation occurred exclusively in the micron silica-based coal tar epoxy coating, while no such observed in case of nano silica coal tar epoxy composite coating. Indeed, the results suggest that the nano silica embedded coal tar epoxy composite coating has significantly superior corrosion resistant properties when compared to the conventional silica-based coal tar epoxy composite coating. This demonstrates the potential benefits of using nano silica in improving corrosion resistance in coatings.

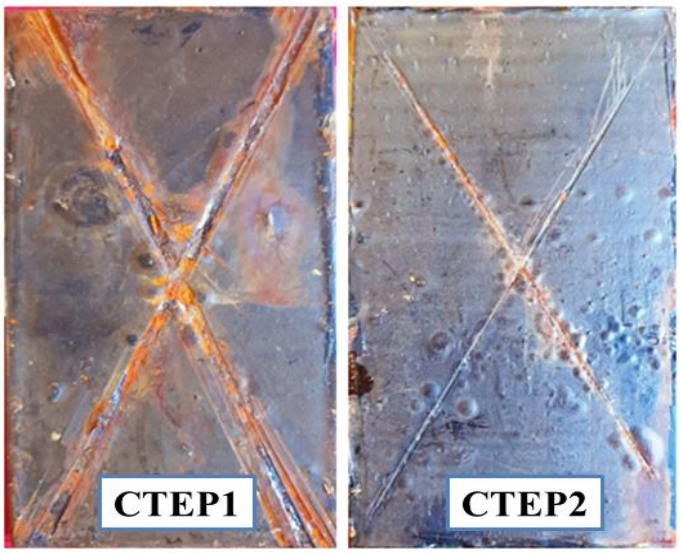


**Fig.5(C).16**: Images of coal tar epoxy coated MS panels of after 2200hrs salt spary test

## 5 (C). 9. Cathodic Disbondment (CD) Study

Complete of experiment then poured phenopthalein indicator on drilled hole at the centre of each cell. There was change of violet colour observed which indicate violet colour zone has been corroted area shown in Fig.5(C).17. Here temperature is

related to disbanding of coating. An increase of the current, a greater expansion of disbonded area observed at higher temperature due to rate of disbonded area (mm/day) and temperature are proportional to each other [28,29]. There are no such experiments measured by temperature effect on the transport of water and ions. At high vapor pressure of water increase vapor of water through surface of composite coating and porosity of coating grows as a result of chemical attack with thermal expansion.

**Table.5(C).7:** Cathodic disbondment result for coal tar epoxy composite coating

| Samples code name | Voltage (V) | Current (mA) | Temp ($^{O}$C) | Duration (Days) | Disbondment area (mm)/Remarks |
|---|---|---|---|---|---|
| CTEP1 | −1.5 | 90-110 | 30-45 | 28 | Full area delaminated and coating comes out |
| CTEP2 | −1.5 | 90-110 | 30-45 | 28 | Small area delaminated and some blister formed |

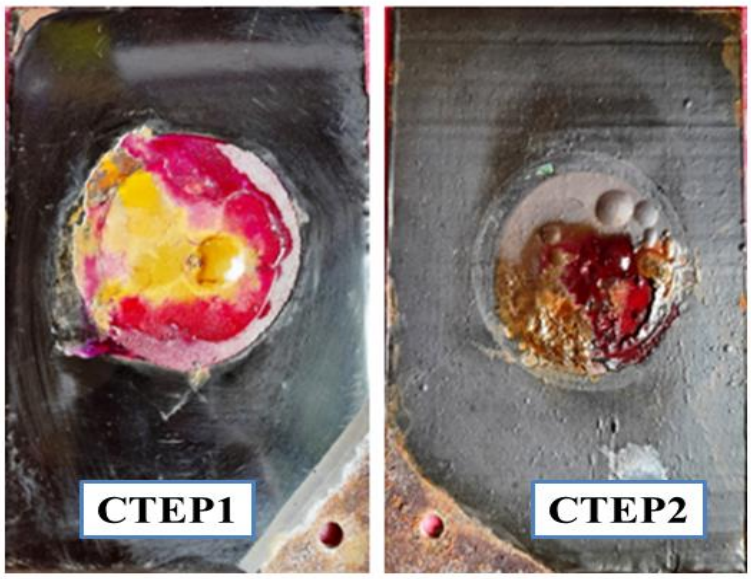


**Fig.5(C).17:** Images of coal tar epoxy coated MS panels after cathodic disbond test for 3.5% Nacl solution 28 days

## 5(C).10. Water and Chemical Resistance Study

The degree of water absorption has been evaluated by using formula of % swell test for 65 days. The nano filler based cured film (CTEP2) showed excellent water resistant than conventional cured film (CTEP1). As result, absorption of water CTEP1 is 26.53% and where as CTEP2 is 5.76%. The resistance behaviors of chemicals of the cured films were studied by in solution of acids (5% $H_2SO_4$ and 5% HCl) and alkali (5% NaOH) immersed for 65 days. The studies exposed that the films, acid and alkali immersion test showed damages and weight loss in acid medium is 30-40% and loss of gloss in alkali of CTEP1. On the other hand small damages and weight loss in acid (8-19%) and little loss of gloss in alkali of CTEP2 observed. CTEP2 shows better water and chemical resistance than CTEP1 due to nano particles completely wetted by tar epoxy and adduct of aliphatic chain from DETA give cured highly crosslink density rigid molecule structure presence of hydrophobic groups of nano organo silane, etc.

## 5(C).11. Conclusions

In summary, we have developed the organo silane epoxy nanocomposite material by simple method and successfully showed excellent result in all experiments. Nano composite material's superior corrosion properties than conventional coating have been confirmed by TEM, XRD, SEM and TGA-DTA studies. The most noticeable thing is that the organo silane nano filler embedded polymeric coating exhibits the lowest lowest corrosion current density, resistance to corrosion as well as more positive corrosion potential and excellent polarization resistance when compared to conventional silica based epoxy coating. Even salt spray chamber test shows better corrosion resistance for nano composite coal tar epoxy compared to conventional epoxy. Nano composite coating shows much lower cathodic

disbondment properties and hence much better corrosion resistance properties. Also, it has been observed that resin can consume 6.5-7 wt% of nanoparticles by optimization**.** With view above coal tar epoxy nanocomposite coating should be used for corrosion mitigation in the practical applications.

# 5(D)

# VINYL ESTER BASED COMPOSITE COATINGS

## 5 (D).1. FTIR spectroscopy

The glass flake-based vinyl ester composite coating system provides a highly compact and rigid structure. As a result, the different intensities of the bands from the different functional groups are not exposed to the IR beam during its path, likely due to the rigid structure that suppresses the normal stretching and bending vibrations. The free volume porosity of such composite coatings is very minimal. The weak vibrational band at 915cm$^{-1}$ [40-42] is associated with the vibration of oxirane ring. The vibrational band in between 1258 to 1460cm-1 can be attributed to the C─O─C and C═C for aromatic symmetric stretching modes of vibration[43]. Two characteristics vibrational bond observed at 1627cm$^{-1}$ for olefinic and 1726 to 1736cm$^{-1}$ for C═O stretch in both composite coatings depicted in Fig.5(D).1 and Fig.5(D).2.

**Table. 5(D).1:** Characteristic bands obtained from FTIR spectra of developed vinyl ester composite coating

| **Wavenumber (cm$^{-1}$)** | **Assignments** |
|---|---|
| 3743 | Free SiOH |
| 3090─3600 | OH of H—OH, Et—OH and Si—OH/N—H of primary and secondary amines |
| 2855─2995 | C—H of $CH_2$, $CH_3$/CH aromatic and aliphatic |
| 1726─1736 | C═O |
| 1627 | Olefinic bond (C═C) |
| 1510 ─1615 | For benzene ring |
| 1460 | —C═C—for aromatic backbone |
| 1258─1287 | —C—O—C— ether group |
| 1185 | Si—O—Si of ≡Si—O—Si≡/C—C—O—C |
| 1060 | Asym. Si—O—Si Stretching |

| | |
|---|---|
| 915 | Oxirane ring |
| 812 | $SiO_4$ tetrahedron ring |
| 474 | O—Si—O |

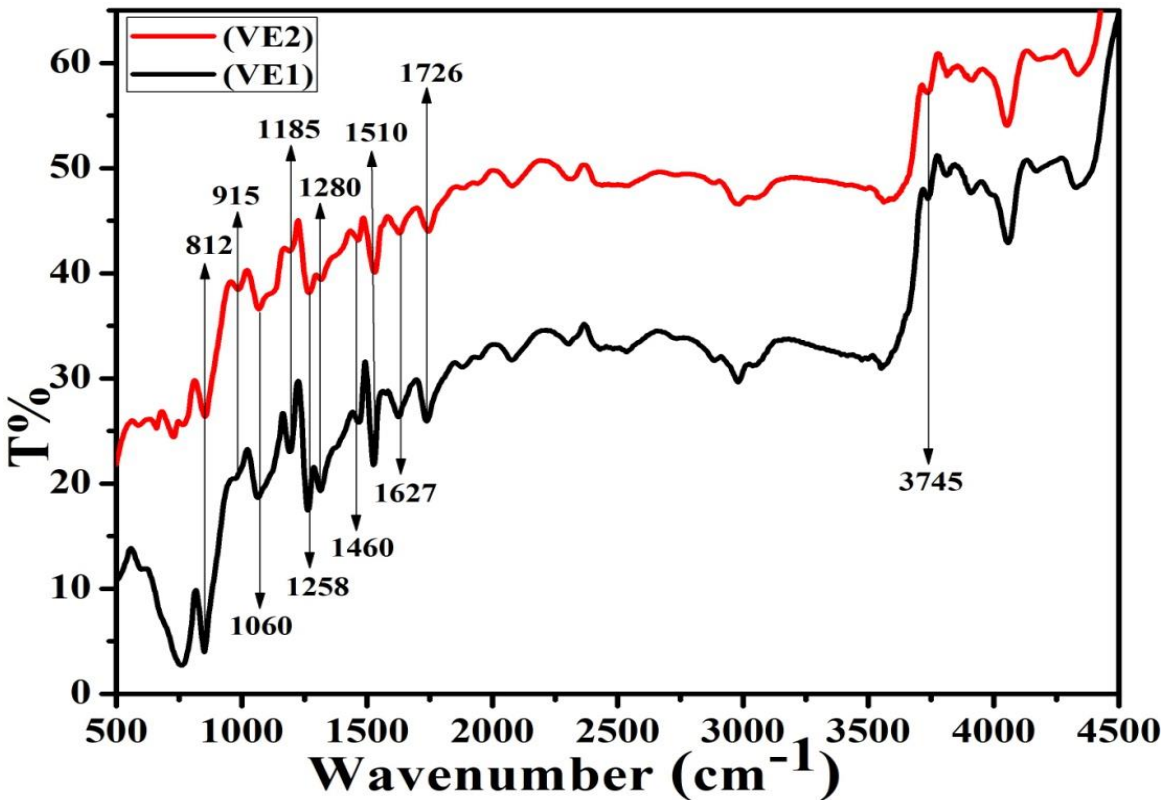


**Fig.5(D).1:** FTIR spectroscopy of composite coatings of VE1 and VE2

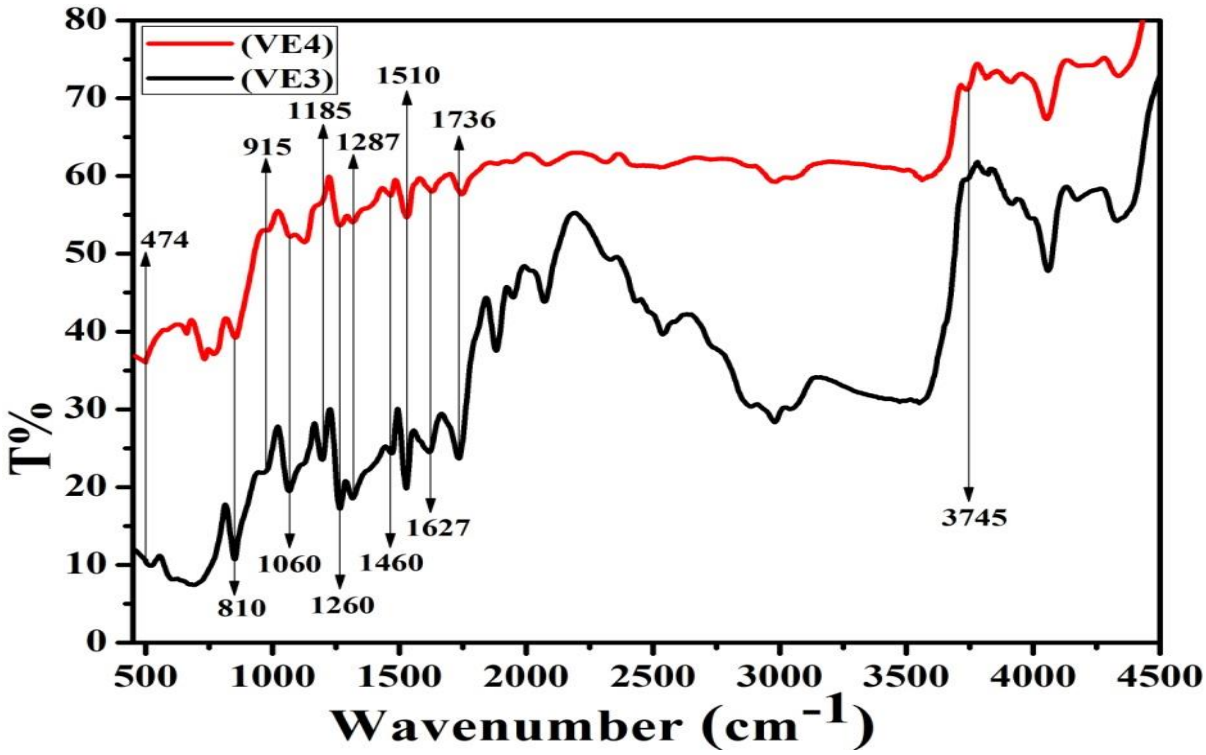


**Fig.5(D).2:** FTIR spectroscopy of composite coatings of VE3 and VE4

After 2200 hours of salt spray exposure, the FTIR spectra of the glass flake vinyl ester composite coatings recorded in Fig.5(D).3 and Fig.5(D).4 indicate that the relative transmittance of the salt-sprayed nano-composite coating closely resembles that of the unprocessed one.

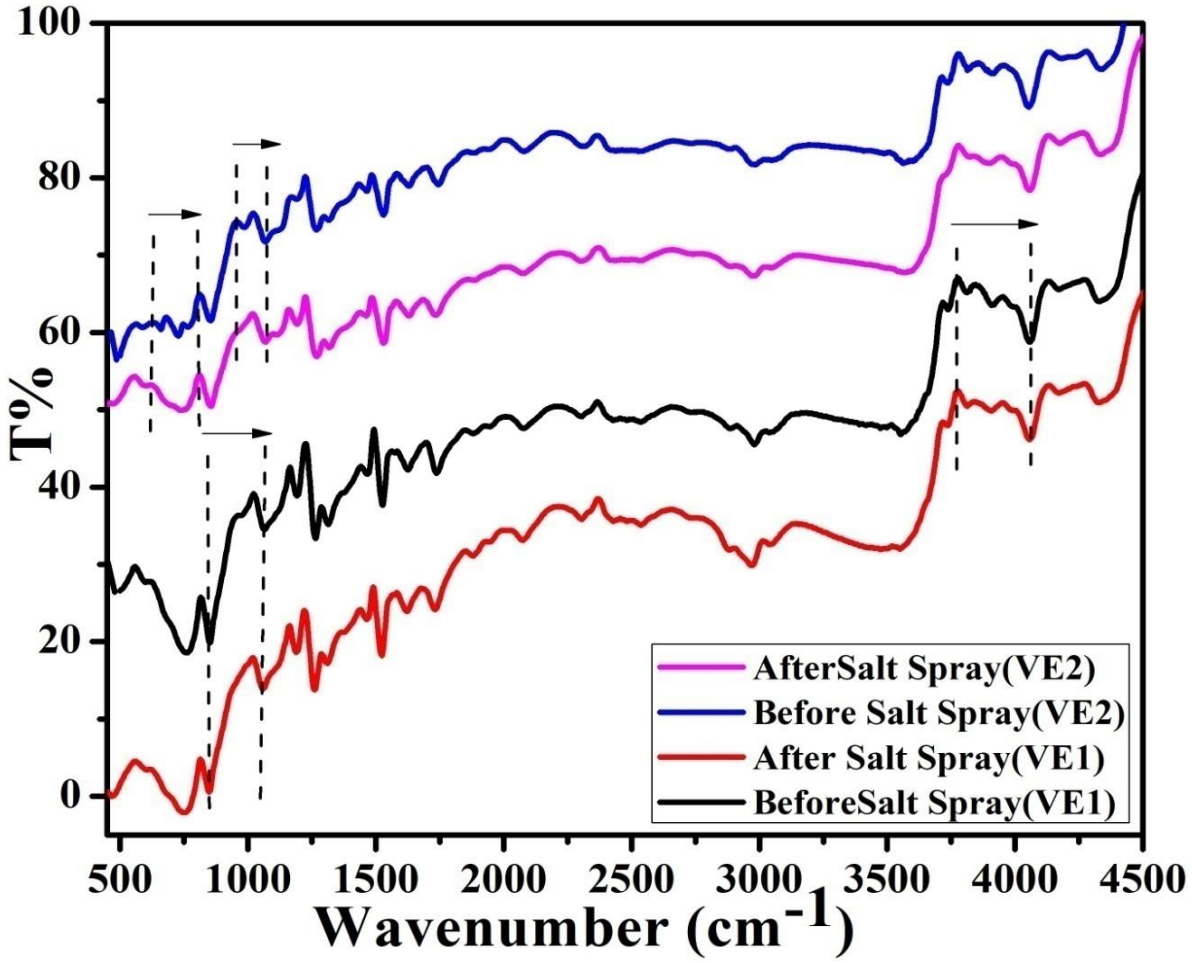


**Fig.5(D).3:** FTIR spectroscopy of VE1 and VE2 after 2200hrs salt spray chamber test

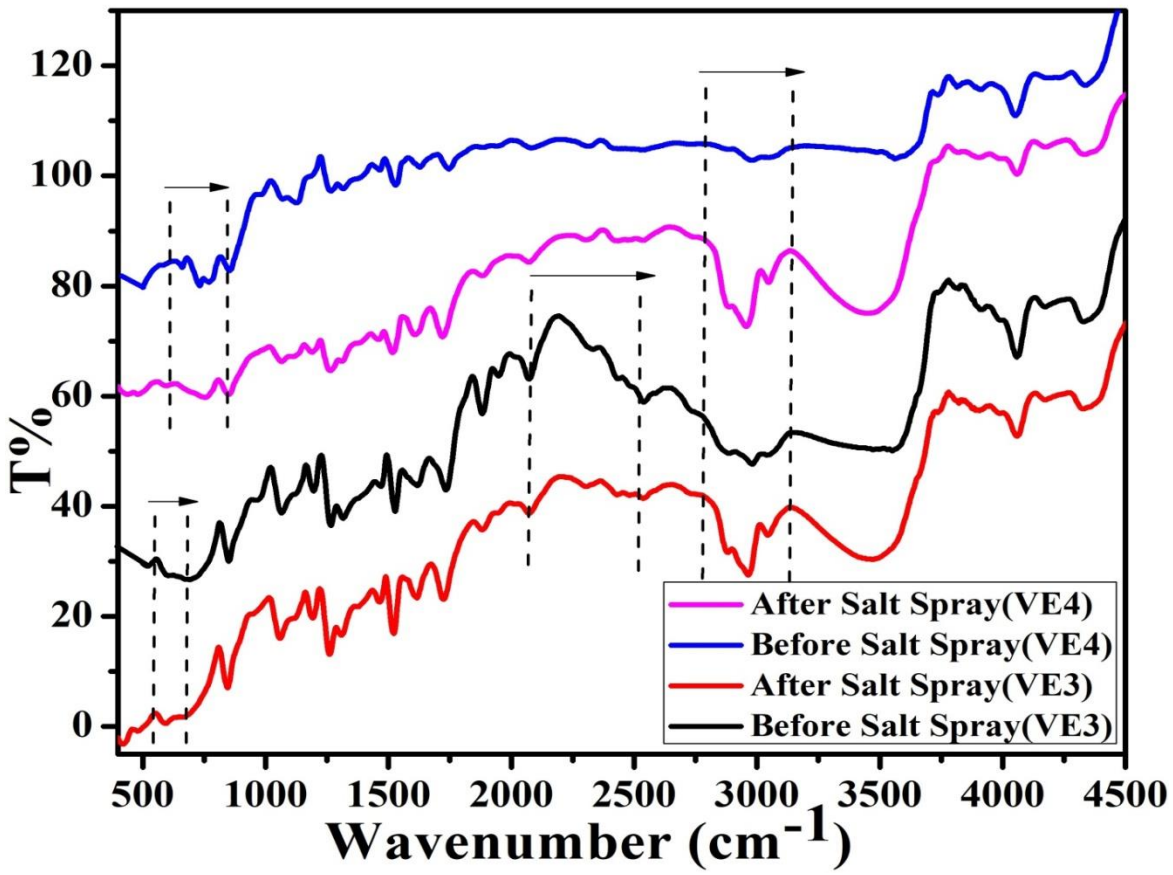


**Fig.5(D).4:** FTIR spectroscopy of VE3 and VE4 after 2200hrs salt spray chamber test

Additional very weak bands (i) 954 to 1073cm$^{-1}$ (ii) 624 to 802cm$^{-1}$ for VE2 and (i) 2785 to 3146 cm$^{-1}$ (ii) 603 to 844 cm$^{-1}$ for VE4 are observed in resin degradation of nanocomposite coatings. The presences of such peaks signify an interaction between the glass flake nanocomposite coating and the salt spray, indicating a very slow corrosion resistance against salt spray. But in case of glass flake conventional vinyl ester composite coatings, additional bands (i) 3764 to 4061 cm$^{-1}$ (ii) 835 to 1067cm$^{-1}$ for VE1 and (i) 543 to 676cm$^{-1}$ (ii) 2075 to 2524cm$^{-1}$ (iii) 2788 to 3147cm$^{-1}$ for VE3 are observed. After the salt spray test of composite films, the transmittance of conventional coatings changed considerably, leading to the conclusion that the coatings have significantly degraded due to the salt spray exposure.

## 5.(D).2. XRD Patterns Analysis

The XRD peaks of organo siliane particles and composite coating of cured film seen in Fig.5(D).5 and Fig.5(D).5. A broad pattern obtained at 2θ = 22.21 compared to the presence of $SiO_2$ crystalline particle it correlate that particles are amorphous in nature. In composite, pigments broad peaks are observed at angles of 2θ values and (*hkl*) planes are 20.90 *(1 1 1)*, 27.03 *(1 2 0)*, 31.02 *(2 1 1)* 39.40 *(130)* and 68.32 *( 3 3 3 )* for quartz silica (Card No: 1010921), 27.7 (*110*), 36.2 *(101)*, 41.4 *(111)*, 44.5 *(210)* 54.3 *(211)* and 56.6 (*200*) for rtile $TiO_2$ respectively (Card No: 21-1276) and additives of soap stone powder observed at angles of 2θ values and (*hkl*) planes are 29.4 *(027)*, 31.29 *(028)*, 51.2 *(0211)* and 60.2 *(330)* respectively (Card No: 10-0036). Now it can say that all composition are fully embedded in vinyl ester matrix matix but nanocompositeS VE2 and VE4 showed more intense peak due to more amorphous nature of organo silane nano filler.

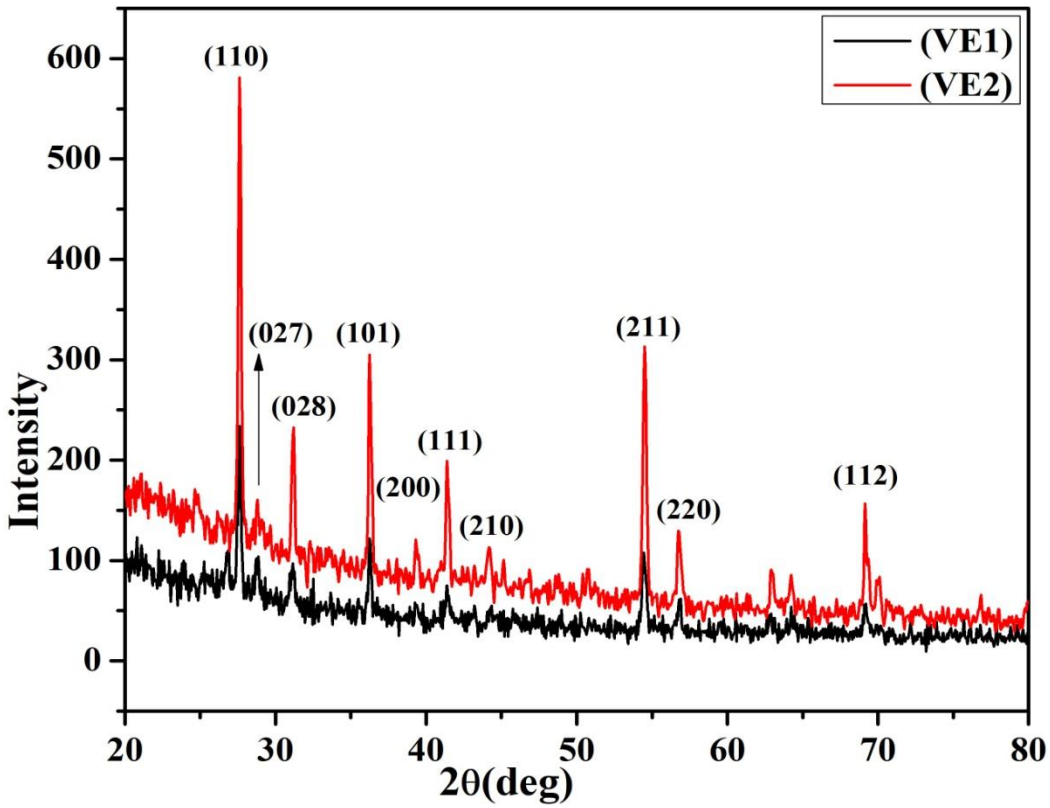


**Fig.5(D).5:** XRD pattern of 160A glass flake embedded vinyl ester composite coatings VE1 and VE2

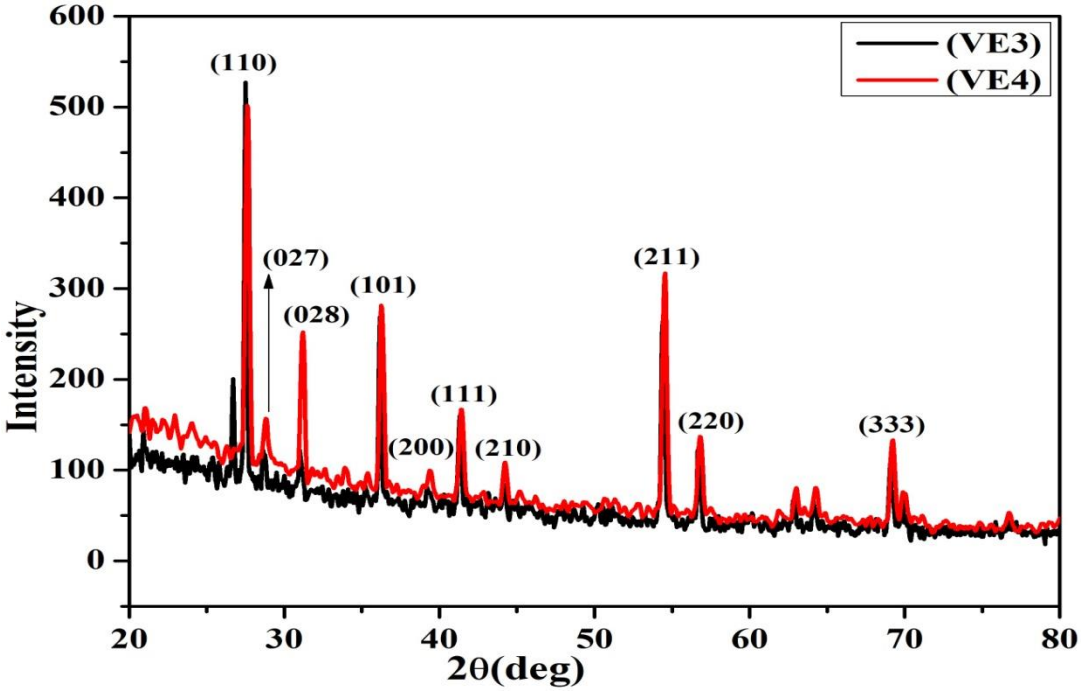


**Fig.5(D).6:** XRD pattern of 160N glass flake embedded vinyl ester composite coatings VE3 and VE4

## 5.(D).3. Morphology Study

### 5.(D).3.1. Scanning Electron Microscope (SEM)

To achieve improved corrosion performance in the nano coating, it is crucial to ensure good wetting of nano-sized particles in the composite. In Fig.5(D).6 to Fig.5(D).7, SEM images at two different magnifications reveal that silica nanoparticles are uniformly distributed within the polymer matrix during the formation of the composite coating. Whereas some micro particle and as well as some pore are observed conventional filler based vinyl ester composite coating. Both magnifications, ranging from 1 to 10 µm, were used for observing the coating, confirming the even dispersion of the silica nanoparticles.

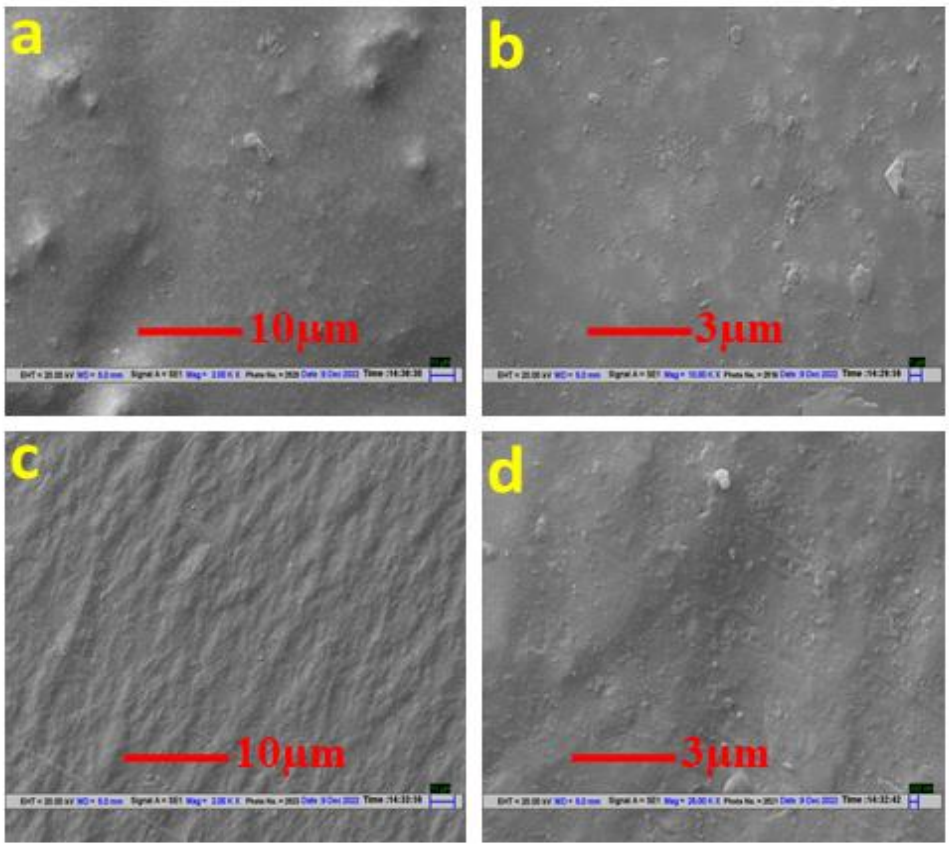


**Fig.5(D).6:** SEM images of conventional composite in (a) and (b) for VE1, dispersed silica nano filler in (c) and (d) for VE2

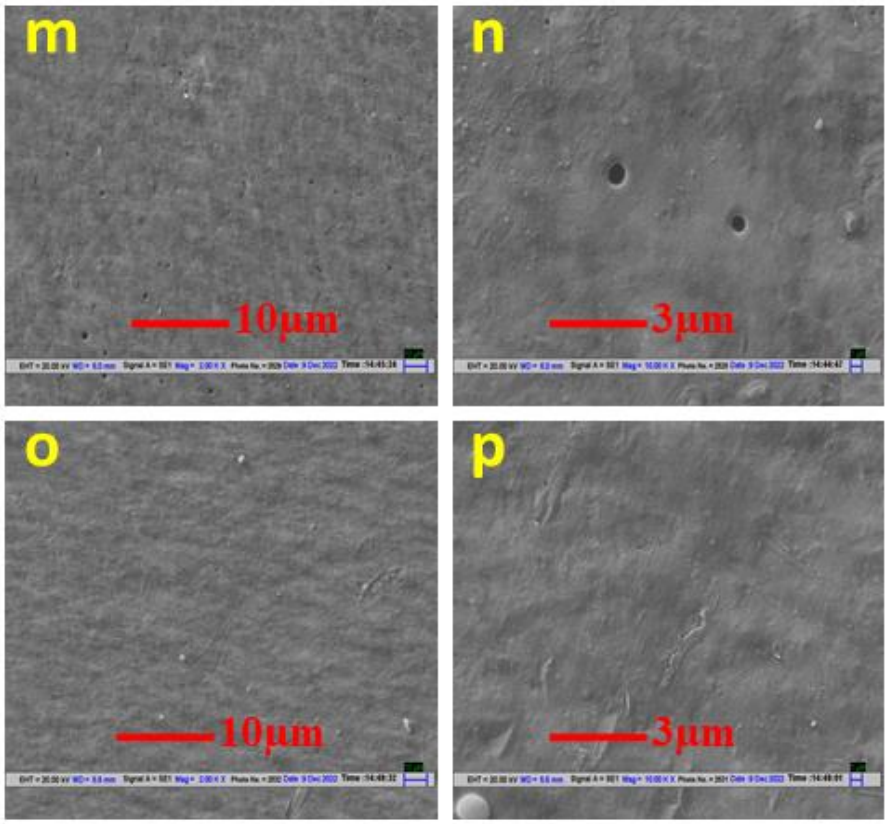


**Fig.5(D).7:** SEM images of conventional composite in (m) and (n) for VE3, dispersed silica nano filler in (o) and (p) for VE4

## 5.(D).3.2. Transmission Electron Microscope (TEM)

The degree of dispersion of $SiO_2$ nanoparticles and their morphology can be analyzed using Transmission Electron Microscopy (TEM) on the surface. The results obtained from TEM will provide valuable insights into the corrosion resistant properties of the nano coatings. Additionally, the use of Image J software can be employed to detect and measure the particle size of organo silane, which has been found to be less than 50nm.

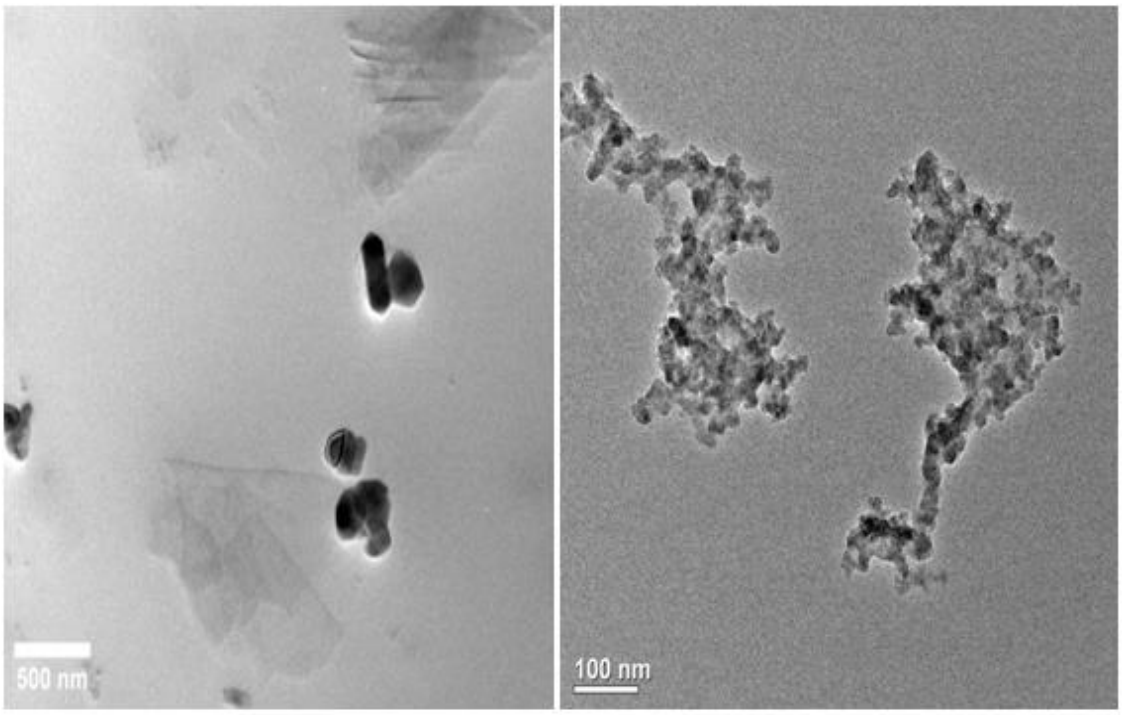


**Fig.5(D).8:** Transmission electron images of 160A glass flkake based nano composite coating of VE2

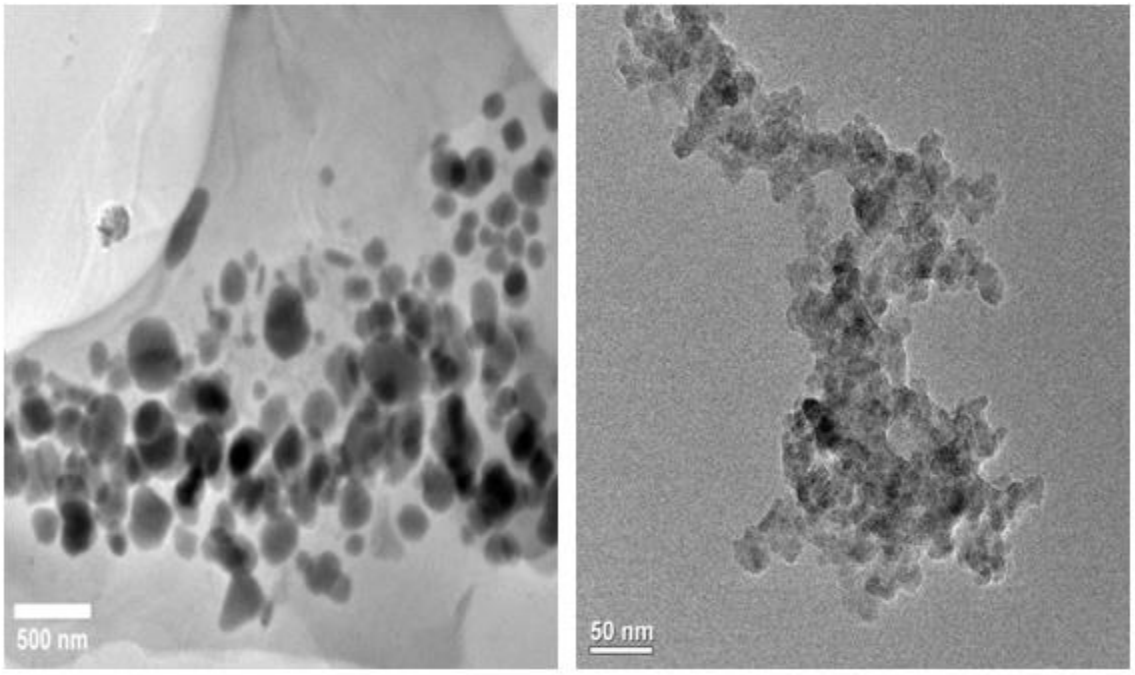


**Fig.5(D).9:** Transmission electron images of 160N glass flkake based nano composite coating of VE4

## 5(D).4. Thermal (TGA-DTA) Analysis

According to Fig.5(D).10 and Fig.5(D).11, the thermal decomposition process exhibits three distinct steps. The first step occurs at 100–200°C, primarily attributed to the evaporation of solvent from the matrix or fillers. The second step takes place in the range of 250–400°C, involving the decomposition of quartz silica fillers and $TiO_2$ the weight loss of from the composites. An additional third step is observed in the temperature range of 400–600°C under nitrogen, which may be attributed to the oxidation of partially decomposed fillers in a nitrogen atmosphere. Similar results have been reported for various types of nanocomposite films [44,45]. Fig.5(D).11 shows that the highest peak temperature is observed for VE4 while the lowest peak temperature is seen for VE1, summarizes the thermal stability get of both their respective nanocomposites than conventional one. Exothermic reaction occurred at 350 to 450$^{O}$C and endothermic reaction occurred at 550 to 650$^{O}$C

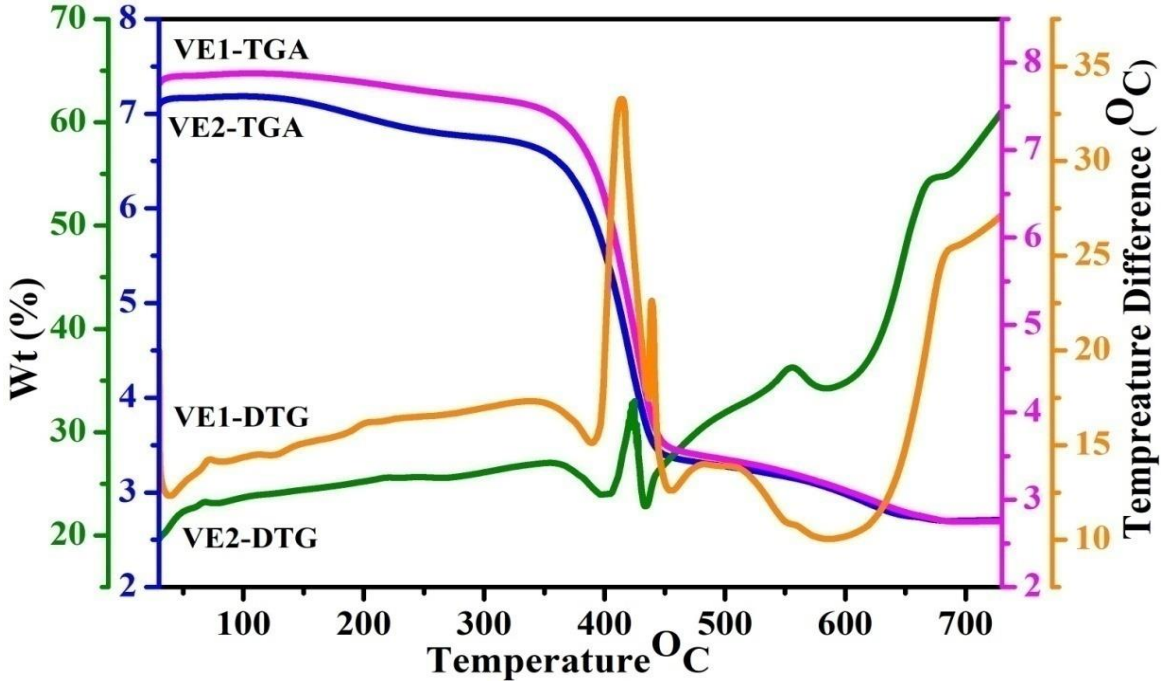


**Fig. 5(D).10:** TGA-DTA thermogram curve of VE1 andVE2

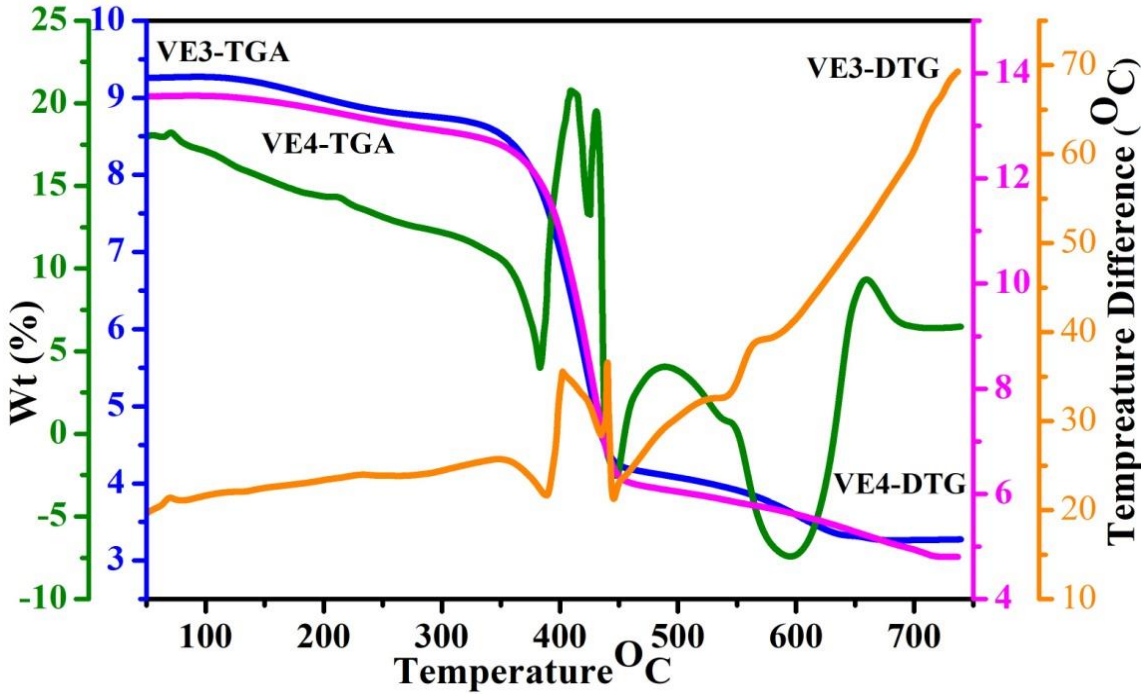


**Fig. 5(D).11:** TGA-DTA thermogram curve of VE3 andVE4

## 5(D).5. Physico-Mechanical Properties

In terms of mixing ability and formation viscosity, the addition of nano organosilane increases viscosity more than conventional quartz silica. This is because silica nanoparticles have a higher surface area for interaction with polymer chains in the composite matrix. Other mechanical properties such as DFT (Dry Film Thickness), flexibility, scratch hardness, pencil hardness, adhesion, falling ball impact, and abrasion resistance of the composite coatings were evaluated. Both types of composite coatings have a DFT in the range of 200±10 microns. The nano composite coating is more flexible than the conventional composite coating. All composite coatings exhibit better scratch and pencil hardness compared to the conventional one, attributed to the hardness and cross-linking density of the composite coating. The falling ball impact test shows good results, indicating uniform dispersion of nano fillers, resulting in a strong cross-linked elastomeric rigid structure. The cross link density of composite thermosets, determined by the

% swelling method in xylene, is higher for VE4 compared to VE1. This is due to the longer hydrophobic chains on the surface of nanoparticles, which significantly enhance interfacial interactions within the polymer segments.

VE1 VE2 VE3 VE4

**Fig. 5(D).12:** Images of flexibility coated VE composite on MS panel

**Table. 5(D).2:** Result of scratch hardnes and pencil hardness of VEcomposite coating on MS panel

| Sample code Name | 500 gm Weight | 1000 gm Weight | 1500 gm Weight | Hardness (6B to 6H) |
|---|---|---|---|---|
| VE1 | Passed | Passed | Passed | Passed |
| VE2 | Passed | Passed | Passed | Passed |
| VE3 | Passed | Passed | Passed | Passed |
| VE4 | Passed | Passed | Passed | Passed |

In VE composite coatings, the addition of nano silica significantly improves abrasion resistance with minimal weight loss compared to using silica micro-particles. Nano silica coatings demonstrate only a 1.2 mg/1000 cycles weight loss, indicating uniform distribution for a stronger network. Adhesion properties in nanocomposite coatings are superior due to increased crosslink density resulting

from the distribution of nano-particles, especially noticeable after a salt spray test. Additionally, at a 60 degree angle, VE4 exhibits better gloss than VE2, suggesting that with nano silica particles composite, has a higher refractive index than the conventional one.

**Table. 5(D).3:** Result of Physico-Mechanical testing of VE composite coating

| Coating code name | Cross link Density (%) | Adhesion Property ($N/mm^2$) | | Impact Test (KG.M) | | Abrasion Test (mg/cycles) | Gloss |
|---|---|---|---|---|---|---|---|
| | | Before Salt Spray | After 2200 hrs Salt Spray Test | Instrusion | Extrusion | | At $60^O$ angle |
| VE1 | 93.43 | 20.9 | 11.7 | >0.8 | >0.7 | 3.2 | 112 |
| VE2 | 98.71 | 34.3 | 23.7 | >0.4 | >0.6 | 1.5 | 123 |
| VE3 | 95.3 | 27.2 | 16.5 | >0.8 | >1.3 | 2.4 | 126 |
| VE4 | 97.8 | 36.8 | 26.8 | >0.5 | >0.7 | 1.2 | 134 |

## 5(D).6. Corrosion Studies

## 5(D).6.1. Tafel curves analysis of the various vinyl ester composite coating

Polarization curves were analyzed for various VE composite coatings and compared with an uncoated MS rod. These studies were conducted at periodic time intervals (initial, 1, 7, 15, and 30 days) through immersion in a 3.5 wt% Nacl solution. The figures, specifically **Fig.8 and Fig.9**, display the polarization curves. In the polarization curves (PD curve), various electrochemical parameters were examined, including corrosion potential ($E_{corr}$), cathode Tafel slope ($\beta_c$), anode

Tafel slope ($\beta_a$), corrosion current ($I_{corr}$), polarization resistance ($R_p$), and corrosion current density ($J_{corr}$). These parameters provide insights into the corrosion behavior and performance of the different coatings and the unncoated MS rod over time.

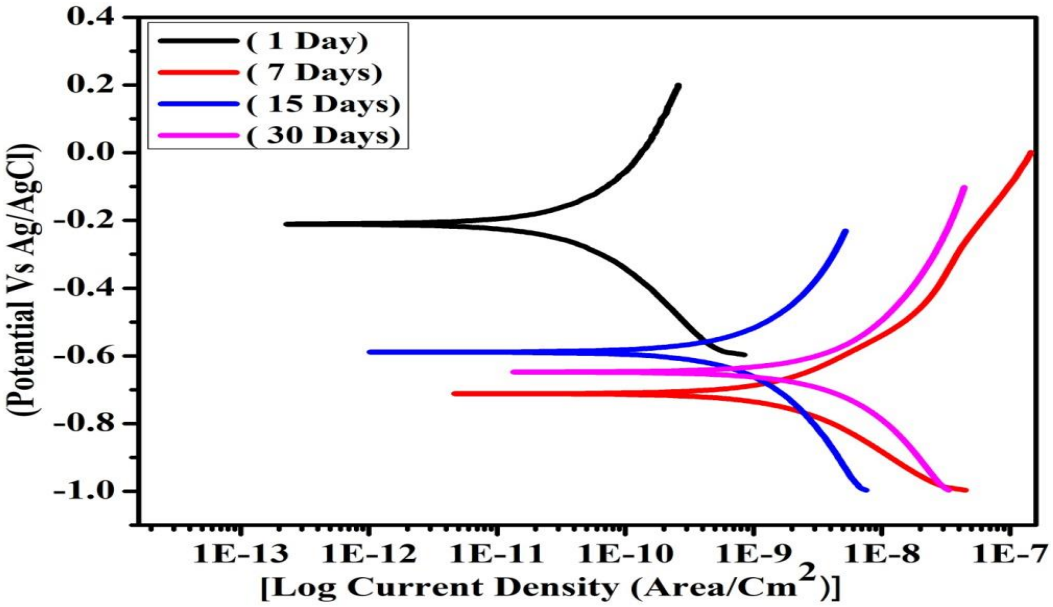


**Fig.5(D).13:** Tafel curves of composite coating of VE1 after (1, 7, 15 and 30) days immersions in 3.5 wt% Nacl aqueous solution

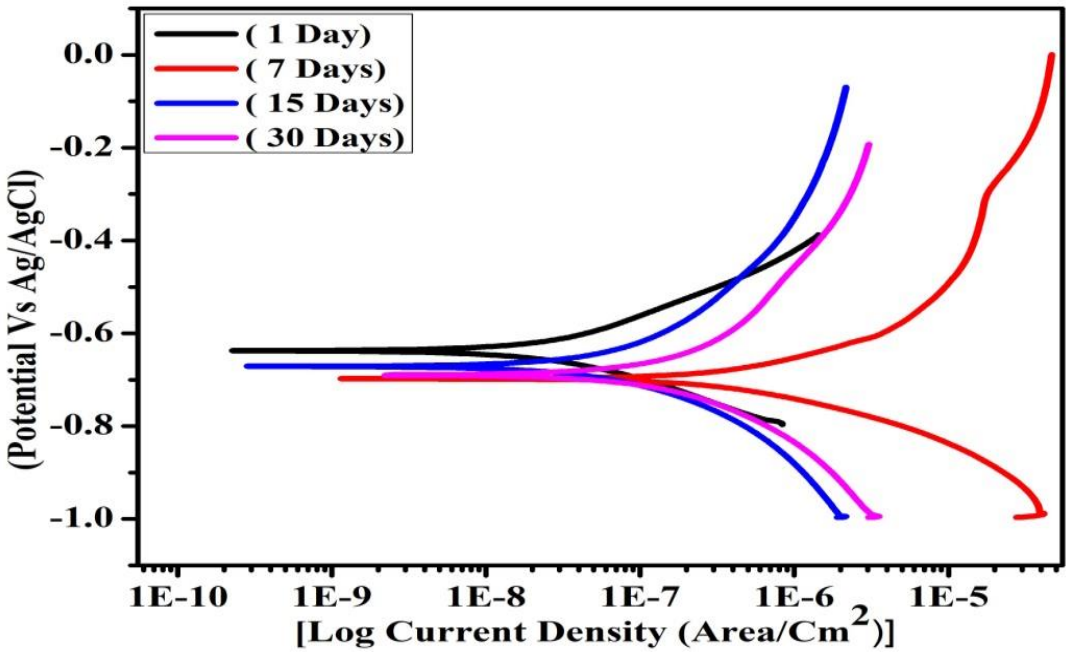


**Fig.5(D).14:** Tafel curves of composite coating of VE2 after (1, 7, 15 and 30) days immersions in 3.5 wt% Nacl aqueous solution

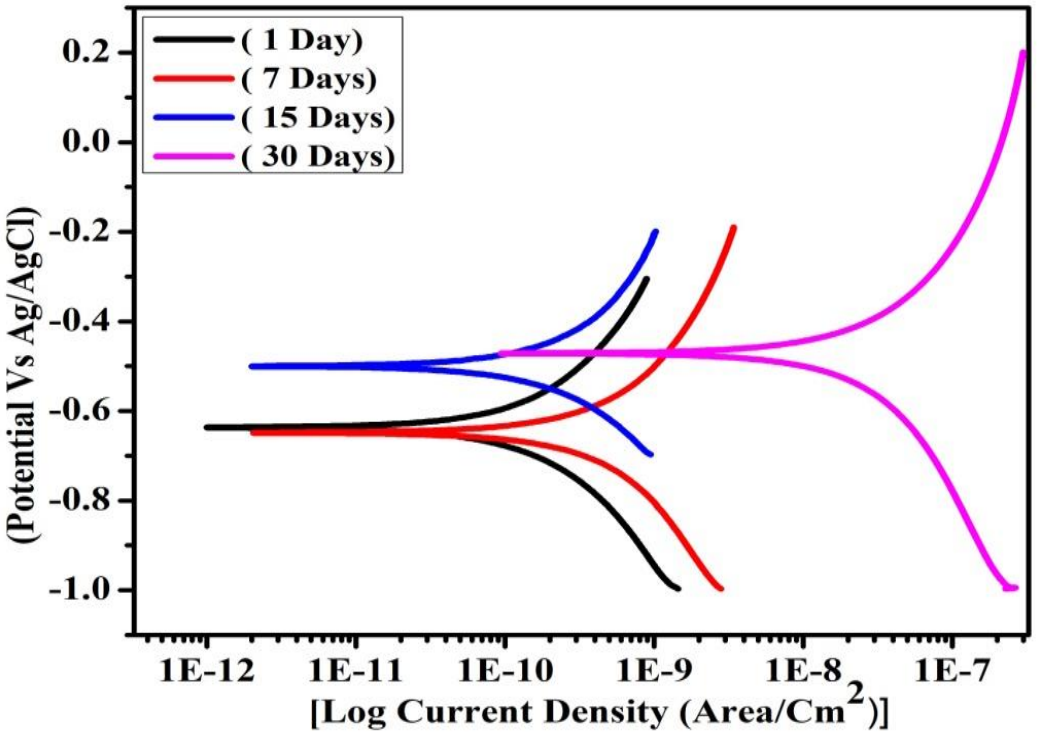


**Fig.5(D).15:** Tafel curves of composite coating of VE3 after (1, 7, 15 and 30) days immersions in 3.5 wt% Nacl aqueous solution

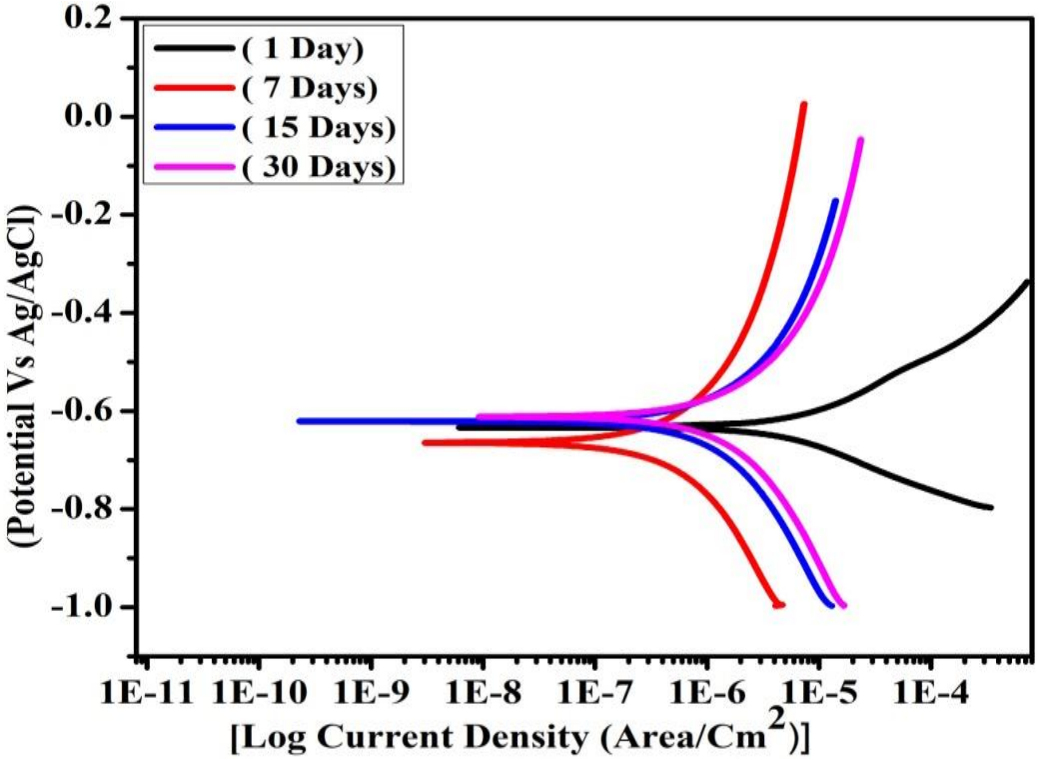


**Fig.5(D).16:** Tafel curves of composite coating of VE4 after (1, 7, 15 and 30) days immersions in 3.5 wt% Nacl aqueous solution

**Table.5(D).4:** Electrochemical parameters after soaking for different time intervals (1, 7, 15 and 30) days of polarization measurements of VE1 &VE2 coated MS rod

| Samples code name | Day(s) | $-E_{corr}$ (V vs SCE) | $J_{corr}$ ($A/cm^2$) | $I_{corr}$ (mA $cm^{-2}$) | Corrosion rate (mm/year) | $R_p$($\Omega$ $cm^2$) | βa (mV $dec^{-1}$) | βc (mV $dec^{-1}$) |
|---|---|---|---|---|---|---|---|---|
| VE1 | 1 | ─0.208 | 1.27E-11 | 1.52E-10 | 1.48E-07 | 1.72E+03 | 0.128 | 0.135 |
| | 7 | ─0.711 | 6.89E-10 | 6.87E-09 | 4.00E-06 | 98319 | 0.108 | 0.105 |
| | 15 | ─0.616 | 3.46E-10 | 4.15E-09 | 0.00004 | 44201 | 0.15 | 0.16 |
| | 30 | ─0.650 | 1.23E-09 | 1.47E-08 | 0.000086 | 22140 | 0.12 | 0.10 |
| VE2 | 1 | ─0.627 | 1.34E-08 | 1.88-07 | 3.52E-06 | 78311 | 0.073 | 0.063 |
| | 7 | ─0.698 | 2.94E-07 | 4.13E-06 | 2.91E-06 | 2.80E+06 | 0.086 | 0.078 |
| | 15 | ─0.682 | 4.08E-08 | 5.73E-07 | 2.21E-06 | 8.27E+06 | 0.138 | 0.10 |
| | 30 | ─0.667 | 3.47E-08 | 1.05E-06 | 1.43E-05 | 2.38E+05 | 0.110 | 0.103 |

**Table.5(D).5:** Electrochemical parameters after soaking for different time intervals (1, 7, 15 and 30) days of polarization measurements of VE3 &VE4 coated MS rod

| Samples code name | Day (s) | $-E_{corr}$ (V vs SCE) | $J_{corr}$ ($A/cm^2$) | $I_{corr}$ (mA $cm^{-2}$) | Corrosion rate (mm/year) | $R_p$($\Omega$ $cm^2$) | βa (mV $dec^{-1}$) | βc (mV $dec^{-1}$) |
|---|---|---|---|---|---|---|---|---|
| VE3 | 1 | ─0.665 | 4.62E-11 | 7.59E-10 | 1.37E-03 | 7865 | 0.125 | 0.123 |
| | 7 | ─0.679 | 1.37E-10 | 2.25E-09 | 0.000743 | 21934 | 0.13 | 0.121 |
| | 15 | ─0.519 | 4.50E-11 | 3.39E-10 | 0.06443 | 96677 | 0.075 | 0.0721 |
| | 30 | ─0.493 | 1.05E-08 | 1.72E-07 | 0.00012 | 9 7162 | 0.179 | 0.224 |
| VE4 | 1 | ─0.602 | 2.66E-09 | 3.81E-05 | 6.89E-08 | 3.56E+07 | 0.061 | 0.070 |
| | 7 | ─0.631 | 2.32E-08 | 2.58E-06 | 4.51E-07 | 1.28E+07 | 0.158 | 0.162 |
| | 15 | ─0.621 | 4.44E-07 | 3.03E-06 | 4.31E-06 | 2.20E+07 | 0.13 | 0.140 |
| | 30 | ─0.614 | 5.54E-06 | 5.67E-06 | 3.23E+06 | 1.73E+06 | 0.169 | 0.198 |

From the table, electrochemical parameters of various composite coatings are put forward. The higher $E_{corr}$, lower $I_{corr}$, and higher Rp values show better corrosion resistive properties. Thus we can say that corrosion potential ($E_{corr}$) of VE4 is higher than that of others composite. Meanwhile, the corrosion current ($J_{corr}$) of VE4>VE2 coatings is the lowest than VE3>VE1. Interestingly, the corrosion potential first increased and then decreased in VE4coating and also corrosion current to be inversely related. Moreover, in term of polarization resistance, VE4 is 1.73E+06Ωcm$^2$ which is about 17.80 more than that of VE3 whereas VE2 is 2.38E+05 i.e about 10.75 times more than VE1, nano composite coating possesses the superior corrosion resistance properties over conventional composite coating.

## 5(D).6.2. Analysis of EIS results of various vinyl ester composite coatings

The Nyquist and Bode plots of the coated MS rod after immersion for various time intervals (1, 7, 15, and 30 days) in corrosion studies are displayed in Fig.5(D).17 to Fig.5(D).24. In the Nyquist plot, a significant semicircle is observed, and the Bode plot indicates capacitance behavior, suggesting high corrosion resistance of the coating. The impedance $|Z|_{0.01}$ at low frequencies exhibits very large values, reaching $5\times10^6$ and the phase angle is around 140 for the for VE4 coating and $2\times10^6$ and the phase angle is around 140 for the for VE2 coating. Whereas, $6\times10^3$ and the phase angle is around 125 for the for VE1 coating and $1.5\times10^3$ and the phase angle is around 90. These observations indicate the presence of a time constant, which is characteristic of the barrier properties of the vinyl ester coating [12,13]. Over the course of 1 to 30 days, the data consistently demonstrate pronounced corrosion resistance behavior.

After 1 and 7 days, a new semi circle appears in the Nyquist plot of VE3 and VE1 respectively, indicating the generation of an ionic path within the coating. This

behavior can be represented by an electrical equivalent circuit comprising a working electrode (W.E), charge transfer resistance, and a constant phase element (CPE) in series with a parallel combination of the coating. Interestingly, such a phenomenon did not occur in the case of VE2 and VE4 coating, suggesting differences in the corrosion behavior and barrier properties between the coatings.

In the Nyquist and Bode plot shown in the nano composite coatings VE2 and VE4 display an increase in the impedance modulus $|Z|_{0.01}$ at low frequencies as corrosion time progresses, particularly noticeable at 15 and 30 days. This behavior suggests that vinyl ester nanocomposite coatings act as an effective protective barrier. Conversely, the conventional based composite coating experiences degradation over time. It is presumed that electrolyte penetration through the coating occurs, creating a path to the MS coated surface, ultimately leading to degradation in the case of conventional coating.

After 15 and 30 days, there is an extension observed in the second time constant of the impedance plots, which is illustrated by the appearance of a second semicircle in the Nyquist plot at lower frequencies. During this stage, the barrier properties of the composite coating gradually deteriorate, leading to exposure of the substrate to the corrosive solution. In this context, the first semi circle in the impedance plot is associated with the barrier characteristics of the VE2 and VE4 coatings, while the second semi circle represents the corrosion process occurring at the interface between the substrate and the damaged area of the coating. This second semicircle reflects the charge transfer process between the substrate and the electrolyte solution. These conditions are depicted by the electrical equivalent circuit shown in Fig.5(C).13.

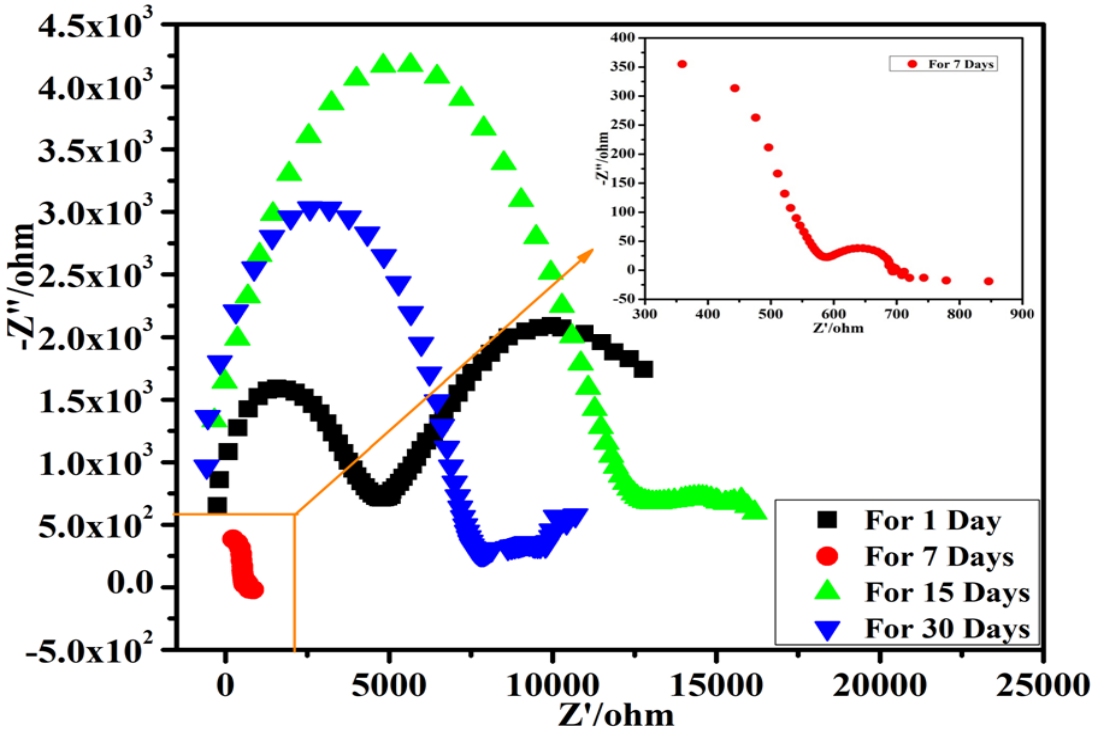


**Fig.5(D).17:** Nyquist plot of VE1 after soaking for 3.5 weight% Nacl aqueous solution for (1, 7, 15 and 30) days

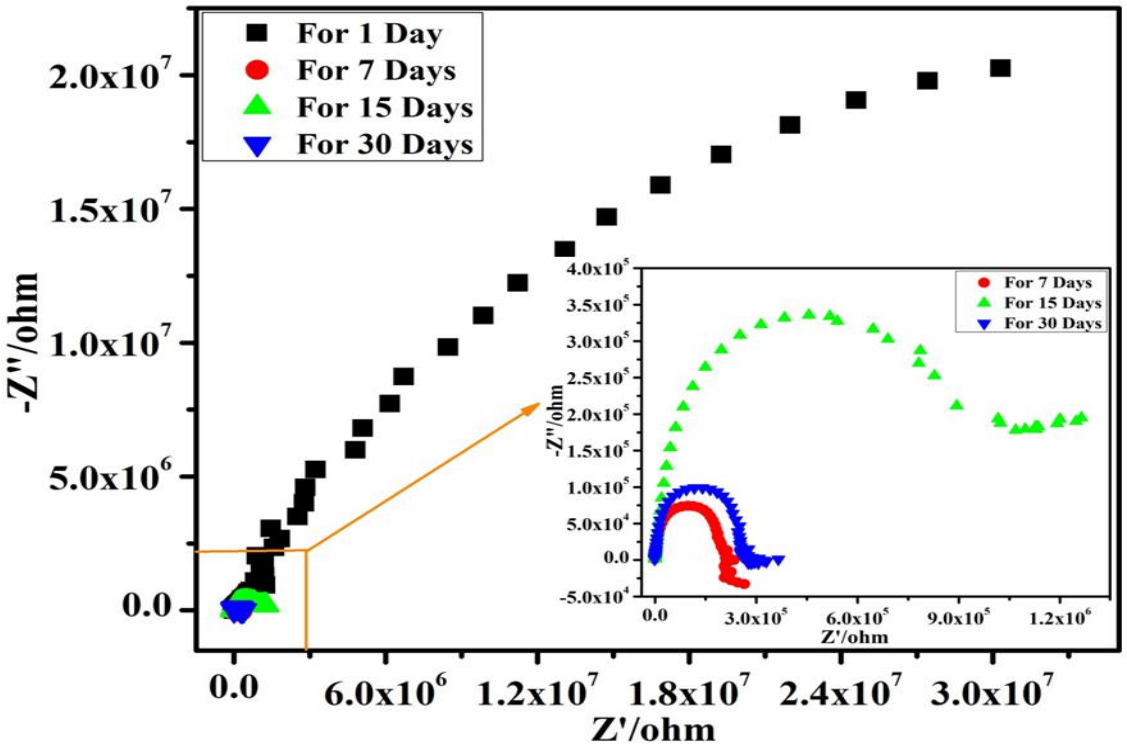


**Fig.5(D).18:** Nyquist plot of VE2 after soaking for 3.5 weight% Nacl aqueous solution for (1, 7, 15 and 30) days

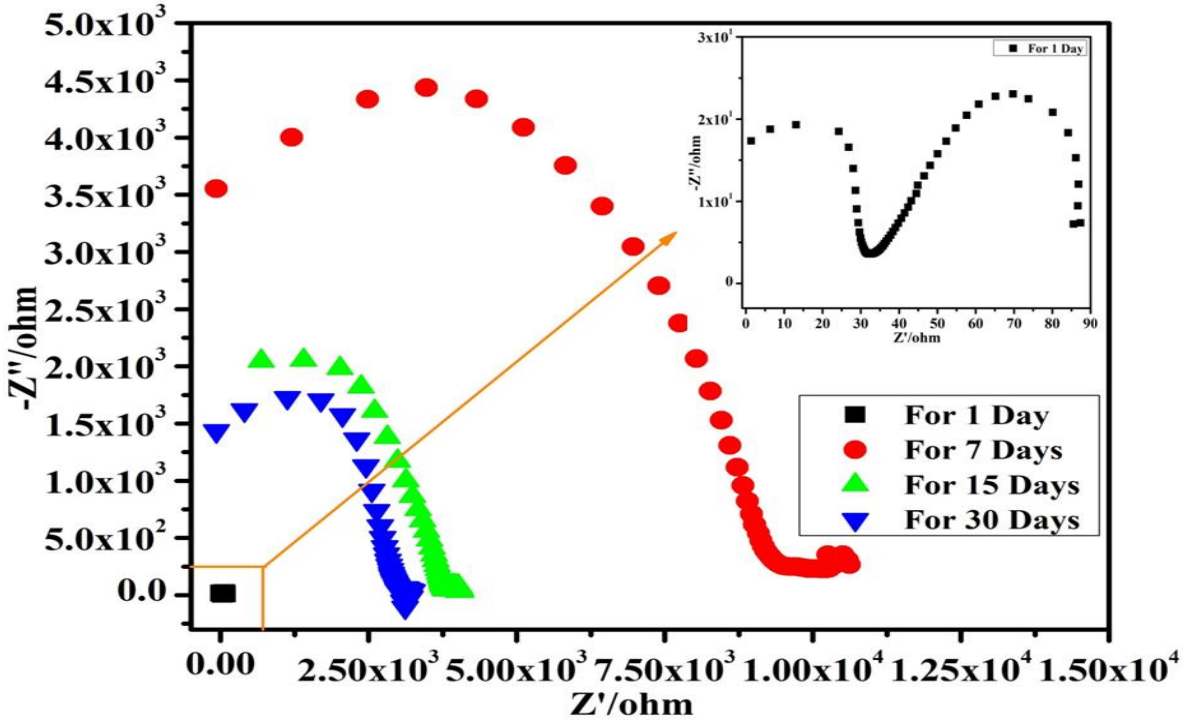


**Fig.5(D).19:** Nyquist plot of VE3 after soaking for 3.5 weight% Nacl aqueous solution for (1, 7, 15 and 30) days

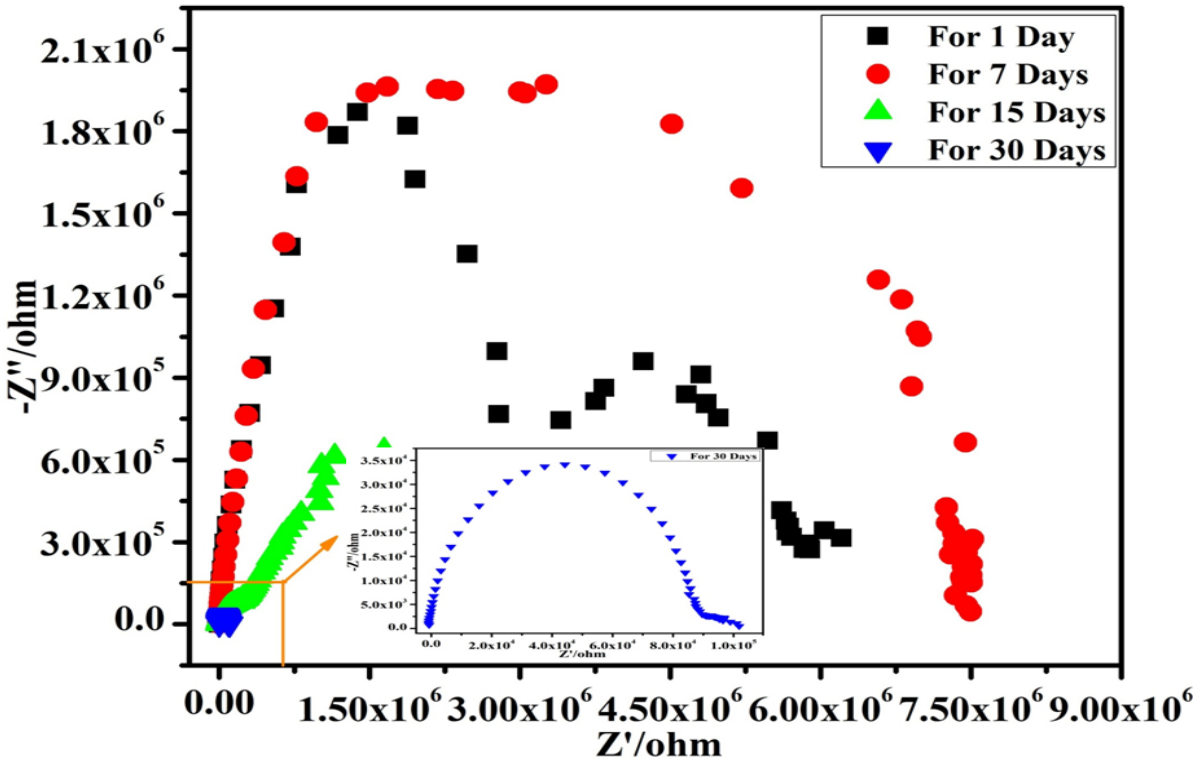


**Fig.5(D).20:** Nyquist plot of VE4 after soaking for 3.5 weight% Nacl aqueous solution for (1, 7, 15 and 30) days

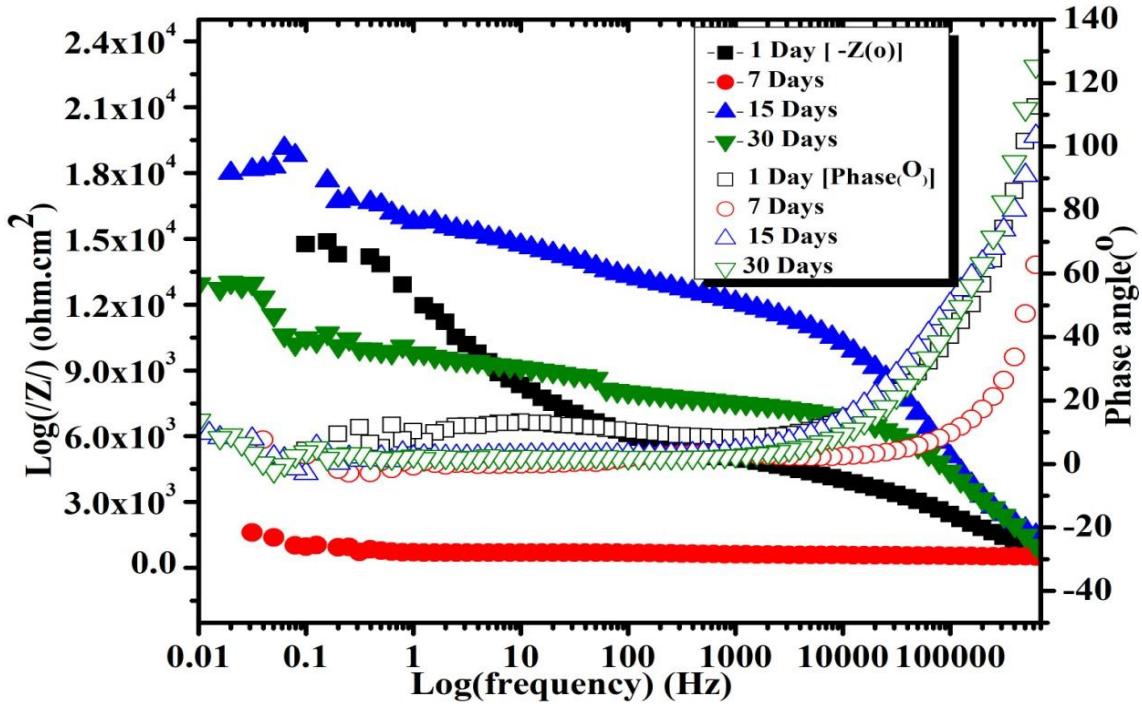


**Fig.5(D).21:** Bode plot of VE1 after soaking for 3.5 weight% Nacl aqueous solution for (1, 7, 15 and 30) days

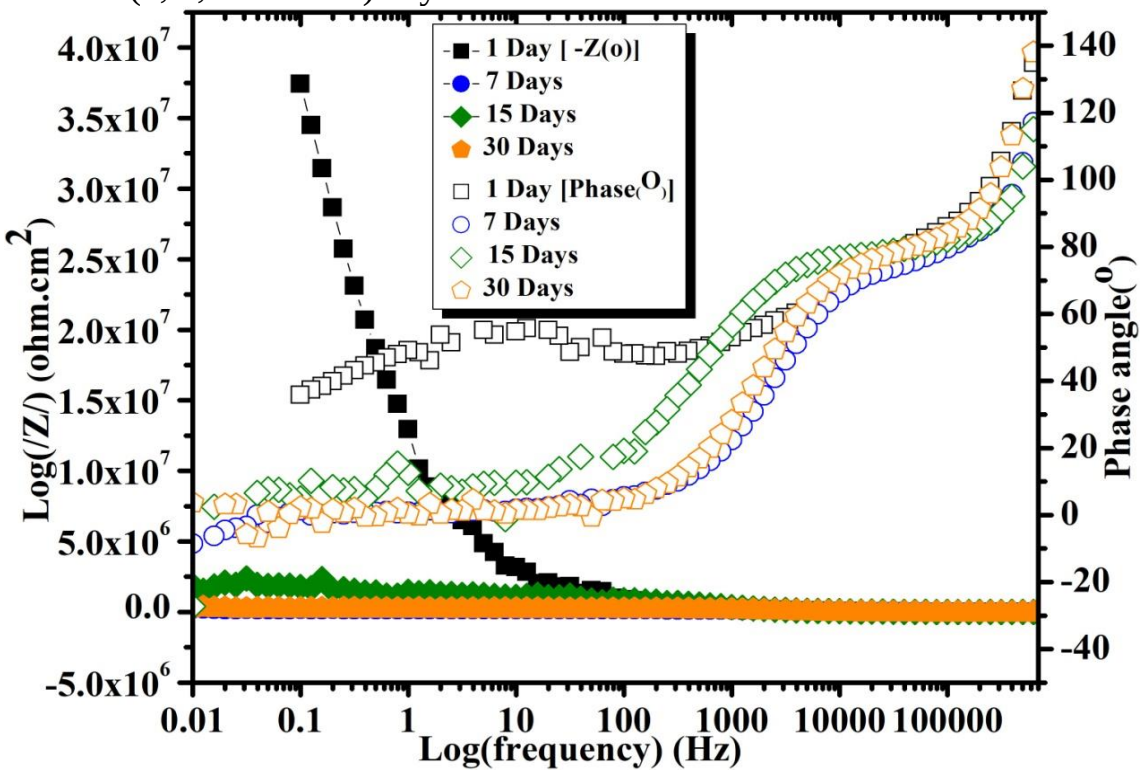


**Fig.5(D).22:** Bode plot of VE2 after soaking for 3.5 weight% Nacl aqueous solution for (1, 7, 15 and 30) days

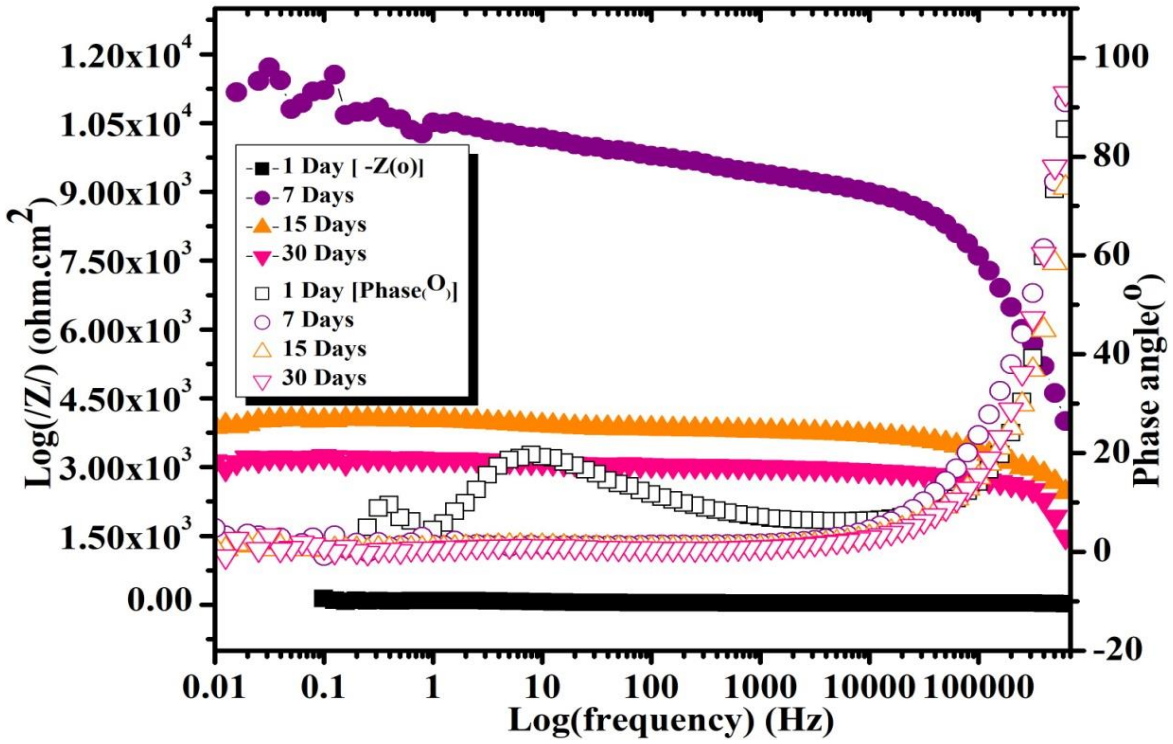


**Fig.5(D).23:** Bode plot of VE3 after soaking for 3.5 weight% Nacl aqueous solution for (1, 7, 15 and 30) days

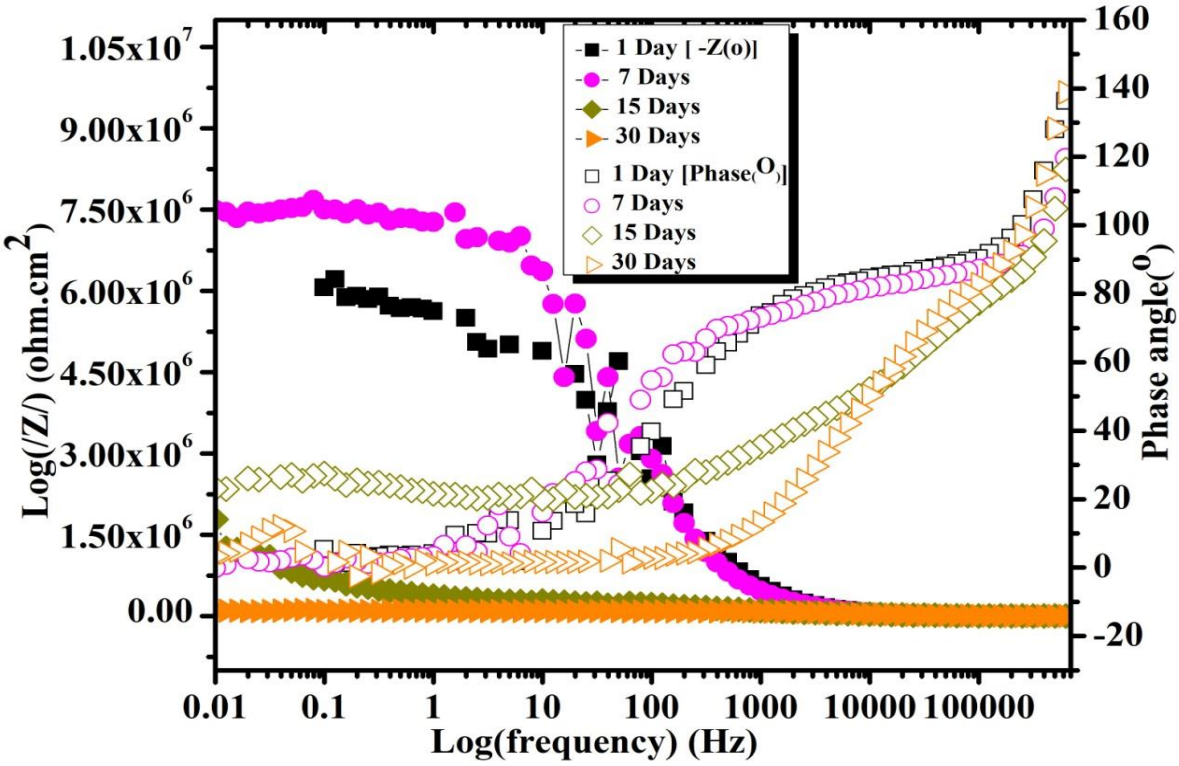


**Fig.5(D).24:** Bode plot of VE4 after soaking for 3.5 weight% Nacl aqueous solution for (1, 7, 15 and 30) days

**Table.5(D).6.** Fitting results of VE1 and VE2

| Samples code name | Day(s) | C.P.E ($Y_o$) | $R_p$(Ω) | C.P.E (N) |
|---|---|---|---|---|
| VE1 | 1 | 4.04E-10F | 5379.7 | 0.7004 |
| | 7 | 3.35E-10F | 727.14 | 1.13 |
| | 15 | 2.41E-10F | 14317 | 0.68 |
| | 30 | 1.97E-10F | 8708.2 | 0.78 |
| VE2 | 1 | 1.67E-08F | 9.50E+07 | 0.606 |
| | 7 | 3.33-10F | 2.17E+05 | 0.840 |
| | 15 | 5.95-10F | 1.19E+06 | 0.713 |
| | 30 | 3.47E-10F | 2.67E+05 | 0.894 |

**Table.5(D).7.** Fitting results of VE3 and VE4

| Samples code name | Day(s) | C.P.E ($Y_o$) | $R_p$(Ω) | C.P.E (N) |
|---|---|---|---|---|
| VE3 | 1 | 0.00033F | 60.86 | 0.817 |
| | 7 | 4.60E-10F | 11426 | 0.875 |
| | 15 | 6.27E-11F | 4934 | 0.993 |
| | 30 | 1.30E-10F | 3273 | 1.120 |
| VE4 | 1 | 8.74E-10F | 5.95E+06 | 0.693 |
| | 7 | 3.4E-10F | 7.42E+06 | 0.863 |
| | 15 | 1.39E-10F | 5.32E+06 | 0.670 |
| | 30 | 3.51E-10F | 92929 | 0.812 |

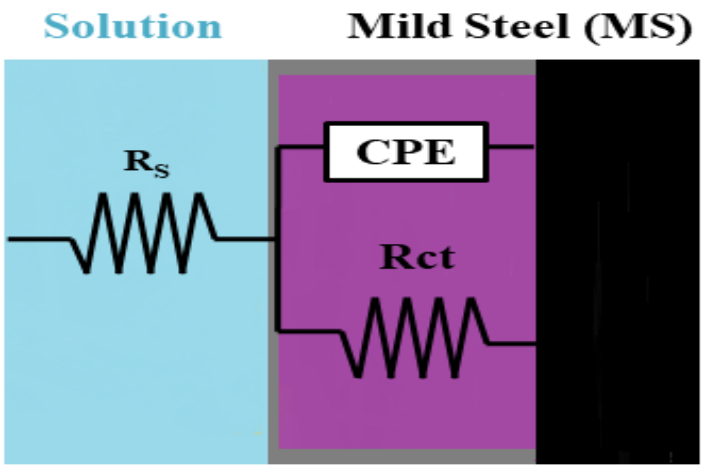


**(a)**

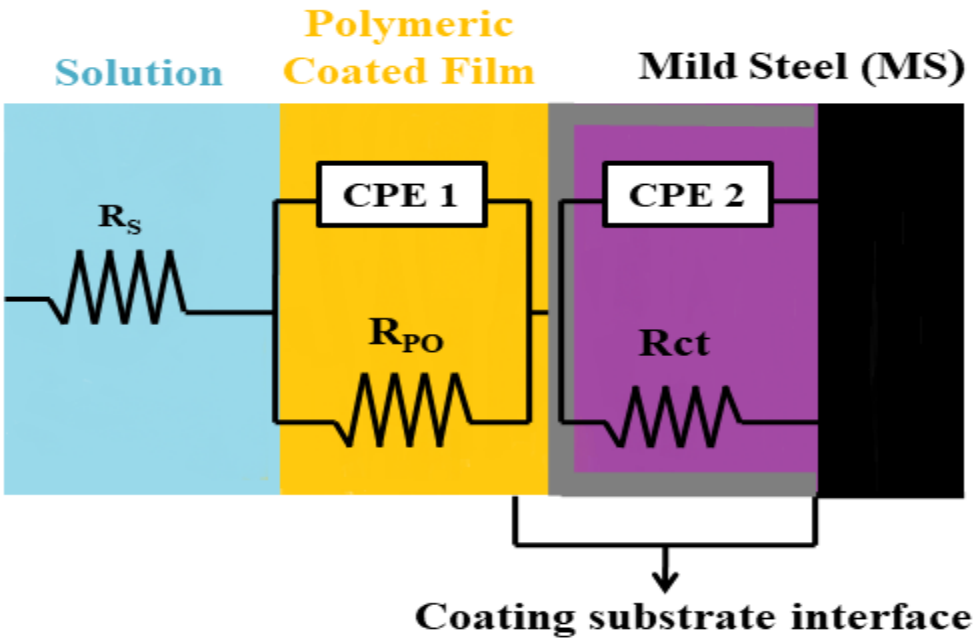


**(b)**

**Fig.5(D).25:** The equivalent electrical circuit models used to simulate EIS measurements of coatings at various immersion stages: (a) for one time constant and (b) for two time constant

**Table.5(D).8:** Inhibition efficiency of VE composite coating from electrochemical parameter after corrosion studies

| **Coating code Name** | **% Corrosion Inhibition Efficiency=** $\frac{I^o_{corr} - I_{corr}}{I^o_{corr}} \times 100$ | **% Rct =** $\frac{Rct - Rct^o}{Rct} \times 100$ | $P = \frac{R_{P(Uncoated)}}{R_{P(Coated)}} \times 10^{-\frac{(\Delta E_{corr})}{ba}}$ |
|---|---|---|---|
| VE1 | 78 | 97.84 | $P=18.06\times10^{-6}$ |
| VE2 | 86.72 | 99.79 | $P=63.49\times10^{-9}$ |
| VE3 | 79.36 | 98.30 | $P=80.99\times10^{-6}$ |
| VE4 | 96.95 | 99.67 | $P=13.87\times10^{-9}$ |

From Table.5(D).6, electrochemical parameter, it has been seen, VE4>VE2>VE3>VE1 increasing order for corrosion inhibition efficiency, VE4>VE2>VE3>VE1 increasing order for charge transfer resistance and VE4>VE2>VE1>VE3 increasing order for porosity measurement of different type of composite coatings respectively. It has suggested that nano filler embedded vinyl ester coating best results in corrosion inhibition efficiency and charge transfer resistance due to dense structure formed when cured with hydrophobic nano silica particle compared to conventional one [27].

## 5(D).7. Surface Analysis of Coatings (Optical Images)

Optical images from Fig.5(D).26 to Fig.5(D).29 were captured before and after the corrosion studies of coatings on an MS rod in electrochemical experiments. After the corrosion test over, it has observed that major number of pits with degradation appeared on the surface of the 160A glass flake with conventional silica based vinyl ester composite VE1 coating compared to 160N glass flake with conventional silica based vinyl ester composite VE3 coating depicted in

Fig.5(D).26 (c) and (d). It has revealed that more swelling occurred in the Nacl medium for the conventional VE1 coating than VE3 coating. The damages observed at the metal coating interface allowed the uptake of electrolyte, indicating the weak resistance nature of the VE1 coating. Few numbers of pits and damages were observed after the corrosion studies of the 160N glass flake with nano silica based vinyl ester composite VE4 coating compared to 160A glass flake with nano silica based vinyl ester composite VE2 coating depicted in Fig.5(D).27 (g) and (h). The presence of nano organosilane at the metal/coating interface effectively prevented the penetration of corrosion ions onto the MS substrate.

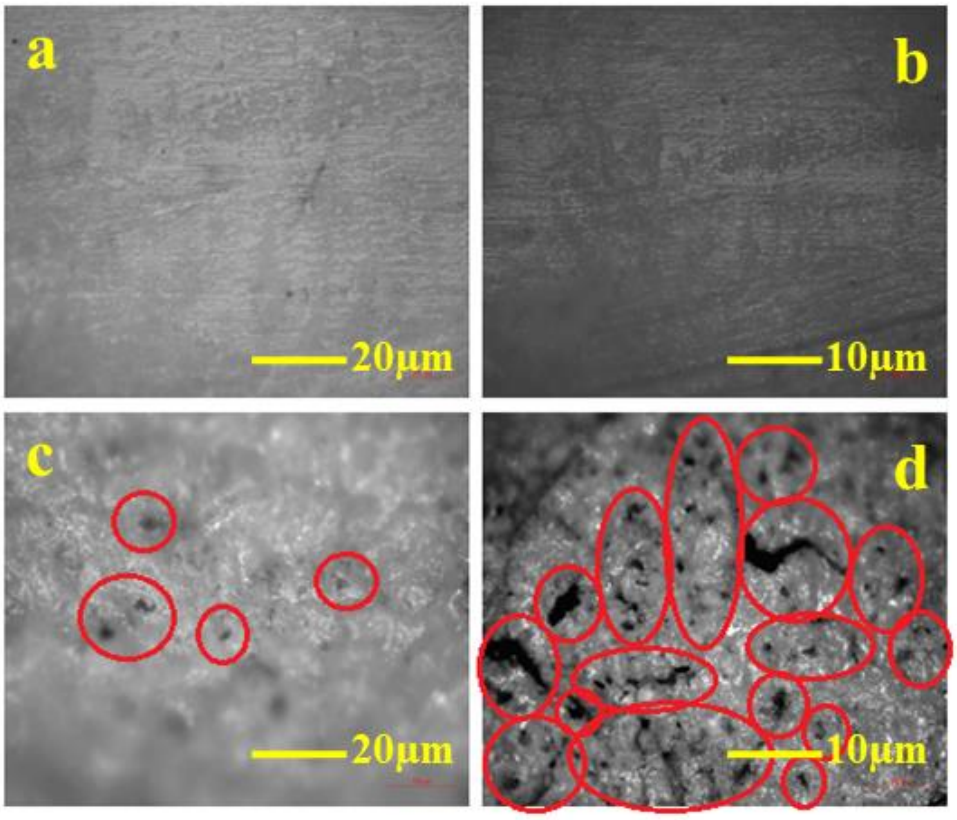


**Fig.5(D).26:** Image shows studies at different magnifications (a) & (b) before corrosion and (c) & (d) after corrosion of VE1

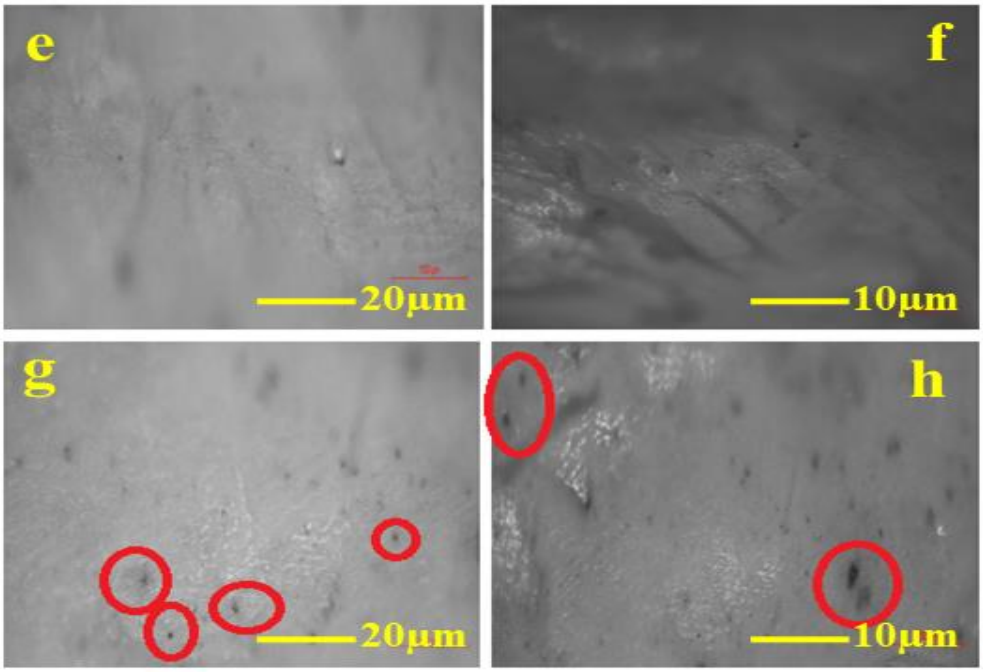


**Fig.5(D).27:** Image shows studies at different magnifications (e) & (f) before corrosion and (g) & (h) after corrosion of VE2

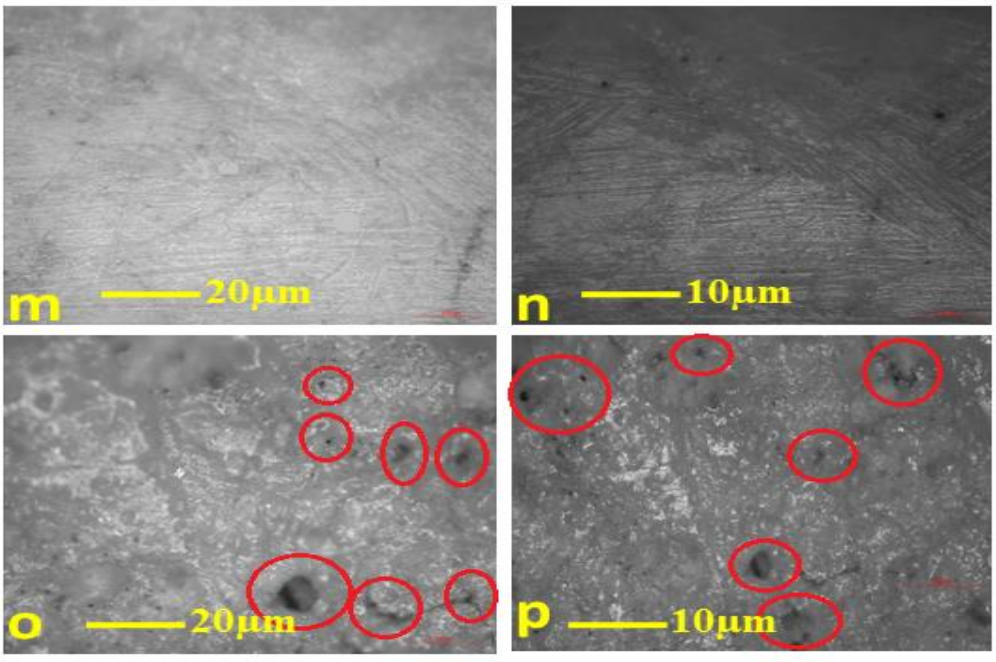


**Fig.5(D).28:** Image shows studies at different magnifications (m) & (n) before corrosion and (o) & (p) after corrosion of VE3

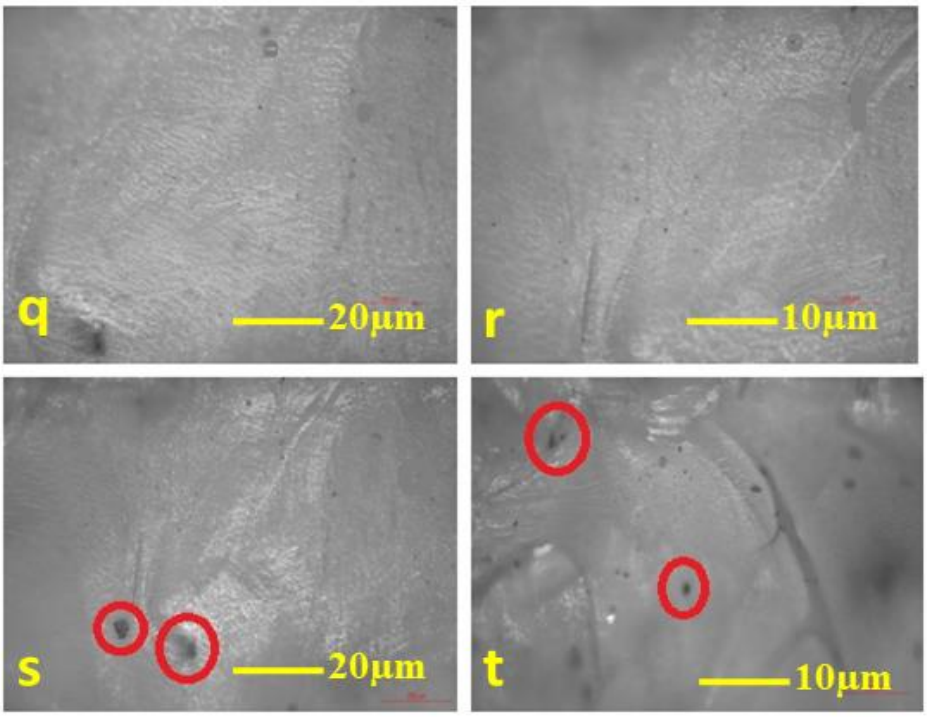


**Fig.5(D).29:** Image shows studies at different magnifications (q) & (r) before corrosion and (s) & (t) after corrosion of VE4

## 5.(D).8. Salt Spray Chamber Study

The salt spray chamber test was conducted continuously for 2200 hours, exposing coated panels to a foggy environment. According to the findings presented in Fig.5(D).29 and Fig.5(D).30**,** it was observed that corrosion and blister formation were exclusive to the micron silica-based vinyl ester composite coatings (VE1 and VE3). In contrast, there was less corrosion and blister formation in the nano silica based vinyl ester composite coatings (VE2 and VE4). These results strongly suggest that vinyl ester composite coatings embedded with nano silica exhibit significantly superior corrosion-resistant properties when compared to conventional vinyl ester composite coatings that use micron silica. This

demonstrates the potential advantages of incorporating nano silica for enhancing corrosion resistance in such coatings.

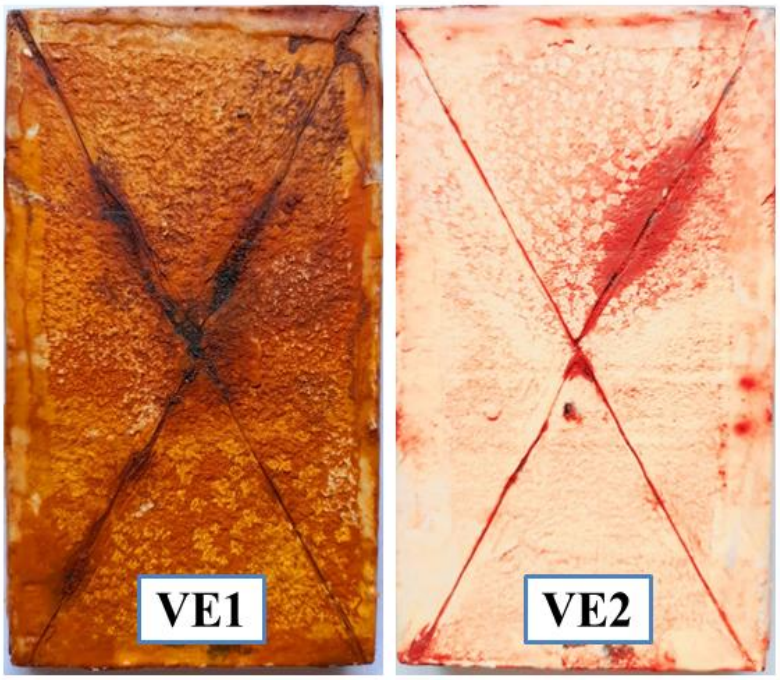


**Fig.5(D).29:** Image shows salt spray studies MS coated panels of VE1 and VE2

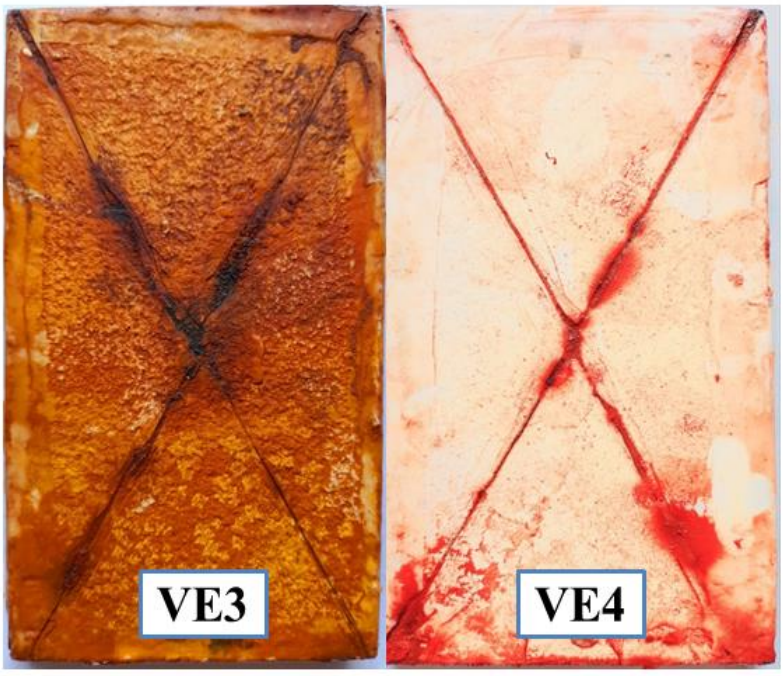


**Fig.5(D).30.** Image shows salt spray studies MS coated panels of VE3 and VE4

## 5(D).9. Cathodic Disbondment Study

After the experiment, phenolphthalein indicator was used to detect violet color changes in drilled holes at the center of each cell, signifying corrosion in the violet color zone, as shown in Fig.5(D).31 and Fig.5(D).32. Temperature plays a crucial role in coating disbonding, with a direct correlation to disbondment rates (mm/day). Higher current leads to increased expansion, especially at elevated temperatures [34, 35]. Increased vapor pressure can elevate coating porosity, allowing more electrolyte permeation through the coating. This leads to chemical attack and thermal expansion of the metal substrate. Additionally, elevated temperatures accelerate the dissolution of interface oxides. The results indicate that the epoxy nano composite sample exhibits significantly less cathodic disbondment area than the conventional one, highlighting its superior corrosion-resistant properties.

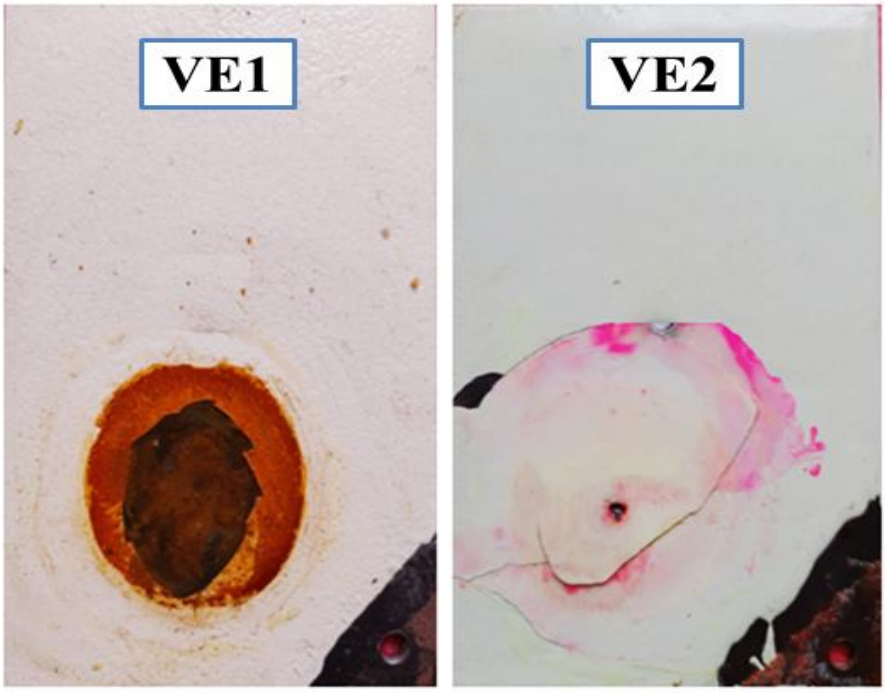


**Fig.5(D).31:** Image shows CD studies MS coated panels of VE1 and VE2

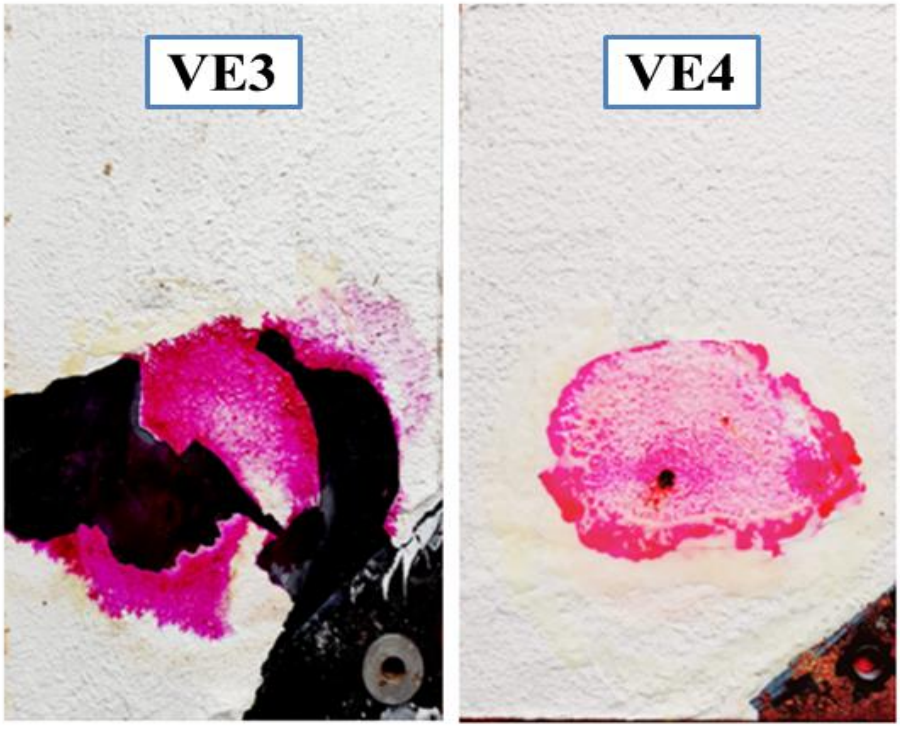


**Fig.5(D).32:** Image shows CD studies MS coated panels of VE3 and VE4

**Table.5(C).9:** Cathodic disbondment result for VE composite coating

| Samples code name | Voltage (V) | Current (mA) | Temp ($^{O}$C) | Duration (Days) | Disbondment (mm)/Remarks |
|---|---|---|---|---|---|
| VE1 | −1.5 | 90-110 | 30-45 | 17 | Full area delaminated and coating comes out |
| VE2 | −1.5 | 90-110 | 30-45 | 28 | Small area delaminated but coating becomes cracked |
| VE3 | −1.5 | 90-110 | 30-45 | 28 | Full area delaminated and coating comes out |
| VE4 | −1.5 | 90-110 | 30-45 | 28 | 6-9.3 |

## 5(D).10. Water and Chemical Resistance Study

The degree of water absorption has been evaluated by using formula of % swell test for 65 days. The nano filler based cured film VE4>VE2> showed excellent water resistant than conventional cured film VE3>VE1.

As result, absorption of water VE3 and VE1 are 16.17%, 21.32% respectively and where as VE4 and VE2 are 5.43%, 3.14% respectively.

The resistance behaviors of chemicals of the cured films were studied by in solution of acids (5% HCl and 5% $H_2SO_4$) and alkali (5% NaOH) immersed continue for 65 days.

These studies exposed that the films, acid and alkali immersion test showed damages and weight loss in acid medium is 13-27% and loss of gloss in alkali of conventional cured film. On the other hand small damages and weight loss in acid (4-12%) and little loss of gloss in alkali of nano filler based cured film observed.

Nano composite coatings show better water and chemical resistance than conventional composite coating due to nano particles completely wetted by vinyl ester resin and cured highly crosslink density rigid molecule structure presence of hydrophobic groups of nano organo silane, etc.

## 5(D).11. Conclusions

In summary, we have successfully developed an organo silane vinyl ester nanocomposite material using a simple method, which has shown excellent results in all experiments. Various studies including TEM, XRD, SEM, and TGA-DTA have confirmed that the nanocomposite material exhibits superior corrosion properties compared to conventional coatings. The organo silane nano filler embedded in the polymeric coating demonstrates the lowest corrosion current density, a more positive corrosion potential, and excellent polarization resistance

when compared to conventional silica-based epoxy coatings. Even in salt spray chamber tests, the nanocomposite coal tar epoxy exhibits better corrosion resistance than conventional epoxy coatings. It also displays significantly lower cathodic disbondment properties, indicating superior corrosion resistance. Optimization has shown that the resin can consume approximately 6.5 to 7 wt% of nanoparticles. Based on these findings, vinyl ester nanocomposite coatings are recommended for practical applications requiring corrosion mitigation.

# CHAPTER-6

# Conclusions

## 6. Conclusion:

Corrosion is prevalent and significantly affects various sectors, including industry, municipalities, and private domains. Polymer nanocomposites have gained significant attention in recent decades for protecting metals from corrosion.

In the current study, the following corrosion inhibitors were successfully integrated silica particle into a polymer matrix such as: incorporating silica particle into epoxy (EP series), polyurethane (PU series), coal tar epoxy (CTEP series), vinyl ester (VE series) resin and cured. The silica particles incorporated in the polymer matrix were analyzed using various techniques, including FTIR, XRD, SEM, TEM, and TGA-DTA. Silica based nanocomposite coatings improve their physical as well as mechanical properties. Incorporating nano silica into the polymer resin, cured coating enhances abrasion resistance and impact strength, owing to the inherent flexibility, smoothness, and stress-dissipating properties of the organo siliane moiety. Conventional silica based coating systems display limited impact and abrasion resistance because of their inherent brittleness and rigidity. Nanocomposite coating systems have lower hardness values compared to conventional composite coating systems due to the inherent coiled and resilient nature of the organo modified silica skeleton. Research on the corrosion protection performance of nano silica based coating systems has showed excellent anti corrosion behavior than conventional coating systems from measurement of electrochemical potential, potentiodynamic polarization, electrochemical impedance measurements, salt spray chamber test and catodic disbondment studies.

In this chapter, the qualitative ranking (1 for highest, 2 for higher, 3 for high, 4 for low, 5 for lower and 6 for lowest) for all coatings are the summarized and final conclusions drawn from the all over studies in below.

## 6.(A). Epoxy Composite Coating

Comparative study of conventional and nano filler based epoxy composite coatings concluded below.

**Table.6.1** FTIR (before & after salt spray) comparative studies of epoxy composite coatings

| Coating code name | FTIR Studies | |
|---|---|---|
| | **Before Salt Spray** | **After 2200 hrs Salt Spray** |
| (a) Conventional filler based epoxy composite coating (EP1) | All characteristics peaks are observed on 3743 to 466 $cm^{-1}$in this region | Additional vibrational bond observed at (i) 3775 to 3963$cm^{-1}$ (ii) 1667 to 2336 $cm^{-1}$ and (iii) 543 to 750$cm^{-1}$,in these region |
| (b) Nano filler based epoxy composite coating (EP2) | The intensity of the peaks increases from nano composite compare conventional composite ones when the number of methyl groups surrounding a Si atom increases more instance. It has seen that at band 3745$cm^{-1}$ maximum level of free SiOH belongs in nano organosiliane powder and nano composite coating. | Vibrational band shifted 1058 to 1470 $cm^{-1}$ But also all characteristics bands are present after salt spray test |
| (c) Conventional filler with 160A glass flake based epoxy composite coating (EP3) | All characteristics peaks are observed on 3743 to 466 $cm^{-1}$in this region | Additional vibrational bond observed at (i) 3554 to 4110$cm^{-1}$ (ii) 1801 to 2283 $cm^{-1}$ and (iii) 509 to 810$cm^{-1}$, in these region |
| (d) Nano filler with 160A glass flake based epoxy composite coating (EP4) | The intensity of the peaks increases in the nano composite compared to the conventional composite when there are more methyl groups surrounding a Si atom. It's observed that the maximum level of free SiOH is found at 3745 $cm^{-1}$ in both nano | Very weak bands observed in resin degradation of nanocomposite coating 1018 to 1145 $cm^{-1}$ in this region |

| | | |
|---|---|---|
| | organo silane powder and the nano composite coating. | |
| (e) Conventional filler with 160N glass flake based epoxy composite coating (EP5) | All characteristics peaks are observed on 3743 to 466 $cm^{-1}$in this region | Additional vibrational bond observed at (i) 3568 to 4030$cm^{-1}$ (ii) 1580 to 2391$cm^{-1}$ and (iii) 550 to 750$cm^{-1}$ in this region. |
| (f) Nano filler with 160N glass flake based epoxy composite coating (EP6) | The intensity of the peaks increases from nano composite compare conventional composite ones when the number of methyl groups surrounding a Si atom increases more instance. It has seen that at band 3745$cm^{-1}$ maximum level of free SiOH belongs in nano organosilane powder and nano composite coating. | Additional very weak bands observed in resin degradation of nanocomposite coating 1005 to 1138 $cm^{-1}$ in this region. So, it can be concluded that there is no significant interaction between the glass flake epoxy nanocomposite coating and the salt spray, indicating limited resin degradation and offering a high level of resistance against corrosion. |

**Table.6.2.** Ranking of epoxy composite coating of FTIR studies after salt spray

| Coating code name | Ranking |
|---|---|
| (a) EP1 | Lowest (6) |
| (b) EP2 | High (3) |
| (c) EP3 | Low (4) |
| (d) EP4 | Higher (2) |
| (e) EP5 | Lower (4) |
| (f) EP6 | Highest (1) |

**Table.6.3.** XRD and morphology (SEM & TEM) comparative studies of epoxy composite coating

| **Coating code name** | **XRD Studies** | **Morphology Studies** | |
|---|---|---|---|
| | | **SEM** | **TEM** |
| (a) EP1 | All ingredients are seen at less instance peak in epoxy composite including quartz silica. Coating showed amorphous in nature. | Some particles are observed at micro level on surfaces of coating and also micrographs also show heterogeneous dispersion of silica particles within the polymer matrix. | × |
| (b) EP2 | All compositions are observed at high intense peak in epoxy composite including nano silica. Developed coating showed amorphous in nature. | Nano silica particles are homogeneously dispersed in the polymer matrix during the formation of nanocomposite coatings. | Nano silica particles are homogeneously dispersed in the polymer matrix during the formation of nanocomposite coatings. |
| (c) EP3 | All ingredients are seen at less instance peak in epoxy composite including quartz silica. Coating showed amorphous in nature. | Some particles are observed at micro level on surfaces of coating and also micrographs also show heterogeneous dispersion of silica particles within the polymer matrix | × |
| (d) EP4 | All compositions are observed at high intense peak in epoxy composite including nano silica. Developed coating showed amorphous in | Nano silica particles are homogeneously dispersed in the polymer matrix during the formation of nanocomposite coatings. | Results from TEM will define corrosion resistant properties of nanocoatings, detected organo silane particle size is |

| | | | |
|---|---|---|---|
| | nature. | | less than 50nm. |
| (e) EP5 | All ingredients are seen at less instance peak in epoxy composite including quartz silica. Coating showed amorphous in nature. | Some particles are observed at micro level on surfaces of coating and also micrographs also show heterogeneous dispersion of silica particles within the polymer matrix. | × |
| (f) EP6 | All compositions are observed at high intense peak in epoxy composite including nano silica. Developed coating showed amorphous in nature. | Nano silica particles are homogeneously dispersed in the polymer matrix during the formation of nanocomposite coatings. | The corrosion performance of the resultant nancoating is influenced by a presence of nano-sized particles in a polymeric matrix, detected organosilane particle size is less than 50nm. |

**Table.6.4.** Ranking of epoxy composite coating of XRD and morphology (SEM & TEM) studies

| **Coating code name** | **XRD** | **SEM** | **TEM** |
|---|---|---|---|
| | **Ranking** | **Ranking** | **Ranking** |
| (a) EP1 | High (3) | Low (4) | × |
| (b) EP2 | Higher (2) | Highest (1) | High (3) |
| (c) EP3 | Lower (5) | Lower (5) | × |
| (d) EP4 | Higher (2) | High (3) | High (3) |
| (e) EP5 | Low (4) | Lower (5) | × |
| (f) EP6 | Highest (1) | Higher (2) | Highest (1) |

**Table.6.5.** Comparative studies of Physico-Mechanical testing of epoxy composite coating

| **Coating code name** | **Cross link Density (%)** | **Adhesion Property ($N/mm^2$)** | | **Impact Test (KG.M)** | | **Abrasion Test (mg/cycles)** | **Thermal Studies (TGA-DTA)** |
|---|---|---|---|---|---|---|---|
| | | **Before Salt Spray** | **After 2200 hrs Salt Spray Test** | **Instrusion** | **Extrusion** | | |
| (a) EP1 | 85 | 23.5 | 7.8 | >1.3 | >1.5 | 7.8 | Coating degrade at $450^{O}C$ |
| (b) EP2 | 97 | 43.7 | 29.8 | >0.7 | >0.9 | 3.8 | Coating degrade at $650^{O}C$ |
| (c) EP3 | 87 | 33.8 | 23.6 | >0.9 | >0.7 | 6.2 | Coating degrade at $500^{O}C$ |
| (d) EP4 | 95.8 | 45.3 | 32.3 | >0.3 | >0.4 | 2.1 | Coating degrade at $750^{O}C$ |
| (e) EP5 | 83.65 | 32.5 | 16.2 | >0.6 | >0.8 | 4.7 | Coating degrade at $550^{O}C$ |
| (f) EP6 | 96.20 | 44.2 | 36.1 | >0.2 | >0.2 | 2.3 | Coating degrade at $860^{O}C$ |

**Table.6.6.** Ranking of epoxy composite coating of Physico-Mechanical testing

| **Coating code name** | **Cross link Density (%)** | **Adhesion Property ($N/mm^2$)** | **Impact Test (KG.M)** | **Abrasion Test (mg/cycles)** | **Thermal Studies (TGA-DTA)** |
|---|---|---|---|---|---|
| | **Ranking** | **Ranking** | **Ranking** | **Ranking** | **Ranking** |
| (a) EP1 | Low (4) | Lowest (6) | Lowest (6) | Lowest (6) | Lowest (6) |
| (b) EP2 | High (3) | Higher (2) | High (3) | Higher (2) | High (3) |
| (c) EP3 | Lower (5) | Low (4) | Lower (5) | Low (4) | Lower (5) |
| (d) EP4 | Higher (2) | Higher (2) | Higher (2) | Highest (1) | High (3) |
| (e) EP5 | Lowest (6) | Lower (5) | Low (4) | Low (4) | Low (4) |
| (f) EP6 | Higher (2) | Highest (1) | Highest (1) | Higher (2) | Highest (1) |

**Table.6.7.** Comparative studies of corrosion studies of epoxy composite coating

| **Corrosion Studies** | | | | | |
|---|---|---|---|---|---|
| **Samples Code Name** | **Potentiodynamic Polarization (PD) (After 30 Days) & Corrosion Inhibition Efficiency (%)** | **Electro chemical Impedance Spectroscopy (EIS) (After 30 Days) & Charge transfer resistance (Rct in %)** | **Cathodic Disbondment (CD) (After 28 Days)** | **Salt Spray Chamber (SSC) Test (After 2200 hrs)** | **Porosity (P) & Optical Images Analysis (After Corrosion Studies)** |
| Uncoated MS Rod | (After 7 Days)<br>$-E_{corr}$(V vs SCE = −0.910<br>$J_{corr}$ ($A/cm^2$) = | (After 7 Days)<br>C.P.E ($Y_o$) = 0.00065<br>$R_P$ (Ω) = 0.821 | × | | |

| | | | | | |
|---|---|---|---|---|---|
| | 4.63E-05<br>$I_{corr}$ ($mAcm^{-2}$) = 1.25E-05<br>Corrosion rate (mm/year) = 0.8721<br>$R_P$ ($\Omega cm^2$) = 177.66 | C.P.E (N) = 0.521<br>Equivalent electrical circuit models: Two time constant | | × | × |
| (a) Conventional filler based epoxy composite coating (EP1) | ─$E_{corr}$(V vs SCE)= ─0.594<br>$J_{corr}$ ($A/cm^2$) = 8.16E-08<br>$I_{corr}$ ($mAcm^{-2}$) = 1.69E-06<br>Corrosion rate (mm/year) = 0.00094<br>$R_P$ ($\Omega cm^2$) = 30446<br>Corrosion inhibition efficiency (%) = 98.70 | C.P.E ($Y_o$) = 1.27E─10F<br>$R_P$ ($\Omega$) =22751<br>C.P.E (N) = 0.853<br>Equivalent electrical circuit models: Two time constant<br>Rct (%) = 98.83 | Disbondment area (mm): 6 ─ 13.2 | Corrosion and blister formation occurred only in micron silica based epoxy composite coating due to porosity formed with micron range of silica | P= $45.78\times10^{-7}$<br>After corrosion study it has been seen that some holes are observed over the surface. It revealed that swelling has occurred in Nacl medium of conventional epoxy coatings. Damages observed at the metal-coating interface uptake electrolyte that implies the weak resistance nature of conventional composite coatings. |
| (b) Nano filler based | ─$E_{corr}$(V vs SCE)= ─0.590<br>$J_{corr}$ ($A/cm^2$) = | C.P.E ($Y_o$) = 1.97E─10F<br>$R_P$ ($\Omega$) = 60783 | Disbondment area (mm): 6 ─ 9.5 | But such type of corrosion not observed in case of nano silica | P=$38.69\times10^{-10}$<br>There are no such |

| | | | | | |
|---|---|---|---|---|---|
| epoxy composite coating (EP2) | 2.01E-08<br>$I_{corr}$ ($mAcm^{-2}$) = 4.73E-07<br>Corrosion rate (mm/year) = 0.00024<br>$R_P$ ($\Omega cm^2$) =108392<br>Corrosion inhibition efficiency (%) = 99.61 | C.P.E (N) = 0.910<br>Equivalent electrical circuit models: One time constant<br>Rct (%) = 99.20 | | based epoxy composite coating This indicates nano silica embedded epoxy is having much better corrosion resistant properties than conventional silica based epoxy coating. | holes and damages observed after corrosion study of nano composite coating. Presence of nano organosiliane at metal/coating interface prevented the penetration of corrosion ions on MS substrate. |
| (c) Conventional filler with 160A glass flake based epoxy composite coating (EP3) | ─$E_{corr}$(V vs SCE)= ─0.677<br>$J_{corr}$ ($A/cm^2$) = 8.03E-09A<br>$I_{corr}$ ($mAcm^{-2}$) = 4.2E-07A<br>Corrosion rate (mm/year) = 0.0002349<br>$R_P$ ($\Omega cm^2$) =1.0402E+04<br>Corrosion inhibition efficiency (%) =99.18 | C.P.E ($Y_o$) = 2.46-10F<br>$R_P$ ($\Omega$) = 41587<br>C.P.E (N) = 0.882<br>Equivalent electrical circuit models: Two time constant<br>Rct (%) = 99.30 | Disbondment area (mm Partially delamination and 1/3 th area of coating comes out): | Corrosion and blister formation occurred in micron silica based epoxy composite coating | P=$20.23\times10^{-7}$<br><br>Some holes are observed over the surface but less than EP1 coating. It revealed that swelling has occurred in Nacl medium of 160A glass flake with conventional silica based epoxy composite coatings. Damages observed at the metal-coating interface uptake electrolyte that |

| | | | | | |
|---|---|---|---|---|---|
| | | | | | implies the weak resistance nature coating. |
| (d) Nano filler with 160A glass flake based epoxy composite coating (EP4) | $-E_{corr}$(V vs SCE)= −0.539<br>$J_{corr}$ (A/cm$^2$) = 2.02E-08A<br>$I_{corr}$ (mAcm$^{-2}$) = 3.49-08A<br>Corrosion rate (mm/year) =<br>$R_P$ (Ωcm$^2$) =9.3407E-05<br>Corrosion inhibition efficiency (%) =99.92 | C.P.E ($Y_o$) = 1.32E-10F<br>$R_P$ (Ω) = 44921<br>C.P.E (N) = 0.707<br>Equivalent electrical circuit models: Two time constant<br>Rct (%) = 99.78 | Disbondment area (mm): 6−8.7 | But such type of corrosion not observed in case of nano silica with 160A glass flake based epoxy composite coating. This indicates nano silica with glass flake embedded epoxy is having much better corrosion resistant properties than conventional silica with glass flake based epoxy coating. | P=10.26×10$^{-12}$<br>There are only two holes are observed after corrosion study of 160A glass flake with nano silica based composite coating. Presence of nano organosiliane at metal/coating interface prevented the penetration of corrosion ions on MS substrate. |
| (e) Conventional filler with 160N glass flake based epoxy composite | $-E_{corr}$(V vs SCE)= −0.699<br>$J_{corr}$ (A/cm$^2$) = 1.01E-08<br>$I_{corr}$ (mAcm$^{-2}$) = 2.06E-07<br>Corrosion rate (mm/year) = 0.00011748<br>$R_P$ (Ωcm$^2$) =2.09E+05<br>Corrosion inhibition | C.P.E ($Y_o$) = 2.60E-10F<br>$R_P$ (Ω) = 38853<br>C.P.E (N) = 0.887<br>Equivalent electrical circuit models: : Two time constant<br>Rct (%) = 99.86 | Disbondment area (mm): 6−9.3 | Corrosion and blister formation occurred in micron silica based epoxy composite coating | P=26.59×10$^{-8}$<br>Some pin holes are observed over the surface but less than EP3 coating. It revealed that swelling has occurred in Nacl medium of 160N glass flake with conventional silica based epoxy |

| | | | | | |
|---|---|---|---|---|---|
| coating (EP5) | efficiency (%) = 99.84 | | | | composite coatings. |
| (f) Nano filler with 160N glass flake based epoxy composite coating (EP6) | ─$E_{corr}$(V vs SCE)= ─0.416<br>$J_{corr}$ (A/cm$^2$) = 1.02E-10<br>$I_{corr}$ (mAcm$^{-2}$) = 1.51E-09<br>Corrosion rate (mm/year) = 1.18E-06<br>$R_P$ (Ωcm$^2$) = 4.62E+07<br>Corrosion inhibition efficiency (%) = 99.90 | C.P.E ($Y_o$) = 1.99E-10F<br>$R_P$ (Ω) = 2.53E+07<br>C.P.E (N) = 1.024<br>Equivalent electrical circuit models: One time constant<br>Rct (%) = 99.96 | Disbondment area (mm): 6─7.3 | But such type of corrosion not observed in case of nano silica with 160N glass flake based epoxy composite coating. This indicates nano silica with glass flake embedded epoxy is having too much better corrosion resistant properties than conventional silica with glass flake based epoxy coating. | P=23.48×10$^{-14}$<br>There are only two pin holes are observed after corrosion study of 160N glass flake with nano silica based composite coating. Presence of nano organosiliane at metal/coating interface prevented the penetration of corrosion ions on MS substrate. |

**Table.6.8.** Ranking of epoxy composite coating of Physico-Mechanical testing

| Sample Code Name | Potentiodynamic Polarization (PD) (After 30 Days) & Corrosion Inhibition Efficiency (%) | Electro chemical Impedance Spectroscopy (EIS) (After 30 Days) & Charge transfer resistance (Rct in %) | Cathodic Disbondment (CD) (After 28 Days) | Salt Spray Chamber (SSC) Test (After 2200 hrs) | Porosity (P) & Optical Images Analysis (After Corrosion Studies) |
|---|---|---|---|---|---|
| | **Ranking** | **Ranking** | **Ranking** | **Ranking** | **Ranking** |
| (a) EP1 | Low (4) | Low (4) | Low (4) | Low (4) | Low (4) |
| (b) EP2 | High (3) | High (3) | Higher (2) | Higher (2) | High (3) |
| (c) EP3 | Lower (5) | Low (4) | Lower (5) | Lower (5) | Lower (5) |
| (d) EP4 | Higher (2) | Higher (2) | Higher (2) | Highest (2) | Higher (2) |
| (e) EP5 | Low (4) | Lowest (6) | Low (4) | Low (4) | Low (4) |
| (f) EP6 | Higher (2) | Highest (1) | Highest (1) | Highest (1) | Highest (1) |

## 6. (B). PU composite Coating

Comparative study of conventional and nano filler based polyurethane composite coatings concluded below.

**Table.6.9.** FTIR (before & after salt spray) comparative studies of Polyurethane composite coatings

| Coating code name | FTIR Studies | |
|---|---|---|
| | **Before Salt Spray** | **After 2200 hrs Salt Spray** |
| (g) Conventional filler based polyurethane composite coating (PU1) | Most observable region are main distinguishable peaks of C─H stretching band (2800─4000cm$^{-1}$) appear. These peaks are mainly associated to urethane linkage | But in case of conventional composite coating of PU1, additional bands (i) 3554 to 4056cm$^{-1}$ (ii) 1560 to 1761cm$^{-1}$ (iii) 1111 to 1332cm$^{-1}$ and (iv) 583 to 844cm$^{-1}$ are observed in resin degradation which signify corrosion occurred in between |

| | | |
|---|---|---|
| | (NHCOO) in a polyurethane film is hydrogen bonded to each other with distinguished functional groups and the qurtz silica doped on the surface of composite coating. | polyurethane and salt spray |
| (h) Nano filler based polyurethane composite coating (PU2) | Moreover, the intensity of the peak nanocomposite coating (PU2) increasesess than conventional composite coating (PU1) for embedded organo siliane nanoparticle due to number of methyl groups surrounding Si atom increases intensifies more. | Additional very weak bands (i) 1078 to 1191$cm^{-1}$ and (ii) 649 to 870 $cm^{-1}$ are observed in resin degradation of nanocomposite coating of PU2. |

**Table.6.10.** Ranking of polyurethane composite coating of FTIR studies after salt spray

| Coating code name | Ranking |
|---|---|
| (g) PU1 | Lowest (6) |
| (h) PU2 | Higher (2) |

**Table.6.11.** XRD and morphology (SEM & TEM) comparative studies of polyurethane composite coating

| Coating code name | XRD Studies | Morphology Studies | |
|---|---|---|---|
| | | SEM | TEM |
| (g) PU1 | All ingredients are seen at less instance peak in PU composite including quartz | SEM images of conventional composite, where some particles are observed at micro level on the surface of coating and also micrographs also show | × |

| | | | |
|---|---|---|---|
| | silica. Coating showed amorphous in nature. | heterogeneous dispersion of silica particles within the polymer matrix. | |
| (h) PU2 | All compositions are observed at high intense peak in PU composite including nano silica. Developed coating showed amorphous in nature. | From the SEM images of nanocomposite coating, it is evident that the silica particle is fully wetted by the epoxy resin during composite formation. The micrographs also show | Organo silane particle size is less than 20nm detected in PU matrix |

**Table.6.12.** Ranking of polyurethane composite coating of XRD and morphology (SEM & TEM) comparative studies

| **Coating code name** | **XRD** | **SEM** | **TEM** |
|---|---|---|---|
| | **Ranking** | **Ranking** | **Ranking** |
| (g) PU1 | Lowest (6) | Lowest (6) | × |
| (h) PU2 | High (3) | Higher (2) | Higher (2) |

**Table.6.12.** Comparative study of Physico-Mechanical testing of polyurethane composite coating

| Coating code name | Cross link Density (%) | Adhesion Property ($N/mm^2$) | | Impact Test (KG.M) | | Abrasion Test (mg/cycles) | Thermal Studies (TGA-DTA) |
|---|---|---|---|---|---|---|---|
| | | Before Salt Spray | After 2200 hrs Salt Spray Test | Instrusion | Extrusion | | |
| (g) PU1 | 87 | 29.5 | 18.8 | >0.5 | >0.7 | 7.8 | Coating degrade at 300 $^{O}C$ |
| (h) PU2 | 92 | 43.7 | 34 | >0.4 | >0.3 | 3.8 | Coating degrade at 500 $^{O}C$ and above |

**Table.6.13.** Ranking of polyurethane composite coating of Physico-Mechanical testing

| Coating code name | Cross link Density (%) | Adhesion Property ($N/mm^2$) | Impact Test (KG.M) | Abrasion Test (mg/cycles) | Thermal Studies (TGA-DTA) |
|---|---|---|---|---|---|
| | Ranking | Ranking | Ranking | Ranking | Ranking |
| (g) PU1 | Lowest (6) | Lowest (6) | Lower (5) | Lowest (6) | Lowest (6) |
| (h) PU2 | Higher (2) | High (3) | Higher (2) | High (3) | High (3) |

**Table.6.14.** Comparative studies of corrosion studies of polyurethane composite coating

| **Corrosion Studies** | | | | | |
|---|---|---|---|---|---|
| **Samples Code Name** | **Potentiodynamic Polarization (PD) (After 30 Days) & Corrosion Inhibition Efficiency (%)** | **Electro chemical Impedance Spectroscopy (EIS) (After 30 Days) & Charge transfer resistance (Rct in %)** | **Cathodic Disbondment (CD) (After 28 Days)** | **Salt Spray Chamber (SSC) Test (After 2200 hrs)** | **Porosity (P) & Optical Images Analysis (After Corrosion Studies)** |
| (g) Conventional filler based polyurethane composite coating (PU1) | $-E_{corr}$(V vs SCE)= 0.746<br>$J_{corr}$ (A/cm$^2$) = 1.66E-05<br>$I_{corr}$ (mAcm$^{-2}$) = 0.00034<br>Corrosion rate (mm/year) = 0.19345<br>$R_P$ ($\Omega$cm$^2$) = 119.71<br>Corrosion inhibition efficiency (%) = 69.70 | C.P.E ($Y_o$) =1.76E-05<br>$R_P$ ($\Omega$) = 34.53<br>C.P.E (N) = 0.541<br>Equivalent electrical circuit models: Two time constant<br>Rct (%) = 75.62 | Disbondment area (mm): Fully area delaminated and coating comes out | Continuous fog on coated panels. From, results shown indicates, more corrosion and blister formation occurred only in micron silica based epoxy composite coating | P=23.74×10$^{-3}$<br>After the corrosion study, it was observed that the major number of pits and degradation occurred on the surface of the PU1. This indicates that swelling occurred in the Nacl medium for the conventional PU1 coating. The damages observed at the metal- |

| | | | | | |
|---|---|---|---|---|---|
| | | | | | coating interface allowed the uptake of electrolyte, indicating the weak resistance nature of the PU1 coating. |
| (h) Nano filler based polyurethane composite coating (PU2) | $-E_{corr}$(V vs SCE)= 0.653<br>$J_{corr}$ (A/cm$^2$) = 1.87E-08<br>$I_{corr}$ (mAcm$^{-2}$) = 4.48E-07<br>Corrosion rate (mm/year) = 0.00021<br>$R_P$ ($\Omega$cm$^2$) =93929<br>Corrosion inhibition efficiency (%) =99.89 | C.P.E ($Y_o$) =1.18E-10F<br>$R_P$ ($\Omega$) = 32883<br>C.P.E (N) = 0.787<br>Equivalent electrical circuit models: One time constant<br>Rct (%) = 99.94 | Disbondment area (mm): ¼ th area of coating delaminated | But such type of corrosion not observed in case of nano silica based PU composite coating. This indicates nano silica with glass flake embedded PU is having too much better corrosion resistant properties than conventional silica with glass flake based PU coating. | P=87.24×10$^{-10}$<br>Very less number of pits or damages was observed after the corrosion study of the PU2 coating. The presence of nano organosilane at the metal/coating interface effectively prevented the penetration of corrosion ions onto the MS substrate. |

**Table.6.15.** Ranking of polyurethane composite coating of Physico-Mechanical testing

| Sample Code Name | Potentiodynamic Polarization (PD) (After 30 Days) & Corrosion Inhibition Efficiency (%) | Electro chemical Impedance Spectroscopy (EIS) (After 30 Days) & Charge transfer resistance (Rct in %) | Cathodic Disbondment (CD) (After 28 Days) | Salt Spray Chamber (SSC) Test (After 2200 hrs) | Porosity (P) & Optical Images Analysis (After Corrosion Studies) |
|---|---|---|---|---|---|
| | **Ranking** | **Ranking** | **Ranking** | **Ranking** | **Ranking** |
| (a) PU1 | Lowest (6) | Lowest (6) | Lowest (6) | Lowest (6) | Lowest (6) |
| (b) PU2 | High (3) | High (3) | High (3) | Higher (2) | High (3) |

## 6. (C). Coal Tar Epoxy Composite Coating

Comparative study of conventional and nano filler based coal tar epoxy composite coatings concluded below.

**Table.6.16.** FTIR (before & after salt spray) comparative studies of coal tar epoxy composite coatings

| Coating code name | FTIR Studies | |
|---|---|---|
| | **Before Salt Spray** | **After 2200 hrs Salt Spray** |
| (i) Conventional filler based coal tar epoxy composite coating (CTEP1) | A peak at 1276cm$^{-1}$ which suggested aliphatic ─C─N─ stretching. At 1510 to 1615cm$^{-1}$ for benzene ring and 1460cm$^{-1}$ for aromatic backbone bands are confirmed. Transmission peaks are confirmed at 2855 to 2995cm$^{-1}$ make sure aliphatic and aromatic ─CH─ linkages respectively. | In the case of the conventional composite coating of CTEP1, additional bands are (i) 3528 to 8970cm$^{-1}$ (ii) 1018 to 1527cm$^{-1}$ (iii) 636 to 844cm$^{-1}$ observed. The changes observed in the transmittance spectra can be attributed to the interaction between the coating and salt spray, resulting in the formation of new C-H bonding. |

| | | |
|---|---|---|
| | Cured films of coal tar epoxy composite undergo stretching vibration ─C─O─C─ oxirane ring at 1045 $cm^{-1}$, ─C─O─ at 1175$cm^{-1}$ and also ─N─H─ of primary amine at 1655$cm^{-1}$. The IR spectrum DETA indicate characteristics peaks are at 2850$cm^{-1}$ for alkyl group, 1460 $cm^{-1}$ for aromatic ─C═C─ and 1276$cm^{-1}$ for aliphatic ─C─N─ stretch. | |
| (j) Nano filler based coal tar epoxy composite coating (CTEP2) | - 1276 $cm^{-1}$ peak: aliphatic ─C─N─ stretching.<br>- 1510 to 1615 $cm^{-1}$ bands: benzene ring.<br>- 1460 $cm^{-1}$ band: aromatic backbone.<br>- 2855 to 2995 $cm^{-1}$ transmission peaks: aliphatic and aromatic ─CH─ linkages.<br>- Cured coal tar epoxy films exhibit vibrations at 1045 $cm^{-1}$ (─C─O─C─ oxirane ring), 1175 $cm^{-1}$ (─C─O─), and 1655 $cm^{-1}$ (─N─H─ primary amine).<br>- DETA's IR spectrum features peaks at 2850 $cm^{-1}$ (alkyl groups), 1460 $cm^{-1}$ (aromatic ─C═C─ bonds), and 1276 $cm^{-1}$ (aliphatic ─C─N─ stretching). | Additional very weak band (i) 944 to 1085$cm^{-1}$ is observed in resin degradation of nanocomposite coating of CTEP2. From the FTIR spectrum, it is evident that the relative transmittances of samples before and after the salt spray test are very similar. This suggests that in this case, the resin system is not degraded in the presence of salt spray. |

**Table.17.** Ranking of coal tar epoxy composite coating of FTIR studies after salt spray

| Coating code name | Ranking |
|---|---|
| (i) CTEP1 | Lower (5) |
| (j) CTEP2 | Higher (2) |

**Table.6.18.** XRD and morphology (SEM & TEM) comparative studies of coal tar epoxy composite coating

| Coating code name | XRD Studies | Morphology Studies |
|---|---|---|
| | | SEM |
| (i) CTEP1 | All ingredients are seen at less instance peak in coal tar epoxy composite including quartz silica. Coating showed amorphous in nature. | SEM images of conventional composite, where some particles are observed at micro level on the surface of coating and also micrographs also show heterogeneous dispersion of silica particles within the polymer matrix. Some cavities and pores are observed on the surface. |
| (j) CTEP2 | All compositions are observed at high intense peak in coal tar epoxy composite including nano silica. Developed coating showed amorphous in nature. | From the SEM images of nanocomposite coating, it is evident that the silica particle is fully wetted by the epoxy resin during composite formation. The micrographs also show uniform dispersion of silica particles within the polymer matrix. However, in epoxy filled of nano $SiO_2$, there are larger agglomerates and aggregates observed. |

**Table.6.19.** Ranking of coal tar epoxy composite coating of XRD and morphology (SEM & TEM) studies

| Coating code name | XRD | SEM |
|---|---|---|
| | Ranking | Ranking |
| (i) CTEP1 | Lowest (6) | Low (4) |
| (j) CTEP2 | High (3) | Highest (1) |

**Table.6.20.** Comparative study of Physico-Mechanical testing of coal tar epoxy composite coating

| Coating code name | Cross link Density (%) | Adhesion Property ($N/mm^2$) | | Impact Test (KG.M) | | Abrasion Test (mg/cycles) | Thermal Studies (TGA-DTA) |
|---|---|---|---|---|---|---|---|
| | | Before Salt Spray | After 2200 hrs Salt Spray Test | Instrusion | Extrusion | | |
| (i) CTEP1 | 85 | 28.9 | 21.7 | >0.8 | >0.7 | 8.7 | Coating degrade at $580^{O}C$ and above |
| (j) CTEP2 | 97 | 41.3 | 36.6 | >0.4 | >0.5 | 1.2 | Coating degrade at $780^{O}C$ and above |

**Table.6.21.** Ranking of coal tar epoxy composite coating of Physico-Mechanical testing

| **Coating code name** | **Cross link Density (%)** | **Adhesion Property ($N/mm^2$)** | **Impact Test (KG.M)** | **Abrasion Test (mg/cycles)** | **Thermal Studies (TGA-DTA)** |
|---|---|---|---|---|---|
| | **Ranking** | **Ranking** | **Ranking** | **Ranking** | **Ranking** |
| (i) CTEP1 | Low (4) | Low (4) | Lower (5) | Low (4) | Low (4) |
| (j) CTEP2 | Higher (2) | Highest (2) | Highest (1) | Higher (2) | High (3) |

**Table.6.22.** Comparative studies of corrosion studies of coal tar epoxy composite coating

| **Samples Code Name** | **Potentiodynamic Polarization (PD) (After 30 Days) & Corrosion Inhibition Efficiency (%)** | **Electro chemical Impedance Spectroscopy (EIS) (After 30 Days) & Charge transfer resistance (Rct in %)** | **Cathodic Disbondment (CD) (After 28 Days)** | **Salt Spray Chamber (SSC) Test (After 2200 hrs)** | **Porosity (P) & Optical Images Analysis (After Corrosion Studies)** |
|---|---|---|---|---|---|
| (i) Conventional filler based coal tar epoxy composite coating (CTEP1) | $-E_{corr}$(V vs SCE)= −0.677<br>$J_{corr}$ ($A/cm^2$) = 3.18E-08<br>$I_{corr}$ ($mAcm^{-2}$) = 6.49E-07<br>Corrosion rate (mm/year) = 0.00037<br>$R_P$ ($\Omega cm^2$) = 70557<br>Corrosion inhibition efficiency (%) =84.30 | C.P.E ($Y_o$) = 2.53E-10F<br>$R_P$ ($\Omega$) = 21905<br>C.P.E (N) = 0.760<br>Equivalent electrical circuit models: Two time constant<br>Rct (%) = 97.54 | Disbondment area (mm): Full area delaminated and coating comes out | Continuous fog exposure was conducted for 2200 hours on coated panels. The results, indicate that corrosion and blister formation occurred exclusively in the micron silica-based coal tar epoxy coating | $P=78.96\times10^{-6}$<br>It has observed that some pits with degradation appeared on the surface of the CTEP1. It was revealed that swelling occurred in the Nacl medium for the |

| | | | | | |
|---|---|---|---|---|---|
| | | | | | conventional coal tar epoxy coating of CTEP1. The damages observed at the metal-coating interface allowed the uptake of electrolyte, indicating the weak resistance nature of the CTEP1 coating. |
| (j) Nano filler based coal tar epoxy composite coating (CTEP2) | ─$E_{corr}$(V vs SCE)= ─0.201<br>$J_{corr}$ (A/cm$^2$) = 3.08E-11<br>$I_{corr}$ (mAcm$^{-2}$) = 7.05E-6<br>Corrosion rate (mm/year) = 3.58E-07<br>$R_P$ (Ωcm$^2$) = 4.34E+07<br>Corrosion inhibition efficiency (%) = 99.85 | C.P.E ($Y_o$) = 7.16E-11F<br>$R_P$ (Ω) = 3.48+07<br>C.P.E (N) = 0.851<br>Equivalent electrical circuit models: One time constant.<br>Rct (%) = 99.87 | Disbondment area (mm): Small area delaminated and some blister formed | While no such observed in case of nano silica coal tar epoxy composite coating. Indeed, the results suggest that the nano silica embedded coal tar epoxy composite coating has significantly superior corrosion-resistant properties when compared to the conventional silica-based coal tar epoxy composite coating. | P=71.92×10$^{-10}$ Only three pits are observed after the corrosion study of the CTEP2. The presence of nano organosilane at the metal/coating interface effectively prevented the penetration of corrosion ions onto the MS substrate. |

**Table.6.23.** Ranking of polyurethane composite coating of Physico-Mechanical testing

| Sample Code Name | Potentiodynamic Polarization (PD) (After 30 Days) & Corrosion Inhibition Efficiency (%) | Electro chemical Impedance Spectroscopy (EIS) (After 30 Days) & Charge transfer resistance (Rct in %) | Cathodic Disbondment (CD) (After 28 Days) | Salt Spray Chamber (SSC) Test (After 2200 hrs) | Porosity (P) & Optical Images Analysis (After Corrosion Studies) |
|---|---|---|---|---|---|
| | **Ranking** | **Ranking** | **Ranking** | **Ranking** | **Ranking** |
| (i) CTEP1 | Low (4) | Lowest (6) | Lower (5) | Lower (5) | Low (4) |
| (j) CTEP2 | Higher (2) | Higher (2) | High (3) | High (3) | High (3) |

## 6. (D). Vinyl Ester Composite Coating

Comparative study of conventional and nano filler based vinyl ester composite coatings concluded below.

**Table.6.24.** FTIR (before & after salt spray) comparative studies of vinyl ester composite coatings

| Coating code name | FTIR Studies | |
|---|---|---|
| | **Before Salt Spray** | **After 2200 hrs Salt Spray** |
| (k) Conventional filler with 160A glass flake based vinyl ester composite coating (VE1) | The weak vibrational band at 915cm$^{-1}$ is associated with the vibration of oxirane ring. The vibrational band in between 1258 to 1460cm-1 can be attributed to the C─O─C and C═C for aromatic symmetric stretching modes of vibration. Two characteristics vibrational bond observed at 1627cm$^{-1}$ for olefinic and | 160A glass flake conventional vinyl ester composite coatings, additional bands (i) 3764 to 4061 cm$^{-1}$ (ii) 835 to 1067cm$^{-1}$ are observed. After the salt spray test of films, the transmittance of conventional coatings changed considerably, leading to the conclusion that the coatings have significantly degraded due to the salt spray exposure. |

| | | |
|---|---|---|
| | 1726 to 1736cm$^{-1}$ for C═O stretch in both composite coatings. | |
| (l) Nano filler with 160A glass flake based vinyl ester composite coating (VE2) | The free volume porosity of nano composite coatings is very minimal. The weak vibrational band at 915cm$^{-1}$ is associated with the vibration of oxirane ring. The vibrational band in between 1258 to 1460cm-1 can be attributed to the C─O─C and C═C for aromatic symmetric stretching modes of vibration. Two characteristics vibrational bond observed at 1627cm$^{-1}$ for olefinic and 1726 to 1736cm$^{-1}$ for C═O stretch in both composite coatings | Additional very weak bands (i) 954 to 1073cm$^{-1}$ (ii) 624 to 802cm$^{-1}$ are observed in resin degradation of nanocomposite coatings. The presences of such peaks signify an interaction between the glass flake nanocomposite coating and the salt spray, indicating a very slow corrosion resistance against salt spray |
| (m) Conventional filler with 160N glass flake based vinyl ester composite coating (VE3) | The weak vibrational band at 915cm$^{-1}$ is associated with the vibration of oxirane ring. The vibrational band in between 1258 to 1460cm-1 can be attributed to the C─O─C and C═C for aromatic symmetric stretching modes of vibration. Two characteristics vibrational bond observed at 1627cm$^{-1}$ for olefinic and 1726 to 1736cm$^{-1}$ for C═O stretch in both composite coatings. | 160N glass flake conventional vinyl ester composite coatings, additional bands (i) 543 to 676cm$^{-1}$ (ii) 2075 to 2524cm$^{-1}$ (iii) 2788 to 3147cm$^{-1}$ are observed. After the salt spray test of films, the transmittance of conventional coatings changed considerably, leading to the conclusion that the coatings have significantly degraded due to the salt spray exposure. |
| (n) Nano filler with 160N glass flake based vinyl ester composite | The free volume porosity of nanocomposite coatings is very minimal. The weak vibrational band | Additional very weak bands (i) 2785 to 3146 cm$^{-1}$ (ii) 603 to 844 cm$^{-1}$ are observed in resin degradation of nanocomposite coatings. The |

| | | |
|---|---|---|
| coating (VE4) | at 915cm$^{-1}$ is associated with the vibration of oxirane ring. The vibrational band in between 1258 to 1460cm-1 can be attributed to the C─O─C and C═C for aromatic symmetric stretching modes of vibration. Two characteristics vibrational bond observed at 1627cm$^{-1}$ for olefinic and 1726 to 1736cm$^{-1}$ for C═O stretch in both composite coatings. | presences of such peaks signify an interaction between the glass flake nanocomposite coating and the salt spray, indicating a very slow corrosion resistance against salt spray. |

**Table.6.25.** Ranking of vinyl ester composite coating of FTIR studies after salt spray

| Coating code name | Ranking |
|---|---|
| (k) VE1 | Lower (5) |
| (l) VE2 | High (3) |
| (m) VE3 | Low (4) |
| (n) VE4 | Higher (2) |

**Table.6.26.** XRD and morphology (SEM & TEM) comparative studies of vinyl ester composite coating

| Coating code name | XRD Studies | Morphology Studies | |
|---|---|---|---|
| | | SEM | TEM |
| (k) VE1 | All ingredients are seen at less instance peak in VE composite including quartz silica. Coating showed amorphous in nature. | SEM images of conventional composite, where some particles are observed at micro level on the surface of coating and also micrographs also show heterogeneous dispersion of silica | × |

| | | | |
|---|---|---|---|
| | | particles within the polymer matrix. | |
| (l) VE2 | All compositions are observed at high intense peak in VE composite including nano silica. Developed coating showed amorphous in nature. | From the SEM images of nanocomposite coating, it is evident that the silica particle is fully wetted by the vinyl ester resin during composite formation. The micrographs also show uniform dispersion of silica particles within the polymer matrix. | Organosilane particle size is less than 50nm detected |
| (m) VE3 | All ingredients are seen at less instance peak in VE composite including quartz silica. Coating showed amorphous in nature. | SEM images of conventional composite, where some particles are observed at micro level on the surface of coating and also micrographs also show heterogeneous dispersion of silica particles within the polymer matrix. The particles are cluster form. Some cavities and pores are observed on the surface. | × |
| (n) VE4 | All compositions are observed at high intense peak in VE composite including nano silica. Developed coating showed amorphous in nature. | From the SEM images of nanocomposite coating, it is evident that the silica particle is fully wetted by the vinyl ester resin during composite formation. The micrographs also show uniform dispersion of silica particles within the polymer matrix. | Organosilane particle size is less than 50nm detected. |

**Table.6.27.** Ranking of vinyl ester composite coating of XRD and morphology (SEM & TEM) studies

| Coating code name | XRD | SEM | TEM |
|---|---|---|---|
| | Ranking | Ranking | Ranking |
| (k) VE1 | Lowest (6) | Low (4) | × |
| (l) VE2 | High (3) | High (3) | High (3) |
| (m) VE3 | Lower (5) | Lower (5) | × |
| (n) VE4 | Higher (2) | Higher (2) | High (3) |

**Table.6.28.** Comparative studies of Physico-Mechanical testing of vinyl ester composite coating

| Coating code name | Cross link Density (%) | Adhesion Property ($N/mm^2$) | | Impact Test (KG.M) | | Abrasion Test (mg/cycles) | Thermal Studies (TGA-DTA) |
|---|---|---|---|---|---|---|---|
| | | Before Salt Spray | After 2200 hrs Salt Spray Test | Instrusion | Extrusion | | |
| (k) VE1 | 93.43 | 20.9 | 11.7 | >0.8 | >0.7 | 3.2 | Coating degrade at $400^{O}C$ and above |
| (l) VE2 | 98.71 | 34.3 | 23.7 | >0.4 | >0.6 | 1.5 | Coating degrade at $480^{O}C$ and above |
| (m) VE3 | 95.3 | 27.2 | 16.5 | >0.8 | >1.3 | 2.4 | Coating degrade at $470^{O}C$ and above |
| (n) VE4 | 97.8 | 36.8 | 26.8 | >0.5 | >0.7 | 2.1 | Coating degrade at $500^{O}C$ and above |

**Table.6.29.** Ranking of vinyl ester composite coating of Physico-Mechanical testing

| **Coating code name** | **Cross link Density (%)** | **Adhesion Property ($N/mm^2$)** | **Impact Test (KG.M)** | **Abrasion Test (mg/cycles)** | **Thermal Studies (TGA-DTA)** |
|---|---|---|---|---|---|
| | **Ranking** | **Ranking** | **Ranking** | **Ranking** | **Ranking** |
| (k) VE1 | Lowest (6) | Lowest (6) | Low (4) | Lower (5) | Lowest (6) |
| (l) VE2 | Higher (2) | High (3) | Higher (2) | Higher (2) | High (3) |
| (m) VE3 | Low (4) | Lowest (5) | Lower (5) | Lower (4) | Low (4) |
| (n) VE4 | High (3) | Highest (1) | Higher (2) | Highest (1) | Higher (2) |

**Table.6.30.** Comparative studies of corrosion studies of vinyl ester composite coating

| **Corrosion Studies** | | | | | |
|---|---|---|---|---|---|
| **Samples Code Name** | **Potentiodynamic Polarization (PD) (After 30 Days) & Corrosion Inhibition Efficiency (%)** | **Electro chemical Impedance Spectroscopy (EIS) (After 30 Days) & Charge transfer resistance (Rct in %)** | **Cathodic Disbondment (CD) (After 28 Days)** | **Salt Spray Chamber (SSC) Test (After 2200 hrs)** | **Porosity (P) & Optical Images Analysis (After Corrosion Studies)** |
| (k) Conventional filler with 160A glass flake based vinyl ester composite coating (VE1) | $-E_{corr}$(V vs SCE)= −0.650<br>$J_{corr}$ ($A/cm^2$) = 1.23E-09<br>$I_{corr}$ ($mAcm^{-2}$) = 1.47E-08<br>Corrosion rate (mm/year) = | C.P.E ($Y_o$) = 1.97E-10F<br>$R_P$ (Ω) = 8708.2<br>C.P.E (N) = 0.78<br>Equivalent electrical circuit models: Two time constant. | Disbondment area (mm): Full area delaminated and coating comes out | It has observed that corrosion and blister formation were exclusive to the 160A glass flake with micron silica-based vinyl ester composite | $P=18.06\times10^{-6}$<br>After the corrosion test, it has observed that major number of pits with degradation appeared on the |

| | | | | | |
|---|---|---|---|---|---|
| | 0.000086<br>$R_P$ ($\Omega cm^2$) = 22140<br>Corrosion inhibition efficiency (%) = 78 | Rct (%) = 97.84 | | coating | surface of the 160A glass flake with conventional silica based vinyl ester composite VE1 coating |
| (l) Nano filler with 160A glass flake based vinyl ester composite coating (VE2) | ─$E_{corr}$(V vs SCE)= ─0.667<br>$J_{corr}$ ($A/cm^2$) = 3.47E-08<br>$I_{corr}$ ($mAcm^{-2}$) = 1.05E-06<br>Corrosion rate (mm/year) = 1.43E-05<br>$R_P$ ($\Omega cm^2$) =1.73E+06<br>Corrosion inhibition efficiency (%) =86.72 | C.P.E ($Y_o$) = 3.47E-10F<br>$R_P$ ($\Omega$) = 2.67E+05<br>C.P.E (N) = 0.894<br>Equivalent electrical circuit models: Two time constant.<br>Rct (%) = 99.79 | Disbondment area (mm): Small area delaminated but coating became cracked | There was less corrosion and blister formation in the160A glass flake with nano silica-based vinyl ester composite coating | P=$63.49\times10^{-9}$<br>Less numbers of pits and damages were observed after the corrosion studies of the 160A glass flake with nano silica based vinyl ester composite coating. |
| (m) Conventional filler with 160N glass flake based vinyl ester composite coating (VE3) | ─$E_{corr}$(V vs SCE)= ─0.493<br>$J_{corr}$ ($A/cm^2$) = 1.05E-08<br>$I_{corr}$ ($mAcm^{-2}$) = 1.72E-07<br>Corrosion rate (mm/year) = | C.P.E ($Y_o$) = 1.30E-10F<br>$R_P$ ($\Omega$) = 3273<br>C.P.E (N) = 1.120<br>Equivalent electrical circuit models: Two time constant. | Disbondment area (mm): Full area delaminated and coating comes out | It has observed that corrosion and blister formation were exclusive to the 160N glass flake with micron silica-based vinyl ester composite | P=$80.99\times10^{-6}$<br>After the corrosion test, it has observed that number of pits with degradation appeared on the surface of the |

| | | | | | |
|---|---|---|---|---|---|
| | 0.00012<br>$R_P$ ($\Omega cm^2$) =9 7162<br>Corrosion inhibition efficiency (%) = 79.36 | Rct (%) = 98.30 | | coating | 160N glass flake with conventional silica based vinyl ester composite VE1 coating compared to VE1 coating. |
| (n) Nano filler with 160N glass flake based vinyl ester composite coating (VE4) | $-E_{corr}$(V vs SCE)= −0.614<br>$J_{corr}$ ($A/cm^2$) = 5.54E-06<br>$I_{corr}$ ($mAcm^{-2}$) = 5.67E-06<br>Corrosion rate (mm/year) = 3.23E+06<br>$R_P$ ($\Omega cm^2$) = 2.38E+05<br>Corrosion inhibition efficiency (%) = 96.95 | C.P.E ($Y_o$) = 3.51E-10F<br>$R_P$ ($\Omega$) = 92929<br>C.P.E (N) = 0.812<br>Equivalent electrical circuit models: Two time constant.<br>Rct (%) = 99.67 | Disbondment area (mm): 6-9.3 | There was less corrosion and blister formation in the160N glass flake with nano silica-based vinyl ester composite coating | $P=13.87\times10^{-9}$<br>Few numbers of pits and damages were observed after the corrosion studies of the 160N glass flake with nano silica based vinyl ester composite VE4 coating compared to 160A glass flake with nano silica based vinyl ester composite VE2 coating |

**Table.6.31.** Ranking of epoxy composite coating of Physico-Mechanical testing

| **Sample Code Name** | **Potentiodynamic Polarization (PD) (After 30 Days) & Corrosion Inhibition Efficiency (%)** | **Electro chemical Impedance Spectroscopy (EIS) (After 30 Days) & Charge transfer resistance (Rct in %)** | **Cathodic Disbondment (CD) (After 28 Days)** | **Salt Spray Chamber (SSC) Test (After 2200 hrs)** | **Porosity (P) & Optical Images Analysis (After Corrosion Studies)** |
|---|---|---|---|---|---|
| | **Ranking** | **Ranking** | **Ranking** | **Ranking** | **Ranking** |
| (a) VE1 | Lowest (6) | Lowest (6) | Loest (6) | Lower (5) | Lowest (6) |
| (b) VE2 | Higher (2) | High (3) | High(3) | High (3) | High (3) |
| (c) VE3 | Lower (5) | Lowest (4) | Lowest (5) | Lower (4) | Lower (5) |
| (d) VE4 | Higher (2) | Higher (2) | Higher (2) | Higher (2) | High (3) |

# 6.1. Final Conclusions:

Insulation property is most important for any painting/coating material. Impedance spectroscopy is directly proportional to dielectric strength as well as insulation property. For over all coating ranking, considering best on results of Electo Chemical Impedance Spectroscopy (EIS), adhesion, Cathodic Disbondment (CD), Potentiodynamic Polarization (PD), Salt Spray Chamber (SSC) test, abrasion, porosity, impact, Fourier Transform Infrared Spectroscopy (FTIR), cross link density, Scanning Electron Microscope (SEM), Transmission Electron Microscope (TEM) and X Ray Diffraction (XRD) respectively.

**Table. 6.32.** Summary of over all ranking of composite coatings for MS substrate

| Coating code name | Ranking | | | | | | | | | | | | | | Over all Rank |
|---|---|---|---|---|---|---|---|---|---|---|---|---|---|---|---|
| | FTIR | XRD | Cross Link Density | SEM | TEM | Adhesion | Impact | Abrasion | TGA-DTA | PD | EIS | CD | SSC | Porosity | |
| (a) EP1 | 6 | 3 | 4 | 4 | × | 6 | 6 | 6 | 6 | 4 | 4 | 4 | 4 | 4 | 8th |
| (b) EP2 | 3 | 2 | 3 | 1 | 3 | 3 | 3 | 3 | 3 | 3 | 3 | 3 | 3 | 3 | 3rd |
| (c) EP3 | 4 | 5 | 5 | 6 | × | 4 | 5 | 5 | 5 | 5 | 4 | 5 | 5 | 5 | 10th |
| (d) EP4 | 2 | 2 | 2 | 3 | 3 | 2 | 2 | 2 | 2 | 2 | 2 | 2 | 1 | 2 | 2nd |
| (e) EP5 | 5 | 4 | 6 | 5 | × | 5 | 4 | 4 | 4 | 6 | 5 | 4 | 4 | 4 | 9th |
| (f) EP6 | 1 | 1 | 2 | 2 | 1 | 1 | 1 | 2 | 1 | 1 | 1 | 1 | 1 | 1 | 1st |
| (g) PU1 | 6 | 6 | 6 | 6 | × | 6 | 5 | 6 | 6 | 6 | 6 | 6 | 6 | 6 | 14th |
| (h) PU2 | 2 | 3 | 2 | 2 | 2 | 3 | 2 | 3 | 3 | 3 | 3 | 3 | 2 | 3 | 6th |
| (i) CTEP1 | 5 | 6 | 4 | 4 | × | 4 | 5 | 4 | 4 | 4 | 6 | 5 | 5 | 4 | 11th |
| (j) CTEP2 | 2 | 3 | 2 | 1 | × | 1 | 1 | 2 | 3 | 2 | 2 | 3 | 3 | 3 | 5th |
| (k) VE1 | 5 | 6 | 6 | 4 | × | 6 | 4 | 5 | 6 | 6 | 6 | 6 | 5 | 6 | 13th |
| (l) VE2 | 3 | 3 | 2 | 3 | 3 | 3 | 3 | 3 | 3 | 2 | 3 | 3 | 3 | 3 | 7th |
| (m) VE3 | 4 | 5 | 4 | 5 | × | 5 | 5 | 4 | 4 | 5 | 6 | 6 | 5 | 5 | 12th |
| (n) VE4 | 2 | 2 | 3 | 2 | 3 | 1 | 2 | 1 | 2 | 2 | 2 | 2 | 2 | 1 | 4th |

Nano filler with 160N glass flake based epoxy composite coating (EP6) coating exhibited superior property in of Electo Chemical Impedance Spectroscopy (EIS), adhesion, Cathodic Disbondment (CD), Potentiodynamic Polarization (PD), Salt Spray Chamber (SSC) test, porosity, impact, Fourier Transform Infrared Spectroscopy (FTIR), Scanning Electron Microscope (SEM), Transmission Electron Microscope (TEM) and X Ray Diffraction (XRD) respectively. Whereas, it has higher in cross link density and abrasion property. Hence it is ranked 1st.

Nano filler with 160A glass flake based epoxy composite coating (EP4) based epoxy composite coating (EP6) coating exhibited higher property in of Electo Chemical Impedance Spectroscopy (EIS), adhesion, Cathodic Disbondment (CD), Potentiodynamic Polarization (PD), Salt Spray Chamber (SSC) test, abrasion, porosity, impact, Fourier Transform Infrared Spectroscopy (FTIR), cross link density and X Ray Diffraction (XRD). Whereas, it has high in Scanning Electron Microscope (SEM)and Transmission Electron Microscope (TEM) respectively. Hence it is ranked 2nd.

Nano filler based epoxy composite coating (EP2) exhibited high results in of Electo Chemical Impedance Spectroscopy (EIS), adhesion, Cathodic Disbondment (CD), Potentiodynamic Polarization (PD), Salt Spray Chamber (SSC) test, abrasion, porosity, impact, Fourier Transform Infrared Spectroscopy (FTIR), cross link density, X Ray Diffraction (XRD) and Transmission Electron Microscope (TEM. Whereas, it has highest in Scanning Electron Microscope (SEM)respectively. Hence it is ranked 3rd.

Nano filler with 160N glass flake based vinyl ester composite coating (VE4) showed highest results in adhesion, abrasion and porosity. Higher results in Electro chemical Impedance Spectroscopy (EIS), Cathodic Disbondment (CD), Potentiodynamic Polarization (PD), Salt Spray Chamber (SSC) test, impact, Scanning Electron Microscope (SEM), Fourier Transform Infrared Spectroscopy (FTIR) and X Ray Diffraction (XRD). Coating showed high result in Transmission Electron Microscope (TEM) and cross link density respectively. Hence it is ranked 4th.

Nano filler based coal tar epoxy composite coating (CTEP2) revealed highest result in adhesion, impact and Scanning Electron Microscope (SEM)studies.

Higher result in abrasion, Higher results in Electro chemical Impedance Spectroscopy (EIS), Potentiodynamic Polarization (PD), cross link density and Fourier Transform Infrared Spectroscopy (FTIR). High result in X Ray Diffraction (XRD), TGA-DTA, Cathodic Disbondment (CD), Salt Spray Chamber (SSC) and porosity respectively. Hence it is ranked $5^{th}$ .

Nano filler based polyurethane composite coating (PU2) expressed higher results in impact Salt Spray Chamber (SSC), crosslink density, Scanning Electron Microscope (SEM), Transmission Electron Microscope (TEM) and Fourier Transform Infrared Spectroscopy (FTIR). High result in adhesion, abrasion, TGA-DTA, Potentiodynamic Polarization (PD), Electro chemical Impedance Spectroscopy (EIS), Cathodic Disbondment (CD), X Ray Diffraction (XRD) and porosity respectively. Hence it is ranked $6^{th}$.

Nano filler with 160A glass flake based vinyl ester composite coating (VE2) showed higher result in crosslink density and Potentiodynamic Polarization (PD). High results in Electo Chemical Impedance Spectroscopy (EIS), adhesion, Cathodic Disbondment (CD), Salt Spray Chamber (SSC) test, porosity, impact, Fourier Transform Infrared Spectroscopy (FTIR), Scanning Electron Microscope (SEM), TGA-DTA, Transmission Electron Microscope (TEM) and X Ray Diffraction (XRD) respectively. Hence it is ranked $7^{th}$.

Conventional filler based epoxy composite coating (EP1) expressed high result in X Ray Diffraction (XRD). Low results in crosslink density, Electro chemical Impedance Spectroscopy (EIS), Cathodic Disbondment (CD), Salt Spray Chamber (SSC) test, porosity, Scanning Electron Microscope (SEM), Potentiodynamic Polarization (PD). Lowest results in adhesion, impact, abrasion, TGA-DTA and Fourier Transform Infrared Spectroscopy (FTIR) respectively. Hence it is ranked $8^{th}$.

Conventional filler with 160N glass flake based epoxy composite coating (EP5) revealed low results in X Ray Diffraction (XRD), impact, abrasion, TGA-DTA, Cathodic Disbondment (CD), Salt Spray Chamber (SSC) test and porosity. Lower results in Fourier Transform Infrared Spectroscopy (FTIR), Scanning Electron Microscope (SEM), adhesion and Electro chemical Impedance Spectroscopy (EIS). Lowest results in cross link density and Potentiodynamic Polarization (PD) respectively. Hence it is ranked 9$^{th}$.

Conventional filler with 160A glass flake based epoxy composite coating (EP3) showed low results in Fourier Transform Infrared Spectroscopy (FTIR), adhesion and Electro chemical Impedance Spectroscopy (EIS). Lower result in X Ray Diffraction (XRD), impact, abrasion, TGA-DTA, Cathodic Disbondment (CD), Salt Spray Chamber (SSC) test and porosity. Lowest results in cross link density and Potentiodynamic Polarization (PD). Lowest result in Scanning Electron Microscope (SEM)respectively. Hence it is ranked 10$^{th}$.

Nano filler based coal tar epoxy composite coating (CTEP2) showed low results in crosslink density, Scanning Electron Microscope (SEM), adhesion, abrasion, TGA-DTA, Potentiodynamic Polarization (PD) and porosity. Lower result in Fourier Transform Infrared Spectroscopy (FTIR), impact, Cathodic Disbondment (CD) and Salt Spray Chamber (SSC). Lowest result in X Ray Diffraction (XRD) and Electro chemical Impedance Spectroscopy (EIS)respectively. Hence it is ranked 11$^{th}$.

Conventional filler with 160N glass flake based vinyl ester composite coating (VE3) revealed low result in crosslink density, abrasion, TGA-DTA and Fourier Transform Infrared Spectroscopy (FTIR). Lower results in X Ray Diffraction (XRD), Scanning Electron Microscope (SEM), adhesion, impact, Potentiodynamic Polarization (PD), and Salt Spray Chamber (SSC) and porosity. Lowest result in

Electro chemical Impedance Spectroscopy (EIS)and Cathodic Disbondment (CD) studies respectively. Hence it is ranked 12th.

Conventional filler with 160A glass flake based vinyl ester composite coating (VE1) showed low results in impact and Scanning Electron Microscope (SEM)studies. Lower results in Fourier Transform Infrared Spectroscopy (FTIR), abrasion and Salt Spray Chamber (SSC) studies. Lowest results in X Ray Diffraction (XRD), crosslink density, adhesion, TGA-DTA, Potentiodynamic Polarization (PD), Electro chemical Impedance Spectroscopy (EIS), Cathodic Disbondment (CD) and porosity studies respectively. Hence it is ranked 13th.

Conventional filler based polyurethane composite coating (PU1) expressed lowest result in Electo Chemical Impedance Spectroscopy (EIS), adhesion, Cathodic Disbondment (CD), Potentiodynamic Polarization (PD), Salt Spray Chamber (SSC) test, porosity, Fourier Transform Infrared Spectroscopy (FTIR), Scanning Electron Microscope (SEM), X Ray Diffraction (XRD), cross link density and abrasion property respectively. Whereas lower result in impact test. Hence it is ranked 14th.

It is concluded that, EP6 (nano filler and 160N glass flake) based nanocomposite coating showed best result out of developed nanocomposite coating all over experimental performance. The glass flake epoxy system features a chemically cross linked structure and reduced film porosity when cured with nano filler. Also the same time organo silane does have pendant methyl bulky group and as well as non polar rigid allyl group which is surface treated on 160N glass flake. The glass flake also strictly restrict water molecule from penetrating in to the polymer matrix and most highly prevents the creation of porosity through tortuous path. Surface activity with well dispersion of nanoparticales truly embedded in the resin through

containing cross linking agent with lot of linkage group and gives three dimensional network rigid structures. These molecular networks form a very high dense structure and reduced porosity and increased metal adhesion synergistically provides high level corrosion resistance with remarkable Physico-Mechanical properties in these systems. Also, it has been studieded that resin can consume 6.5 to 7wt% of nanoparticles by optimization.

The organo silane modified nano filler based polymeric nanocomposite coating systems developed in the recent investigation can serve as highly effective protective coatings for steel structures, surpassing conventional coatings and providing excellent protection against atmospheric corrosion and marine corrosion due to fouling.

# References:

# Introduction:

[1] R. Parsons, ***Pure Appl. Chem.***, 37 **(1979)** 503.

[2] Corrosion of Metals and Alloys, Terms and Definitions, Draft International Standard ISO/DIS 8044, TC, 156, **(1985)**.

[3] K. E. Heusler, D. Landolt and S. Trasatti, Electrochemical Corrosion Nomenclature (Recommendation 1998), ***Electrochim. Acta***, 35 **(1990)** 295.

[4] L.S. Van Delinder, Corrosion Basics, An Introduction, ed. (Houston, TX: NACE), **(1984)**.

[5] H. H. Uhlig, The Cost of Corrosion in the United States. Chemical and Engineering News, 27 **(1949)** 2764.

[6] L. Losana, ***11th Int. Congr. On Metallic Corrosion***, Florence, Itali, 1 **(1990)** 1.

[7] L.H. Bennet, J. Kruger, R. I. Parker, E. Passiglia, C. Reimann, A. W. Ruff, H. Yakowitz and E. B. Berman, "Economic Effects of Metallic Corrosion in the United States", National Bureau of Standards Special Publication 511, Washington, DC, **(1978)**.

[8] G. H. Koch, M. P. H. Brongers, N. G. Thompson, Y. P. Virmani and J. H. Payer, “Corrosion Costs and Preventive Strategies in the United States”. Report by C.C Technologies Laboratories, Inc. to Federal Highway Administration (FHWA), Office of Infrastructure Research and Development, Publication no. FHWARD-01-156, March, **(2002)**.

[9] J. Haque, V. Srivastava, C. Verma and M. A. Quraishi, ***J. Mol. Liq.***, http://dx.doi.org/101016/j.molliq.2016.11.011 **(2016)**.

[10] K. S. Rajagopalan, ***10th Int. Congr. On Metallic Corrosion***, Chennai, Oxford & IBH, New Delhi, 2 **(1987)** 1765.

[11] A. S. Khanna, ***News Letter***, NACE, India, 4 **(1997)** 3.

[12] Umoren S. A & Solomon M.M., Protective polymeric films for industrial substrates: A critical review on fast and recent applications with conducting polymers and polymer composites/ nanocomposites, Progress in Material science, 104, 380-450, (2019).
[13] Xu. H & Zhang. Y., A review on conducting polymers and nanopolymer composite coatings for steel corrosion protection, Coatings, 9, 807, (2019)

## Literature Survey and Scope of Insvestigation:

[1] Pourhashem, S., Vaezi, M.R., Rashidi, A.M and Bagherzadeh, M.R., Exploring corrosion protection properties of solvent based epoxy-graphene oxide nanocomposite coatings on mild steel, Corrosion Science, 115, pp-78-92, (2017)

[2] Frigione, M & Lettieri, M., Recent advances and trends of nanofilled/ nanostructured epoxies, Materials 13, p-15 (2020)
[3] Naeem. M, Kuan H.C, Michelmore. A, Meng. Q, Qiu. A, Aakyiir. M, Losic. D, Zhu. S, Ma. J., A new method for preparation of functionalized graphene and its epoxy nanocomposites, Compos. Part B Eng, 196, 108096 (2020)
[4] Zeng. L, Huang. X, Li. X, Li. R, Li. Y, Xiong. Y., A gelatin-treated carbon nanofiber/epoxy nanocomposite with significantly improved multifunctional properties, Mater, Today Commun, 24 (2020)
[5] Liu, S., Gu, L., Zhao, H., Chen, J and Yu, H., Corrosion Resistance of Graphene-Reinforced Waterborne Epoxy Coatings, Journal of Materials Science & Technology, 32, pp. 425-431 (2016)
[6] Xiong. H, Qi. F, Zhao. N, Yuan. H, Wan. P, Liao. B, Ouyang. X., Effect of organically modified sepiolite as inorganic nanofiller on the anti-corrosion resistance of epoxy coating, Materials. Letters, 260, 126941 (2020).

[7] Tomić M. D., Dunjić B., Bajat J. B., Likić V., Rogan J., & Djonlagić J., Anticorrosive epoxy/clay nanocomposite coatings: rheological and protective properties, Journal of Coatings Technology and Research, 13(3), 439-456 (2016)
[8] Madhup M. K., Shah N. K., & Parekh N. R., Investigation and improvement of abrasion resistance, water vapor barrier and anticorrosion properties of mixed clay epoxy nanocomposite coating, Progress in Organic Coatings, 102, 186-193 (2017)
[9] Milena. S & Jiri. B., A view from inside to the surface of nanocomposite coatings, Polymer nanocomposite coatings, Chapter 6, C.R.C Press (2014)
[10] Odegard G. M et al., Modelling of the mechanical properties of nanoparticles/polymer composites, Polymer; 46; 553-562 (2005)
[11] Navarchian. A. H, Joulazadeh. M & Karimi. F., Investigation of corrosion protection performance of epoxy coatings modified by polyaniline/clay nanocomposites on steel surfaces, Progress in Organic coating, 77, 347-353 (2014)
[12] Caldas. C. M, Calheiros. L. F & Soares. B. G., Silica-polyaniline hybrid materials prepared by inverse emulsion polymerization for epoxy based anti corrosive coating, Journal of Applied Polymer Science, 10.1002, 45505 (2017)
[13] Abd El-Fattah. M, El Saeed A.M, Azzam. A. M, Abdul Rahim. A. R. M & Hefni H.H.H., Improvement of Corrosion resistance, antimicrobial activity, mechanical and chemical properties of epoxy coating by loading chitosan as a natural renewable source, Progress in organic coatings, 101, 288-296 (2016)
[14] Alam M.A.; Abdus Samad U.; Alam M.; Anis A.; Al-Zahrani S.M., Enhancement in Nanomechanical, Thermal, and Abrasion Properties of $SiO_2$ Nanoparticle-Modified Epoxy Coating, Coatings, 10, 310 (2020)
[15] Alam M.A.; Samad U.A.; Sherif E.-S.M.; Poulose A.M.; Mohammed J.A.; Alharthi N.; Al-Zahrani S.M., Influence of $SiO_2$ Content and Exposure Periods on the Anticorrosion Behavior of Epoxy Nanocomposite Coatings, Coatings, 10, 118, 2020.

[16] Ray S.S, Okamoto. M, Polymer/layered silicate nanocomposites: a review from preparation to processing, Prog. Polym. Sci. 28, 1539–1641 (2003)
[17] G.. Tsaneva, V. Kozhukharov, S. Kozhukharov, M. Ivanova, J. Gerwann, M. Schem, T. Schmid, Functional nanocomposite coatings for corrosion protection of aluminum alloy and steel, Journal of the University of Chemical Technology and Metallurgy, 43, 2, 2008, 231-238
[18] Yanhong Li, Bing Li and weixing Chen, A study on the reactive diluent for the solvent-free epoxy anticorrosive coating, J. Chem. Pharm. Res., 2014, 6(7):2466-2469
[19] LU HongBin, GU MinHao, HUANG JianFeng, HU Yong & MENG XiangKang, *In-situ* polymerized nanosilica/acrylic/epoxy hybrid coating: Preparation, microstructure and properties, *Sci China Ser E-Tech Sci.*, 8, 52, pp.2204–2209 (2009)

[20] S. K. Dhoke1, Narayani Rajgopalan2, A. S. Khanna, Effect of Nano-Zinc Oxide Particles on the Performance Behavior of Waterborne Polyurethane Composite Coatings, IJMSCI Vol.2 Iss.2 2012 PP.47-55
[21] Shu-Xue Zhou,1 Li-Min Wu,1 Jian Sun,1,2 Wei-Dian Shen, Effect of Nanosilica on the Properties of Polyester-Based Polyurethane, Journal of Applied Polymer Science, Vol. 88, 189–193 (2003)
[22] Gnanaprakasam Christopher, Manickam Anbu Kulandainathan, Gurusamy Harichandran, Highly dispersive waterborne polyurethane/ZnO nanocomposites for corrosion protection, J. Coat. Technol. Res., 12 (4) 657–667, 2015
[23] Moussa Tamboura, Anna M. Mikhailova, Meng Qiu Jia, A Comparative Study of Anticorrosion Paints Based on Silicone-Urethane Binders: a Multilayer Primer, Silicon (2014) 6:45–56

[24] Iris Holken, Mathias Hoppe, Yogendra K. Mishra, Stanislav N. Gorb, Rainer Adelunga and Martina J. Baum, Complex shaped ZnO nano- and microstructure based polymer composites: mechanically stable and environmentally friendly coatings for potential antifouling applications, *Phys. Chem. Chem. Phys.*, 2016, 18, 7114─7123

[25] Guo Jia-Hu, ab Liu Yu-Cun, Chai Tao, Jing Su-Ming, Ma Hui, Qin Ning, Zhou Hua, Yan Taoa and He Wei-Ming, Synthesis and properties of a nano-silica modified environmentally friendly polyurethane adhesive, RSC Adv., 2015, 5, 44990–44997

[26] Arifin, A. M. T.1, Supri, A. G., Hassan, M. F., Rahman, M.N.A., Haq, R.H.A., Taib, I., Adzila, S., Effect of Filler Loading on Properties of Polyurethane/ClayComposite, Materials Science and Engineering , 607 (2019) 012003

[27] Priyanka Adapala, Swati Gaur, Ravindra G. Puri, Anand S. Khanna, Development and Evaluation of Nano-Silica Dispersed Polyurethane Based Coatings for Improved Anti-Graffiti and Scratch Resistance, Open Journal of Applied Sciences, 2015,5,808-818

[28] Y. Gonzalez-Garcı, S. Gonzalez, R.M. Souto, Electrochemical and structural properties of a polyurethane coating on steel substrates for corrosion protection, Corrosion Science ,49 (2007) 3514–3526

[29] K.A. Thomas, Shiny Nair, R. Rajeswari, A.V. Ramesh kumar, V. Natarajan, T. Mukundan,Reji John, Electrochemical behaviour of PANi/polyurethane antifouling coatingin salt water studied by electrochemical impedance spectroscopy, Progress in Organic Coatings, 89 (2015) 267–270

[30] Cristóbal Valentini, Jorge Fiora, Gabriel Ybarra, A comparison between electrochemical noise and electrochemical impedance measurements performed on

a coal tar epoxy coated steel in 3% NaCl, Progress in Organic Coatings 73 (2012) 173– 177

[31] M. Atapour, S. Abdollahi , S. M. Monir Vaghefi, The Effect of Erosion on Corrosion Protection Properties of Coal Tar Epoxy Coating, International Journal of ISSI, Vol.11 (2014), No.2, pp.17-22

[32] Otilio B.F. Di´ogenes a, Davi R. de Oliveira b, Lucas R.R. da Silva a, ´Italo Gomes Pereira c, Selma Elaine Mazzetto , Walney S. Araujo a, Diego Lomonaco Development of coal tar-free coatings: Acetylated lignin as a bio-additive for anticorrosive and UV-blocking epoxy resins, Progress in Organic Coatings 161 (2021) 106533

[33] S.D. Jagtap, S.P. Tambe, R.N. Choudhari, B.P. Mallik, Mechanical and anticorrosive properties of non toxic coal-tar epoxyalternative coating, Progress in Organic Coatings 77 (2014) 395– 402

[34] Xiuzhi Zhang, Fuhui Wang, Yuanlong Du, Protective performance of epoxy resin modified with coal tar coating studied by electrochemical impedance spectroscopy, Progress in Organic Coatings 53 (2005) 302–305

[35] Kim, Bum Sung Kim, Se Kyoung Lee, Hee Chul, Tar-free epoxy/amine curing system for corrosion protection of ballast tanks, Corrosion Science and Technology, 31(5); p. 411-417

[36] R. BabićM. Metikoš-HukovićH. Radovčić, The study of coal tar epoxy protective coatings by impedance spectroscopy, Progress in Organic Coatings, Volume 23, Issue 3, February 1994, Pages 275-286

[37] Fujian Tang, Genda Chen, Jeffery S. Volz, Richard K. Brow, and Michael Koenigstein, Corrosion Behavior of Enamel Coated Steel Rebar by EIS, Advanced Materials Research Vols. 450-451 (2012) pp 445-453

[38] Fujian Tang, Genda Chen, Richard K. Brow, Jeffery S. Volz, Michael L. Koenigstein, Corrosion resistance and mechanism of steel rebar coated with three types of enamel, Corrosion Science 59 (2012) 157–168

[39] Jyoti Chaudhary, Synthesis ,Characterization and Curing of Vinyl ester resin, J. Environ. Nanotechnol, Volume 2 (2013) 42-45 pp.

[40] Timucin Bardak a, Ali Naci Tankut b, Nurgül Tankut b, Eser Sozen b, Deniz Aydemir, The effect of nano-$TiO_2$ and $SiO_2$ on bonding strength and structural properties of poly (vinyl acetate) composites, Measurement 93 (2016) 80–85

[41] Azam Ghadami, Morteza Ehsani and Hossein Ali Khonakdar, Vinyl ester/ glass flake nanocomposites: An overview of chemical and physical properties, Journal of Composite Materials, 2014, Vol. 48(13) 1585–1593

[42] Salim Barbhuiya, and Mohammad Ikbal Choudhury, Nanoscale Characterization of Glass Flake Filled Vinyl Ester Anti-Corrosion Coatings, Coatings 2017, 7, 116

[43] Mohsen Khademian, Hossein Eisazadeh, Alireza Shakeri, and Mohsen Ghorbani, Effect of HPC-PANI/$SIO_2$ Emulsion Nanocomposite in Poly(vinyl acetate) for Corrosion-Resistant Coatings, Polymer-Plastics Technology and Engineering, 54: 1051–1056, 2015

[44] Jyoti Chaudhary, Supriya Dadhich, Suman Jinger and Giriraj Tailor, Epoxy Based Vinyl Ester Resins: Synthesis and Characterization, International Journal of Chemical Engineering Research, Volume 9, Number 1 (2017), pp. 99-104

[45] H. M. KANG,1 T. H. YOON,1 M. BUMP,2 J. S. RIFFLE, Effect of Solubility and Miscibility on the Adhesion Behavior of Polymer Coated Carbon Fibers with Vinyl Ester Resins, Journal of Applied Polymer Science, Vol. 79, 1042–1053 (2001)

[46] Katherine Dean, Wayne D. Cook, Laurent Rey, Jocelyne Galy, and Henry Sautereau, Near-Infrared and Rheological Investigations of Epoxy-Vinyl Ester Interpenetrating Polymer Networks, Macromolecules 2001, 34, 6623-6630

[47] Nishar Hameed, P.A. Sreekumar, V.S. Valsaraj, Sabu Thomas, High Performance Composite From Epoxy and Glass Fibers: Morphology, Mechanical, Dynamic Mechanical, and Thermal Analysis, Polymer Composites, 2009

[48] Dipa Ray, Suparna Sengupta, S. P. Sengupta, Amar K. Mohanty, Manjusri Misra, Preparation and Properties of Vinylester Resin/Clay Nanocomposites, Macromol. Mater. Eng. 2006, 291, 1513–1520

[49] Xi Zhang, Vahid Bitaraf, Suying Wei, and Zhanhu Guo, Henry A. Colorado, Vinyl Ester Resin: Rheological Behaviors, Curing Kinetics, Thermomechanical, and Tensile Properties, AIChE Journal January 2014 Vol. 60, No. 1

[50] Umoren S. A & Solomon M.M., Protective polymeric films for industrial substrates: A critical review on fast and recent applications with conducting polymers and polymer composites/ nanocomposites, Progress in Material science, 104, 380-450, (2019).

[51] Xu. H & Zhang. Y., A review on conducting polymers and nanopolymer composite coatings for steel corrosion protection, Coatings, 9, 807, (2019)

[52] Charles G. Munger. Corrosion protection by protective coatings/NACE Publication: 73, (1984).

[54] May, C.A., Epoxy resins in Engineered Materials Handbook, The Materials Information Society, ASM International: Novelty, OH, USA, Volume 1, pp. 66–77 (1989)

[55] Sukanya P, Priyanka P, Smitha M & Sanjay K.N., Polymer-Plastics Technology and Engineering", 55, 8, 862-877 (2016)

[56] Kaur, M & Jayakumari, L.S., Eco-friendly cardanol-based phenalkamine cured epoxy-cenosphere syntactic foams: Fabrication and characterization, J. Appl. Polym. Sci. 44189, (2016)

[57] Ionescu, M. *Chemistry and Technology of Polyols for Polyurethanes*; Ionescu, M., Ed.; Rapra Technology: Shawbury, UK, 2005.

[58] Petrović ZS, Fajnik D, Preparation and properties of castor oil based polyurethanes, J. Appl Polym Sci 1984; 29(4): 1031-1040.

[59] Mutlu H, Meier MR, Castor oil as a renewable resource for the chemical industry", Eur J Lipid Sci Technol 2010; 112(1): 10-30.

[60] http://www.acme-hardesty.com/product/hydrogenated-castor-oil

[61] Randall, D.; Lee, S. (2003). *The Polyurethanes Book*. New York: Wiley. ISBN 978-0-470-85041-1.

[62] S.M. Singh, Paint India 7 (1984) 23.

[63] Warnes, A.R; Coal tar distillation and working up of tar products, JOHN ALLAN AND COM PANY THE GAS WORLD" OFFICES, 8 BOUVERIE STREET, E.C.London, 1913.

[14] *Eller, K.; Henkes, E.; Rossbacher, R.; Höke, H. "Amines, Aliphatic". Ullmann's Encyclopedia of Industrial Chemistry. Weinheim: Wiley-VCH.*

[65] *Brydson, J. A. (1999). "Epoxide Resins". In J. A. Brydson (ed.). Plastics Materials (Seventh ed.). Oxford: Butterworth-Heinemann. pp. 744–777.*

[66] Cassis, F.A., and Talbot, R.C., 1998, Polyester and Vinyl Ester Resins. *Handbook of Composites* (Peters, S.T., Editor), 2nd Eition, London: Chapman & Hall.

[67] Li, Hui; Synthesis, Characterization and Properties of Vinyl Ester Matrix Resins, PhD thesis, Blacksburg, Virginia, 1998.

[68] Lambourne. 1987. Paint and surface coatings/ Ellis Horwood Ltd./ New York: 111.

[69] Thamaphat K, Limsuwan P and Ngotawornchai B; Phase Characterization of TiO2 Powder by XRD and TEM, Kasetsart J. (Nat. Sci.) 42 : 357 - 361 (2008)

[70] Paint additives, 1970. Noyes Data Corporation/ Park Ridge/ New Jersey/ U.S.A.

[71] Nied D, Rasmussen K E, Hopital E L, Skibsted J and Lothenbach B; Properties of magnesium silicate hydrates (M-S-H), Cement and Concrete Research 79 (2016) 323–332

[72] Junior Tavares, J.F., Costa, L.M., Cetlin, P.R., Paulino Aguilar, M.T., Influence of quartz powder and silica fume on the performance of Portland cement, Sci Report, 10(1):21461, (2020).

[73]Jharimune S, Gu X, Lim M L, Dent M, Rakers N, Lee C Y, He H, Mubarak A, Hui C, Effect of glass flake in Anti-corrosive coatings for extreme conditions, AMPP-2022-17923

[74] Martens.C.R. 1958. Technology of paintS/ varnishes and lacquers/ New York.

[75] C. K. Lam & K. T. Lau., Localized elastic modulus distribution of nanoclay/epoxy composites by using nanoindentation, Composite Structures, vol. 75, no 1-4, pp. 553–558 (2006)

[76] G. Shi, M. Q. Zhang, M. Z. Rong, B. Wetzel & K. Friedrich., Friction and wear of low nanometer Si3N4 filled epoxy composites, Wear, vol. 254, no. 7-8, pp. 784–796 (2003)

[77] A. Hartwig, M. Sebald, D. Putz, and L. Aberle., Preparation, characterisation and properties of nanocomposites based on epoxy resins - An overview, Macromolecular Symposia, vol. 221, pp. 127– 135 (2005)

[78] F. Dietsche, Y. Thomann, R. Thomann, and R. Mulhaupt., Translucent acrylic nanocomposites containing anisotropic laminated nanoparticles derived from intercalated layered silicates, Journal of Applied Polymer Science, vol. 75, no. 3, pp. 396– 405 (2000)

[79] Ammar S, Ramesh K, Vengadaesvaran B, Ramesh S, Arof AK., Amelioration of anticorrosion and hydrophobic properties of epoxy/PDMS composite coatings containing nano ZnO particles, Prog Org Coating, 92: 54–65 (2016)

[80] Ghazizadeh A, Haddadi SA, Mahdavian M., The effect of sol-gel surface modified silver nanoparticles on the protective properties of the epoxy coating, RSC Adv, 6 (2016)

[81] Haddadi S.A, Mahdavian M, Karimi E., Evaluation of the corrosion protection properties of an epoxy coating containing sol–gel surface modified nano-zirconia on mild steel, RSC Adv, 5:28769–77 (2015)

[82] Yu Y, Yeh J, Liou S, Chen C, Liaw D, Lu H., Preparation and properties of polyimide–clay nanocomposite materials for anticorrosion application, J Appl Polym Sci; 92:3573–82 (2004)

[83] Zea C, Barranco-García R, Chico B, Díaz I, Morcillo M, de la Fuente D., Smart mesoporous silica nanocapsules as environmentally friendly anticorrosive pigments, Int J Corros, 2015, Article Id 426397 (2015)

[84] Palimi MJ, Rostami M, Mahdavian M, Ramezanzadeh B., A study on the corrosion inhibition properties of silane-modified Fe2O3 nanoparticle on mild steel and its effect on the anticorrosion properties of the polyurethane coating, J Coating Technol Res;12:277–92 (2015)

[85] Arash Haddadi S, Amini M, Ghaderi S, Ramazani A., Synthesis and cation-exchange behavior of expanded MoS2 nanosheets for anticorrosion applications, Mater, Today Proc 5 (2018)

[86] Dias S.A.S, Lamaka S.V, Nogueira C.A, Diamantino T.C, Ferreira M.G.S., Sol–gel coatings modified with zeolite fillers for active corrosion protection of AA2024, Corrosion Sci;62:153–62 (2012)

[87] Abdullayev.E, Price.R, Shchukin.D, Lvov.Y., Halloysite tubes as nanocontainers for anticorrosion coating with benzotriazole, ACS Appl Mater Interfaces, 1:1437-43 (2009)

[88] Akbarzadeh S, Ramezanzadeh M, Ramezanzadeh B, Mahdavian M, Naderi R., Fabrication of highly effective polyaniline grafted carbon nanotubes to induce active protective functioning in a silane coating, Ind Eng Chem Res, 58: 20309–22 (2019)

[89] Ramezanzadeh B, Ghasemi E, Mahdavian M, Changizi E, Mohamadzadeh Moghadam MH., Covalently-grafted graphene oxide nanosheets to improve barrier and corrosion protection properties of polyurethane coatings, Carbon N Y, 93: 555–73 (2015)

[90] Qiu S, Li W, Zheng W, Zhao H, Wang L., Synergistic effect of polypyrroleintercalated graphene for enhanced corrosion protection of aqueous coating in 3.5% NaCl solution, ACS Appl Mater Interfaces, 9:34294–304 (2017)

[91] Geim AK, Novoselov KS., The rise of graphene, Nanosci. Technol. A collect. Rev. From nat. Journals. World Scientific, p. 11–9 (2010)

[92] Liu D, Zhao W, Liu S, Cen Q, Xue Q., Comparative tribological and corrosion resistance properties of epoxy composite coatings reinforced with functionalized fullerene C60 and graphene, Surf Coating Technol, 286:354–64 (2016)

[93] Fatemeh Dolatzadeh, Siamak Moradian , Mohammad Mehdi Jalili, Influence of various surface treated silica nanoparticles on the electrochemical properties of $SiO_2$/polyurethane nanocoatings, Corrosion Science, 53 (2011) 4248–4257.

[94] Kerstin Muller et al., Review on the processing and properties of polymer nanocomposites and nanocoatings and their applications in the packaging, automotive and solar energy fields, Nanomaterials, 7, 74-121 (2014)

[95] Jones D.A., Principles and Prevention of Corrosion, 2nd ed.; Prentice- Hall Inc.: Upper Saddle River, NJ, USA, ISBN 0133599930 (1996)

[96] Schuh C.A.; Nieh T.G.; Iwasaki H., The effect of solid solution W additions on the mechanical properties of nanocrystalline Ni, Mater., 51, 431–443 (2003)

[97] Andreatta F., Aldighieri P., Paussa L., Di Maggio R., Rossi S & Fedrizzi L., Electrochemical behaviour of $ZrO_2$ sol–gel pre-treatments on AA6060 aluminium alloy, Electrochim. Acta, 52, 7545–7555 (2007)

[98] Sriraman K.R.; Strauss H.W.; Brahimi S.; Chromik R.R.; Szpunar J.A.; Osborne J.H.; Yue S., Tribological behavior of electrodeposited Zn, Zn–Ni, Cd and Cd–Ti coatings on low carbon steel substrates, Tribiol. Int., 56, 107–120 (2012)

[99] Wang Y.; Zhang L.; Hu Y.; Li C., Comparative Study on Optical Properties and Scratch Resistance of Nanocomposite Coatings Incorporated with Flame Spray Pyrolyzed Silica Modified via in-situ Route and ex-situ Route, J. Mater. Sci. Technol., 32, 251–258 (2016)

[100] M.; Dubois P., Polymer-Layered silicate nanocomposites: Preparation, properties and uses of a new class of materials, Mater. Sci. Eng. R-Rep., 28, 1–63 (2000)

[101] Shi. X et al., Effect of nanoparticles on the anticorrosion and mechanical properties of the epoxy coating, Surface and coatings technology, vol.204, no.3, 237-245 (2009)

[102] Nguyen. T. A et al., Effect of nanoparticles on the thermal and mechanical properties of epoxy coatings, Journal of Nanoscience and Nanotechnology, vol.16, no.9, pp. 9874-9881 (2016)

[103] Phuong Nguyen-Tri et al., Nanocomposite coatings: Preparation, Characterization, properties and applications, International Journal of Corrosion, article id 4749501(2018)

[104] Ray S.S and Okamoto. M., Polymer/layered silicate nanocomposites: a review from preparation to processing, Progress in Polymer Science, vol.28, no.11, pp. 1539-1641 (2003)

[105] Tsagaropoulos. G & Eisenberg. A., Dynamic mechanical study of the factors affecting the two glass transition behaviour of filled polymers. Similarities and differences with random ionomers, Macromolecules, vol. 28, no. 18, pp. 6067–6077 (1995)

[106] Mayes A. M., Softer at the boundary, Nature Materials, vol. 4, no. 9, pp. 651-652 (2005)

[107] Starr F. W, Schrøder T. B, and Glotzer S. C., Effects of a nanoscopic filler on the structure and dynamics of a simulated polymer melt and the relationship to ultrathin films, Physical Review E: Statistical, Nonlinear, and Soft Matter Physics, vol. 64, no. 2 (2001)

[108] Shi. X, Nguyen T. A, Suo. Z, Liu. Y & Avci. R., Effect of nanoparticles on the anticorrosion and mechanical properties of epoxy coating, Surface & Coatings Technology, vol. 204, no. 3, pp. 237–245 (2009)

[109] Schmidt H., New type of non-crystalline solids between inorganic and organic materials, J. Non-Cryst. Solids 73, 681–691 (1985)

[110] Novak B.M., Hybrid nanocomposites materials between inorganic glasses and organic polymers. Adv. Mater. 5, 422–433 (1993)

[111] Zhang Y.; Choi J.R.; Park S.-J., Interlayer polymerization in amineterminated macromolecular chain-grafted expanded graphite for fabricating highly thermal conductive and physically strong thermoset composites for thermal management applications, Compos. Part A Appl. Sci. Manuf. 109, 498–506 (2018)

[112] Thakur V.K.; Kessler M.R., Self-healing polymer nanocomposite materials: A review, Polymer 69, 369–383 (2015)

[113] Jawaid M.; Qaiss A.K.; Bouhfid R., Nanoclay Reinforced Polymer Composites: Nanocomposites and Bionanocomposites, Springer: Singapore (2016)

[114] Babu Valapa R.; Loganathan S.; Pugazhenthi G.; Thomas S.; Varghese T.O., An Overview of Polymer–Clay Nanocomposites. In Clay-Polymer Nanocomposites; Elsevier: Amsterdam, The Netherlands, pp. 29–81 (2017)

[115] Vo V.S.; Mahouche-Chergui S.; Babinot J.; Nguyen V.H.; Naili S.; Carbonnier B., Photo-induced SI-ATRP for the synthesis of photoclickable intercalated clay nanofillers, RSC Adv., 6, 89322– 89327 (2016)

[116] Beyer G., Nanocomposites: A new class of flame retardants for polymers, Plast. Addit. Compd., 4, 22–28 (2002)

[117] Gurses A., Introduction to Polymer-Clay Nanocomposites; Pan Stanford: Singapore (2015)

[118] Martin C., Twin Screw Extruders as Continuous Mixers for Thermal Processing: A Technical and Historical Perspective, AAPS PharmSciTech 17, 3–19 (2016)

[119] Huang Y.; Yang K.; Dong J.Y., Copolymerization of Ethylene and 10-Undecen-1-ol using a Montmorillonite-Intercalated Metallocene Catalyst: Synthesis of Polyethylene/Montmorillonite Nanocomposites with Enhanced Structural Stability, Macromol. Rapid Commun., 27, 1278–1283 (2006)

[120] Cardoso R.S.; Aguiar V.O.; Marques M.D.F.V., Master batches of polypropylene/clay obtained by in situ polymerization and meltblended with commercial polypropylene, J. Compos, Mater., 51, 3547–3556 (2017)

[121] Cherifi Z.; Boukoussa B.; Zaoui A.; Belbachir M.; Meghabar R., Structural, morphological and thermal properties of nanocomposites poly (GMA)/clay

prepared by ultrasound and in-situ polymerization, Ultrason. Sonochem., 48, 188–198 (2018)
[122] Xia H.S.; Wang Q., Preparation of conductive polyaniline/nanosilica particle composites through ultrasonic irradiation, J. Appl. Polym. Sci., 87, 1811–1817 (2003)
[123] Lapshin S.; Swain S.K.; Isayev A.I., Ultrasound aided extrusion process for preparation of polyolefin-clay nanocomposites, Polym. Eng. Sci. 48, 1584–1591 (2008)
[124] Kumar R.V.; Koltypin Y.; Palchik O.; Gedanken A., Preparation and characterization of nickel-polystyrene nanocomposite by ultrasound irradiation, J. Appl. Polym. Sci., 86, 160–165 (2002)
[125] Isayev A.I.; Hong C.K.; Kim K.J., Continuous mixing and compounding of polymer/filler and polymer/polymer mixtures with the aid of ultrasound, Rubber Chem. Technol, 76, 923–947 (2003)
[126] Wunderlich, W., The Atomistic Structure of Metal/Ceramic Interfaces is the Key Issue for Developing Better Properties, Metals, 4, 410–427 (2014)
[127] Agarwala, V.; Agarwala, R.C.; Daniel, B.S.S., Development of nanograined metallic materials by bulk and coating techniques, Synth. React. Inorg. Met.-Org. Nano-Met. Chem., 36, 3–16 (2006)
[128] Ramezanzadeh. B et al., Studying the effects of micro and nano sized ZnO particles on the corrosion resistance and deterioration behavior of an epoxy-polyamide coating on hot dip galvanized steel, Progress in Organic coatings, 71(3), 314-328 (2011)
[129] Sharifi. M et al., Preparation and characterization of a high performance powder coating base on epoxy/clay nanocomposite, Progress in Organic coatings, 106, 69-76 (2017)

[130] Wang. N et al., Effect of nano-sized mesoporous silica MCM-41 and MMT on corrosion properties of epoxy coating, Progress in Organic coatings, 75(4), 386-391 (2012)

[131] Chen, L.; Song, R.G.; Li, X.W.; Guo, Y.Q.; Wang, C.; Jiang, Y., The improvement of corrosion resistance of fluoropolymer coatings by $SiO_2$/poly(styrene-co-butyl acrylate) nanocomposite particles, Appl. Surf. Sci., 353, 254–262 (2015)

[132] Huttunen-Saarivirta et al., Characterization and corrosion protection properties of epoxy powder coatings containing nanoclays, Progress in Organic Coatings, 76(4), 757-767 (2013)

[133] Tomic et al., The use of nanoclay in preparation of epoxy anticorrosive coatings, Progress in Organic Coatings, 77(2), 518-527(2014)

[134] Reig C.S.; Lopez A.D.; Ramos M.H.; Ballester V.A.C., Nanomaterials: A map for their selection in food packaging applications, Packag. Technol. Sci., 27, 839–866 (2014)

[135] Kim J.Y.; Han S.-I.; Kim S.H., Crystallization behaviours and mechanical properties of poly(ethylene 2,6-naphthalate)/multiwall carbon nanotube nanocomposites, Polym. Eng. Sci., 47, 1715–1723 (2007)

[136] De Moura M.R.; Aouada F.A.; Avena-Bustillos R.J.; McHugh T.H.; Krochta J.M.; Mattoso L.H.C., Improved barrier and mechanical properties of novel hydroxypropyl methylcellulose edible films with chitosan/tripolyphosphate nanoparticles, J. Food Eng., 92, 448–453 (2009)

[137] De Moura M.R.; Lorevice M.V.; Mattoso L.H.C.; Zucolotto V., Highly stable, edible cellulose films incorporating chitosan nanoparticles., J. Food Sci., 76, N25–N29 (2011)

[138] Hare C.H, The Design of anticorrosive coatings for ferrous substrates, Coatings world, July/August 24 (1997)

[139] Leclerq M. J, Protective Coatings and Linings, 7(3), 57 (1990)
[140] Choudalakis G.; Gotsis A.D., Permeability of polymer/clay nanocomposites: A review, Eur. Polym. J., 45, 967–984 (2009)
[141] Duncan T.V., Applications of nanotechnology in food packaging and food safety: Barrier materials, antimicrobials and sensors, J. Colloid Interface Sci., 363, 1–24 (2011)
[141] Sun L.; Boo W.J.; Clearfield A.; Sue H.J.; Pham H.Q., Barrier properties of model epoxy nanocomposites, J. Membr. Sci., 318, 129–136 (2008)
[142] Picard E.; Gauthier H.; Gérard J.F.; Espuche E., Influence of the intercalated cations on the surface energy of montmorillonites: Consequences for the morphology and gas barrier properties of polyethylene/montmorillonites nanocomposites, J. Colloid Interface Sci, 307, 364–376 (2007)
[143] Yongxing Zhang et al., Excellent corrosion protection performance of epoxy composite coatings filled with silane functionalized silicone nitride, Journal of Polymer research, 25, 130 (2018)
[144] Fornes T.; Paul D., Modeling properties of nylon 6/clay nanocomposites using composite theories, Polymer, 44, 4993–5013 (2003)
[145]. Sen S.; Thomin J.D.; Kumar S.K.; Keblinski P., Molecular underpinnings of the mechanical reinforcement in polymer nanocomposites, Macromolecules, 40, 4059–4067 (2007)
[146] Vaia R.; Giannelis E., Liquid crystal polymer nanocomposites: Direct intercalation of thermotropic liquid crystalline polymers into layered silicates. Polymer, 42, 1281–1285 (2001)
[147] Jang J.S.; Bouveret B.; Suhr J.; Gibson R.F., Combined numerical/experimental investigation of particle diameter and interphase effects on coefficient of thermal expansion and young's modulus of $SiO_2$/epoxy nanocomposites, Polym. Compos., 33, 1415– 1423 (2012)

[148] Yu S.; Yang S.; Cho M., Multi-Scale modeling of cross-linked epoxy nanocomposites, Polymer, 50, 945–952 (2009)
[149] Choi J.; Yu S.; Yang S.; Cho M., The glass transition and thermoelastic behavior of epoxy-based nanocomposites: A molecular dynamics study, Polymer, 52, 5197–5203 (2011)
[150] Tsai J.L.; Tzeng S.H., Characterizing mechanical properties of particulate nanocomposites using micromechanical approach, J. Compos. Mater., 42, 2345–2361 (2008)
[151] Yang S.; Cho M., Scale bridging method to characterize mechanical properties of nanoparticle/polymer nanocomposites, Appl. Phys. Lett.,93, 043111 (2008)
[152] Goertzen W.K.; Kessler M., Thermal expansion of fumed silica/cyanate ester nanocomposites, J. Appl. Polym. Sci. 109, 647– 653 (2008).

## Experimental

[1] Kathalewar, M and Sabnis, A, Effect of molecular weight of phenalkamines on the curing, mechanical, thermal and anticorrosive properties of epoxy based coatings, Progress in Organic Coatings, 84 (2015) 79–88.

[2] Palraj, S., Selvaraj, M., Maruthan, K and Rajagopal,G., Corrosion and wear resistance behavior of nano-silica epoxycomposite coatings, Progress in Organic Coatings, 81, 132–139, 2015
[3] Zhang, J-T., Hu, J., Zhang, J-Q and Cao, C-N., Studies of water transport behavior and impendence models of epoxy-coated metals in NaCl solution by EIS, Progress in Organic Coatings, 51 (2), 145-151, 2004

[4] Pathak, S-K and Rao, B-S., Structural Effect of Phenalkamines on Adhesive Viscoelastic and Thermal Properties of Epoxy Networks, Journal of Applied Polymer Science, Vol. 102, 4741–4748 (2006)

[5] Kaur, M and Jayakumari, L-S., Eco-friendly cardanol-based phenalkamine cured epoxy-cenosphere syntactic foams: Fabrication and characterization, J. APPL. POLYM. SCI. 44189, 2016,

[6] Banerjee, D., Ghosh, C-K., Duari, B., Dey, R and Chaudhuri, B., Failure Analysis of Resin of Different Coating Materials By Infrared Spectroscopy, International Journal of Latest Research in Science and Technology, Volume 3, Issue 3: Page No. 105-108, 2014

[7] Popovic, M.M. and Grgur, B.N., Corrosion studies on electrochemically deposited PANI and PANI/epoxy coatings on mild steel in acid sulfate solution. Prog. Org. Coat., 2005, **52** (4), 359-365.

[8] M. Behzadnasab, S.M. Mirabedini, K. Kabiri, S. Jamali, Corrosion performance of epoxy coatings containing silane treated $ZrO_2$ nanoparticles on mild steel in 35% NaCl solution, Corros. Sci. 53 (2011) 89–98.

[9] Yu ,Z., Di, H., Ma, Y., He, Y., Liang, L., Lv, L., Ran, X., Pan,Y. and Luo, Z., Preparation of graphene oxide modified by titanium dioxide to enhance the anti-corrosion performance of epoxy coatings. *Surf. Coat. Technol.*, 2015, **276**, 471-478.

[10] Tang, L-C., Wan,Y-J., Yan, D., Pei, Y-B., Zhao, L., Li, Y-B., Wu, L-B., Jiang, J-X. and Lai, G-Q., The effect of grapheme dispersion on the mechanical properties of grapheme/epoxy composites. *Carbon*, 2013, **60**, 16-27.

[11] Mirabedini, S.M., Moradian, S., Scantlebury, J.D. and Thompson, G.E., Characterization and corrosion performance of powder coated aluminium alloy. *Iran. Polym. J.*, 2003, **12**, 261–269.

[12] Kendig, M., Mansfeld F, F. and Tsai, S., Determination of the long term corrosion behavior of coated steel with A.C. impedance measurements, *Corros. Sci.*, 1983, **23**, 317–322.

[13] Liu, A., Tian, H., Li, S., Ju, X., Yang, H., Sun, Y., Wang, L. and Li, W., Bioinspired layered hybrid coatings with greatly enhanced barrier effect and active corrosion protection performance. *Prog. in Org. Coat.*, 2021, **152**, 106131.

[14] Yu, Z., Di, H., Ma, Y., Lv, L., Pan, Y., Zhang, C. and Y. He., Fabrication of graphene oxide–alumina hybrids to reinforce the anti-corrosion performance of composite epoxy coatings. *Appl. Surf. Sci.*, 2015, **351**, 986-996.

[15] Sarojini Swain, Ram Avatar Sharma, Subhendu Bhattacharya, and Lokesh Chaudhary, Effects of Nano-silica/Nano-alumina on Mechanical and Physical Properties of Polyurethane Composites and Coatings, Tra on Ele & Elec Mat, Vol. 14, No. 1, pp. 1-8, February 25, 2013

[16] Khudyakoy, I-V., Designed Monomers and Pol ymer, 12 (2009) 279-290

[17] M. Zubielewicz, W. Gnot, Mechanisms of non-toxic anticorrosive pigments in organic waterborne coatings, Prog. Org. Coat, 49 (2004) 358–371.

[18] R.L. De Rosa, D.A. Earl, G.P. Bierwagen, Statistical evaluation of EIS and ENM data collected for monitoring corrosion barrier properties of organic coatings on Al-2024-T3, Corros. Sci. 44 (2002) 1607–1620.

[19] M. Zubielewicz, W. Gnot, Mechanisms of non-toxic anticorrosive pigments in organic waterborne coatings, Prog. Org. Coat. 49 (2004) 358–371.

[20] M. Mahdavian, M.M. Attar, Another approach in analysis of paint coatings with EIS measurement: phase angle at high frequencies, Corros. Sci. 48 (2006) 4152–4157.

[21] Barna, E., Bommer, B., Kursteiner, J., Vital, A., Trzebiatowski, O.V., Kochb, W., Schmidc, B and Graule, T. (2005). Innovative, scratch proof nanocomposites for clear coatings, *Composit. Part A*, vol. 36, pp. 473-480.

[22] Fatemeh Dolatzadeh, Siamak Moradian, Mohammad Mehdi Jalili, Influence of various surface treated silica nanoparticles on the electrochemical properties of $SiO_2$/polyurethane nanocoatings, Corrosion Science 53 (2011) 4248–4257

[23] Graziella Trovati, Edgar Ap Sanches, Salvador Claro Neto, Yvonne P. Mascarenhas, Gilberto O. Chierice, Characterization of Polyurethane Resins by FTIR, TGA, and XRD, Journal of Applied Polymer Science, Vol. 115, 263–268 (2010)

[24] Yanfang Zhu, Jinping Xiong, Yuming Tang, Yu Zuo, EIS study on failure process of two polyurethane composite coatings, Progress in Organic Coatings 69 (2010) 7–11

[25] Mirabedini, S.M., Moradian, S., Scantlebury, J.D. and Thompson, G.E., Characterization and corrosion performance of powder coated aluminium alloy. *Iran. Polym. J.*, 2003, **12**, 261–269.

[26] Liu, A., Tian, H., Li, S., Ju, X., Yang, H., Sun, Y., Wang, L. and Li, W., Bioinspired layered hybrid coatings with greatly enhanced barrier effect and active corrosion protection performance. *Prog. in Org. Coat.*, 2021, **152**, 106131.

[27] Yu, Z., Di, H., Ma, Y., Lv, L., Pan, Y., Zhang, C. and Y. He., Fabrication of graphene oxide–alumina hybrids to reinforce the anti-corrosion performance of composite epoxy coatings. *Appl. Surf. Sci.*, 2015, **351**, 986-996.

[28] Holub, J. and T. Wong, D., Analysis of CDT Methods and Factors Affecting Cathodic Disbondment, Marissa Tan Shaw Cor Ltd, Corporate Research & Development, 25 Bethridge Rd. Toronto, Ontario, Canada, 2015.

[29] NACE international conference, 25 Bethridge Rd. Toronto, Ontario, Canada, 200

[30] M.M. Jalili, S. Moradian, Prog. Org. Coat. 66 (2009) 359.

[31] X.D. Chen, Z. Wang, Z.F. Liao, Y.L. Mai, M.Q. Zhang, Polym. Test. 26 (2007) 202.

[32] J. Douce, J.-P. Boilot, J. Biteau, L. Scodellaro, A. Jimenez, Thin Solid Films 466 (2004) 114.

[33] F. Bauer, H.-J. Gla sel, E. Hartmann, H. Langguth, R. Hinterwaldner, Int. J. Adhes. Adhes. 24 (2004) 519.

[34] Fatemeh Dolatzadeh, Siamak Moradian, Mohammad Mehdi Jalili, Corrosion Science 53 (2011) 4248–4257

[35] H. Chen, S. Zhou, G. Gu, L. Wu, Modification and dispersion of nanosilica, J. Dispersion Sci. Technol. 25 (2005) 837–848.

[36] Mukesh Kathalewar, Anagha Sabnis, Effect of molecular weight of phenalkamines on the curing, mechanical, thermal and anticorrosive properties of epoxy based coatingsProgress in Organic Coatings 84 (2015) 79–88.

[37] Tseng, F. P.; Chang, F. C.; Lin, S. F.; Lin, J. J. J Appl Polym Sci 1999, 71, 2129.

[38] Sandeep K. Pathak, B. S. Rao, Structural Effect of Phenalkamines on Adhesive Viscoelastic and Thermal Properties of Epoxy Networks

[39] J.R. Agger, M.W. Anderson, M.E. Pemble, O. Terasaki, Y. Nozue, J. Phys. Chem. B102 (1998) 3345–3353.

[40] Jiri Holub, Dennis T. Wong, Marissa Tan Shaw Cor Ltd Corporate Research & Development

[41] Jyoti Chaudhary, Supriya Dadhich, Suman Jinger and Giriraj Tailor, Epoxy Based Vinyl Ester Resins: Synthesis and Characterization, International Journal of

Chemical Engineering Research. ISSN 0975-6442 Volume 9, Number 1 (2017), pp. 99-104

[42] Jyoti Chaudhary / J. Environ. Nano technol., Vol. 2 , 42-45, (2013)

[43] Azam Ghadami, Morteza Ehsani and Hossein Ali Khonakdar, Vinyl ester/ glass flake nanocomposites: An overview of chemical and physical Properties, Journal of Composite Materials 48(13)

[44] S. Wang, L. Chen, Y. Tong, Structure–property relationship in chitosan-based biopolymer/montmorillonite nanocomposites, J. Polym. Sci. Part A: Polym. Chem. 44 (2006) 686–696.

[45] S. Tunc, H. Angellier, Y. Cahyana, P. Chalier, N. Gontard, E. Gastaldi, Functional properties of wheat gluten/montmorillonite nanocomposite films processed by casting, J. Membr. Sci. 289 (2007) 159–168

# PhD Thesis

ORIGINALITY REPORT

**1%**

SIMILARITY INDEX

PRIMARY SOURCES

| | | |
|---|---|---|
| 1 | ir.amu.ac.in<br>Internet | 247 words — 1% |
| 2 | Fatemeh Dolatzadeh, Siamak Moradian, Mohammad Mehdi Jalili. "Influence of various surface treated silica nanoparticles on the electrochemical properties of SiO2/polyurethane nanocoatings", Corrosion Science, 2011<br>Crossref | 215 words — 1% |

ON < 1%

ON < 10 WORDS

Ujjwal Ghosh 12/07/2023

12/7/2023

1. 12/07/2023

Dr. Akshay Kr. Pramanick
Professor
Department of Metallurgical & Material Engineering
Jadavpur University, Kolkata-700 032

NACE CORROSION SPECIALIST CERT. NO. 14687

SSPC COATING SPECIALIST

NACE COATING SPECIALIST CERT. NO. 14687

# PhD Thesis

ORIGINALITY REPORT

1%
SIMILARITY INDEX

PRIMARY SOURCES

| | | |
|---|---|---|
| 1 | ir.amu.ac.in<br>Internet | 247 words — 1% |
| 2 | Fatemeh Dolatzadeh, Siamak Moradian, Mohammad Mehdi Jalili. "Influence of various surface treated silica nanoparticles on the electrochemical properties of SiO2/polyurethane nanocoatings", Corrosion Science, 2011<br>Crossref | 215 words — 1% |

| | | | |
|---|---|---|---|
| EXCLUDE QUOTES | ON | EXCLUDE SOURCES | < 1% |
| EXCLUDE BIBLIOGRAPHY | ON | EXCLUDE MATCHES | < 10 WORDS |